

**DESIGN, SYNTHESIS, PHARMACOLOGICAL AND
MOLECULAR MODELING EVALUATION OF NOVEL
PYRAZOLOPYRIMIDINE DERIVATIVES AS HUMAN A₃
ADENOSINE RECEPTOR ANTAGONISTS**

GOPALAKRISHNAN VENKATESAN
M.Pharm (Birla Institute of Technology, India)

**A THESIS SUBMITTED
FOR THE DEGREE OF DOCTOR OF PHILOSOPHY
DEPARTMENT OF PHARMACY
NATIONAL UNIVERSITY OF SINGAPORE**

2013

DECLARATION

I hereby declare that the thesis is my original work and it has been written by me in its entirety. I have duly acknowledged all the sources of information which have been used in the thesis.

This thesis has also not been submitted for any degree in any university previously.

V Gopalakrishnan

Gopalakrishnan Venktesan

20 August 2013

Acknowledgements

With immense pleasure and profound sense of gratitude, I take this opportunity to express my deep sense of gratitude and heartfelt indebtedness to my respected supervisor Assoc. Prof. Giorgia Pastorin, for her precious guidance, constant encouragement, affectionate behaviour and patience throughout the duration of the thesis work.

I express my sincere thanks to Prof. Klotz Karl-Norbert and Ms. Sonja Kachler (Institute for Pharmacology, University of Würzburg, Germany) for the pharmacological assays of the synthesized compounds, as well as Asst. Prof. Yap Chun Wei for his invaluable help to carry out the QSAR study for the synthesized compounds.

I render my sincere thanks to Assoc. Prof. Goh Mei Lin for allowing us to use the molecular modeling software. I am highly thankful to my ex-labmate Dr. Siew Lee Cheong for her timely help in the various aspects .

I extend my thanks to post-doctorate fellow of our laboratory Dr. Priyanakar Paira for correcting the experimental section of this thesis and to Dr.Vamsi Krishna for his valuable suggestions to perform molecular docking.

I am highly grateful to laboratory technologists Ms. Sek Eng, Ms. Pey Pey, Ms. Bee Jen and Ms. Tang Booy for their valuable technical support and lab officer Mr. Jeremy Goh for his assistance.

I am also eternally grateful to the research scholarship award offered by National University of Singapore throughout my Ph.D candidature.

A few lines or pages seem less to express my sincere indebtedness and love to my parents and siblings (Tharani & Gowri) for their affections, constant encouragement and invaluable suggestions without which it seems impossible to come to this stage.

Lastly, very grateful to the almighty for the blessings.

List of Publications

Published abstracts (Poster presentations):

1. Venkatesan, G., Pastorin, G, “Synthesis of novel pyrazolo[3,4-*d*]pyrimidine as human adenosine A₃ receptor antagonists”, Annual Pharmacy Research Symposium, April 2012, Singapore.
2. Venkatesan, G., Vamsi krishna, K., Pastorin, G, “Synthesis and Molecular Docking studies of novel pyrazolo[3,4-*d*]pyrimidine as human adenosine A₃ receptor antagonists, AAPS-NUS 7th PharmSci@Asia Symposium, June 2012, Singapore (Awarded the best poster presentation).
3. Venkatesan, G., Pastorin, G, “Synthesis, pharmacological evaluation and SAR study of novel pyrazolo[3,4-*d*]pyrimidine as human adenosine A₃ receptor antagonists”, Annual Pharmacy Research Awareness Symposium, April 2013, Singapore.

Journal Articles :

1. Venkatesan, G., Paira, P., Cheong, S.L., Vamsikrishna, K., Federico, S., Klotz, K.N., Spalluto, G., Pastorin, G, Discovery of simplified N²-substituted pyrazolo[3,4-*d*]pyrimidine derivatives as novel adenosine receptor antagonists: efficient synthetic approaches, biological evaluations and molecular docking studies. *Bioorg. Med. Chem.* **2013**, *In Press*.
2. Venkatesan, G., Cheong, S.L., Paira, P., Vamsikrishna, K., Federico, S., Klotz, K.N., Spalluto, G., Pastorin, G, Novel pyrazolo[3,4-*d*]pyrimidine-4-carboxylates as human A₃ adenosine receptor antagonist: Discovery, Lead Optimization, Biological and Molecular Modeling evaluation- Manuscript under preparation.
3. Paira, P., Chow, M.J., Venkatesan, G., Kosaraju, V.K., Cheong, S.L., Klotz, K.N., Ang, W.H., Pastorin, G, Organoruthenium Antagonists of

Human A₃ Adenosine Receptors, *Chem. Eur. J.* **2013**, **19**(25), **8321-8330**.

4. Cheong, S L., Federico, S., Venkatesan, G., Mandel, A.L., Shao, Y.M., Moro, S., Spalluto, G., Pastorin, G, The A₃ adenosine receptor as multifaceted therapeutic target: pharmacology, medicinal chemistry and insilico approaches, *Med. Res. Rev*, **2013**, **33**(2), **235-335**.
5. Cheong, S L., Federico, S., Venkatesan, G., P Paira., Y M Shao., G Spalluto., Yap, C. W., Pastorin, G, "Pharmacophore elucidation for a new series of 2-aryl-pyrazolo-triazolo-pyrimidines as potent human A₃ adenosine receptor antagonists". *Bioorg. Med. Chem. Lett*, **2011**, **21**(10), **2898-2905**.
6. Cheong, S L., Venkatesan, G., Paira, P., Ramasamy, J., Mendel, A.L., Federico, S., Spalluto, G., Pastorin, G, "Pyrazolo derivatives as potent adenosine receptor antagonists: An overview on the structure-activity relationships", *Int. j. med. chem*, volume **2011** (2011), Article ID **480652**, **15 pp**.

Book Chapter:

1. Li, J., Venkatesan, G., Pastorin, G. Biomedical applications III: Delivery of Immunostimulants and vaccines. **Carbon Nanotubes: from bench Chemistry to promising Biomedical applications**, Singapore: Pan standford, 2010, 333pp.

Table of Contents

Acknowledgements.....	ii
List of Publications.....	iii
Table of Contents.....	iv
Summary.....	xii
List of Tables.....	xvi
List of Chart/Schemes.....	xvii
List of Figures.....	xviii
List of Abbreviations.....	xxii
Chapter 1 General Introduction	1
1.1 Introduction.....	1
1.2 Characterization and physiological significance of adenosine receptors subtypes.....	2
1.3 Pharmacology and therapeutic applications of A ₃ adenosine receptors.....	5
1.3.1 Role of A ₃ receptor in central nervous system.....	6
1.3.2 Role of A ₃ receptor in the cardiovascular system.....	7
1.3.3 Role of A ₃ AR in inflammation and other related pathological conditions.....	8
1.3.4 Role of A ₃ AR in eye disorders.....	10
1.3.5 Significance of A ₃ receptor in cancer.....	10
1.3.6 Role of Adenosine deaminase.....	12
1.4 Overview on different classes of ligands as Adenosine ReceptorAntagonists.....	14
1.4.1 Xanthine derivatives as A ₃ AR antagonists.....	15
1.4.2 Nonxanthine derivatives as A ₃ AR antagonist.....	16
1.4.2.1 Monocyclic scaffolds.....	16
1.4.2.2 Bicyclic scaffolds.....	17
1.4.2.3 Tricyclic scaffolds.....	18
1.5 Overview of structure-activity relationships profile of pyrazolo pyrimidines as A ₃ AR Antagonists.....	21
1.6 Overview of structure - activity relationships profile of pyrazolo-triazolo- pyrimidine as hA ₃ AR Antagonist.....	23

1.7	Other therapeutic applications of pyrazolo[3,4- <i>d</i>]pyrimidines.....	26
1.7.1	Pyrazolo[3,4- <i>d</i>]pyrimidines as adenosine deaminase (ADA) inhibitors.....	27
1.7.2	Pyrazolo[3,4- <i>d</i>]pyrimidines as ATP-Competitive inhibitors of kinases.....	27
1.7.2.1	The mammalian target of rapamycin (mTOR).....	27
1.7.2.2	EGF-R PTK Inhibitors.....	28
1.7.2.3	CDK inhibitors with antiproliferative activity.....	29
1.7.3	Pyrazolo[3,4- <i>d</i>]pyrimidines as DNA polymerase inhibitors.....	29
1.8	Molecular Modeling on hA ₃ AR and its ligands.....	30
1.8.1	Quantitative structure-activity relationship (QSAR) studies.....	30
1.8.2	Homology modeling of hA ₃ receptor.....	34
1.8.2.1	Progress of hA ₃ AR homology modeling.....	35
1.8.2.2	hA ₃ AR models.....	36
1.8.2.3	Evaluations of hA ₃ AR model.....	38
1.8.3	Molecular Docking Simulations.....	38
1.8.3.1	Pyrazolo[4,3- <i>d</i>]pyrimidinones.....	39
1.8.3.2	Pyrazolo[3,4- <i>d</i>]pyrimidines.....	39
1.8.3.3	Pyrazolo-triazolo-pyrimidines.....	40
	Chapter 2 Statement of Purpose.....	44
	Chapter 3 Design, Synthesis, Pharmacological and Molecular Modeling Evaluation of a Novel Series of 4-chloro-Pyrazolopyrimidine Derivatives...	47
3.1	Introduction.....	47
3.2	Rationale of drug design.....	47
3.3	Chemical Considerations.....	51
3.3.1	Synthesis of 4-chloro-2-(ar)alkyl-2 <i>H</i> -pyrazolo[3,4- <i>d</i>]pyrimidin-6-amine (81-84), N-(4-chloro-2-(ar)alkyl-2 <i>H</i> -pyrazolo-[3,4- <i>d</i>]pyrimidin-6-yl)benzamide (101-116), N-benzoyl-N-(4-chloro-2-(ar)alkyl-2 <i>H</i> -pyrazolo[3,4- <i>d</i>]pyrimidin-6-yl)benzamide (117-120), and N-(4-chloro-2-(ar)alkyl-2 <i>H</i> -pyrazolo[3,4- <i>d</i>]pyrimidin-6-yl)-2-phenylacetamide (121-124).....	52
3.3.2	Experimental Methods.....	57
3.3.2.1	Chemistry.....	57

3.3.2.2	General procedure for the synthesis of 3-amino-1-alkyl or aralkyl-1 <i>H</i> -pyrazole-4- carbonitriles (65-68).....	58
3.3.2.3	General procedure for synthesis of methyl 3-amino-1-(alkyl or aralkyl)-1 <i>H</i> -pyrazole-4-carbimidates (69-72).....	59
3.3.2.4	General procedure for synthesis of ethyl 2-(alkyl or aralkyl)-4-oxo-4,5-dihydro-2 <i>H</i> -pyrazolo[3,4- <i>d</i>]pyrimidin-6-ylcarbamates (73-76).....	59
3.3.2.5	General procedure for synthesis of 6-amino-2-(alkyl or aralkyl) -2 <i>H</i> -pyrazolo[3,4- <i>d</i>]pyrimidin-4(5 <i>H</i>)-one (77-80).....	61
3.3.2.6	General procedure for synthesis of 3-amino-1-(alkyl or aralkyl)-1 <i>H</i> -pyrazole-4-carboxamide (85-88).....	61
3.3.2.7	General procedure for synthesis of 3-(3-benzoylthioureido)-1-(alkyl or aralkyl)-1 <i>H</i> -pyrazole-4-carboxamide (89-92).....	62
3.3.2.8	General procedure for synthesis of (E)-methyl N'-benzoyl-N-(4-carbamoyl-1-(alkyl or aralkyl)-1 <i>H</i> -pyrazol-3-yl) carbamimidothioate (93-96).....	63
3.3.2.9	General procedure for synthesis of (Z)-3-(2-benzoylguanidino)-1-(alkyl or aralkyl)-1 <i>H</i> -pyrazole-4-carboxamide (97-100).....	64
3.3.2.10	General procedure for synthesis of 6-amino-2-(alkyl or aralkyl)-2 <i>H</i> -pyrazolo[3,4- <i>d</i>]pyrimidin-4(5 <i>H</i>)-one (77-80).....	65
3.3.2.11	General procedure for synthesis of 4-chloro-2-(alkyl or aralkyl)-2 <i>H</i> -pyrazolo[3,4- <i>d</i>]pyrimidin-6-amine (81-84).....	65
3.3.2.12	General procedure for synthesis of N-(4-chloro-2(alkyl or aralkyl)-2 <i>H</i> -pyrazolo[3,4- <i>d</i>]pyrimidin-6-yl) benzamide (101-104, 105-108, 109-112, 113-116).....	67
3.3.2.13	General procedure for synthesis of N-benzoyl-N-(4-chloro-2-(alkyl or aralkyl)-2 <i>H</i> -pyrazolo[3,4- <i>d</i>]pyrimidin-6-yl) benzamide (117-120).....	71
3.3.2.14	General procedure for synthesis of N-(4-chloro-2-(alkyl or aralkyl)-2 <i>H</i> -pyrazolo[3,4- <i>d</i>]pyrimidin-6-yl)-2-phenyl acetamide (121-124).....	72
3.3.3	X-ray crystallographic studies.....	73
3.3.4	Conclusion.....	74

3.4	Pharmacological Evaluation of a Novel Series of 4-chloro Pyrazolopyrimidine Derivatives.....	75
3.4.1	Introduction.....	75
3.4.2	Binding affinity towards human A ₁ , A _{2A} and A ₃ adenosine receptors.....	75
3.4.3	Adenylyl cyclase activity at human A _{2B} adenosine receptors.....	76
3.4.4	Experimental Methods.....	76
3.4.4.1	Preparation of CHO membrane.....	76
3.4.4.2	Binding assay of human cloned A ₁ , A _{2A} , A ₃ adenosine receptor.....	77
3.4.4.3	Adenylyl cyclase activity assay.....	78
3.4.4.4	Data analysis.....	78
3.4.5	Results and Discussion.....	78
3.4.5.1	Structure-affinity relationships.....	78
3.4.6	Conclusion.....	86
3.5	Quantitative Structure-Activity Relationship (QSAR) Study on a New Series of PyrazoloPyrimidine Derivatives.....	88
3.5.1	Introduction.....	88
3.5.2	Experimental Methods.....	89
3.5.2.1	Selection and preparation of dataset.....	89
3.5.3	Results and discussion.....	90
3.5.4	Conclusion.....	93
3.6	Homology Modeling of Human A ₃ Adenosine Receptor and Molecular Docking Evaluation of PyrazoloPyrimidine derivatives.....	94
3.6.1	General Introduction.....	94
3.6.2	Homology Modeling of Human A ₃ Adenosine Receptor.....	94
3.6.2.1	Introduction.....	94
3.6.2.2	Experimental Methods.....	94
3.6.2.3	Results and Discussion.....	96
3.6.3	Molecular Docking Simulations.....	98
3.6.3.1	Introduction.....	98
3.6.3.2	Experimental Methods.....	99
3.6.3.3	Results and Discussion.....	101

3.6.3.4 Conclusion.....	111
Chapter 4 Rationale of Further Ligand Modification.....	113
Chapter 5 Design, Synthesis, Pharmacological and Molecular Docking	
Evaluation of Pyrazolo[3,4-<i>d</i>]Pyrimidine-4-carboxylate derivatives.....	116
5.1 Introduction.....	116
5.2 Chemical Considerations.....	116
5.2.1 Synthesis of ethyl 6-amino-2-(alkyl or aralkyl)-2 <i>H</i> - pyrazolo[3,4- <i>d</i>]pyrimidine-4-carboxylate (133-136), ethyl 6-benzamido-(alkyl or aralkyl)-2 <i>H</i> -pyrazolo[3,4- <i>d</i>]pyrimidine -4-carboxylate (137-153), ethyl 6-(<i>N</i> -benzoylbenzamido)-2- methyl-2 <i>H</i> -pyrazolo[3,4- <i>d</i>]pyrimidine-4-carboxylate (154-158), ethyl 2-(alkyl or aralkyl)-6-(2-phenylacetamido)-2 <i>H</i> - pyrazolo[3,4- <i>d</i>]pyrimidine-4-carboxylate (159-162).....	118
5.2.2 Experimental section.....	120
5.2.2.1 Chemistry.....	120
5.2.2.2 General procedure for synthesis of 6-amino-2-(alkyl or aralkyl)- 2 <i>H</i> -pyrazolo[3,4- <i>d</i>] pyrimidine-4-carbonitrile (125-128).....	121
5.2.2.3 General procedure for synthesis of 6-amino-2-(alkyl or aralkyl)- 2 <i>H</i> -pyrazolo[3,4- <i>d</i>]pyrimidine-4-carboxamide (129-132).....	122
5.2.2.4 General procedure for synthesis of ethyl 6-amino-2-(alkyl or aralkyl)-2 <i>H</i> -pyrazolo[3,4- <i>d</i>]pyrimidine-4-carboxylate (133-136)	123
5.2.2.5 General procedure for synthesis of ethyl 6-benzamido-(alkyl or aralkyl)-2 <i>H</i> -pyrazolo[3,4- <i>d</i>]pyrimidine-4-carboxylate (137-151)	125
5.2.2.6 General procedure for synthesis of ethyl 6-(<i>N</i> -benzoyl benzamido) -2-methyl-2 <i>H</i> -pyrazolo[3,4- <i>d</i>]pyrimidine-4- carboxylate (154-158).....	129
5.2.2.7 General procedure for synthesis of ethyl 2-(alkyl or aralkyl)- 6-(2-phenylacetamido)-2 <i>H</i> -pyrazolo[3,4- <i>d</i>] pyrimidine-4- carboxylate (159-162).....	131
5.2.3 Conclusion.....	132
5.3 Pharmacological Evaluation of a Novel Series of PyrazoloPyrimidine-4- Carboxylate Derivatives.....	133
5.3.1 Introduction.....	133

5.3.2	Experimental Methods.....	133
5.3.3	Results and discussion.....	134
5.3.3.1	Binding affinity towards human A ₁ , A _{2A} and A ₃ adenosine receptors: Structure-affinity relationships.....	134
5.4	Docking Evaluation of a Novel Series of PyrazoloPyrimidine-4- Carboxylate Derivatives.....	144
5.4.1	Introduction.....	144
5.4.2	Results and Discussion.....	144
5.4.3	Conclusion.....	153
Chapter 6	Pharmacological and docking evaluations of pyrazolopyrimidine derivatives as adenosine deaminase inhibitors.....	155
6.1	Introduction.....	155
6.1.1	Experimental Methods.....	156
6.1.2	Results and Discussion.....	156
6.1.2.1	Biological Evaluation.....	156
6.2	Docking Studies.....	160
6.2.1	Conclusion.....	164
Chapter 7	Concluding Remarks and Future Perspective.....	165

Summary

A₃ adenosine receptor (A₃AR) subtype is implicated in several pathological conditions such as cardiac and cerebral ischemia, neurodegenerative diseases as well as chronic inflammatory diseases including rheumatoid arthritis, asthma and cancer. It has been suggested that the selective inhibition of A₃ARs by antagonists could be useful as therapy for the various diseases conditions (**CHAPTER 1**). In the past few years, there has been an intensive effort to develop different heterocyclic scaffolds as hA₃AR antagonists. Among them, the pyrazolo[4,3-*e*]-1,2,4-triazolo-[1,5-*c*]pyrimidine (PTP) tricyclic scaffold has demonstrated good affinity towards the hA₃ receptor and broad selectivity range over other receptor subtypes. Recently, our group has reported new potent and selective pyrazolo-triazolo-pyrimidine (PTPs) derivatives with phenyl ring at C² position and various substituents at N⁵ and N⁸ positions. However, these PTP derivatives and also most of the tricyclic compounds, have a number of limitations such as poor aqueous solubility due to high molecular weight and a complex nature of the structure, which makes the synthetic preparation difficult and time consuming. Moreover, these problems may affect the drug like properties of the analogues. Taking into account these drawbacks, in this thesis the tricyclic PTP scaffold is simplified into the bicyclic pyrazolopyrimidine scaffold in an attempt to identify a lead compound with better physico chemical properties and similar pharmacological profile as PTP counterpart (**CHAPTER 2**).

In this project, a new series of pyrazolopyrimidines bearing a chloro group at C⁴ position and various substitution at C⁶ and N² positions were designed and synthesized as a result of a molecular simplification of parent PTP ligands (**CHAPTER 3**). The objective of the work was to investigate the effect of substituents at N², C⁶, C⁴ positions of the PPs on the hA₃ adenosine receptor affinity and selectivity over hA₁, hA_{2A}, hA_{2B} receptor subtypes.

Binding evaluation of new 4-chloro-2-(*ar*)alkyl-2*H*-pyrazolo[3,4-*d*]pyrimidin-6-amine derivatives with C⁶-free amino, benzamides and phenylacetamide (**81-84**, **101-120** & **121-124**) showed moderate affinity at hA₃AR and

selectivity at other receptor subtypes (**CHAPTER 4**). Especially, analogue **116**, with a phenyl ethyl substitution at N² position and a *para*-methylbenzamide at C⁶ position, displayed the best hA₃ affinity profile (K_i hA₃ = 1.5 μM) and about 7 fold selectivity at the hA₁ and hA_{2A} ARs. Further, analogues **115 & 120** of the same series emerged for their high selectivity (**115**, hA₁/A₃ = 21 and **120**, hA₁/A₃=35) against the hA₁ adenosine receptors, while showed almost equal (**115**, K_i hA₃ = 2.8 μM & **120**, K_i hA₃ = 2.9 μM) affinity at the hA₃AR. Similarly, some of the N²-neopentyl derivatives also displayed good affinity and moderate selectivity; for example compound **112**, with N² neopentyl, and C⁶ *p*-toluamide substituents showed a moderate affinity at the hA₃AR (K_i hA₃ = 5.0 μM) and its *para*-CF₃ analogue **111** displayed the best combined affinity and selectivity profile with K_i hA₃ = 6.6 μM; hA₁/A₃ >15, hA_{2A}/A₃ >15 in the whole series.

To rationalize the experimental hA₃ affinity and selectivity profiles of the initial 4-chloro-PP series, molecular modeling investigations were also performed on the newly synthesized PP derivatives. Among them, 3D-QSAR (quantitative structure activity relationship) methodology such as Topomer CoMFA (Comparative molecular field analysis) studies were conducted to investigate the contribution of the structural features at the N² and C⁶ positions of the bicyclic nucleus for recognition at the hA₃AR (**CHAPTER 5**). The final topomer CoMFA model displayed average correlation and predictability ($r^2 = 0.561$; $q^2 = 0.325$) and the model demonstrated that both steric effects & electrostatic effects were predominant for the ideal interaction of the antagonists with the hA₃ receptor.

Additionally, molecular docking studies were performed on 4-chloro PP derivatives (**CHAPTER 6**) using newly constructed hA_{2A} based hA₃ homology model and hA_{2A}AR crystal structure to depict the hypothetical binding mode and interactions of these derivatives. Binding interactions of 4-chloro PP derivatives summarized that hydrophobic interactions around N² & C⁶ phenyl of the benzamide chain, π - π stacking interaction with pyrazolopyrimidine ring and hydrogen bonding with C⁶amide are essential for hA₃ affinity. However, derivatives of 4-chloro-PP's lost one of the stabilizing H-

bonding interaction with Asn250 (TM6), which was deemed essential for hA₃AR affinity.

Considering the low affinity and poor selectivity profile of the 4chloro-PP analogues, further ligand modification was carried out to design a better series, in which the lipophilic chloro group at C⁴ was replaced by hydrogen bond acceptor ester substituent (**CHAPTER 7**).

In this new study, 6-amino-2-(alkyl or aralkyl)-2*H*-pyrazolo[3,4-*d*]pyrimidines bearing ester substituents at C⁴ position and various other substitutions at C⁶ and N² positions were designed and synthesized (**CHAPTER 8**). The objective of this work was to investigate the significance of the ester substituents and additional electron withdrawing and or electron donating *para* substituents of the C⁶ benzamide on the hA₃AR affinity and selectivity. Based on the binding experiments (**CHAPTER 9**), the newly synthesized pyrazolopyrimidine-4-carboxylate derivatives displayed a better affinity profile (2-3 fold increment) at hA₃AR but also ameliorated (about 15-17 fold) the selectivity against other adenosine receptor subtypes. In addition, these new derivatives showed better physico chemical properties than PTP derivatives, hence enhanced the drug like properties of the lead compounds.

Indeed, in the pyrazolopyrimidine-4-carboxylates series, most of the compounds showed very low micro molar range affinity at hA₃AR and over 100 fold improvement in the selectivity against adenosine receptor subtypes as compared to 4-chloro-pyrazolopyrimidines. In particular, compound **133**, bearing N² methyl and C⁶ free amino groups, showed the best affinity in the whole series with $K_i \text{ hA}_3 = 0.7 \mu\text{M}$, which is >142 fold more potent than its 4-chloro-PP counterpart (**81**, $K_i \text{ hA}_3 = >100 \mu\text{M}$). Similarly, compound **147**, bearing N² neopentyl and C⁶ *para*-toluamide groups, showed the best combined affinity and selectivity profile with $K_i \text{ hA}_3 = 0.9 \mu\text{M}$; $\text{hA}_1/\text{A}_3 = >111$, $\text{hA}_{2A}/\text{A}_3 = >111$. In addition, another compound (**146**) from the same N² neopentyl series displayed almost equal affinity ($K_i \text{ hA}_3 = 1.3 \mu\text{M}$) and selectivity profile ($\text{hA}_1/\text{A}_3 = >77$, $\text{hA}_{2A}/\text{A}_3 = >77$) as compound **147**. Subsequently, steric *para* substituted benzamide compounds **153** and **155** displayed comparable affinity and selectivity as compound **147**.

Consequently, molecular docking investigations were carried out on this new series of PP-4-carboxylate derivatives (**CHAPTER 9**) using newly constructed hA_{2A} based hA₃ homology model and hA_{2A}AR crystal structure to depict the hypothetical binding mode and interactions. Docking analysis showed that these analogues retained all of the essential interactions displayed by the 4-chloro PP derivatives. Similarly, they also showed additional stabilizing hydrogen bonding interactions with ‘N’ of the pyrimidine, pyrazole and also with carbonyl of the ester substituent. In addition, *para* substituents of the benzamide chains showed additional hydrophobic interactions with Val169, Val259 and Ile253, which are crucial for hA₃ affinity and selectivity over other receptor subtypes.

Eventually, new PP derivatives were also tested for their ADA inhibitory activity (**CHAPTER 10**). Some of the compounds showed promising inhibitory potency, which could be further improved by the additional substitution at the N² position of the pyrazole ring.

In summary, the molecular simplification of PTP ligands and further ligand modification of 4-chloro-pyrazolopyrimidines to pyrazolo[3,4-*d*]pyrimidine-4-carboxylates have given rise to a new class of potent and selective hA₃AR antagonists. Molecular modeling evaluation employed in our study has provided new perspectives on the structural features and binding interactions responsible for the hA₃ affinity of new PP derivatives.

List of Tables

Table 1. Binding affinity of PTP analogues (K_i) at hA₁, hA_{2A}, hA_{2B} and hA₃ receptors and selectivity against hA₁ and hA_{2A} receptors.

Table 2. Structures of new pyrazolo[3,4-*d*]pyrimidines derivatives.

Table 3. Binding affinity (K_i) of synthesized compounds at hA₁, hA_{2A}, and hA₃ adenosine receptors^[a] and selectivity against hA₁ and hA_{2A} receptors (R denote N² position).

Table 4. Fragments of training sets of 4-chloro-pyrazolopyrimidine derivatives.

Table 5. Results of the Topomer CoMFA analysis.

Table 6. Average pIC₅₀ value contributions of different substituents for R and R¹ group at pyrazolopyrimidine derivatives in topomer CoMFA with an intercept of 2.85.

Table 7. Ramachandran Plot Summary from Procheck.

Table 8. Ramachandran Plot Summary from Richardson Lab's Molprobit.

Table 9. Global quality scores.

Table 10. RMS deviations of hA₃ Model and its respective templates.

Table 11. Binding affinity (K_i) of synthesized compounds at hA₁, hA_{2A}, and hA₃ adenosine receptors^[a] and selectivity against hA₁ and hA_{2A} receptors (R denote N² position).

Table 12. ADA inhibition data of pyrazolo[3,4-*d*]pyrimidine derivatives (R denotes N² position, R₁ denotes C⁶ position).

List of Charts/Schemes

Chart 1. Rationale for the design of 2-(alkyl and aralkyl substituted)-2*H*-pyrazolo[3,4-*d*]pyrimidine derivatives (Molecular simplification of PTP into PP, R denotes N² position, R₁ denotes C⁶ position).

Chart 2. Proposed mechanism of formation of **65-68**.

Chart 3. Proposed mechanism for the formation of compounds **73-76**.

Chart 4. Structural features of pyrazolo[3,4-*d*]pyrimidines and proposed changes (R denotes N² position, R₁ denotes C⁶ position).

Chart 5. Proposed mechanism of formation of **125-128**.

Chart 6. Proposed mechanism of formation of **129-132**.

Chart 7. Proposed mechanism of formation of **133-136**.

Scheme 1. Synthetic scheme for derivatives **81-84**.

Scheme 2. Synthetic scheme for derivatives **101-124**.

Scheme 3. Synthetic scheme for derivatives **133-136**.

Scheme 4. Synthetic scheme for derivatives **137-162**.

List of Figures

Figure 1. Structure of adenosine.

Figure 2. Schematic view of A₁AR with TM domains as representative example of adenosine receptors.

Figure 3. Different subtypes of endogenous adenosine its second messenger interactions with G protein subunit Gi or Gs.

Figure 4. Schematic representation of signaling pathways involved in the A₃AR modulation.

Figure 5. Schematic view of the therapeutic application of A₃AR ligands in various patho physiological conditions.

Figure 6. Structures of (2) A₃ agonist, IB-MECA (3) A₃ agonist, Cl-IB-MECA; (4) QAF805, A_{2B}AR and A₃AR antagonist (used for inflammatory conditions); (5) MRS1523, (6) cordycepin, (7) pyrazolo[3,4-*d*]pyrimidine effective in cancer; (8) KF26777 (used for asthma); (9) MRS3558 (used for autoimmune inflammatory diseases); (10) OT- 7999, (used for glaucoma).

Figure 7. General pathway of adenosine metabolism.

Figure 8. Novel class of ADA inhibitors.

Figure 9. Structures of hA₃AR antagonists: xanthine-based structures.

Figure 10. Structures of hA₃AR antagonists: Non xanthine-based monocyclic structures.

Figure 11. Structures of hA₃AR antagonists: Non xanthine-based bicyclic Structures.

Figure 12. Structures of hA₃AR antagonists: Non xanthine-based tricyclic structures.

Figure 13. Molecular simplification of tricyclic pyrazolo[3,4-*c*]quinolone to pyrazolo[4,3-*d*]pyrimidinone.

Figure 14. Structures of pyrazolopyrimidine and related ligand as hA₃AR antagonists.

Figure 15. Structures of Pyrazolo-triazolo-pyrimidines as hA₃AR antagonists.

Figure 16. Structure-affinity relationship for the novel series of 2-aryl-PTP derivatives.

Figure 17. Structures of pyrazolo[3,4-*d*]pyrimidines as various enzyme inhibitors.

Figure 18. A. Distribution of steric and electrostatic effects in the 2-aryl-pyrazolo triazolopyrimidine derivative. The distances (Å) among the three pharmacophoric points constituted by the N⁵-phenyl ring, N⁸-methyl and C²-aryl ring are indicated. B. Combined steric and electrostatic contour plots observed for PTP analogue.

Figure 19. Topology of (A) bovine rhodopsin-based hA₃ homology model (B) human β₂ adrenergic receptor-based hA₃ homology model (C) hA_{2A} adenosine receptor-based hA₃ homology model.

Figure 20. Hypothetical binding interactions of new series of 2-aryl-PTPs

Figure 21. Essential features for PP analogue.

Figure 22. X-ray crystal structure of compound **81** (CCDC-937929). All the atoms are represented by spheres of arbitrary radii.

Figure 23. Overview of structure-affinity relationship (SAR) profile for the new series of 4-Chloro-PP derivatives **81-84** & **101-124**. ^aSpecific for N² phenylethyl substitution.

Figure 24. The steric and electrostatic effects at the N² position in compound **116** (green region favours the bulky substituents).

Figure 25. The steric and electrostatic effects at the C⁶ position in compound **116** (green region denotes steric effects, blue and red regions denotes electrostatic effects).

Figure 26. General flow chart of homology modeling.

Figure 27. General topology of the hA₃ 'hybrid' homology model.

Figure 28. The crystallographic pose of ZM241385 inside the binding cavity of hA_{2A} receptor reproduced using different docking programmes A. MOE-Dock (rmsd 2.25) B. PLANTS (rmsd 2.48) C. Autodock (rmsd 2.94).

Figure 29. Common binding interactions of new series of 4-Chloro PPs (**81-84** & **101-124**) at N² & C⁴ position with residues at hA₃AR.

Figure 30. Common binding interactions of new series of 4-Chloro PPs (**81-84** & **101-124**) at C⁶ position with respective residues in hA₃AR. ^aResidues found to interact with N² methyl substitution only, ^bResidues found to interact with N² isopropyl substitution only.

Figure 31. A. Hypothetical binding mode of compound **116** obtained after docking simulations inside the hA₃AR binding site. Poses are viewed from the membrane side facing TM6, TM7, and TM1. The view of TM7 is

omitted. B. 2D view of binding residue with ligand **116** inside hA₃AR binding site.

Figure 32. (A) Crystallographic binding mode of ZM-241385 inside the hA_{2A} receptor (PDB code 3EML) and hypothetical binding mode of compound **116** obtained after docking simulations (B) inside the hA_{2A}AR binding site and poses are viewed from the membrane side facing TM6, TM7, and TM1. The view of TM7 is omitted.

Figure 33. Binding orientation of ZM-241385 (grey) and analogue **118** (magenta) inside the hA_{2A}AR binding site. The view of TM7 is voluntarily omitted.

Figure 34. A. Hypothetical binding mode of analogue **118** inside the hA_{2A}AR binding site. The view of TM7 is voluntarily omitted. B. 2D view of binding residue with ligand **118** inside hA_{2A} AR binding site.

Figure 35. Hypothetical binding mode of PTP inside the hA₃AR binding site. The view of TM7 is voluntarily omitted.

Figure 36. Binding orientation of **125 (PTP)** (magenta) and analogue **116** (grey) inside the hA₃AR binding site. The view of TM7 is voluntarily omitted.

Figure 37. Overview of structure-affinity relationship (SAR) profile for the new series of PP-4-carboxylate derivatives **129-162**.^a N²-methyl group favoured high hA₃ affinity.

Figure 38. Common binding interactions of new series of PP-4-carboxylates (**133-162**) with N² substitution ^aResidues found to interact with C⁶ free amino substitution only.

Figure 39. Common binding interactions of new series of PP-4-carboxylates (**133-162**) with C⁶ substitution. ^aResidues found to interact with N² neopentyl substitution only.

Figure 40. Hypothetical binding mode of compound **133** obtained after docking simulations inside the hA₃AR binding site. Poses are viewed from the membrane side facing TM6, TM7, and TM1. The view of TM7 is omitted.

Figure 41. A. Hypothetical binding mode of compound **155** obtained after docking simulations inside the hA₃AR binding site. Poses are viewed from the membrane side facing TM6, TM7, and TM1. The view of TM7 is omitted. B. 2D view of binding residue with ligand **155** inside hA₃AR binding site.

Figure 42. A. Hypothetical binding mode of compound **147** obtained after docking simulations inside the hA₃AR binding site. (B) compound **147** inside the hA_{2A}AR binding site. Poses are viewed from the membrane side

facing TM6, TM7, and TM1. The view of TM7 is omitted.

Figure 43. **A.** Hypothetical binding mode of compound **153** obtained after docking simulations inside the hA₃AR binding site. Poses are viewed from the membrane side facing TM6, TM7, and TM1. The view of TM7 is omitted. **B.** 2D view of binding residue with ligand **153** inside hA₃AR binding site.

Figure 44. Binding orientation of **125 (PTP)** (magenta) and analogue **147** (blue) inside the hA₃AR binding site. The view of TM7 is voluntarily omitted.

Figure 45. Crystal structure of Adenosine deaminase.

Figure 46. **A.** Binding mode of reference ligand (+)-EHNA into the ADA binding cavity. **B.** 2D view of the reference compound (+)-EHNA inside the ADA.

Figure 47. **A.** Binding mode of compound **151** inside the ADA binding cavity, **B.** 2D view of the compound **151** inside the ADA binding cavity.

Figure 48. Superimposition of ligand **151** (blue) & **162** (magenta) inside ADA binding cavity.

List of Abbreviations

ARs: adenosine receptors

ADA: adenosine deaminase

AMP: adenosine monophosphate

ATP: Adenosine triphosphate

β 1AR : beta1-adrenergic receptor

β 2AR : beta2-adrenergic receptor

Bcl : B cell lymphoma

CREB: cAMP response element-binding protein

cAMP :cyclic adenosine monophosphate

CDK2: Cyclin-dependent kinase 2

CGS15943: 5-amino-9-chloro-2-(2-fury1)-[1,2,4]triazolo[1,5-*c*]quinazoline

CHO cells: Chinese hamster ovary cells

Cl-IB-MECA: 2-chloro-N⁶-(3-iodobenzyl)-5'-N-methylcarboxamidoadenosine

CoMFA: Comparative Molecular Field Analysis

CNS: Central nervous system

DAG: Di acyl glycerol

DIPEA: diisopropylethylamine

DMF: dimethylformamide

ECL: extracellular loop

EL: Extra cellular

EGFR: epidermal growth factor receptor

ERK1/2: extracellular signal-regulated kinases

EtOAc: ethyl acetate

ER: endoplasmic reticulum

Gi: inhibitory G proteins

GIT: Gastrointestinal tract

GPCR: G protein-coupled receptor
GnRH : Gonadotropin- releasing hormones
Gq: Gq family of G proteins
GSK3 β : glycogen synthase kinase 3 β
GTP: guanosine triphosphate
hA₂₁AR: human A₁ adenosine receptor
hA_{2A}AR: human A_{2A} adenosine receptor
hA_{2B}AR: human A_{2B} adenosine receptor
hA₃AR: human A₃ adenosine receptor
HIF-1 α : Hypoxia-inducible factor 1-alpha
HMQC: Heteronuclear Multiple-Quantum Correlation
[³H]-CCPA: [³H]-2-chloro-6-cyclopentyl adenosine
[³H]-NECA: [³H]-N-ethylcarboxamido adenosine
I-ABOPX: 2-[4-[3-[(4-amino-3-iodophenyl)methyl]-2,6-dioxo-1-propyl-7*H*-
purin-8-yl]phenoxy]acetic acid
IB-MECA: N⁶-(3-iodobenzyl)-5'-N-methylcarboxamidoadenosine
IGluR: ionotropic glutamate receptor
IKK: I κ B kinase
IL : intracellular
IOP : Intra ocular pressure
IP3 : inositol triphosphate
IPC: ischemic preconditioning
K_{ATP}: ATP-sensitive potassium channel
KF26777: 2-(4-bromophenyl)-4-propyl-7,8-dihydro-1*H*-imidazo[1,2-*i*]purin-
5(4*H*)-one
LBHM: ligand-based homology modeling
LH : Luteinizing hormone
MAPK: mitogen-activated protein kinase
MEK: mitogen-activated pyotein kinase
MEP: molecular electrostatic potential

MIP- α : macrophage inflammatory protein alpha

MOE: Molecular Operating Environment

mRNA: messenger Ribonucleic acid

MRS1067: 3,6-dichloro-2-(4-chloro-2-isopropylphenyl)-4*H*-chromen-4-one

MRS1191: 3-benzyl 5-ethyl 6-methyl-2-phenyl-4-(phenylethynyl)-1,4-dihydropyridine-3,5-dicarboxylate

MRS134: 3-ethyl 5-(4-nitrobenzyl) 2-methyl-6-phenyl-4-(phenylethynyl)-1,4-dihydropyridine-3,5-dicarboxylate

MRS1220: N-(9-chloro-2-(furan-2-yl)-[1,2,4]triazolo[1,5-*c*]quinazolin-5-yl)-2-phenylacetamide

MRS1292: 3,6-dichloro-2-(4-chloro-2-isopropylphenyl)-4*H*-chromen-4-one

MRS1523: 5-propyl-2-ethyl-4-propyl-3-(ethylsulfanylcarbonyl)-6-phenylpyridine-5-carboxylate

MRS3558: (1*S*,2*R*,3*S*,4*S*,5*S*)-4-(2-chloro-6-(3-chlorobenzylamino)-9*H*-purin-9-yl)-2,3-dihydroxy-N-methylbicyclo [3.1.0] hexane-1-carboxamide

MRS3771: 3,6-dichloro-2-(4-chloro-2-isopropylphenyl)-4*H*-chromen-4-one

mTOR: mammalian target of rapamycin

NECA: N-ethylcarboxamido adenosine

NF- κ B: nuclear factor kappa-B

OT-7999: 5-n-butyl-8(4-trifluoromethylphenyl)-3*H*-[1,2,4]triazolo-[5,1-*i*]purine

PDB: Protein database

PI3K: phosphoinositide 3-kinase

PKA and PKB/Akt: protein kinases A and B

PKC: protein kinase C

PLC and PLD: phospholipase C and phospholipase D

PLS: partial-least-square

PTK: protein tyrosine kinase

PP: pyrazolopyrimidine

PTP: pyrazolo-triazolo-pyrimidine

QAF805 : 3-(5-(2-methyl-1*H*-imidazol-1-yl)-2-(pyrazin-2-ylamino)thiazol-4-yl)benzotrile

QSAR: quantitative structure-activity-relationship
RMSD: root-mean-squared deviation
R-PIA: R-N⁶-phenylisopropyladenosine
r²_{pred}: predictive r²
SCID: serious combined immunodeficiency disease
SAR: structure-affinity/activity relationship
TLC: thin-layer chromatography
TM: transmembrane
TMS: tetramethylsilane
TNF- α : tumor necrosis factor alpha
TRH : Thyrotropin- releasing hormone
TSH : Thyroid stimulating hormone
MV: molecular volume
RMSD: root mean square deviation
VUF8504: 3,6-dichloro-2-(4-chloro-2-isopropylphenyl)-4*H*-chromen-4-one
VUF5574: 1-(4-methoxyphenyl)-3-(2-(pyridin-3-yl)quinazolin-4-yl)urea

Chapter 1 General Introduction

The information pertained to this chapter has been compiled from our below review article:

- Cheong, S. L.; Federico, S.; Venkatesan, G.; Moro, S.; Spalluto, G.; Pastorin, G. Human A₃ adenosine receptor as multifaceted therapeutic target: pharmacology, medicinal chemistry and in silico approach. *Med. Res. Rev.* 33 (2), 235-335, 2013. doi:10.1002/med.20254.

1.1 Introduction

Adenosine is a nucleoside made up of adenine attached to a ribose moiety through a β -N⁹-glycosidic linkage (**Figure 1**). In our body, adenosine acts as an endogenous modulator that regulates many physiological processes through activation of specific human adenosine receptors (hARs). These receptors, which consist of seven transmembrane domains, are members of G protein-coupled receptor (GPCR) family and are activated by different stimuli such as photons, neurotransmitters, neuromodulators, biogenic amines (e.g. catecholamines and histamine), peptides (e.g. gonadotropin-releasing hormones (GnRH), thyrotropin-releasing hormone (TRH)) and glycoproteins (luteinizing hormone (LH) and thyroid stimulating hormone (TSH)).¹

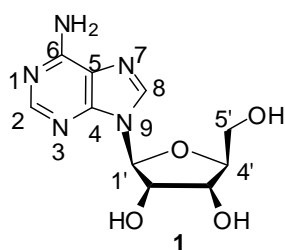


Figure 1. Structure of adenosine

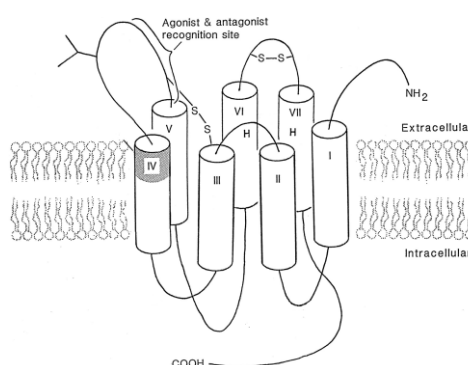


Figure 2. Schematic view of A₁AR with TM domains as representative example of adenosine receptors²

These receptors possess a common central domain consisting of seven transmembrane (TM 1–7) helices (approximately 20–25 amino acids for each helix). These helices are connected via three intracellular (IL1, IL2 and IL3) and three extracellular loops (EL1, EL2 and EL3). The extracellular region of the protein is composed of the amino terminus and several loops, comprising the ligand-binding cavity. The carboxyl end is located at the cytoplasmic side of the membrane. Moreover, the helix contains two cysteine residues, observed in TM3/EL1 interface and EL2, which form a vital disulfide linkage (Figure 2). This linkage is considered to be important for the packing and stabilization of the conformations of these seven TM domains. Consequently, the specific properties of these receptors are conferred by these domains.³ Moreover, TM domains of GPCRs contain the primary sequence homology and the most conserved residues are situated within the TM domains and constitute the important structural determinants of receptor function.

1.2 Characterization and physiological significance of adenosine receptor subtypes

Adenosine receptors are categorized into four subtypes, such as A₁, A_{2A}, A_{2B} and A₃ adenosine receptors (Figure 3).⁴ All of these ARs possess their own distinct different tissue localization, biochemistry and pharmacological character.

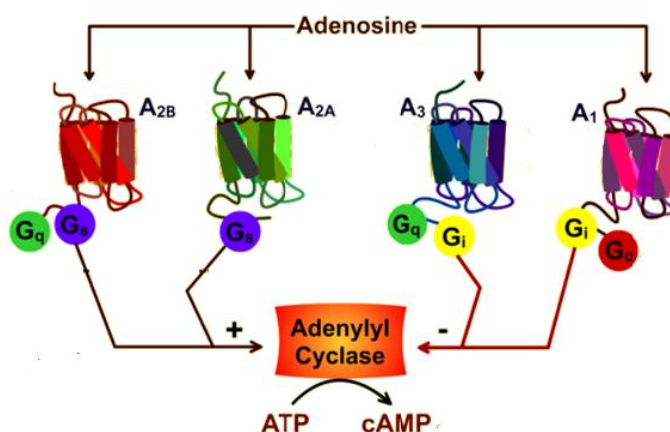


Figure 3. Different subtypes of endogenous adenosine receptors and their second messenger interactions with G protein subunit G_i or G_s.

A₁ Adenosine receptors (A₁ARs). The A₁ARs are the most conserved adenosine receptor subtype across different species⁵ and they are found at the highest density in the brain (cortex, cerebellum, and hippocampus) and adipose tissue. Moderate to high density level of A₁ARs appear to be present on specialized cells of spinal cord, thyroid, kidney, adrenal gland, eye, sinoatrial and atrio ventricular nodal tissue of the heart. Human (h)A₁AR are expressed in low density in the cardiac ventricles, lung, pancreas, liver and GI tract.⁶ Activation of the A₁ARs inhibits adenylyl cyclase activity, activates K⁺ channels, blocks transient Ca⁺ channels and increases intracellular Ca⁺ and inositol-1,4,5-trisphosphate levels by activating phospholipase C (PLC).

A_{2A} Adenosine receptors (A_{2A}ARs). A_{2A}ARs are found in the spleen, thymus and leukocytes in high level, whereas moderate levels are observed in the heart and lung. Moreover, the highest concentration of the receptor is found in *striatum* of the brain.^{7,8} Similarly, activation of A_{2A}ARs induces the cyclic AMP-protein kinase A (PKA) pathway by conjugating through G_s protein⁵ in peripheral tissues or G_{olf} protein^{9,10} in the brain. A_{2A}ARs interact with various neurotransmitters in the brain and regulate the motor, psychiatric effects and the sleep-wake cycle. In peripheral tissues, A_{2A}ARs play a vital role such as oxygen consumption of myocardium, and coronary blood flow.¹¹

A_{2B} Adenosine receptors (A_{2B}ARs). Among all four adenosine receptors, A_{2B}ARs are the most adenosine-insensitive receptor which are widely expressed, but in low abundance. A_{2B}AR requires micromolar concentrations which are rarely achieved under physiological conditions. During conditions including hypoxia, ischaemia, the adenosine level is increased and genetic and pharmacological studies have described the functional roles of A_{2B}ARs including tissue adaptation to hypoxia¹², increased ischaemia tolerance^{13,14}.

A₃ Adenosine receptors (A₃ARs). Recently, the hA₃AR has been cloned and characterized pharmacologically.⁴ The amino acid sequence of the hA₃AR is 61%, 54% and 52% identical in sequence to hA₁AR, hA_{2A}AR and hA_{2B}AR subtypes, respectively.¹⁵ The hA₃AR shares sequence homology of about 74% with ratA₃AR and 85% of identical homology with sheep A₃AR.¹⁶ In addition, mRNA of A₃AR was mainly found in various brain areas at limited levels, whereas high levels were found in rat testis, heart and lungs.¹⁷ Similarly,

mRNA of hA₃AR has been expressed in peripheral tissues, with low levels in testis and CNS.¹⁸ As a consequence, the evaluation of therapeutic characteristics in animal models is hampered due to species dependent tissue distribution and pharmacology of A₃ARs.¹⁹ Thorough investigation on A₃AR suggests that A₃ARs are principally expressed in the liver, lung, and primary cells (e.g. macrophages, monocytes, eosinophils) involved in inflammation. Whereas, A₃AR minor expression is found in kidney, brain, heart, and GIT tissues.⁵ In terms of signalling transduction pathways (**Figure 4**), activation

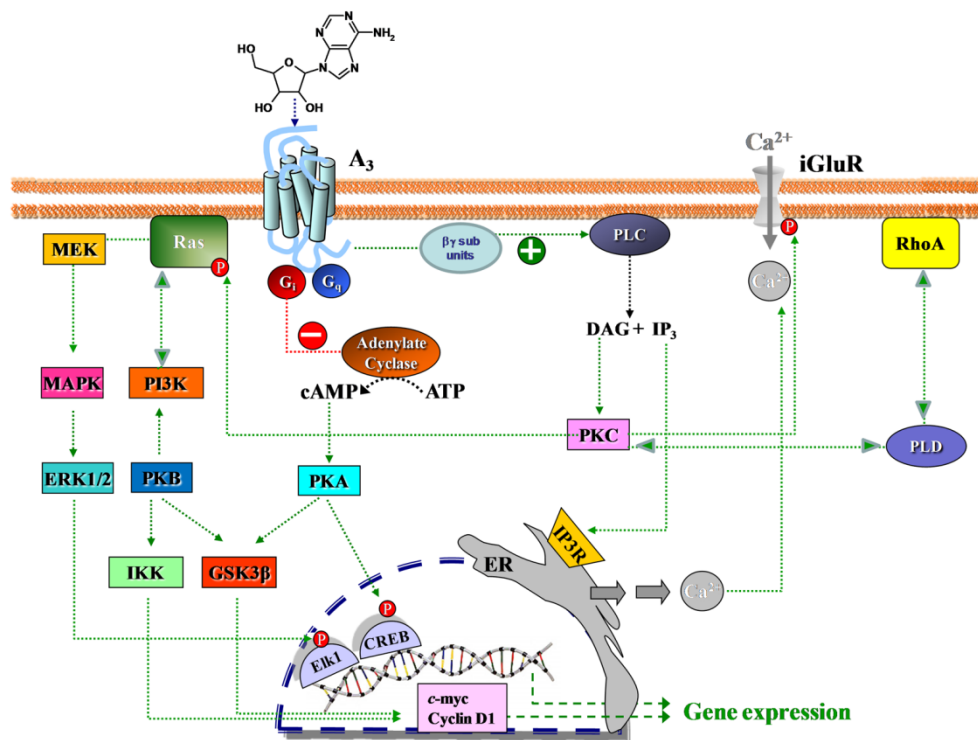


Figure 4. Schematic representation of signalling pathways involved in A₃AR modulation (adopted from Cheong *et al.*).¹⁵

of the A₃ARs results in the (i) inhibition of adenylyl cyclase through the interaction with inhibitory G_i protein mediation, followed by decrease in cyclic adenosine monophosphate (cAMP) level; (ii) increase in the phospholipase C (PLC) activity mediated by G_q protein; (iii) mobilization of Ca⁺ ion.^{20,21} Other secondary pathways related to A₃AR have also been reported, such as (iv) activation of ATP sensitive K⁺ channel (K_{ATP}) in the heart, or (v) activation of RhoA by A₃AR mediation with phospholipase D (PLD) and protein kinase C (PKC) stimulations consequently. These signalling pathways are proven to play a crucial role in protective function of

cardio myocytes.²² (vi) Similarly, through the activation of Ras, A₃AR regulate phosphoinositide 3-kinase (PI3K) or extracellular signal-regulated kinase (ERK1/2) activities.²³ The phosphoinositide 3-kinase/phospholipase B (PI3K/PKB) and mitogen-stimulated protein kinase/extracellular signal influenced kinase (MEK1/ERK1/2) pathways are found to be involved in cell survival processes and related to A₃AR induced preconditioning in cardio myocytes from newborn rats during hypoxia or reoxygenation.²⁴ Through above signalling pathways, the modulation of such receptor is implied in cardio protective and cerebro protective functions. Further, due to selective activation of A₃AR, the cellular growth is also modulated.²⁵⁻²⁸

Similarly, its inhibition by selective antagonists has been described to be useful in the treatment of pathologic conditions such as glaucoma, inflammatory diseases and cancer.^{29,30} The wide spread distribution of A₃ARs in various cells and tissues, could suggest their possible involvement in various disease conditions and the potential use as a selective pharmacological target. As such, the A₃ARs are deemed promising therapeutic targets that propel the research on the development of potential A₃AR ligands targeting this particular receptor. In fact, a large number of A₃ ligands i.e. agonists and antagonists, have been investigated, and various classes of derivatives indicating good A₃ affinity with wide ranges of selectivity towards other AR subtypes have been synthesized and tested successfully as A₃AR ligands. Due to the still enigmatic role of A₃AR, we decided to focus our studies on this adenosine receptor subtype. Therefore, in the next section, pertinent therapeutic applications associated with the modulation of A₃AR by selective compounds are discussed in more details.

1.3 Pharmacology and therapeutic applications of A₃ adenosine receptors

The diverse physiological functions of adenosine highlight the significant benefits of developing therapeutics for the regulation of adenosine receptors. The vast amount of effort invested in adenosine research is driven by the therapeutic potential for drugs which elicit their actions at adenosine receptors. However, the ubiquitous distribution of adenosine receptors in mammalian cell types, the existence of at least four distinct subtypes together with the variability of physiological responses mean that exploiting this

potential requires ligands that are highly selective in their action (with respect to receptor subtype and tissue type) to be of value as therapeutics. To-date, there are increasing studies that indicate the A₃ receptor could be involved in several patho physiological conditions that occur especially in the central nervous, cardiovascular systems, as well as in inflammatory disorders and cancer (**Figure 5**).

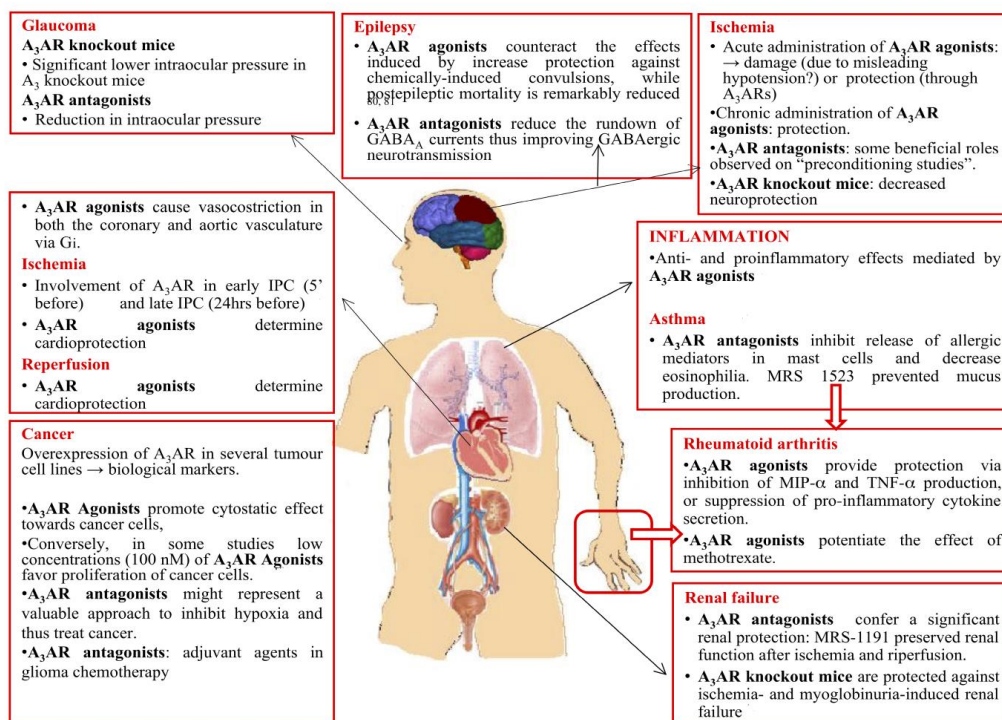


Figure 5. Schematic view of the therapeutic application of A₃AR ligands in various patho physiological conditions

1.3.1 Role of A₃ receptor in central nervous system

A₃ARs are distributed in the central nervous system substantially but at low levels with a diminished affinity and the role of A₃ARs in various pathological conditions is controversial, although they may contribute to neurotransmission.³¹ Recently, Chen *et al.*³⁰ examined the protective role of the A₃AR agonists in brain cells by *in vitro* and *in vivo* study. However, these results differ predominantly from those obtained by Von Lubitz *et al.*,³² who proved that the intra peritoneal pre-treatment with A₃AR agonists before ischemia exacerbated the condition in stroke-afflicted mice. In addition, other research groups hypothesized about the absence of this receptor subtype or its

mRNA in the CNS, suggesting that the described evidence on A₃AR was due to the overlapping affinity of A₃AR ligands for A₁AR.³³ Subsequent studies proved that A₃AR activation has different actions depending on the A₃AR agonists concentration used: higher concentrations (>10 μM) exhibited a cytotoxic effect, whereas lower concentrations displayed a cytoprotective effect. These dual and opposite effects of the A₃AR's activation are observed in conditions such as tissue protection in inflammatory cells or in tumoral tissues. Studies have shown that chronic pre-treatment with an A₃AR agonist resulted in remarkable neuro protection of ischemic gerbils.²⁸ In contrast, neuronal damage was worsened due to acute treatment with an A₃AR agonist.²⁶ It has been reported that the activity of anti depressant-sensitive serotonin transporters (SERTs) is rapidly increased by A₃ARs stimulation.³⁴ A₃AR-stimulated SERT activity is primarily mediated by p38 MAPK-linked pathways, supporting the potential use of agents that block A₃ARs (i.e. antagonists) and selectively diminish SERT surface expression and activation. Therefore, it is suggested the use of A₃AR antagonists for the treatment of mood disorders characterized by hypo serotonergic states.³⁴

1.3.2 Role of A₃ receptor in the cardiovascular system

ARs have been widely distributed in cardiac myocytes, and A₂AR subtypes also highly expressed on endothelial cells.³⁵ During increased oxygen consumption (e.g. exercise), adenosine is formed and channeled out of the cardiac system and further it reaches the interstitial space and carries information of cardiac myocytes to smooth muscle of arteriolar for dilatation, till the conditions reach the normal ranges. Some studies proved the involvement of A₃AR in ischemic preconditioning (IPC), mainly in early ischemia (5 min before the onset)^{36,37} and late IPC (24 hr before inducing ischemia).³⁸ It was noticed that the activation of PKC along with A₃AR-induced opening of the K_{ATP} channels are responsible for the ischemic phenomenon.³⁹

Interestingly, activation of A₃AR by its agonists IB-MECA (**2** in **Figure 6**) and Cl-IB-MECA (**3**) during reperfusion and acute myocardial ischemia was also accounted to be related with cardio protection. Consequently, A₃AR antagonists could block the beneficial effects, which

were observed either before ischemia or during reperfusion.⁴⁰ Nevertheless, a few research groups have performed the preclinical studies investigating the beneficial effects of adenosine administration⁴¹ or the treatment of an acute myocardial ischemia reperfusion injury by AR agonist administration.⁴² Consequently, the results have shown no clear advantages from the infusion of such agents, especially in patients without anterior myocardial infarction, which could probably be attributed to suboptimal doses or too small clinical trials.

A multi factorial large arteries disease called atherosclerosis is the major reason for heart disease and stroke. It was discovered that environmental and genetic risk factors seemed to be involved with this pathology.⁴³ Recently, it has been discovered that HIF-1 α accumulation by activating ERK 1/2 pathway was stimulated by adenosine in hypoxic foam cells. Further, VEGF secretion in a HIF-1 α dependent way was also activated by A₃ARs. In addition, adenosine induced formation of foam cell is strongly reduced A₃AR antagonists and by HIF-1 α silencing. So as a consequence, A₃AR antagonists could be used to block the essential steps of the atherosclerotic plaque development.⁴⁴

1.3.3 Role of A₃AR in inflammation and other related pathological conditions

Adenosine receptors expressed in the inflammatory cells such as mast cells,⁴⁵ neutrophils,⁴⁶ eosinophils⁴⁷ and macrophages⁴⁸ have been modulated by adenosine, thereby it plays a important role in the inflammation process. It has been proven that the activation of A₃ARs could be both pro- or anti-inflammatory, depending on the cell type investigated or on the animal species studied.⁴⁹ Several studies reported that apoptosis and the chemo taxis process of eosinophils are inhibited by A₃ARs, present on human eosinophils.⁵⁰ It has been exhibited that over expressed A₃ARs in lymphocytes, Jurkat cells, and a human leukemic cell line caused the inhibition of adenosine cyclase and calcium modulations.⁵¹ These effects seem to be an indication of an anti-inflammatory effect of this receptor subtype produced by A₃AR activation of macrophages.

In some studies that are aimed at evaluating the role of ARs in inflammatory diseases, for instance asthma, it was observed that mast cells required A₃AR in their degranulation process via PI3K activation and increase in intracellular Ca²⁺ levels.⁵² Besides, the A₃ARs density on eosinophils of

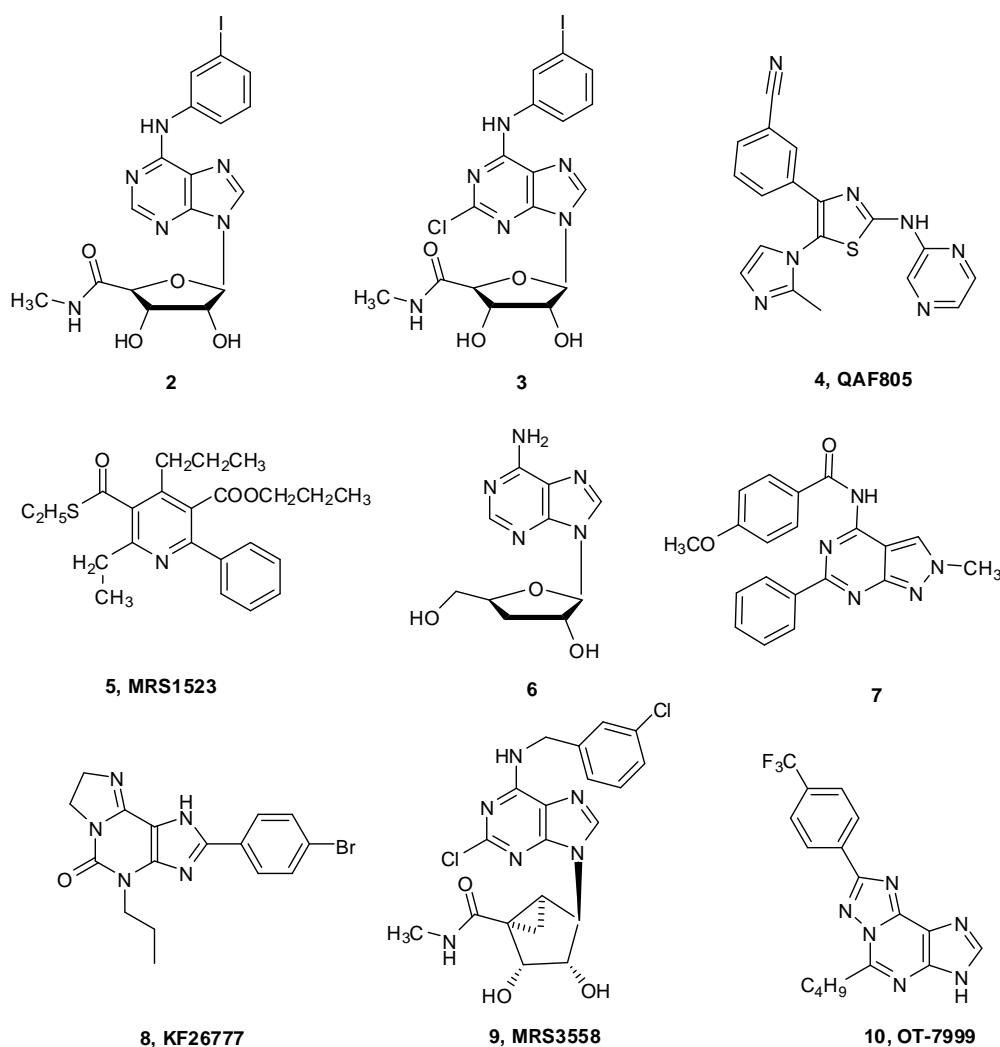


Figure 6. Structures of **(2)** A₃ agonist, IB-MECA **(3)** A₃ agonist, Cl-IB-MECA; **(4)** QAF805, A_{2B}AR and A₃AR antagonist (used for inflammatory conditions); **(5)** MRS1523, **(6)** cordycepin, **(7)** pyrazolo[3,4-*d*]pyrimidine (effective in cancer); **(8)** KF26777 (used for asthma); **(9)** MRS3558 (used for autoimmune inflammatory diseases); **(10)** OT-7999, (used for glaucoma).

patients suffering from asthmatic conditions was also found to be elevated.⁵³ On the other hand, in a rabbit model, it was reported that theophylline counterbalanced the broncho constriction stimulated by adenosine, which was a natural antagonist of adenosine receptors.⁵⁴ Such observations inferred a vital role for A₃AR antagonists for the treatment of asthma. In fact, the pharma

company Novartis developed QAF805 (**4, Figure 6**), as a dual A_{2B}AR and A₃AR antagonist and has been proposed as an antiasthmatic agent.⁵⁵ However, Phase Ib clinical trials of this asthmatic agent were not successful.

In the case of another chronic inflammatory disease, namely rheumatoid arthritis, it was recently noted that TNF- α inhibition involved also the A₃AR,⁵⁶ in particular, the A₃AR agonists were observed to supply a protective effect via inhibition of alpha (MIP- α) and TNF- α secretion, or suppression of cytokine production by involving the PI3K-NF κ B pathway.⁵⁷

1.3.4 Role of A₃AR in eye disorders

A₃ARs have been implicated in ocular diseases such as dry eye, glaucoma or uveitis.⁵⁸ In the past study, lower intracellular pressure observed in the the A₃AR knockout mouse, suggested the role for A₃AR antagonists in glaucoma treatment.⁵⁹ In addition, A₃AR antagonists may be considered as a substitute for treating ocular hypertension associated with pseudoexfoliation syndrome in patients.⁶⁰ On the contrary, in pseudo exfoliation syndrome with glaucoma condition, the level of A₃AR mRNA was found to be increased at the non pigmented ciliary epithelium of the eye while compared to normal eye.⁶¹ Over expression of A₃AR in retinal ganglion cells, seemed to be reduced by agonist treatment and also showed reduced calcium levels and cell rescue from apoptosis.⁶²

1.3.5 Significance of A₃ receptor in cancer

A high concentration of adenosine is found in cancer tissues and also in the interstitial fluid related to various tumors, at sufficient concentrations to interact with ARs. Moreover, up regulation of the A₃AR level in cancer cells proved the important functions of A₃ARs as biological markers or target. In fact such over expression seems to be well correlated with the severity of the disease. More precisely, it is mainly because of enhancement of transcription factor NF- κ B and Wnt signaling caused by expression of the A₃AR.⁶³ Primary examples of A₃AR over expressions (about 2.3 fold) are represented by colon and breast carcinomas in comparison to adjacent normal tissues. In most cases, at least 1.6 fold

increase of A₃AR density has been observed as compared to normal specimens.

Moreover, higher concentration of mRNA of A₃AR was also found in lymph node metastases suggesting that disease progression stage could be indicated by A₃AR levels.⁶⁴ Notably, overexpression of the the A₃AR levels also found in remote tumor tissue along with the tumor origin. This seems to be associated to TNF- α upregulation, a raise in NF-kB and Wnt signaling. Moreover, several studies confirmed that down regulation of A₃AR occurred rapidly after the tumor removal.⁶⁵ More precisely, inhibition of adenylate cyclase by A₃AR causes, decrease in cAMP level, and consequent effects on PKA and PKB/Akt, control the cell cycle, which results in arrest of cell proliferation and inhibition of tumor growth. In fact, it has been recently exhibited that phosphorylative pathways such as ERK 1/2, p38, and Akt are involved in cell proliferation of glioblastoma cells mediated by A₃AR.⁶⁶

The A₃AR agonists such as IB-MECA and CI-IB-MECA, have been widely investigated for their proliferation effects on various tumour cells. Interestingly co-administration of such agonists, with 5-fluorouracil,⁶⁷ seem to be responsible for the cytostatic effect towards cancer cells, as indicated by cell cycle arrest at the G₀/G₁ phase.⁶⁸ The cancer cell function was completely recuperated after administration of a selective A₃AR antagonist (**MRS1523, 5** in **Figure 6**).⁶⁹ In addition, IB-MECA and CI-IB-MECA were found to exclusively activate A₃ARs and inhibit the growth of primary murine melanoma tumors,⁶⁹ human prostate cancers, or colon cancers⁷⁰ in *in vivo* experiments.⁶⁸ In addition, these compounds added value in cancer treatment, by promoting (i) chemoprotective effect;⁷¹ (ii) up-regulation of IL-12 in carcinoma bearing mice,⁷⁰(iii) natural killer cell activity⁷².

On the contrary, low concentrations (100nM) of CI-IB-MECA induced the proliferation of cancer cells, as demonstrated by Gessi *et al.*⁷³ Abbracchio and collaborators have substantiated these results and observed increased Rho expression⁷⁴ and an enhanced anti-apoptotic protein Bcl-XL production. Further, they suggested that A₃AR agonists stimulation might determine different effects depending on cell type and experimental conditions (e.g. concentrations). In fact, both a receptor-dependent or -independent inhibitory effect towards cancer cell proliferation through the arrest at the

G₀/G₁ phase was observed by using high concentrations (10-60 μM) of the above-mentioned A₃AR agonists⁷⁵ or cordycepin (i.e. 3'-deoxyadenosine, **6**)⁷⁶. Recently, a newly synthesized A₃AR antagonist (**pyrazolo[3,4-d]pyrimidine, 7**) was shown to counteract the A₃AR agonists CI-IB-MECA and IB-MECA-induced proliferation of the glioma cells via inhibition of A₃AR agonist-regulated ERK 1/2 activation.⁷⁷ This observation was in accordance with the studies which exhibited that ERK 1/2, p38 and Akt could be the phosphorylative pathways responsible for A₃AR regulated cell proliferation in glioblastoma. These findings implied that A₃AR antagonists could be represented as promising adjuvant agents in the glioma chemotherapy.

On the whole, A₃AR ligands are a class of therapeutically relevant agents that could play an important role in the neuro- and cardio-protection, as well as inflammatory diseases and cancer. Nevertheless, issues on the peculiar physiological role of A₃AR activation, which may produce effects that are species-dependent, or produce opposite effects depending on duration and level of activation as well as concentration of A₃ agonist used, have not yet been satisfactorily explained. In spite of these unclear observations, some promising A₃AR ligands have progressed into the clinical trials, particularly i) adenosine itself (Adenocard), used to treat arrhythmias and supraventricular tachycardia; ii) IB-MECA and CI-IB-MECA (A₃ agonists) in Phase II clinical studies for arthritis, psoriasis and liver cancer, (iii) QAF805 (A_{2B}AR/A₃AR antagonist, **4**) and KF26777, (A₃AR antagonist, **8**), indicated for asthma; (iv) MRS3558 (**CF502, 9** in **Figure 6**) in preclinical studies for autoimmune inflammatory diseases⁷⁸ and (v) OT-7999 (A₃AR antagonist, **10**)⁷⁹ which is expected to enter clinical trials for the treatment of glaucoma.

1.3.6 Role of Adenosine deaminase

Adenosine deaminase (ADA) (EC 3.5.4.4) is considered to be a key endogenous enzyme in purine metabolism and catalyzes the irreversible deamination of adenosine and 2'-deoxyadenosine to inosine and 2'-deoxyinosine, respectively. During electrical stimulation or energy depletion, adenosine is generated, mostly at the intracellular level, and subsequently released by a process involving a transporter.⁸⁰ Subsequently, inactivation of

extracellular adenosine is believed to happen largely by uptake across the cell membrane, followed by either rephosphorylation to 5'-AMP, catalyzed by adenosine kinase (adenosine 5'-phosphotransferase, EC 2.7.1.20) or deamination to inosine, which is catalysed by adenosine deaminase (adenosine aminohydrolase, EC 3.5.4.4). The general pathway of adenosine metabolism is depicted in **Figure 7**.⁸⁰

Generally, adenosine deaminase (ADA) is ubiquitous in all human tissues and plays a vital role in the development of the immune system and the genetic ADA deficiency results in severe immunodeficiency disease caused by damage of lymphoid cells differentiation and maturation.⁸¹ Consequently, it is reported that ADA inhibition may be useful for the selective treatment of lymphoproliferative malignancies.^{82, 83}

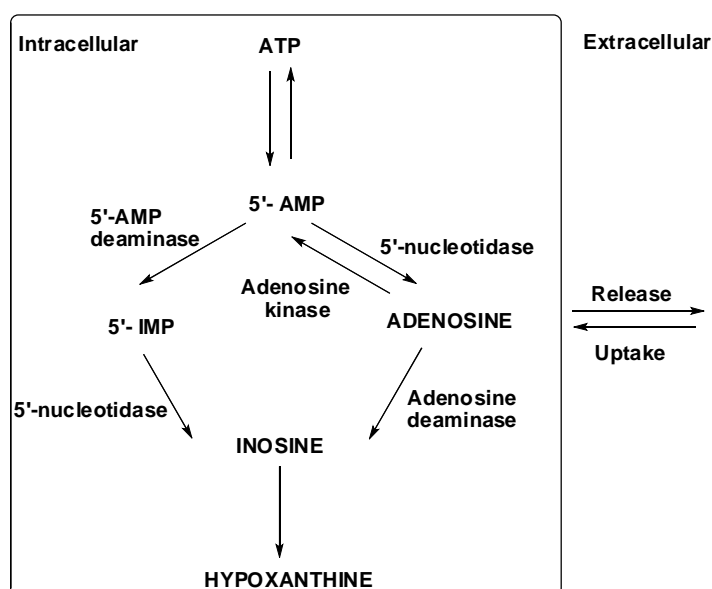


Figure 7. General pathway of adenosine metabolism (adopted from Lloyd *et al*)⁸⁰

ADA abnormalities have also been reported in other diseases, such as rheumatoid arthritis and leukemia.⁸⁴ Moreover, it is described that adenosine concentration is increased in inflammatory lesions, hence it is considered as an important factor in the attenuation of inflammation as well.⁸⁵

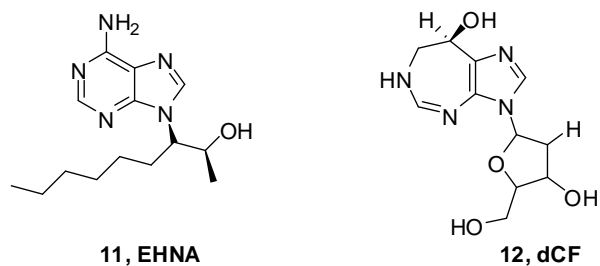


Figure 8. Novel class of ADA inhibitors.

Additionally, ADA has been the focus of interest mainly because its congenital defect in humans causes serious combined immunodeficiency disease (SCID), in turn resulting in the impairment of both B-cell and T-cell development.⁸⁶ Considering the wide therapeutic application, there has been a continuous interest in the development of new ADA inhibitors.

Numerous ADA inhibitors have been reported in the literature. Generally, ADA inhibitors are divided into two classes, namely I) ground-state inhibitors⁸⁷ (**11**, (+)-Erythro-9-(2-hydroxy-3-nonyl)adenine, (+)-EHNA, in **Figure 8**), which have common structure of endogenous adenosine and II) transition state inhibitors⁸⁸ (**12**, 2'-deoxycoformycin, dCF, in **Figure 8**), which resembles the structure of the tetrahedral transition-state intermediate in the deamination process catalyzed by the enzyme. Apart from the natural products, i.e. ADA inhibitors such as (+)-EHNA and deoxycoformycin, several synthetic heterocyclic compounds have been tested for ADA activity. Among them pyrazolo[3,4-*d*]pyrimidine-4-one, imidazo[4,5-*d*]pyridazine-7-one, imidazole-4-amide, 2-hydroxy-3-nonyl-azoles and purine riboside analogues are reported to be potent inhibitors of adenosine deaminase. For more details on ADA inhibition, please refer to **Chapter 10**.

1.4 Overview on different classes of ligands as Adenosine Receptor Antagonists

Over the past two decades, numerous research groups have made intense efforts in exploring suitable ligands for the A₃AR subtype. In particular, an investigation on the selective A₃AR antagonists was carried out enormously because of their potential therapeutic applications, and their preference for pharmacological characterization of receptors. Most of the synthetic A₃AR agonists share a structural similarity with the physiological

agonist adenosine (**1**) and have been developed by various substitutions at the N⁶, C², and 5'-positions.^{89, 90} On the other hand, most of the A₃AR antagonists possess some common structural features. Mostly, they are planar in nature, aromatic, or π -electron-rich heterocycles and it lacks the essential ribose moiety, for agonist activity. In contrast to agonists, AR antagonists are novel in structure as compared to adenosine. The following paragraphs demonstrate the different classes of A₃ antagonists.

1.4.1 Xanthine derivatives as A₃AR antagonists

The xanthines (e.g., caffeine and theophylline) are the classical natural adenosine receptor shows low affinity for the hA₃AR subtypes (in the high μ M range) and they are inactive at the rat AR.¹⁶ As a consequence, structural modification was carried out on the xanthine nucleus by many research groups to improve the affinity at the hA₃AR. Consequently, I-ABOPX (**13**, **Figure 9**, with K_i hA₃AR = 15 nM), with increased affinity for hA₃AR was synthesized by the introduction of 8-phenyl substitution and large 3-substituents on the purine nucleus.⁹¹ Similarly, the cyclization of positions 7 and 8 of the purine nucleus led to the improvement of the affinity (**14**, with K_i hA₃AR = 4.0 nM), while further addition of a 8-methoxy group increased the affinity at hA₃AR and selectivity against other ARs (**15**, with K_i hA₃AR = 2.2 nM).

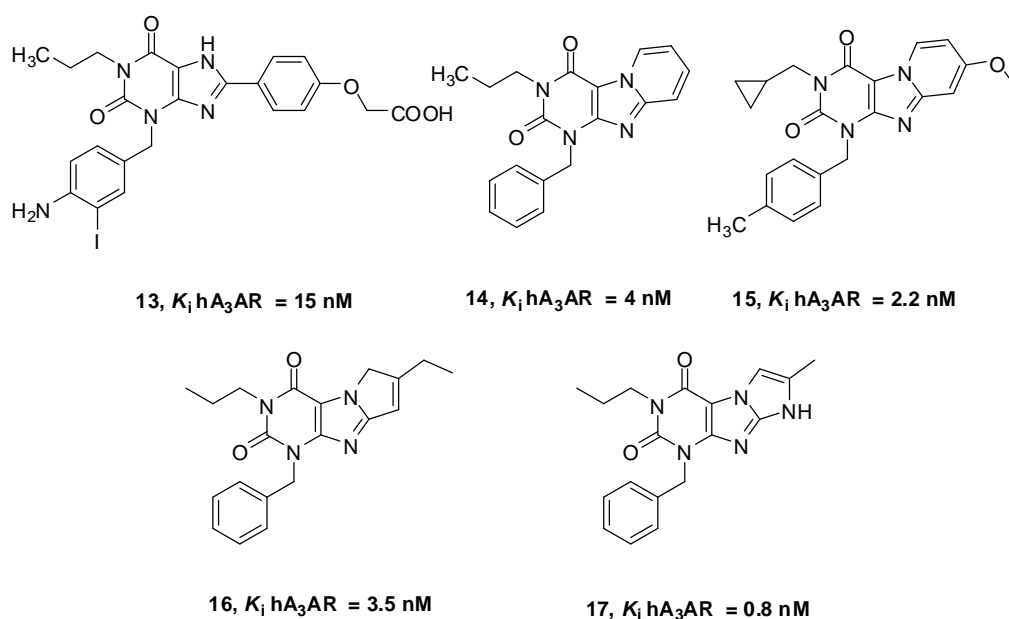


Figure 9. Structures of hA₃AR antagonists: xanthine-based structures.

Similarly, incorporation of an imidazole or pyrrole ring at the 7th and 8th positions gave rise to a new highly potent and selective hA₃AR antagonists (**16**, with K_i hA₃AR = 3.5 nM, and **17**, with K_i hA₃AR = 0.8 nM).⁹²

1.4.2 Nonxanthine derivatives as A₃AR antagonist

Several nonxanthine-based poly heterocyclic derivatives have been described as potential hA₃AR antagonists. These derivatives are generally classified into different subgroups, namely (i) monocyclic scaffolds; (ii) bicyclic scaffolds; and (iii) tricyclic scaffolds.

1.4.2.1 Monocyclic scaffolds

Dihydropyridines and pyridines. The 1,4-dihydropyridine (DHP) derivatives, are also found to possess antagonistic effect to ARs.⁹³ It was noticed that sterically bulky groups at the 4-, 5- and 6-positions are favoured for the hA₃AR affinity. The combination of bulky groups such as phenyl ethynyl at the 4th position, benzylester at the 5th position, and phenyl group at 6th position (**Figure 10**, **MRS1191**, **18**, with K_i hA₃AR = 31.4 nM) displayed the best affinity profile towards hA₃AR. Further incorporation of an electron-withdrawing nitro group at the 4th position of the benzyl ester (**MRS1334**, **19**, with K_i hA₃AR = 2.69 nM, $rA_1AR/hA_3AR=>37174$, $rA_{2A}AR/hA_3AR=>37174$), led to a compound with improved affinity at hA₃AR and selectivity against the other subtypes. Simultaneously, the hA₃AR affinity of the pyridine compounds resulting from the oxidation of 4-dihydropyridines, has also been investigated.

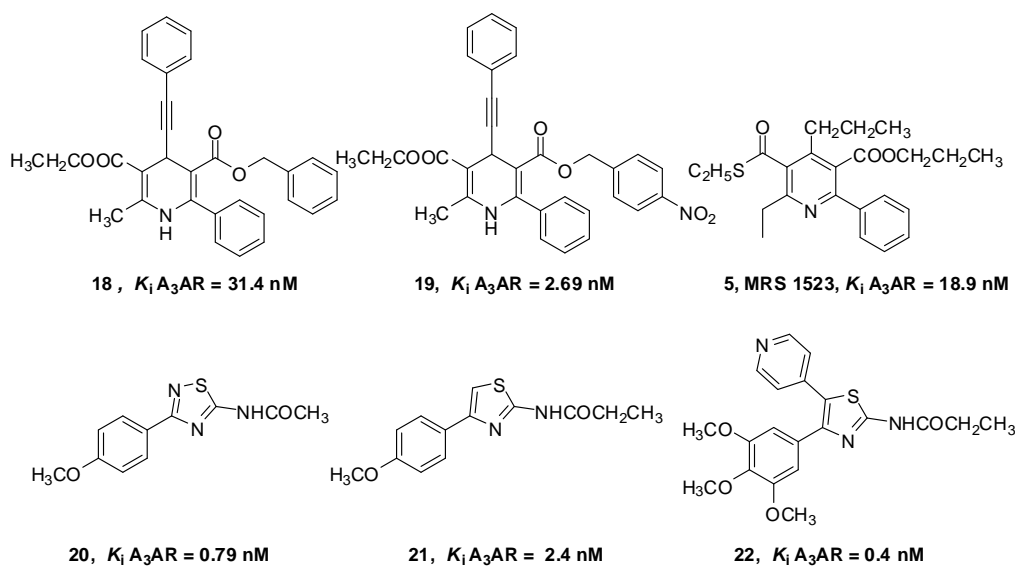


Figure 10. Structures of hA₃AR antagonists: Non xanthine-based monocyclic structures.

Furthermore, a thioester substitution at the 3-position led to a greater affinity at the hA₃AR than oxygen analog (**MRS1523**, **5**, with K_i hA₃AR = 18.9 nM).⁹⁴

Thiadiazoles and thiazoles. Analogues of thiadiazoles (**20**, with K_i hA₃AR = 0.79 nM) and thiazoles (**21**, with K_i hA₃AR = 2.4 nM) derivatives have been reported by some research groups as potent and selective hA₃AR antagonists. From the study, it was observed that further incorporation of a 5-(pyridine-4-yl) moiety in compound **21** enhanced the affinity and selectivity toward hA₃AR (**22**, with K_i hA₃AR = 0.4 nM; hA₁/hA₃ = 425,000; hA_{2A}/hA₃ = 425,000).⁹⁵ On the other hand, this derivative also showed high selectivity at rat A₃AR in animal studies. Such scaffolds could be useful for the development of new potential A₃AR antagonists, considering the relatively shorter synthetic procedures and polar nature as compared with other bicyclic and tricyclic derivatives.

1.4.2.2 Bicyclic scaffolds

Flavonoids. Flavonoids were found to be hA₃AR antagonists in the micromolar concentration from the broad screening of phytochemicals. Further, using SAR and molecular docking studies, a structural optimization was carried out, which gave rise to **MRS1067** (**23** in **Figure 11**, with K_i

hA₃AR, = 561 nM), as the most potent and selective compound of the series for hA₃AR.⁹⁶

Isoquinolines and quinazolines. Ijzerman *et al.* developed the isoquinoline derivatives and the corresponding quinazoline derivatives (with a bio isosteric replacement of a carbon by a nitrogen atom at the 4-position) as novel hA₃AR antagonists.⁹⁷ SAR studies showed that substitution of *meta*- or *para*- pyridyl substituent at the 3-position of the bicyclic nucleus increased the hA₃AR affinity. Moreover, a *para*-methoxyphenyl ring connected to the 1-position via an amide or urea spacer group, was important for high A₃AR affinity and selectivity. The examples of potent and selective A₃AR antagonists among the isoquinoline and quinazoline derivatives are **VUF8504 (24)**, with K_i hA₃AR = 17 nM) and **VUF5574 (25)**, with K_i hA₃AR = 4 nM) respectively.

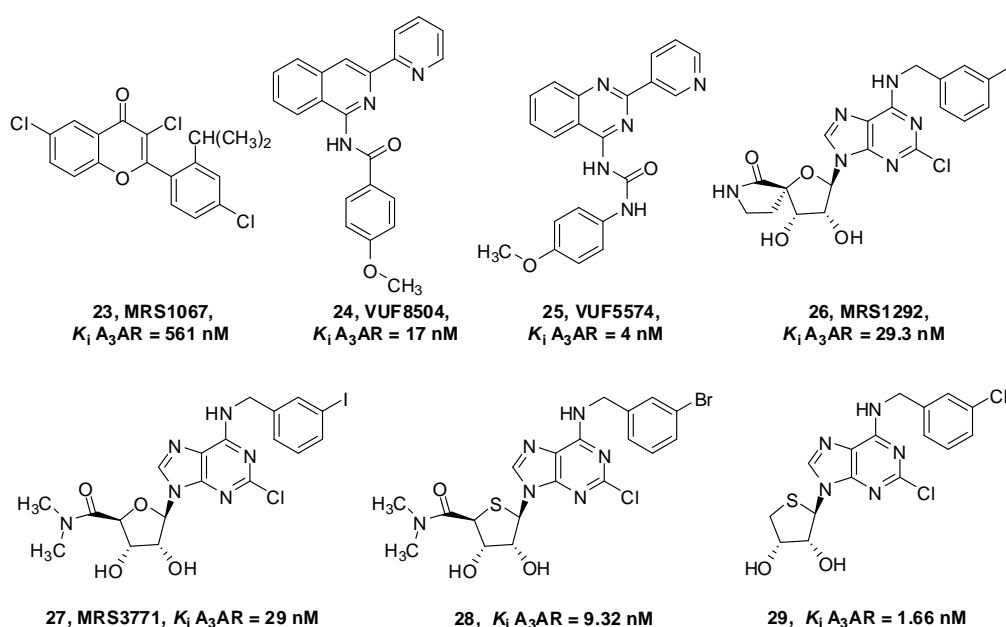


Figure 11. Structures of hA₃AR antagonists: Non xanthine-based bicyclic structures.

Adenosine - and adenine - based derivatives

Some studies have focused on the design of adenosine-based analogues as A₃AR antagonists, since adenosine binds well to the A₃AR across different species. From the molecular modeling studies, it was reported that the flexibility of the 5'-region in the ribose moiety played an essential role in complete activation of hA₃AR. Conversely, the steric bicyclic constraint of

the 5'-region, induced the A₃AR's inhibition, as shown by potent A₃AR antagonist **MRS1292** (**26**, with K_i hA₃AR = 29.3 nM).⁹⁸ Subsequently, it was observed that bisalkyl substitution at 5'-N-uronamide led to the identification of selective antagonists; for example, derivatives were obtained by N-dimethylation (**MRS3771**, **27**, with K_i hA₃AR = 29 nM and **28**, with K_i hA₃AR = 9.32 nM) or a removal of 5'-position substituents (**29**, with K_i hA₃AR = 1.66 nM).⁹⁹

1.4.2.3 Tricyclic scaffolds

Triazolo quinazolines. The first tricyclic heterocycles to be discovered as promising AR antagonists were the triazoloquinazoline derivatives. Among the different compounds synthesized, **CGS15943** (**30**, **Figure 12**, with K_i hA₃AR = 13.8 nM), is reported as a non-selective AR antagonist, and served as a starting template for further development of potent and selective hA₃AR antagonists. Notably, the acylation of N⁵ amino group with aryl or aralkyl moieties has enhanced both the hA₃AR affinity and selectivity (e.g. **MRS1220**, **31**, with K_i hA₃AR = 0.65 nM).¹⁰⁰

Triazolopurines. Triazolopurine derivatives were developed by incorporation of a triazole ring between 1st and 6th position of the purine nucleus, which led to the highly potent and selective hA₃AR antagonists (**32**, K_i hA₃AR = 0.18 nM; **10**, K_i hA₃AR = 0.95 nM).^{79,101} In addition, introduction of a bulky 2-phenyl ring and a butyl chain enhanced hA₃AR affinity and the selectivity. Moreover, very potent and selective derivative **10** (**OT-7999**) showed lowering of IOP in animal models, thus indicating a promising application in the treatment of glaucoma.

Triazoloquinoxalines. The triazolo-[4,3-*a*]quinoxalines (TQX) and triazolo-[1,5-*a*]quinoxalines are examples of class of hA₃AR antagonists, which also share structural similarities with a non-selective AR antagonist **CGS15943** (**30**). In the triazolo[4,3-*a*]quinoxaline series, the acylation of the 4-aminogroup with alkyl or aralkyl substituents with subsequent introduction of the carbonyl group proved to be essential for hA₃AR affinity and selectivity.^{102,103}

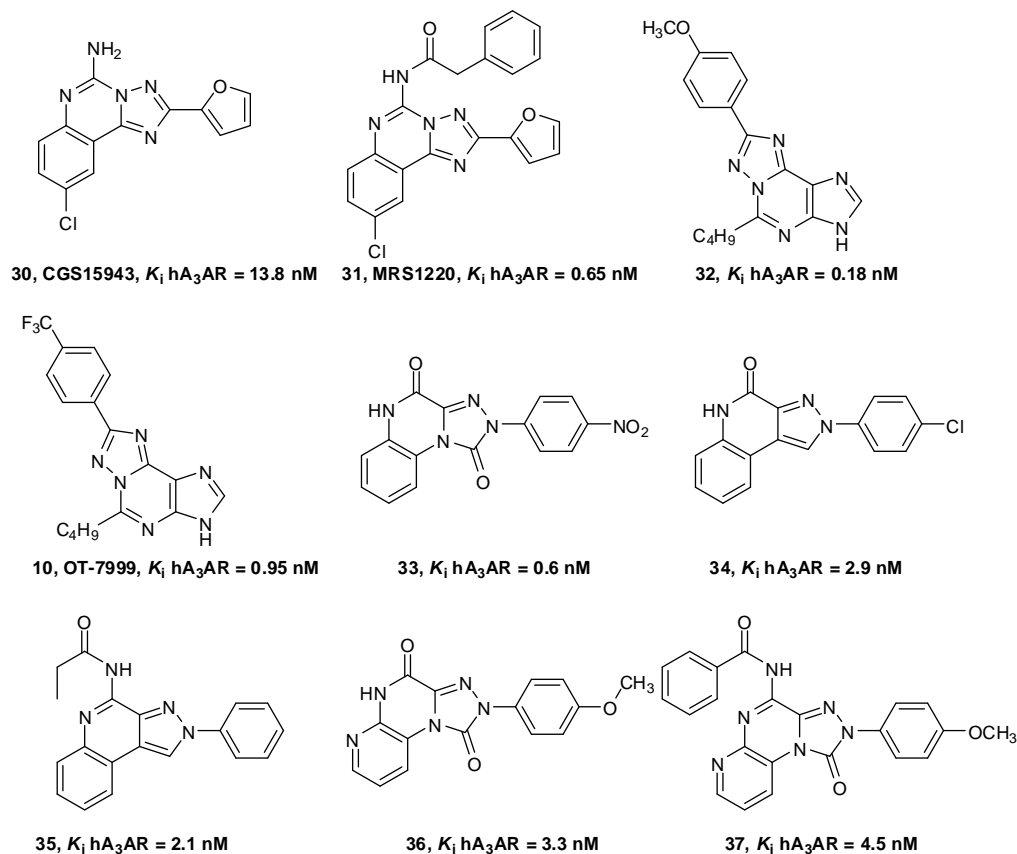


Figure 12. Structures of hA₃AR antagonists: Non xanthine-based tricyclic structures.

Furthermore, the hA₃AR affinity and selectivity was modulated by different substituents on the 2-phenyl ring, especially electron withdrawing and donating substituents such as *para*-methoxy, *para*-methyl, and *para*-chloro. It was observed that the *para*-NO₂ substitution at the 2-phenyl chain was essential for the A₃AR affinity and selectivity in the 1,4-diones series (**33**, with K_i hA₃AR = 0.6 nM).

Pyrazoloquinolines. The series of pyrazoloquinolin-4-ones and pyrazoloquinolines were identified as potent and selective hA₃AR antagonists^{104,105} sharing a common central nucleus with the TQX series. Similar to the TQX, the substituent on the 2-phenyl ring play a crucial role in modulating A₃AR affinity, while a nuclear (e.g. oxogroup) or extranuclear (e.g. amide group) C=O proton acceptor substitution at the 4-position led to potent and selective A₃AR antagonists. At the 2-position, the presence of 4-chloro,4-methoxy, 4-methyl and 3-methyl on the phenyl ring resulted in enhancements of the

hA₃AR affinity in the 4-one (**34**, K_i hA₃AR, 2.9 nM). The introduction of an acyl group and carbamoyl residue (**35**, with K_i hA₃AR, = 2.1 nM) at the 4-position, resulted in retention of the hA₃AR affinity and selectivity, confirming the significance of the C=O group with the receptor site interactions.

Pyrido-triazolo-pyrazinones. Pyrido-triazolo-pyrazinone is a novel scaffold that exhibits SAR similar to TQXs at the hA₃AR receptor.¹⁰⁶ Also in this series, *para*-methoxy group at the 2-phenyl ring displayed high binding affinity in the 4-oxo series (**36**, with K_i hA₃AR = 3.3 nM). Similarly the same substitution in the 4-amido series (compound **37**, with K_i hA₃AR = 4.5 nM) showed high affinity, as compared to the unsubstituted 2-phenyl derivatives. When the 4 amino group was substituted, particularly by acyl groups, the hA₃AR affinities and selectivities were significantly increased (**37**).¹⁰⁶

1.5 Overview of structure-activity relationships profile of pyrazolopyrimidines as A₃AR Antagonists

Pyrazolopyrimidines represent a novel, recently reported series of bicyclic scaffold-derived hA₃AR antagonists that display improved hA₃AR affinity and selectivity profiles compared with their isosterically related derivatives, the imidazole [1,2-*a*][1,3,5] triazines. Lenzi *et.al* synthesised a series of 2-phenyl pyrazolo[4,3-*d*]pyrimidine-7-one derivatives as a result of molecular simplification from the tricyclic scaffold of pyrazolo[3,4-*c*]quinolin-4-one (**38**, **Figure 13**) modified at C⁵ position by different alkyl (H, Me, Et) and aryl (Ph, CH₂Ph) groups in order to investigate the lipophilicity and steric tolerance at this position. From the SAR analysis it was noticed that both the C⁵- and N² substituents of the bicyclic nucleus were essential for hA₃AR affinity and selectivity. Small methyl group substitution at the C⁵-position along with *para* methoxy-substituted phenyl group at the N²-position (**39**, with K_i hA₃AR = 1.2 nM), afforded the most potent and selective hA₃AR antagonist in this series of derivatives. However, A₃AR binding affinity was unfavourable when the C⁵-position was substituted by aryl/aralkyl groups.¹⁰⁷

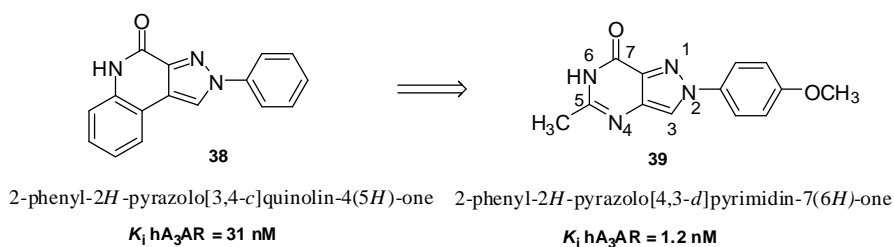


Figure 13. Molecular simplification of tricyclic pyrazolo[3,4-*c*]quinolin-4-one to pyrazolo[4,3-*d*]pyrimidinone

Moreover, in another study, the SAR profile of an isomer of this series indicated that amido (**40**, **Figure 14**) or ureido moieties (**41**) at the C⁴-position, along with a phenyl ring at the C⁶-position at the bicyclic scaffold, were key pharmacophoric elements for the recognition at the ARs and essential for promoting A₃AR affinity and selectivity. As small methyl group (**40**) and bulkier benzyl moiety (**41**) were well tolerated, it is speculated that the N²-position is associated with a good degree of steric tolerance. Compound **40**, with low nanomolar affinity at the A₃AR and the high selectivity against other AR subtypes (**40**, K_i hA₃AR = 0.18 nM; hA₁/hA₃ = 5,761 nM; hA_{2A}/hA₃ = 17,661 nM and **41**, K_i hA₃AR = 2.9 nM; hA₁/hA₃ = 3448; hA_{2A}/hA₃ = 3448), has been suggested as a potential lead compound for the development of other potent analogues. Subsequent test of compound **40** on human glioma U87MG cells counteracted the A₃AR agonist-mediated proliferation of the glioma cells via the inhibition of ERK 1/2 activation. Therefore, this compound might also represent a potential starting template for the development of adjuvant agents in the glioma chemotherapy.^{77,108}

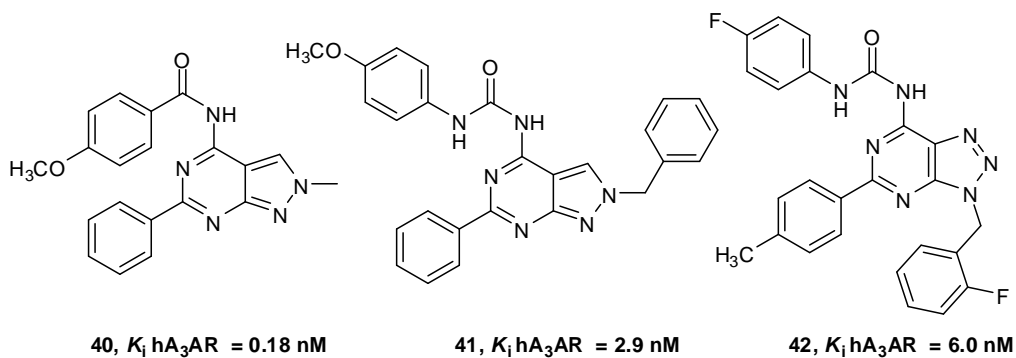


Figure 14. Structures of pyrazolopyrimidine and related ligand as as hA₃AR antagonists.

A series of [1,2,3]triazolo[4,5-*d*]pyrimidines, which could be considered bioisosteres of pyrazolo[3,4-*d*]pyrimidines, was synthesized by Biagi *et al.*¹⁰⁹ From the SAR study, it was noticed that an aryl carbamoyl chain at the N⁶-position and a (substituted)phenyl at the C²-position (corresponding to N⁴- and C⁶- positions in pyrazolo[3,4-*d*]pyrimidines, respectively) led to compound **42** (K_i hA₃AR = 6.0 nM; hA₁/hA₃ =72; hA_{2A}/hA₃ =1,341)¹⁰⁹ that was less potent and less selective towards hA₃AR when compared with pyrazolo[3,4-*d*]pyrimidine derivatives.

1.6 Overview of structure - activity relationships profile of pyrazolo-triazolo-pyrimidine as hA₃AR Antagonist

The pyrazolo-triazolo-pyrimidines (PTPs) are hybrid molecules derived from a hA_{2A}AR antagonist and an A₃AR agonist which resembles the triazoloquinazoline nucleus of the nonselective antagonist **CGS15943 (30)**,^{110,111,112} When the N⁵-position of PTP scaffold of a known hA_{2A} antagonist was substituted with a *para*-methoxy phenyl carbamoyl moiety, an optimal A₃AR affinity was observed. Moreover, such rational design resulted in compound **43 (Figure 15)**, with K_i hA₃AR = 0.6 nM), with very high hA₃AR affinity and selectivity.¹¹³ Subsequently, from different studies, methyl group at the N⁸-position and unsubstituted phenyl group at the N⁵-position were identified as crucial features for hA₃AR affinity which was confirmed by compound **44** (K_i hA₃AR = 0.16 nM).^{114,115,116} Compound **45**, with water solubility of 11mg/ml attained by N⁵ pyridinium salt substitution, which also significantly improved hA₃AR affinity (K_i hA₃AR = 0.01 nM).¹¹⁷

On the contrary, replacement of the N⁵-phenyl moiety with different N⁵-heteroaryl rings resulted in a general loss of hA₃AR affinity and selectivity. Recently, our group¹¹⁸ has synthesized a series of pyrazolo-triazolo-pyrimidines (PTP) derivatives as potent and highly selective hA₃ adenosine receptors antagonists. From the binding assay it was confirmed that the presence of a free amino group at C⁵ position of PTP analogue lowered hA₃AR (**50**, K_i hA₃AR = 75 nM) but it also showed good interaction at both hA₁ and hA_{2A}AR. Moreover, subsequent substituents incorporation at the C⁵ position, significantly decreased the affinity at hA₁ and hA_{2A} AR, thus

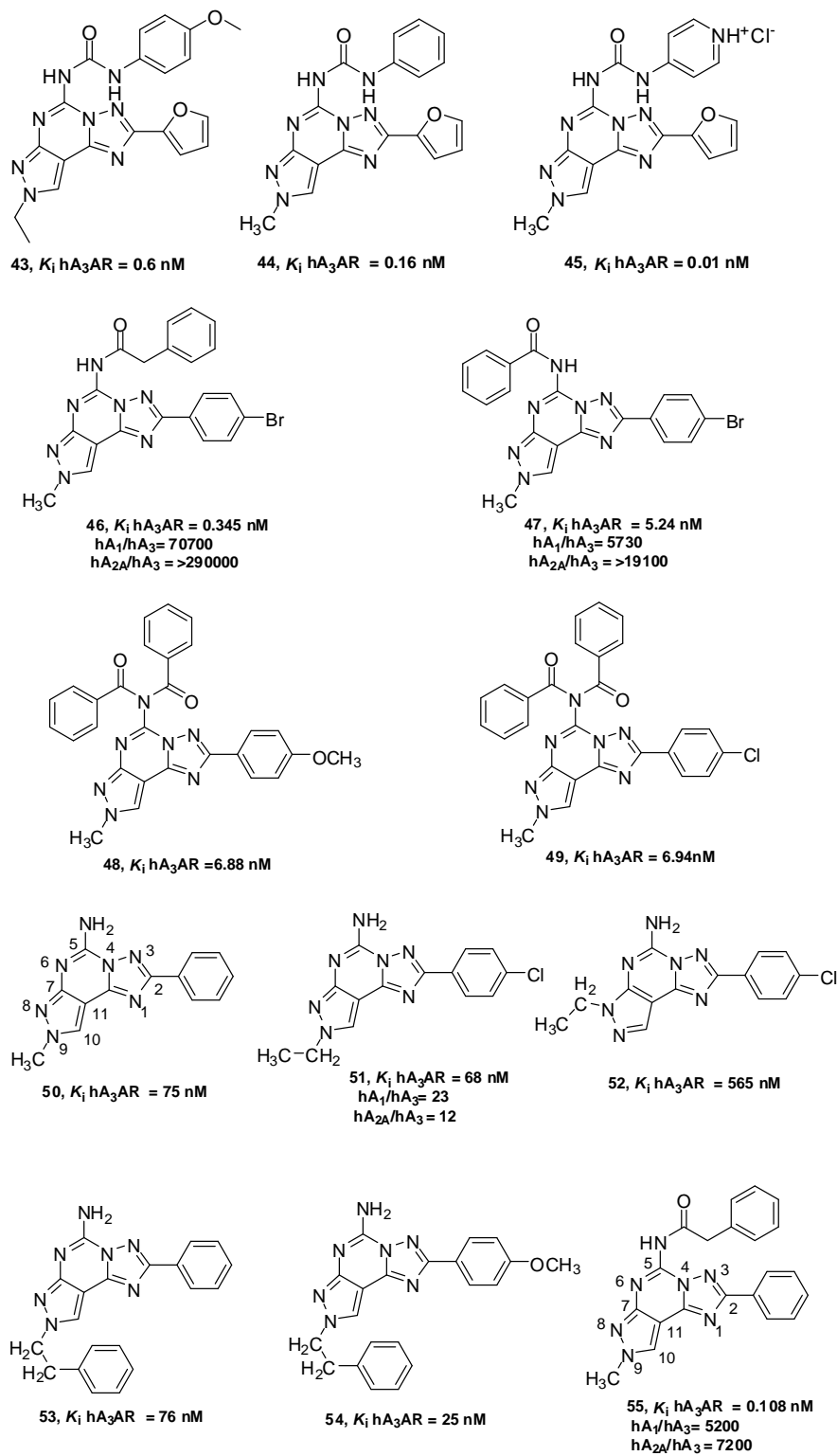


Figure 15. Structures of Pyrazolo-triazolo-pyrimidines as hA₃AR antagonists

improving the hA₃ subtype selectivity. This finding seems to imply that the hA₃ binding cavity around the C⁵ position is rather spacious accommodating extended chains such as benzoyl and phenylacetyl groups. Between these two substituents, the longer phenylacetyl group (e.g. **46**, **Table 1** and **Figure 15**, with K_i hA₃= 0.345 nM, hA₁/hA₃= 70700; hA_{2A}/hA₃>290000) showed relatively better binding profile than the shorter benzoyl chain (**47**, K_i hA₃= 5.24nM, hA₁/hA₃>5730; hA_{2A}/hA₃>19100). Moreover, the vacant NH at C⁵ was not crucial because substitution with an additional benzoyl chain (as in compound **48**, with K_i hA₃= 6.88 nM and **49**, with K_i hA₃= 6.94 nM), although less favorable than a single chain, still retained affinity at hA₃ receptor and good selectivity (>1400) against other receptor subtypes.

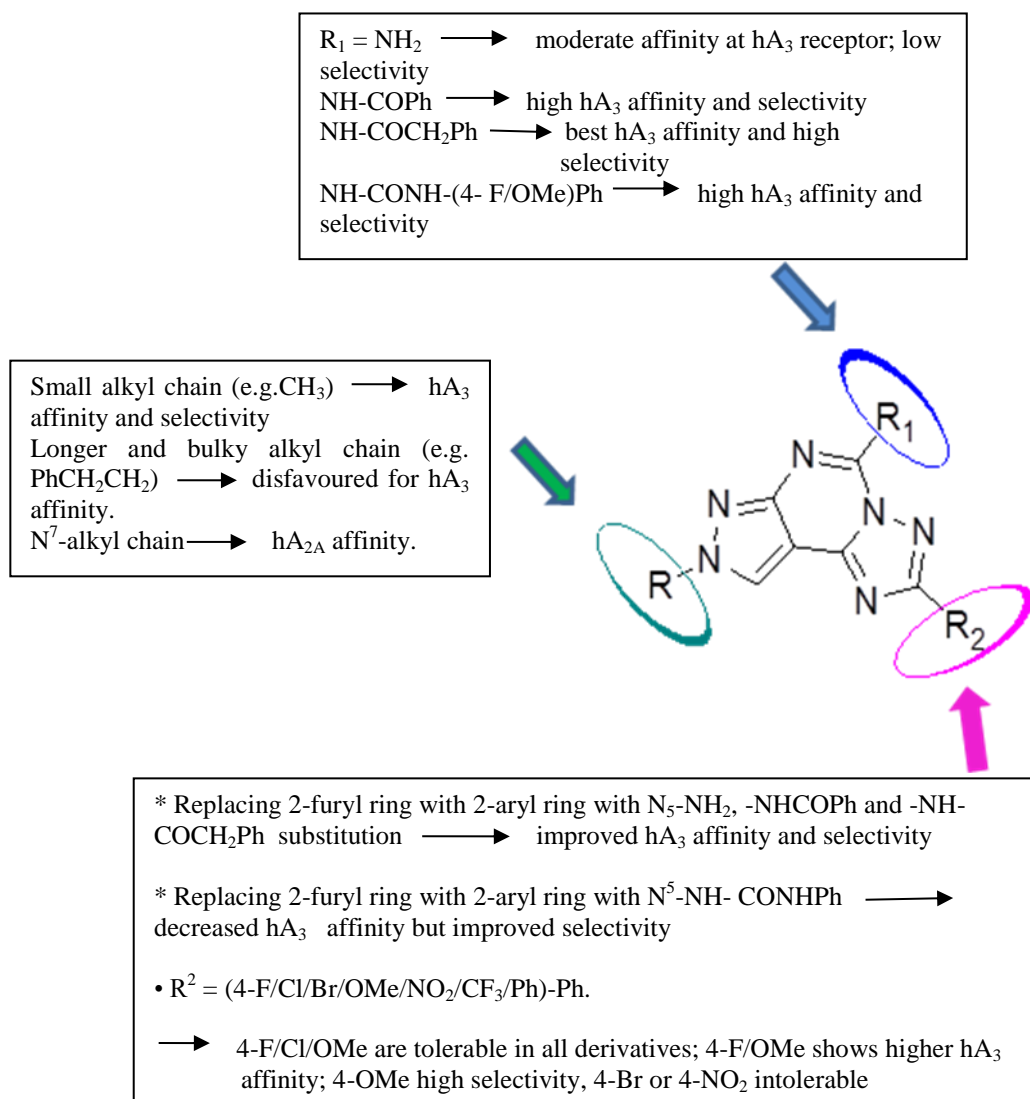


Figure 16. Overview of structure-affinity relationship for the novel series of 2-aryl-PTP derivatives

This finding again supported the predication that the binding pocket of hA₃ receptor around this C⁵ position was roomy enough to accommodate the bulky and branched imide substituent, while there was limited space available for such bulky groups at A₁ and A_{2A} subtypes and resulted in decrease of affinity.

Further in the study, it was found that C⁵ amino compound **50**, with a small alkyl group at N⁸, showed a preference for hA₃ receptors, regardless of substitution at C⁵ and C² positions. This was further confirmed by the introduction of a slightly longer alkyl chain (e.g., an ethyl group in compound **51**, with K_i hA₃= 68.7 nM; hA₁/hA₃= 22.9; hA_{2A}/hA₃= 12.3), which still showed hA₃ antagonism and moderate selectivity. Notably, when the same substituent was shifted from position N⁸ to N⁷ (as in compound **52**, with K_i hA₃= 565 nM) the affinity at hA₃ receptors dropped by at least 8 fold, with the resulting binding affinity profile inclined toward hA_{2A} receptors (K_i hA_{2A}= 83.8 nM). Conversely, when a group bigger than ethyl was introduced at N⁸ (e.g. phenylethyl group in compound **53**, with K_i hA₃= 76.7 nM), a decrease of affinity at hA₃ receptor was observed as similar to compound **50**. In derivatives with free amino group at C⁵ position, the introduction of a methoxy group in *para* position of the phenyl in C² position (**54**, with K_i hA₃=25.0 nM) improved the hA₃ affinity.

Interestingly, when a substitution was introduced at the C⁵ position and a small alkyl group was kept in N⁸ position, affinity increased remarkably towards the hA₃AR. In fact compound **55**, with a phenyl at C², a methyl group at N⁸ and a phenyl acetamide at C⁵, showed the best hA₃ affinity profile of this class of compounds (K_i hA₃=0.108nM) and good selectivity against the other AR receptor (hA₁/hA₃ =5200; hA_{2A}/hA₃ =7200). **Figure 16** displays the overview of structure-affinity relationship for the novel series of 2-aryl-PTP derivatives. On the whole, these results supported the importance of the introduction, in the PTP system, of (a) small substituents (e.g. CH₃) at the N⁸ position to maintain affinity and selectivity at hA₃AR and (b) a lengthy chain such as a phenyl acetyl group at the C⁵ position to obtain a higher affinity and a improved selectivity towards hA₁ and hA_{2A} receptors.

1.7 Other therapeutic applications of pyrazolo[3,4-*d*]pyrimidines

Pyrazolopyrimidines are popular synthetic pharmacophores with numerous reported biological activities partially because of their structural similarity to purines. Purine-containing small molecules (such as ATP and GTP) are widely distributed in nature, and can be recognized by various proteins such as kinases and GTPases. Consequently, pyrazolopyrimidines have been exploited as adenosine deaminase inhibitors¹¹⁹, ATP competitive inhibitors of kinases (mTOR, EGFR and CDK2)¹²⁰⁻¹²² and inhibitors of DNA polymerase.¹²³

1.7.1 Pyrazolo[3,4-*d*]pyrimidines as adenosine deaminase (ADA) inhibitors

The synthesis of a number of 1- and 2-alkyl derivatives of the 4-amino pyrazolo[3,4-*d*]pyrimidine (APP) nucleus and their evaluation as inhibitors of ADA from bovine spleen was reported by Da Settimo *et al.*¹¹⁹ From the pharmacological assay, the 2-substituted amino pyrazolopyrimidines proved to be potent ADA inhibitors and most of them exhibited K_i values in the nanomolar range. The inhibitory activity of this series was enhanced with the increase in alkyl chain length, attaining a maximum with the n-decyl substituent at the N¹ position. Insertion of a 2'-hydroxy group in the n-decyl chain led to compound **56** (Figure 17), which displayed the highest inhibitory potency of the series (**56**, $K_i = 0.053$ nM).

1.7.2 Pyrazolo[3,4-*d*]pyrimidines as ATP-Competitive inhibitors of kinases

1.7.2.1 The mammalian target of rapamycin (mTOR)

Recently, Verheijen *et al.*¹²⁰ reported a series of 4-morpholino-6-aryl-1*H*-pyrazolo[3,4-*d*]pyrimidines as potent and selective mTOR inhibitors. In this study, the 6-aryl substituent of the scaffold was extensively modified to obtain inhibitors of mTOR with subnanomolar inhibitory concentrations. Subsequent, 6-aryllureidophenyl substituents resulted in potent mixed inhibitors of mTOR and phosphatidylinositol 3-kinase R (PI3K-R). However, 6-alkylureidophenyl moiety produced a highly selective mTOR inhibitors.

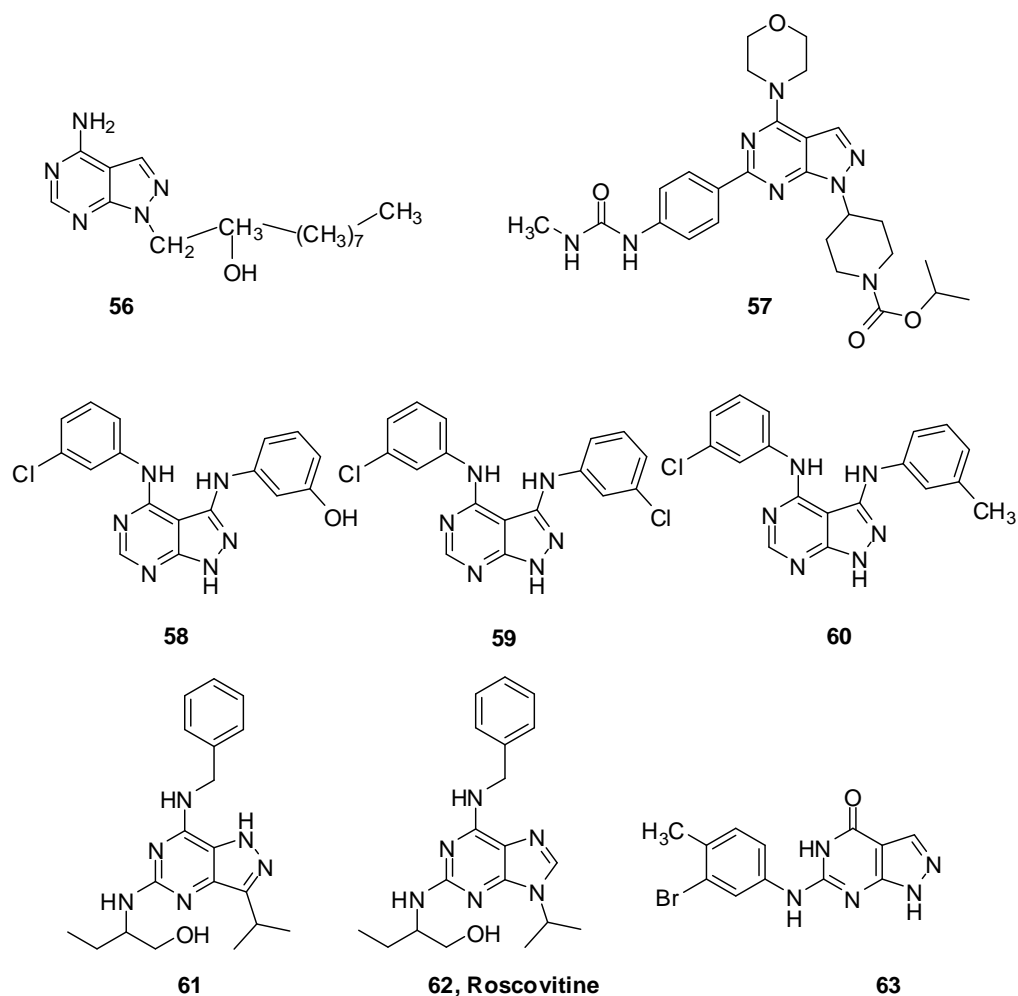


Figure 17. Structures of pyrazolo[3,4-*d*]pyrimidines as various enzyme inhibitors

Similarly, 6-alkylureidophenyl groups were combined with 1-carbamoyl piperidine substitution (e.g. **57**, $IC_{50} = 0.2$ nM) resulted in potent mTOR inhibitor with IC_{50} in subnanomolar range and selectivity of 1000-fold over PI3K-R. In addition, several 6-arylureidophenyl-1*H*-pyrazolo[3,4-*d*]pyrimidines were substituted at the 4-position of the arylureido moiety with water solubilizing groups as a result of structure based drug design approach. Subsequently, these compounds displayed potent mTOR inhibition ($IC_{50} < 1$ nM) with novel cellular proliferation activity in assays ($IC_{50} < 1$ nM).

1.7.2.2 EGF-R PTK Inhibitors

Pyrazolo[3,4-*d*]pyrimidines class was designed based on a pharmacophore model for ATP-competitive inhibitors which interact with epidermal growth factor receptor (EGF-R) protein tyrosine kinase (PTK) active site, this led to the development series of 4-(phenylamino)- substituted

pyrazolo[3,4-*d*]-pyrimidines as potent EGF-R tyrosine kinase inhibitors. Moreover, the derivatives of 4-(phenylamino)-pyrazolopyrimidines were shown to be selective tyrosine kinase inhibitors with potent *in vitro* and cellular activity and combined *in vivo* efficacy.¹²¹ Mostly, compounds of this series showed inhibition with IC₅₀ values of below 10 nM. Among them, compound **58** showed highest activity of 1nM against EGF-R PTK. In addition, compounds **59** and **60** showed satisfactory oral bioavailability in mice and presented improved *in vivo* efficacy at doses of 12.5 and 50 mg/kg using EGF-R overexpressed A431 cell line in a nude mouse tumor model.

1.7.2.3 CDK inhibitors with antiproliferative activity

A new series of pyrazolo[4,3-*d*]pyrimidine scaffold as potent CDK2 inhibitor was reported by Jorda *et al.*¹²² Compound **61** was prepared using a known CDK inhibitor roscovitine (**62**) as bioisotere. In several biochemical and biological assays, the effects of compound **61** were compared with those of its bioisoster, roscovitine. These analyses showed similar kinase selectivity profiles of roscovitine (**62**) and compound **61**, yet apparently higher efficiency of the latter compound. The overall molecular and cellular effects of compound **61** were consistent with its ability to inhibit CDKs and furthermore, exhibited evidence for a role of CDKs in maintenance of DNA repair by homologous recombination (HR); The data suggest that blocking HR-mediated repair by compound **61** and perhaps also by other CDK inhibitors could potentially be exploited in cancer. Importantly, enhanced anticancer activities were observed for pyrazolo[4,3-*d*]pyrimidine **61** compared to its bioisostere roscovitine (**62**). Hence, the reported compound **61** could be preferred for cancer treatment.

1.7.3 Pyrazolo[3,4-*d*]pyrimidines as DNA polymerase inhibitors

Ali *et al* reported a series of 6-anilino substituted pyrazolo[3,4-*d*]pyrimidin-4-ones as inhibitor of enzyme DNA polymerase III replication in *staphylococcus aureus*. The scaffold was considered as a novel dGTP analogues that inhibited other Grampositive (Gr+) bacteria as well.¹²³ To

enhance the potential of these inhibitors as antimicrobials, further structure-activity relationship studies was performed on this scaffold involving substitutions at the 2, 4, and pyrazolo NH positions. All the new inhibitors were investigated for their ability to inhibit *S.aureus*-DNA pol III and Gr⁺ bacteria in culture. Consequently, substitution of 2-anilino groups along with *meta* or *para* position substitution of small hydrophobic groups (**63**, MIC= 8 µg/ml) enhanced both antipolymerase and antimicrobial activity. These pyrazolo[3,4-*d*]pyrimidine derivatives resulted in development of a new class of antimicrobials with promising Gr⁺ bacteria antagonistic activities.

1.8 Molecular Modeling on hA₃AR and its ligands

Presently, most of the drug discovery process involves the combination of computational strategies with conventional synthetic procedures. Generally, computational strategies identifies the structural features of ligands attributing to biological activity, and guiding to the optimization of lead compounds. Moreover, these theoretical methodologies unveil the important atomic level ligand-receptor interactions. Several molecular modeling studies such as quantitative structure–activity relationship (QSAR), homology modeling and molecular docking have been performed on the hA₃AR and its ligands. Among these modeling studies, the molecular docking simulations and QSAR studies performed on the pyrazolo pyrimidine (PP) and pyrazolo-triazolo-pyrimidine (PTP) derivatives as hA₃AR antagonists are discussed in the following sections.

1.8.1 Quantitative structure-activity relationship (QSAR) studies

QSAR has been a useful technique for improving drug discovery of hA₃AR ligands. In such a computational approach, molecular descriptors (different structural features) are chosen to build a theoretical model. The molecular recognition of hA₃AR is depend on the descriptors. Topological and electrostatic potential descriptors are examples of such molecular descriptors which comprise of related information particular to an individual compound.¹²⁴ Moreover, such a constructed model could also assist in the structure optimization of the lead compounds and in the discovery of new potent adenosine ligands.^{125,126} The following sections illustrate some

examples of QSAR studies performed on pyrazolo-triazolo-pyrimidine derivatives as potent hA₃AR antagonists.

Pyrazolo-triazolo-pyrimidines. Moro *et al* recently proposed a receptor-based and ligand-based drug design approach to define a pharmacophore for PTP derivatives .¹¹⁵ In this study, QSAR was performed using docking-based structure super imposition for the PTPs through Comparative Molecular Field Analysis (CoMFA). CoMFA model produced good correlation coefficients (non-crossvalidation r^2) and predictive ability (q^2 and r^2_{pred}). Similarly, the steric and electrostatic contour plots seemed to be consistent with the ligands hypothetical binding interactions of molecular docking simulations. CoMFA suggested that, sterically bulky substituents are favoured for affinity as a green polyhedron (favours bulky groups) was observed around N⁵-aryl carbamoyl moiety. Similarly, a N⁵-phenyl ring was surrounded by blue polyhedron (favours electron positive groups). Both of these contours surrounding the N⁵-substituents were complementary to the surrounding nonpolar residues such as Ile98, Ile186, and Leu244. Moreover, N⁸-substituents and the N⁵-carbamoyl moiety were surrounded by red polyhedra which in turn reflected by surrounding polar residues Ser175, His95, Ser247, and His272 in the docking study.

On the other hand, Tafi *et al.*¹²⁷ defined the pharmacophore map using ligand-based structural alignment to obtain the hA₃ antagonists via the catalyst program. The docking simulation for the PTP derivatives was later performed based on the best catalyst-driven pharmacophoric frame work. The model suggested that hydrophobic groups at the N⁵-, N⁸- and C²- positions, an aromatic appendage at the tricyclic core and a H-bond acceptor at the amidic group were vital for the hA₃ receptor antagonism.

Similarly, Cheong *et al*¹²⁸ elucidated a pharmacophore model for the novel series of 2-aryl-PTP derivatives. A ligand-based pharmacophore was obtained for a new series of 2-unsubstituted and 2-(*para*-substituted)phenyl-pyrazolo-triazolo-pyrimidines as potent antagonists of hA₃AR. CoMFA studies deeply examined the structural features at the N⁵-, N⁸- and C²-positions of the tricyclic nucleus, with more emphasis given to the unprecedentedly explored C²-position. According to the CoMFA model, blue contour was observed in close proximity to the C² position phenyl ring in the

tricyclic nucleus. It was deduced that the delocalization of electrons towards the pseudo aromatic tricyclic core has exerted its effect on the phenyl ring, thus rendering the surrounding region to be more electron deficient. Similarly, the green contour was seen around the phenyl ring at both the N⁵-positions of the tricyclic nuclei, indicating that bulky groups were tolerable around this region.

Consistently, a red contour was seen at the *para*-position of such N⁵-phenyl ring in the PTP derivatives (**Figure 18-B**). This observation was further substantiated by the good hA₃ affinity profile of compounds ranging from 0.2 to 0.4 nM, which bear electro negative groups at the *para*-position. Similarly, the presence of *p*-F or *p*-OMe on the phenyl ring of N⁵-arylcarbamoyl chain in the newly synthesized 2-aryl-PTPs was found favourable for the hA₃ affinity as well. A small patch of yellow contour was found between the *meta* and *para*-positions of the phenyl ring in PTP derivatives bearing the aryl carbamoyl chain, suggesting that only substituents of certain size were acceptable at these two positions. Likewise, a red contour was also seen around the CONH- group at N⁵ position of the scaffold, indicating that the presence of an electro negative group (e.g. carbonyl group) was favoured for hA₃ affinity. Interestingly, electron-withdrawing effect of

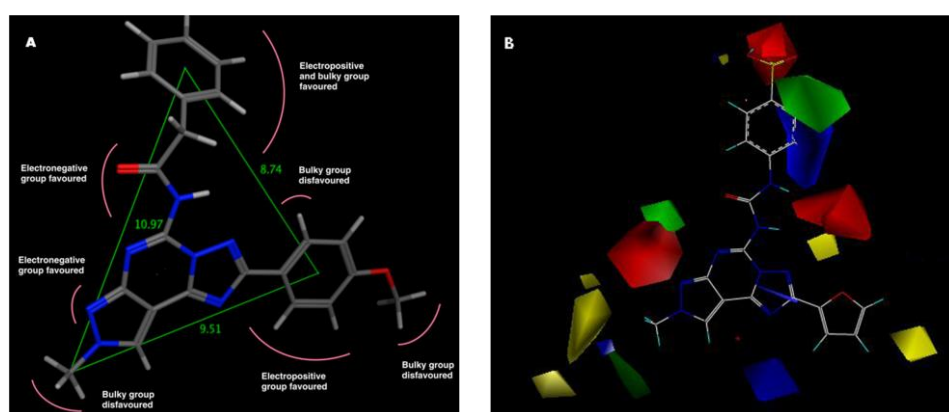


Figure 18. A. Distribution of steric and electrostatic effects in the 2-aryl-pyrazolo-triazolopyrimidine derivative. The distances (Å) among the three pharmacophoric points constituted by the N⁵-phenyl ring, N⁸-methyl and C²-aryl ring are indicated. B. Combined steric and electrostatic contour plots observed for PTP analogue (adopted from Cheong *et al.*).¹²⁸

para-substituents at phenyl ring and delocalization of electrons in the nearby carbamoyl and amidic group made the phenyl ring electron-deficient as that of C²-phenyl ring.

Moreover, a green contour observed around the substituent at N⁸-position of PTPs (**Figure 18-B**) implied that incorporation of the less bulky methyl group was more favourable at the N⁸-position as compared to the bulky alkyl chains such as phenyl ethyl group to provide good affinity at hA₃ receptors. Obviously, an inverse relationship was observed between the binding affinity and the molecular volume (MV) of the substituent at position N⁸. In addition, N⁷ of the pyrazole ring in PTPs was surrounded by a red contour. On the other hand, N⁸-position of PTPs was covered by a small blue contour. The electrostatic effect at this position seemed negligible; whereas the steric effect at this position was assumed to determine an essential role towards the hA₃ affinity.

Overall, the CoMFA-based model confirmed that steric effect was prominent at the N⁵, N⁸-positions and at the *para*-position of 2-phenyl ring (**Figure 18-A**). In addition bulky groups were unfavorable at both the N⁸-position and *para*-position of 2-phenyl ring, while the N⁵-position of the tricyclic nucleus favours the bulky groups. For the electrostatic effect, *para*-position of amidic group at N⁵ favours the electro negative groups, whereas C²- and N⁵-positions favour the electropositive group. Overall, the steric effect was found to be relatively more predominant than electronic effect for antagonists interaction to the hA₃ receptor.¹²⁹

Although CoMFA methodology has been widely used in the research field, yet CoMFA possesses some weaknesses. The most challenging is its input requirement that each ligand structure can be represented as a 3D model, by selecting an absolute orientation of a single conformational alignment. Sometimes, the alignment can yield excellent models with superior predictive ability.¹³⁰ However, only one method exists for validating the alignment procedure, which is the maximization of various q² (cross-validated r²) statistics.¹³¹ This averages the internal predictive accuracy for every structure-activity observation. Similarly, the other major difficulty of the CoMFA method is in its results application. These two CoMFA difficulties is

addressed by “Topomer CoMFA” a completely objective and universal methodology for generating an alignment for structural fragments, both a conformation and its orientation in a cartesian space. By definition, structural fragments contain a common feature. Topomer CoMFA is a 3D-QSAR tool which automatically generates a model for predicting the biological activity or properties of compounds.^{132,133} Basically, structural fragments possess common features such as “open valence” or “attachment bond”. The topomer methodology overlaps this common feature to offer an absolute orientation for any fragment. A single fragment conformation is then generated from a standardized 3D model by rule based adjustments to acyclic single bond torsions and chiralities. Topomer CoMFA has been applied to the four different cases, where structure/activity observations are converted into sets of mutually comparable fragments. These are

[i] A purely congeneric series, for example, a combinatorial library sharing a common nucleus. Differing portions of the structures contribute to the differences in activity. Consequently, the variables responsible for the differences in potency, can be removed from the common core, to become the set(s) of topomerically modeled fragments.

[ii] A roughly homologous series, with each individual structure consisting of more than one large group connected by one or more acyclic bonds, but within one of those large groups identical throughout the series.

[iii] A roughly homologous series containing only one large group, which is similar though not identical across the series.

[iv] Series having negligible homology. In the absence of recognizable commonalities, it may be helpful to identify subseries, each having both a structural commonality.

1.8.2 Homology modeling of hA₃ receptor

Characterization of the GPCRs are usually hampered by the technical difficulties in X-ray crystallography and NMR experiments. Due to that reason 3D structure of the hA₃AR has not been elucidated yet. Nevertheless, construction of hA₃ receptors have been performed using a computational approach. This hA₃ receptor model, through molecular docking analysis aid in

the potential binding pocket predictions and also plays an essential role in the structure-based drug design.

1.8.2.1 Progress of hA₃AR homology modeling

Moro *et al.*¹³⁴ constructed the human A₃ adenosine receptor models utilizing low resolution electron density maps (EDM) of rhodopsin, via the “cross-docking” methodology. The high resolution crystal structure of bovine rhodopsin (PDB Code: 1F88) at 2.8 Å was discovered in the year 2000. Since then, the homology model of hA₃AR are constructed using such a template.¹⁰⁶ Although the transmembrane systems are similar as that of adenosine receptors, very limited sequence identity was observed for the bovine rhodopsin with A₃ receptors (less than 20% sequence ID).¹³⁵ Recently, the crystallographic structure of human beta2 (β₂)-adrenergic GPCR (PDB Code: 2RH1)¹³⁶ and human A_{2A} receptor (PDB Codes: 3EML)¹¹³ at 2.4 Å and 2.6 Å has been resolved respectively. Subsequently, hA₃ receptor homology models are constructed using these alternative templates.⁷⁷ Interestingly, due to relatively high percentage of about 43% of sequence identity, the hA_{2A} receptor is considered as an desirable template for hA₃ receptor homology modeling,¹³⁷

Evers *et al.* introduced ligand assisted homology modeling as an alternative to conventional homology modeling, where the binding site is incorporated with ligand molecules to model a GPCRs by homology.¹³⁸ In this approach, accurate geometries of the protein binding sites are obtained by keeping the ligand molecules bound to the models as restraints. Recently, Moro and his co-workers applied a similar strategy, namely ligand-based homology modeling (LBHM), on the hA₃AR.¹³⁹ In this study multi-conformational space of the antagonists were explored along with ligand binding inducing possible receptor reorganization. Validation of this method was carried out by analysis of more than 200 known hA₃AR antagonists in the corresponding putative ligand binding site. Through this multi-conformational states approach, a consensus binding motif among all known antagonists has been found, and a novel ‘Y-shaped’ 3D-pharmacophore has been deduced by obtaining a consensus binding motif based on this multi-conformational states approach. Applying such receptor-

based pharmacophore, the potential hit could be screened from the available compound database.

1.8.2.2 hA₃AR models

In general, the TM regions of GPCRs comprise of the same overall topology and the most conserved residues in each helix guide the sequence alignment. Nonetheless, the loops constitute the most variable regions. Particularly, the extracellular loop 2 (ECL2) is of particular interest in homology modeling of adenosine receptors. The highly conserved disulfide bond formed between the cysteine 166 (ECL2) and cysteine 83 (TM3) plays an important role in ligand recognition. The formation of disulfide bond is considered critical for determining the conformation of the ligands binding pocket. To-date, a number of A₃AR models have been built based on the bovine rhodopsin template (**Figure 19 (A)**) which describe the hypothetical binding modes and binding interactions with known A₃AR ligands of different scaffold.¹³⁷

Recently, the A₃AR models have also been constructed based on the human β_2 -adrenergic receptor (**Figure 19 (B)**) and the hA_{2A}AR receptor (**Figure 19 (C)**) template.^{77, 137} Among these models, the main differences were observed at the ECL2, ICL3 and extracellular end of TM1.¹³⁷ As the ECL2 is deemed essential for ligand recognition, differences in the ECL2 between the models widely affect the structure based drug design. The bovine rhodopsin-based homology model consists of a seven-helical bundle with a central cavity surrounded by helices 3, 5, 6 and 7. The access of the ligands into the central cavity is governed by the ECL2, which possesses a β -sheet secondary structure. As mentioned earlier, this model has been widely used to identify putative ligand-receptor interactions and rationalize the structure-affinity relationship of known hA₃AR antagonists and agonists. For the human β_2 -adrenergic receptor-based homology model, the location of the hA₃AR antagonist is found similar between the models obtained from the rhodopsin and the β_2 -adrenergic receptor, despite the fact that there are structural differences in the ligand binding sites between the two models. The presence of a α -helix on ECL2 in models (opened to extracellular site) from human β_2 -adrenergic receptor and hA_{2A}AR, rendered the volume

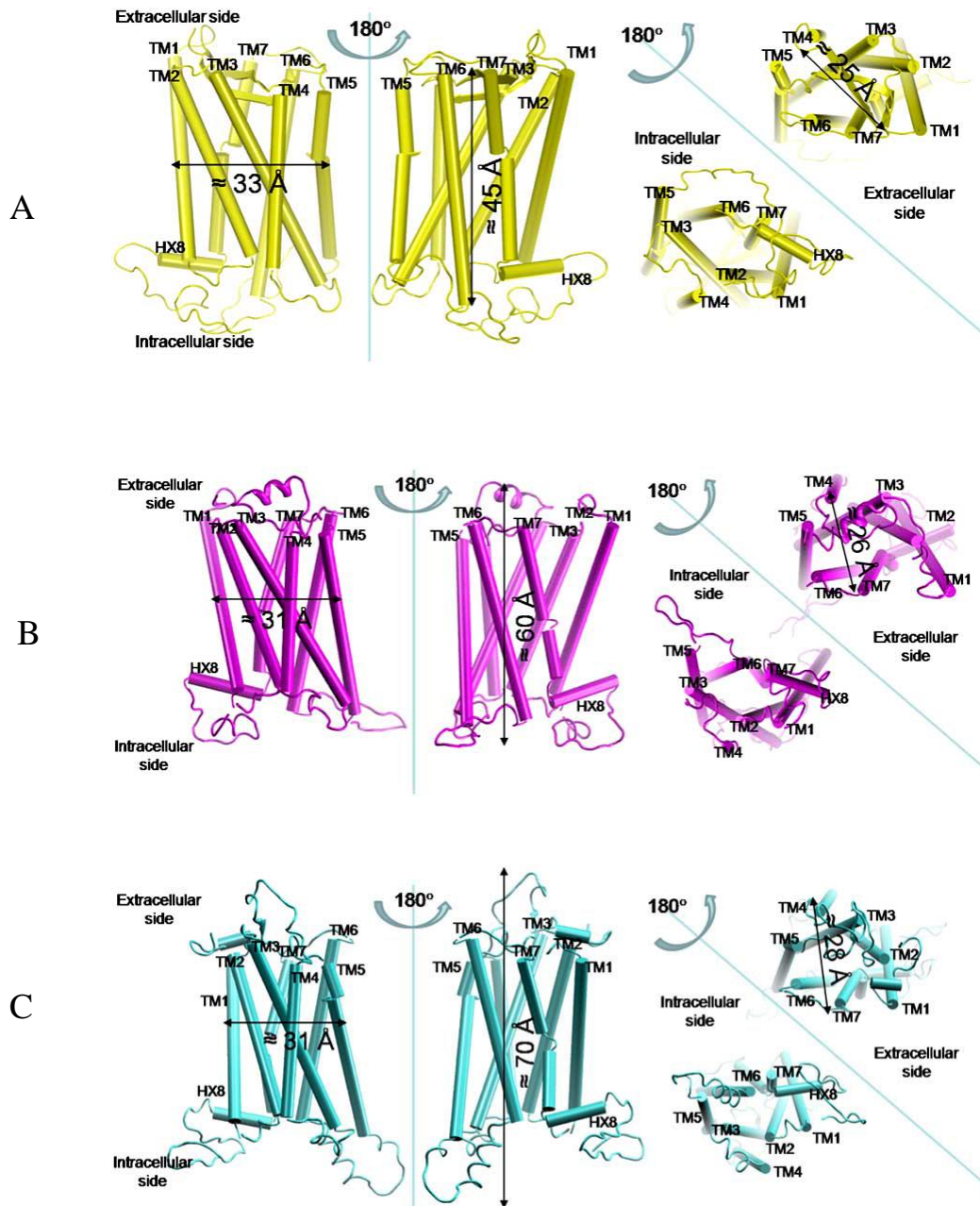


Figure 19. Topology of (A) bovine rhodopsin-based hA₃ homology model (B) human β_2 adrenergic receptor-based hA₃ homology model (C) hA_{2A} adenosine receptor-based hA₃ homology model (adopted from ref 137).¹⁴⁰

measurement difficult. They are measured as 1620 Å³ and 1930 Å³ respectively. However, these models are not comparable to the model which enables the accessibility of ligands into the central binding sites. In the hA_{2A}AR-based homology model, the helical arrangement is similar to other homology models. Nevertheless, the helices are shifted, and the differences among their relative positions results in an RMSD around 2.5 Å.¹³⁷ The

binding pocket of ligands for such a model shifted closer to the TM6 and TM7 and open to the extracellular side. With regards to the volume of binding site, both A₃AR bovine rhodopsin-based model, where the binding site is enclosed, and the estimated volume is 660 Å.¹³⁴

1.8.2.3 Evaluations of hA₃AR model

Evaluation of hA₃ receptor model is a crucial factor in confirming the accuracy of homology modeling. The commonly employed strategies are:

(i) Checking the protein stereochemistry using Ramachandran Plot, χ plot, clash contact reports, and Dope Score¹⁴¹

(ii) the concordance with data from site-directed mutagenesis of hA₃AR; the residues that mutagenesis studies have been identified to play a significant role in ligand-receptor recognition should be involved in ligand-hA₃AR model interactions¹⁴²

(iii) the affinity and selectivity profile of newly synthesized derivatives should be rationalized by models through analysis of the hypothetical binding interaction between the ligand and the respective residues in the docking studies.¹⁴² Based on such receptor-based structural information, new compounds are rationally designed and synthesized;

(iv) the model should also be able to suggest the mutation of residues that the model predicts to be important for ligand-receptor interaction, which is then validated by mutagenesis studies.¹⁴²

1.8.3 Molecular Docking Simulations

Molecular docking simulations relies mainly on the interactions of ligands with the receptor target in a three dimensional environment. For hA₃AR, the affinity of the hA₃ ligands to such a receptor is a result of structural and chemical complementarities, which can be determined through identification of binding modes and interactions of ligands inside the receptor cavity. All the docking studies are performed on a hA₃ receptor homology model, since the crystal structure of hA₃ receptor has not been resolved yet. Through the hA₃ models, the binding modes of different scaffolds of hA₃ ligands are depicted and experimental hA₃ binding affinities of these ligands are therefore rationalized. The majority of these hA₃ models

are based on the bovine rhodopsin template based homology models, with increasing number of models constructed from the recently resolved hA_{2A} receptor crystal structure. The following sections illustrate some examples of molecular docking studies carried out on pyrazolo- pyrimidine (PP) and pyrazolo-triazolo-pyrimidine (PTP) derivatives that have been described as potent hA₃AR antagonists.

1.8.3.1 Pyrazolo[4,3-*d*]pyrimidinones

Lenzi *et al* performed the molecular docking simulation for the series of pyrazolopyrimidinone derivatives (compound **39**) using hA_{2A}AR crystal structure based homology model.¹⁰⁷ In the docking experiments, it was observed that carbonyl group at the 7-position and the N atoms of the pyrazole ring interacted with aminoacid residue Asn250(TM6) by stabilizing hydrogen bonding interactions. Moreover the ligand made various hydrophobic interactions with binding residues, especially, the aromatic π - π stacking interaction was observed between 2-phenyl ring and Phe168(ECL2). Similarly, pyrazolopyrimidin-7-one core made hydrophobic interaction with highly conserved residue Trp243 (TM6). It was also noticed that small electron donor groups such as methyl and methoxy at *para* position of 2-phenyl moiety strengthened the π - π stacking interaction of 2-phenyl group with receptor.

1.8.3.2 Pyrazolo[3,4-*d*]pyrimidines

The docking studies were performed for the pyrazolo[3,4-*d*]pyrimidine derivatives (compound **40**) on an hA₃AR model derived from the homology modelling using hA_{2A}AR crystal structure as template.⁷⁷ It was noted that the methyl group of the scaffold was pointed towards the extracellular membrane and made potential interaction with with Phe168(ECL2) and Leu246(TM6). Subsequently acyl chain at N⁴-position was enclosed in the cleft between TM2 and TM3, and its branch 6-phenyl ring was accommodated inner side of the TM5 and TM6. As expected, the pyrazolo pyrimidine scaffold was interacted with Phe168 by a π - π stacking interaction. In addition two H-bonds were observed between its N¹ and N⁷ nitrogens and the Asn250 (TM6) of receptor. Moreover, the 6-phenyl ring

and acyl moiety of the ligand were sited in the hydrophobic clefts and made essential hydrophobic interactions with nearby residues.

1.8.3.3 Pyrazolo-triazolo-pyrimidines

Baraldi *et al* explored the binding modes and interactions of PTPs scaffold as a class of hA₃AR antagonists.¹¹⁴ From the study, it was hypothesized that these derivatives of PTP mainly interacted with residues belong to TMs 3, 5, 6, and 7. The C²-furan ring of the scaffold pointed towards extracellular side and interacted with Asn250 (TM6) via π - π interaction. The carbamoyl moiety of the N⁵-position was surrounded in the middle of TM6 and TM7, and forms a stabilizing H bonding interaction with Ser275 (TM7). The N⁵-substituents were surrounded by the small binding pocket with hydrophobic residues like Val235 (TM6), Leu236 (TM6) and Asn278 (TM7). Therefore, the *para* and *meta* positions of the N⁵-phenyl ring seemed to be involved with stringent steric control. Similarly, the N⁸-alkyl group made important hydrophobic interactions with residues such as Leu90 (TM3), Phe182 (TM5), Ile186 (TM5), and Leu190 (TM5). Maconi *et al.*¹¹⁷ reported that the furan ring at C² position was seemed to interact with Phe168 (ECL2) and Phe182 (TM5) through a π - π interaction, whereas the carbamoyl group was interacted with His95 (TM3) and Ser247 (TM6) via H-bonding. The N⁵-substituents were located in a hydrophobic region and made hydrophobic interactions with nonpolar residues such as Ile98 (TM3), Ile186 (TM5), and Leu244 (TM6). Conversely, Tafi *et al.*¹²⁷ suggested that the PTP core nucleus was stabilized by π - π stacking interactions with Trp243 (TM6). Similarly, the carbonyl of the amidic group at N⁵ position formed an H-bonding interaction with residue Asn250. In addition the N⁸-alkyl group, C²-furan ring and phenyl ring at N⁵- of PTP were defined by three lipophilic pockets, composed of Phe239, Trp243, His272 (HYD1), Leu102 (HYD2), His95, Phe182, Trp185 and Tyr254 (HYD3) respectively. Moreover, it was deduced that the H-bond present between the N⁵-pyridyl ring and the residue Tyr254 (TM6) mainly favoured hA₃AR affinity and selectivity.

Very recently, our group has performed the docking simulation of 2-(*para*-substituted) phenyl-PTP derivatives as a new class of potent hA₃

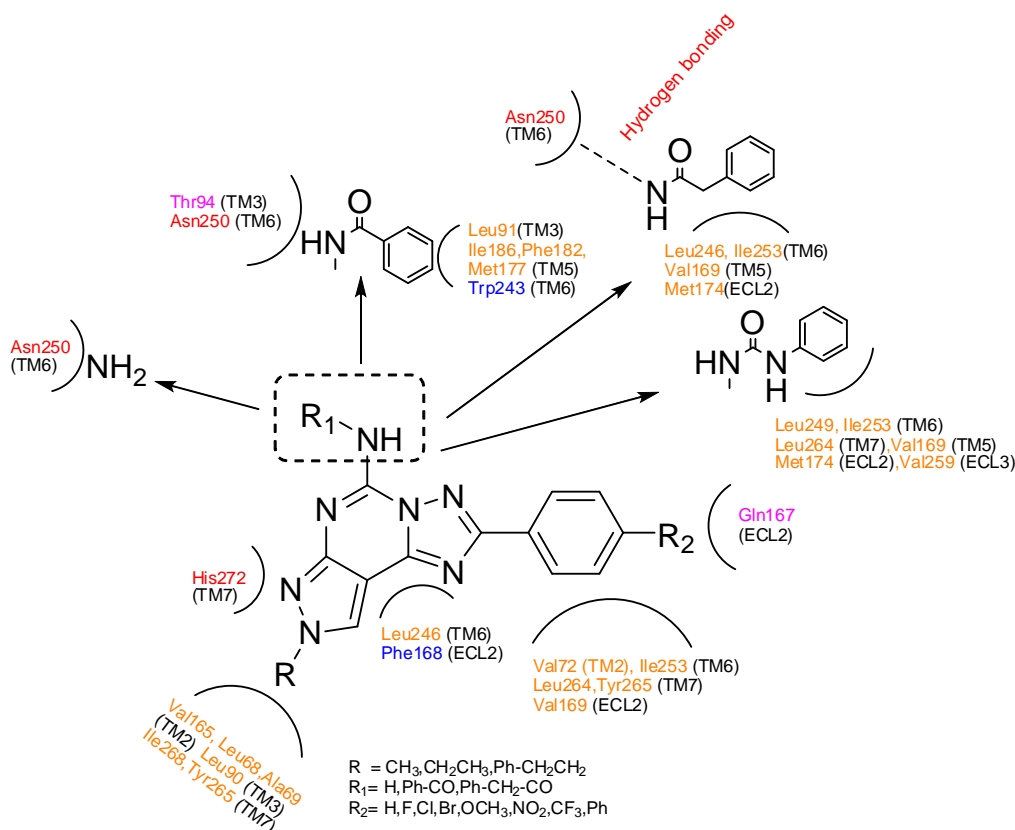
antagonist on A₃AR homology model, based on the crystal structure of the hA_{2A}AR.¹¹⁸ In this study, the ligand-receptor recognition mechanism was analysed in quantitative manner using interaction energy calculation. Moreover, binding interactions of various substituents at the different position of the tricyclic scaffold was analysed.

Binding interactions at the tricyclic nucleus and C²-position of PTP

The tricyclic core of the PTP scaffold was shown to interact mostly with the nonpolar residues such as Leu246 (TM6) and Phe168 (ECL2) through hydrophobic packing and π - π interactions, respectively. The immediate phenyl ring at C²-position of the tricyclic nucleus in N⁵-amine sat inside a hydrophobic pocket surrounded by the side chains of non-polar residues at TMs 6, 7 and ECL2, such as Ile253, Leu264, Tyr265 and Val169 (**Figure 20**). Nevertheless, the bulky side chains of these non-polar residues limited the hydrophobic pocket size around the phenyl ring, and only certain substituents with appropriate sizes were allowed at the 4th position of 2-phenyl ring. Therefore, the introduction of bulky substituents, such as NO₂, CF₃ and phenyl at the *para*-position has resulted in relatively low affinity at the hA₃ receptor mainly due to the steric hindrance imposed by these bulky groups. In addition, van der Waals interactions were also observed between the 2(*para*-(un)substituted)-phenyl ring and the Gln167 on ECL2.

Binding interactions at N⁵-position of PTP

The free NH₂, -CONH, -NHCONH groups (of benzamide, phenylacetamide, phenylcarboamyl) at the N⁵-position formed H-bond with nearby -C=O or NH- group on the side chain of Asn250(TM6), which was highly conserved among all the adenosine receptors. This amino acid was shown to be a crucial residue involved in antagonist recognition at adenosine receptors, as determined from site-directed mutagenesis experiments. In addition, the side chain of Asn250 was also likely to interact with the N⁵-amino or amide group via van der Waals forces. The phenyl ring of benzamide moiety was able to form π - π stacking interactions with the Trp243 (TM6)



- Residue:** Involved in Hydrogen bonding
- Residue:** Involved in Hydrophobic interaction
- Residue:** Involved in π - π stacking interaction
- Residue:** Van der Waals interaction

Figure 20. Hypothetical binding interactions of new series of 2-aryl-PTPs

(Figure 20), which is considered to be an important residue in adenosine receptor activation and antagonist recognition. The corresponding phenyl ring also accommodated within the boundary of a hydrophobic pocket formed by a group of non-polar residues at TM3 (Leu91) and TM5 (Ile186, Phe182, Met177) and interacted with those residues through typical hydrophobic forces. Among these residues, Met177 and Phe182 were exhibited to be essential for the hA₃ receptor antagonist recognition. The presence of the hydrophobic interactions around the N⁵-position appeared crucial for the hA₃ receptor recognition. In addition, the N⁵-phenylacetamide chain of the PTP made hydrophobic interactions with residues like Leu246(TM6), Ile253(TM6), Val169(ECL2) and Met174(TM5). Similarly, phenyl ring of the N⁵-arylcarbamoyl moiety also formed the hydrophobic

interactions with Val169, Met174(ECL2) Leu249, Ile253 (TM6), Val259(ECL3) and Leu264(TM7).

Binding interactions at N⁸-and N⁷-positions of PTP

N⁸-position of the pyrazole ring with methyl and phenylethyl substitution were situated within the boundary of hydrophobic pocket consisting of a group of hydrophobic residues at TM2 (Leu68, Ala69), TM3 (Leu90), TM5(Val165) and TM7(Tyr265, Ile268). All the important binding interactions between C²-, N⁵-N⁸-substituents of 2-aryl-PTPs and the corresponding residues in hA₃ receptor were summarized in the **Figure 20**. Generally, the binding interactions found between the ligands and the residues in hA₃ model were as follows: (i) hydrophobic interactions between N⁸-, N⁵- and C²-substituents and residues deemed crucial for conferring hA₃ affinity; (ii) electron accepting amidic group at N⁵, N⁴/N¹ on triazole ring and sp² N⁷ on pyrazole ring in engaging H-bond with nearby residues; (iii) aromatic moieties like triazolo/pyrimidine ring on the tricyclic nucleus and phenyl ring of benzoyl group at N⁵ position form π - π interaction with the nearby aromatic residues; (iv) van der waals interaction (e.g. dipole-dipole) between the polar moiety (such as amidic group at N⁵, polar substituents at *para*-position of 2-phenyl ring) and the polar residues.

Chapter 2 Statement of Purpose

In the last 15 years, intensive efforts in medicinal chemistry to design and synthesize new derivatives able to interact with adenosine receptors have led to the discovery of potent and selective ligands (with either agonistic or antagonistic properties) for the A₁, A_{2A}, A_{2B} and A₃ ARs. More precisely, while various agonists and antagonists for the A₁ and A_{2A} receptor subtypes have been reported, the role of A_{2B} and A₃ receptors has not been elucidated yet. The reason at the basis of such phenomenon could be attributed to the fact that A_{2B} and A₃ receptors are the latest to be discovered, hence less research has been conducted on these receptor subtypes. Nevertheless, selective inhibition of human A₃ adenosine receptor (hA₃AR) by potent antagonists has been shown to have promising application in the treatment of several pathological conditions, including glaucoma, inflammatory diseases and cancer.^{30, 31, 74} Therefore, the identification of new compounds able to selectively inhibit this adenosine receptor subtype is deemed crucial in improving several pathological conditions. On the basis of these observations, the focus of this thesis is to explore new A₃AR antagonists, with the purpose of providing a better understanding of this still unknown receptor towards promising biomedical applications.

Recent research by our group on the pyrazolo-triazolo-pyrimidine (PTP) scaffold, centered on the replacement of the conventional furan ring at position C² with a 2-(*para* substituted) phenyl ring and various substituents at N⁵ and N⁸ position,¹¹⁸ led to the identification of potent and selective analogues at human A₃AR. However, also in the case of the PTP scaffold and in the most of the tricyclic heterocyclic derivatives described previously in the literature, these compounds have a number of limitations such as

- (i) complex structure of the ligands make the synthetic preparation difficult (due to more steps involved), time consuming and expensive;
- (ii) low yields (15-17%), undetected side products and problems in purification;
- (iii) critical steps in the synthesis of PTPs involve high temperature reactions (160°C & 260°C) for long time;

(iv) some of the PTP compounds show deviation from the Lipinski's rule of five such as high molecular weight and high lipophilicity. Moreover, these problems may affect the ADME properties of the compounds, causing poor pharmacokinetic profiles (solubility & permeability).^{143, 144} As such, these observations have suggested the need to further investigate simplified heterocyclic structures in order to improve the ADME properties as well as to maintain or improve the affinity and selectivity towards the hA₃AR.^{107, 145, 146} A recent study on a molecular simplification of complex tricyclic structures to bicyclic structures resulted in simplified analogues with potent activity in the nanomolar range with improved selectivity towards the hA₃AR as compared to the parent compound. Overall, this study proved the significance of simplified structures, which can act as hA₃AR antagonists to the same extent as more complex structures, while overcoming several limitations including higher propensity for metabolic instability and more complicated syntheses.¹¹⁸

Moreover, from SAR and molecular modelling studies of previously synthesized PTP derivatives, we observed that the pyrazolo [3,4-*d*] pyrimidine (PP) nucleus represents the core domain in the interaction with A₃AR's binding site, suggesting that its presence is critical in affecting the binding of this structure to the receptor of interest. Therefore, PP scaffold was chosen as pharmacophore for this thesis, which is based on a simplified structure of PTP compounds. In addition, we also deduced that certain features included in the new PP scaffold could improve or preserve the hA₃ receptor antagonistic activity, while maintaining the selectivity towards other receptor subtypes. Moreover, we postulated that our PP derivatives would be able to bind equally well to the hA₃AR in comparison to the PTP counterparts, by preserving the key interactions with the same crucial amino acids. The rationale at the basis of such selection is explained in more detail in **Chapter 3**.

Hypothesis 1:

Therefore, based on the above mentioned structural benefits, it is hypothesised that the molecular simplifications of tricyclic PTP to bicyclic PP, together with other substitutions at the N², N⁶ and C⁴-positions of the bicyclic nucleus (corresponding to N⁸ & C⁵ positions, and to the triazole ring, respectively, of the PTP parent scaffold) will ultimately maintain affinity and selectivity at this receptor subtype, while reducing the synthetic procedures

and potentially improving the physico-chemical properties of the derivatives in comparison to the parent compounds (for more details, please refer to **Chapter 3, Chart 1**).

Hypothesis 2:

It is also hypothesized that pertinent molecular modeling investigations can be used to rationalize the experimental data obtained from the pharmacological characterization of new PP derivatives by providing new insights on (i) important structural features associated with their selective inhibition of hA₃AR (via QSAR analysis) and (ii) essential binding interactions between ligands and specific residues responsible for the hA₃ affinity (through molecular docking simulations on the hA₃AR homology model), particularly at the N² & N⁶ position of the tricyclic nucleus.

Main objectives

To test these hypotheses, the following investigations were planned and carried out:

- a) Design, synthesis and characterization of a new series of 4 chloro-pyrazolo [3,4-*d*] pyrimidine derivatives bearing a chloro functional group at the C⁴-position, in conjunction with various substituents at N²- and N⁶-positions of the bicyclic scaffold as simplified analogues of PTPs (**Chapter 3**).
- b) Pharmacological investigation of the importance of structural parameters at each position of PP bicyclic nucleus towards the affinity and selectivity profile at the hA₃AR through binding affinity assays at the hA₁, hA_{2A} and hA₃ receptors as well as functional assays at the hA_{2B} (**Chapter 4**).
- c) Detailed analyses of the SAR for the new series of 4 chloro-pyrazolo [3,4-*d*] pyrimidines towards hA₃AR subtype (**Chapter 4**).
- d) Rationalization of the experimental binding affinity data through molecular modeling investigations, including quantitative structure activity relationship analysis (**Chapter 5**), hA₃AR homology modeling and docking simulations (**Chapter 6**) of the new series of 4 chloro-pyrazolo [3,4-*d*] pyrimidine derivatives (**Chapter 4**).

Chapter 3 Design, Synthesis, Pharmacological and Molecular Modeling Evaluation of a Novel Series of 4-chloro-Pyrazolopyrimidine Derivatives

*Pharmacological assays were performed by our collaborator, Professor Karl-Norbert Klotz, at the Institute for Pharmacology and Toxicology, University of Würzburg, Germany.

* QSAR was performed by our collaborator Asst. Prof. Yap Chun Wei at the Dept of Pharmacy, National university of Singapore.

3.1 Introduction

This section describes the rationale for the design, synthesis, pharmacological and pharmacological evaluation of a new series of pyrazolo[3,4-*d*]pyrimidines bearing a chloro substituent at the C⁶-position (based on the hypothesized structural modification as mentioned in Chapter 2 Statement of Purpose) concurrently with different substituents at the N²- and N⁶-positions of the tricyclic nucleus. The discussion will first elaborate on the factors influencing the design of the library, followed by chemical considerations of the synthetic routes and the binding affinities of the novel series of pyrazolo[3,4-*d*]pyrimidines at the human A₁, A_{2A} and A₃ adenosine receptor subtypes and molecular modelling evaluations of 4-chloro-pyrazolopyrimidine derivatives.

3.2 Rationale of drug design

Based on the details and information available from literature as described in the previous chapter, a new series of adenosine antagonists, particularly targeted at hA₃ receptors, has been designed (**Figure 21**). In our previous work, we have synthesized various tricyclic pyrazolo triazolo pyrimidine (PTP) derivatives as hA₃AR antagonists.¹¹⁸ Among those PTP derivatives, we have found that some of them showed high affinity towards hA₃ receptor in the nM range. Molecular modeling studies of those compounds showed that the introduction of some substituents in the original scaffold could be vital for potency. Thus, to develop a new class of compounds targeting the A₃ receptor, we performed a molecular simplification of the tricyclic PTP structure to a bicyclic pyrazolo[3,4-*d*]pyrimidine (PP) bearing

key substituents, hoping that these new compounds could preserve their pharmacological profile at the hA₃AR while simplifying the synthetic procedures.

From the structure-activity relationship (SAR) studies of previously synthesized PTP derivatives^{118, 128} we deduced the following features that could be vital for the hA₃AR antagonistic activity:

I) The pyrazolo[3,4-*d*]pyrimidine (PP) nucleus has shown to represent the core domain in the interaction with AR's binding sites, suggesting that its presence is critical in affecting the binding of this structure to the receptor of interest. Therefore, we proposed a new series of hA₃AR antagonists, in which the core PP domain was kept intact (**Chart 1**).

II) The size of the substituents at N² position of the PP bicyclic nucleus (corresponding to N⁸ position of the PTP scaffold) could play an important role in determining the affinity and selectivity towards A₃AR. Our previous studies showed that small alkyl groups (e.g., methyl or ethyl) are well tolerated at the hA₃AR, since there is a steric control in the receptor pocket

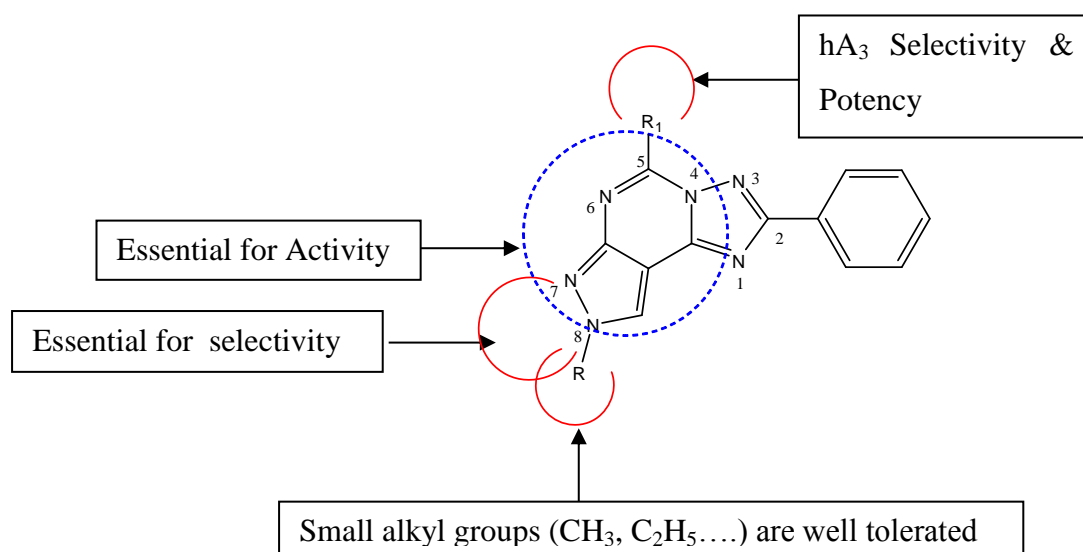


Figure 21. Essential features for **PP** analogue

surrounding that position.¹¹⁴ Hence, we introduced various substituents with different lipophilicity and steric hindrance such as alkyl (methyl **81**, isopropyl **82**, and neopentyl **83**) and phenyl ethyl (**84**) functions at N² position.

III) Assuming that substituents at C⁶ position (correspondent to position C⁵ of PTP scaffold) are essential for retaining the selectivity and potency,¹²⁸ various

acyl groups (benzoyl, para substituted benzoyl and phenylacetyl) were substituted at C⁶ position in the new series of analogues. In fact, these moieties have given rise to potent hA₃AR antagonists when introduced at the C⁵ position of the PTP scaffold.

IV) Differently from the previous triazole ring in the PTP series, a small group needed to be introduced at C⁴ position to keep the scaffold simple and, at the same time, enabling a further point of functionalization. To reiterate, we proposed a lipophilic chloro functional group at the C⁴ of the bicyclic nucleus to maintain the steric constraints unaltered at this position, which could also help the nucleus to attain the same binding pose as PTP due to restricted rotation of C⁴ position. Moreover, this group enables the easy introduction of different chains and functionalities if additional structural modification is deemed essential for further improvement of activity.

Molecular Simplification:

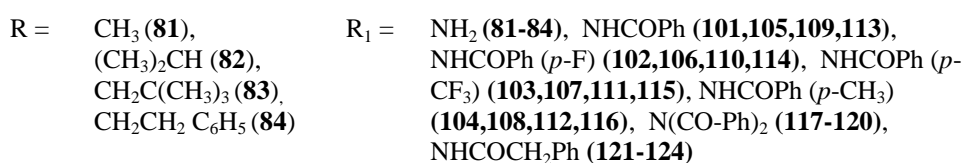
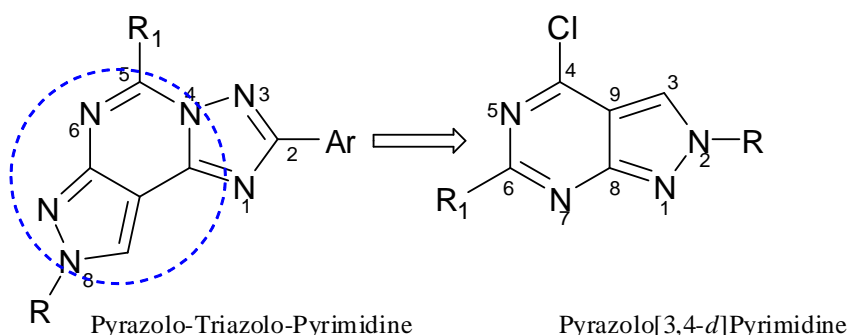
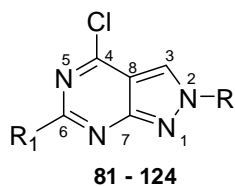


Chart 1. Rationale for the design of 2-(alkyl and aralkyl substituted)-2*H*-pyrazolo[3,4-*d*]pyrimidine derivatives (Molecular simplification of **PTP** into **PP**, R denotes N² position, R₁ denotes C⁶ position).

On the basis of the potential structural benefits of the simplified PP derivatives, a novel structure-affinity relationship evaluation was conducted through the rational design and synthesis of a new series of pyrazolo[3,4-*d*]pyrimidines (compounds **81-84**, **Chart 1** and **Table 2**).

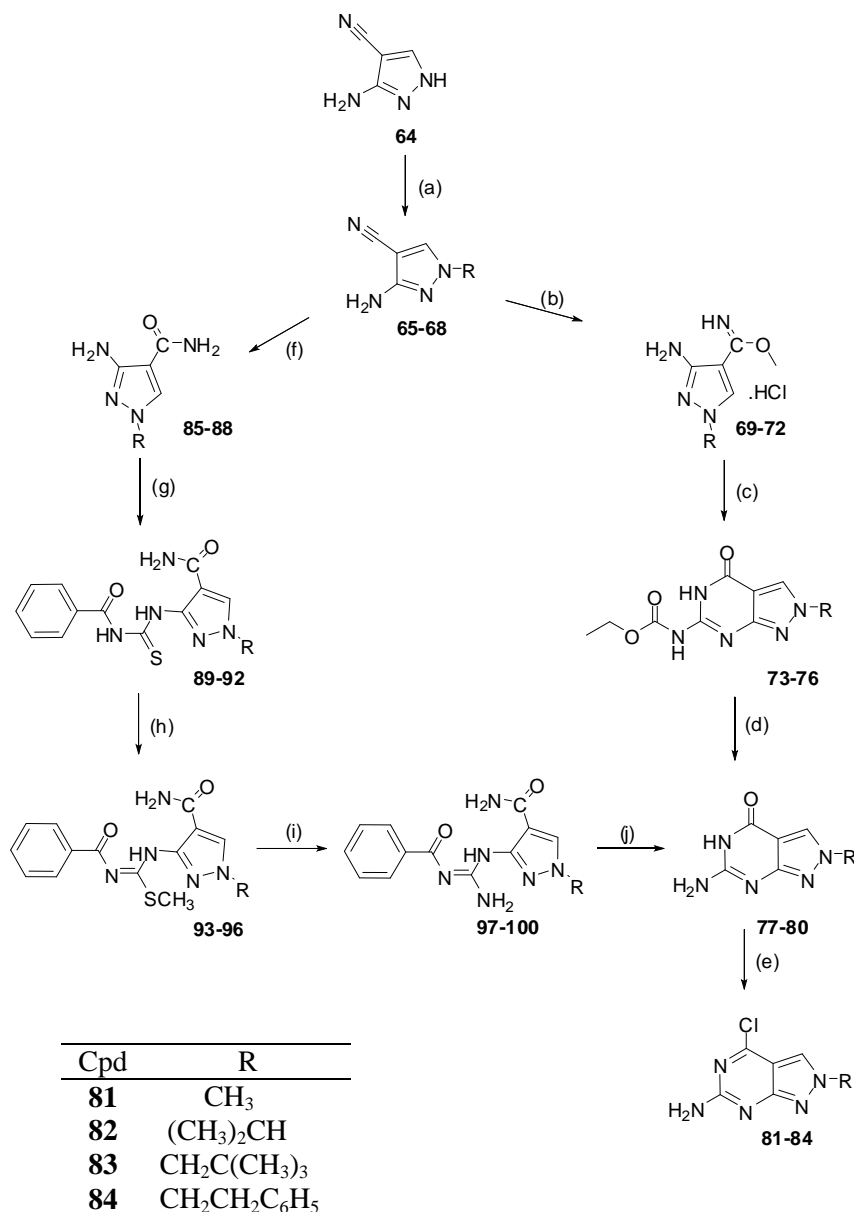
Table 2. Structures of new pyrazolo[3,4-*d*]pyrimidines derivatives.

Compound	Substituents at R	Substituents at R ₁
81	CH ₃	NH ₂
82	CH(CH ₃) ₂	NH ₂
83	CH ₂ C(CH ₃) ₃	NH ₂
84	CH ₂ CH ₂ C ₆ H ₅	NH ₂
101	CH ₃	NHCOPh
102	CH ₃	NHCOPh (<i>p</i> -F)
103	CH ₃	NHCOPh (<i>p</i> -CF ₃)
104	CH ₃	NHCOPh (<i>p</i> -CH ₃)
105	CH(CH ₃) ₂	NHCOPh
106	CH(CH ₃) ₂	NHCOPh (<i>p</i> -F)
107	CH(CH ₃) ₂	NHCOPh (<i>p</i> -CF ₃)
108	CH(CH ₃) ₂	NHCOPh (<i>p</i> -CH ₃)
109	CH ₂ C(CH ₃) ₃	NHCOPh
110	CH ₂ C(CH ₃) ₃	NHCOPh (<i>p</i> -F)
111	CH ₂ C(CH ₃) ₃	NHCOPh (<i>p</i> -CF ₃)
112	CH ₂ C(CH ₃) ₃	NHCOPh (<i>p</i> -CH ₃)
113	CH ₂ CH ₂ C ₆ H ₅	NHCOPh
114	CH ₂ CH ₂ C ₆ H ₅	NHCOPh (<i>p</i> -F)
115	CH ₂ CH ₂ C ₆ H ₅	NHCOPh (<i>p</i> -CF ₃)
116	CH ₂ CH ₂ C ₆ H ₅	NHCOPh (<i>p</i> -CH ₃)
117	CH ₃	N(CO-Ph) ₂
118	CH(CH ₃) ₂	N(CO-Ph) ₂
119	CH ₂ C(CH ₃) ₃	N(CO-Ph) ₂
120	CH ₂ CH ₂ C ₆ H ₅	N(CO-Ph) ₂
121	CH ₃	NHCOCH ₂ Ph
122	CH(CH ₃) ₂	NHCOCH ₂ Ph
123	CH ₂ C(CH ₃) ₃	NHCOCH ₂ Ph
124	CH ₂ CH ₂ C ₆ H ₅	NHCOCH ₂ Ph

At the N² position, alkyl groups with different steric effects, ranging from a small methyl and isopropyl to a long and bulky groups like neopentyl and phenylethyl chain, were incorporated. At the C⁴-position, a chloro group was introduced. At the N⁶, a free amine or different lengths of amide moieties, for instances (bis-) benzamide, phenylacetamide and substituted benzamide with *para*-substituents of different electronic effects, for examples those with electron-withdrawing effect (e.g. 4-F, 4-CF₃) as well as groups with electron-donating effect (e.g. 4-CH₃) were substituted at such position.

3.3 Chemical Considerations

The new series of the 6-amino-4-chloro-pyrazolo[3,4-*d*]pyrimidine derivatives **81-84** & **101-124** were prepared following two synthetic pathways, as depicted in **Schemes 1&2**. **Scheme 1** illustrates the synthesis of analogues **81-84** and **Scheme 2** depicts the synthesis of derivatives **101-124**.



Scheme 1. Reagents: (a) RI or RBr/ K₂CO₃/ DMF, 90 °C, 10h; (b) MeOH/ HCl_(g), 0-10 °C, 18h; (c) C₂H₅OCONCS/ TEA /DCC /DMF, rt, 18h; (d) 2M NaOH/ MeOH, 60 °C, 12h; (e) POCl₃/ dimethylaniline, 110 °C reflux, 24h; (f) conc.H₂SO₄, 0 °C to rt, 5h; (g) C₆H₅CONCS/ acetone, reflux, 12h; (h) CH₃I/ 0.1N NaOH, rt, 3 h; (i) 2% aq.NH₃/ DMF, 120 °C sealed tube, 3 h; (j) 1N NaOH, 110 °C reflux, 12 h.

3.3.1 Synthesis of 4-chloro-2-(ar)alkyl-2H-pyrazolo[3,4-d]pyrimidin-6-amine (81-84), N-(4-chloro-2-(ar)alkyl-2H-pyrazolo[3,4-d]pyrimidin-6-yl)benzamide (101-116), N-benzoyl-N-(4-chloro-2-(ar)alkyl-2H-pyrazolo[3,4-d]pyrimidin-6-yl)benzamide (117,118), and N-(4-chloro-2-(ar)alkyl-2H-pyrazolo[3,4-d]pyrimidin-6-yl)-2-phenylacetamide (119-122)

Alkylation of 3(5)-amino-4-cyano-pyrazoles was performed by Baraldi *et al.*¹¹⁴ The inseparable mixture of N¹ and N² regioisomers of alkylated 3(5)-amino-4-cyano-pyrazoles derivatives were synthesized using a strong base NaH. As according to the reported procedure, the 3(5)-amino-4-cyano-pyrazole was dissolved in dimethylformamide (DMF) and alkylated through a reaction with iodoalkane or bromoalkane and sodium hydride (NaH) under ice bath condition. The NaH, which is a strong base, promotes deprotonation of the acidic proton on the nitrogen atom of the pyrazole ring. As a result, the electron rich nitrogen atom readily attacks the electron deficient alkyl group on the iodoalkane or bromoalkane with ensuing alkylation. Such alkylation process gave rise to a mixture of two inseparable regioisomers, the N¹ and N² regioisomers in a 1:1 ratio. In order to improve the yield of the product, it was decided to use the weak base such as K₂CO₃ instead of NaH. Subsequently, the intended N² regioisomer (**65-68**) was obtained as major product (**Chart 2**) with good yield by under standard heating condition. Among them, compounds **65&68** were already reported by our group.^{118, 147} In addition, compound **66** was also reported in the literature and was prepared by a different procedure in this piece of work.¹⁴⁸

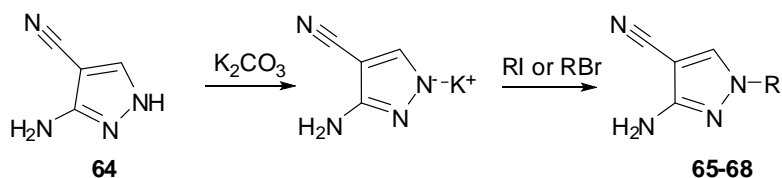


Chart 2. Proposed mechanism of formation of **65-68**

Subsequently, the nitrile group was transformed into carbimide by nucleophilic addition reaction as established by Shrivastava *et al.*¹⁴⁹ Corresponding nitrile derivatives **65-68** were treated with dry hydrogen chloride in dry methanol at 0°C for one hour, followed by stirring at the same temperature for 18 hours to obtain a carbimide as HCl salt (**69-72**). Extra

care was taken for maintaining the temperature at 0°C, as any drastic change in the reaction temperature during the course of the reaction, resulted in the decomposition of the product. The resulting product was unstable and was directly taken to the subsequent reaction without any further purification.

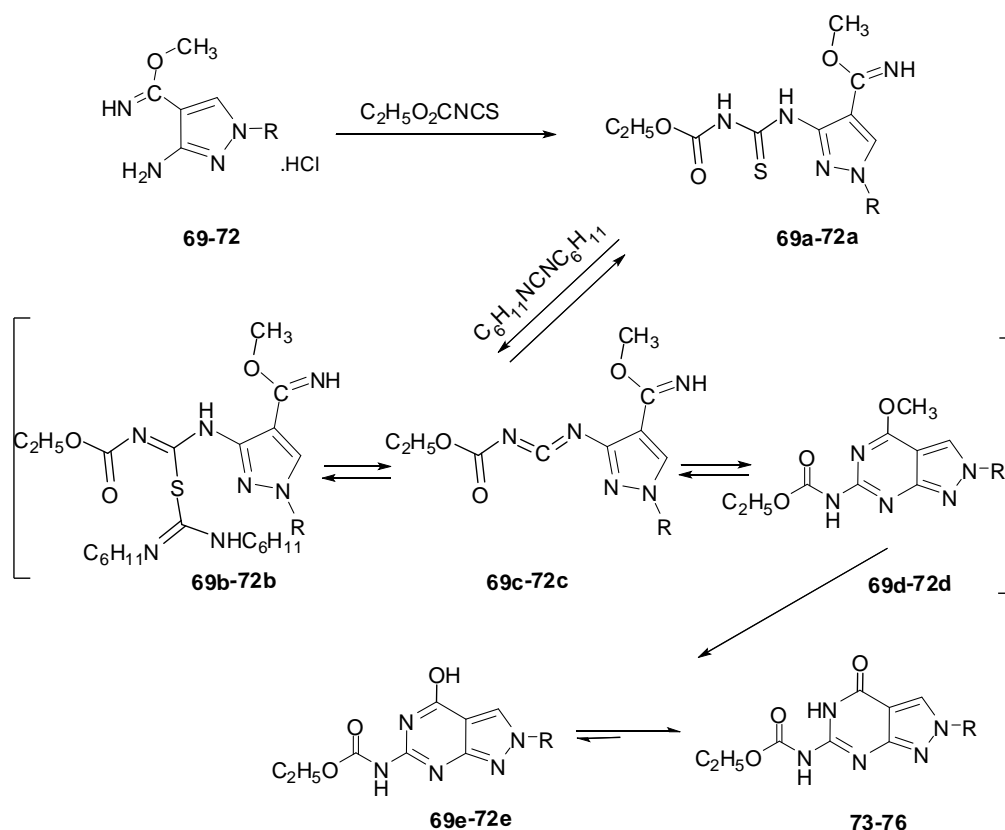


Chart 3. Proposed mechanism for the formation of compounds **73-76**

Intermediate compounds (**69-72**) were cyclized to corresponding carbamates (**73-76**) derivatives using mild alkoxycarbonylisothionate/DCC annulation methodology.¹⁵⁰ Alkylcarbonyl isocyanates are highly reactive reagents and the reaction of an ortho-substituted heterocyclic amine with such a reagent (**Chart 3**), affords a 3-(alkoxycarbonyl)-1-thio-uriedo-substituted derivative (**69a-72a**), which undergoes cyclodesulfurative conditions and finally transformed into the annulated heterocyclic compounds.

In this reaction, intermediates (**69-72**) were condensed with ethoxy carbonylisothiocyanate in DMF at room temperature to obtain a desired ethoxycarbonyl thiouriedos derivative (**Chart 3, 69a-72a**). Subsequent

cyclodesulfurization was effected by addition of dicyclohexylcarbodiimide (DCC) at room temperature and continuous stirring for 18 h under the same temperature resulted in the annulated carbamates (**73-76**). These carbamates (**73-76**) were readily hydrolyzed to corresponding amines **77-80** under basic conditions in methanol at 60°C for 12 hours (steps (a)-(d) in **Scheme 1**). The ethoxy carbonyl protecting group was easily cleaved under standard conditions.

The yield of compounds **73-76** (from 15% to 20%) and **77-80** (from 24 % to 28%) were quite low. As mentioned earlier, PTP compounds were obtained with low yield and the objective of this new design was to obtain all the intermediates and final compounds in good yields. Since the library of these new PP derivatives consists of a large number of compounds, it was deemed unfeasible to continue subsequent reactions with these low yields. Hence, a new synthetic route (steps (f)-(j) in **Scheme 1**) was further developed to obtain the target bicyclic derivatives **81-84** in good yields. In this method, 3-amino-*N*¹-substituted-4-pyrazolocarboxamides (**65-68**) were hydrolyzed to corresponding carboxamides (**85-88**) under acidic conditions at cold temperature for 30 minutes, followed by stirring at ambient temperature for 5 hours. The conversion of nitrile to amide was confirmed by H¹ NMR analysis and two broad singlets were observed for CONH₂ proton as specified in the literature.^{151, 152} Among the carboxamide derivatives (**85-88**), compound **85** was already reported in the literature¹⁵³ and compound **86** was commercially available.

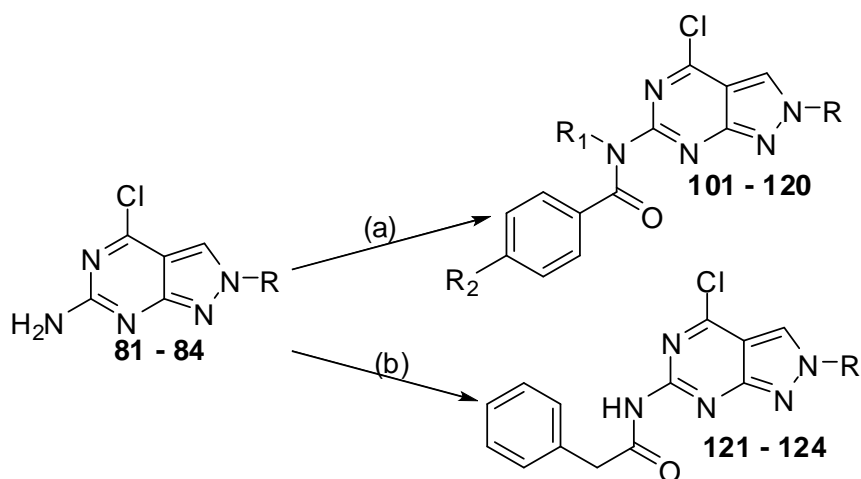
Yamazaki *et.al*¹⁵⁴ synthesized guanosine derivatives by condensation of 5-amino-4-imidazole-carboxamide with benzoyl isothiocyanate followed by methylation and ring closure. Similarly, subsequent steps of the synthetic scheme were performed using these established procedures with some modification. As per literature method, the carboxamide was allowed to react with benzoyl isothiocyanate in water at room temperature, but the corresponding benzoylthioureido derivatives were not obtained. When the reaction was carried out in 50% aqueous acetone at elevated temperature (80-100°C), thiourido derivatives were obtained with low yield, probably because of partial decomposition of benzoyl isothiocyanate in aqueous condition. Hence, the reaction was performed in dry acetone followed by condensation

with benzoylthiocyanate under reflux condition for 12 hours. Upon cooling, the benzoylthioureido (**89-92**) was obtained as yellow solids with good yield.

It is known that methylmercapto group activated by the electron-attracting tendency of benzoyl group would be more reactive. Hence, the methylation reaction was performed by treating intermediate compounds **89-92** with a methyl iodide in aqueous sodium hydroxide solution at ambient temperature for 3 hours to obtain a methylthio derivatives (**93-96**). After adjusting the pH to 6, the corresponding carbamidothioates (**93-96**) were obtained as white solid.

Subsequently, the nucleophilic substitution of SCH₃ group by NH₂ was carried out with vigorous heating in a sealed tube. As expected the electron poor carboamyl carbon was easily attacked by nucleophile NH₂. In this reaction, the methyl mercapto derivatives **93-96** were heated in DMF containing 2% ammonia at 120°C for 3 hours in a sealed tube to afford benzoylguanidino derivatives **97-100** and completion of the reaction was confirmed by the odour of methyl mercaptan from the reaction vessel. Interestingly, the synthesized compounds **97-100** were insoluble in any of the solvent. Hence, they were directly taken to the next reaction. Afterwards, benzoyl guanidinos **97-100** were easily cyclized to amine derivatives **77-80** upon treatment with 1 N sodium hydroxide under reflux condition. Upon cooling, the pH of the reaction mixture was adjusted to 6 to obtain a precipitate. As expected, the nitrogen atom of the carboamyl group attacked the carbon atom of the methenamine group followed by elimination of ammonia and benzoic acid from the reaction. The traces of benzoic acid was easily separated by stirring the product in hot ethanol. Interestingly, compounds **77-80** were obtained with higher yields (from 68 to 81 %) than those obtained from the synthetic route **1**.

Chlorination of the heterocyclic amide has been reported by several researchers. Among them, combination of reagents such as POCl₃ and *N,N*-dimethylaniline or diethylaniline has been widely used in the field of chemistry.^{155, 156} POCl₃ is considered to be one of the strong chlorinating agent for the heterocycle compounds. Hence, chlorination of the 6-amino-2-alkyl-2*H*-pyrazolo[3,4-*d*]pyrimidin-4(5*H*)-ones (**77-80**) was carried out with phosphoryl trichloride (POCl₃) in the presence of *N,N*-dimethyl aniline under



	R	R ₁	R ₂		R	R ₁	R ₂
81	CH ₃	-	-	111	CH ₂ C(CH ₃) ₃	H	CF ₃
82	(CH ₃) ₂ CH	-	-	112	CH ₂ C(CH ₃) ₃	H	CH ₃
83	CH ₂ C(CH ₃) ₃	-	-	113	CH ₂ CH ₂ C ₆ H ₅	H	H
84	CH ₂ CH ₂ C ₆ H ₅	-	-	114	CH ₂ CH ₂ C ₆ H ₅	H	F
101	CH ₃	H	H	115	CH ₂ CH ₂ C ₆ H ₅	H	CF ₃
102	CH ₃	H	F	116	CH ₂ CH ₂ C ₆ H ₅	H	CH ₃
103	CH ₃	H	CF ₃	117	CH ₃	C ₆ H ₅ CO	H
104	CH ₃	H	CH ₃	118	(CH ₃) ₂ CH	C ₆ H ₅ CO	H
105	(CH ₃) ₂ CH	H	H	119	CH ₂ C(CH ₃) ₃	C ₆ H ₅ CO	H
106	(CH ₃) ₂ CH	H	F	120	CH ₂ CH ₂ C ₆ H ₅	C ₆ H ₅ CO	H
107	(CH ₃) ₂ CH	H	CF ₃	121	CH ₃	-	-
108	(CH ₃) ₂ CH	H	CH ₃	123	(CH ₃) ₂ CH	-	-
109	CH ₂ C(CH ₃) ₃	H	H	123	CH ₂ C(CH ₃) ₃	-	-
110	CH ₂ C(CH ₃) ₃	H	F	124	CH ₂ CH ₂ C ₆ H ₅	-	-

Scheme 2. Reagents: (a) substituted benzoyl chloride/DIPEA/toluene, 120°C, reflux, 24 h ; (b) phenylacetyl chloride /DIPEA/toluene, 120°C, reflux, 24 h.

reflux condition for 24 hours. After completion of the reaction the excess POCl₃ was carefully removed and the crude product was purified by column chromatography to obtain the corresponding chloro analogues (**81-84**) as solid. Among them, compound **81** was already reported in the literature in low yield using different procedures.¹⁵⁷ All the corresponding final compounds **81-84** were confirmed by ¹H NMR, ¹³C NMR, HMQC and mass spectra (ESI) analysis.

Later, acylation of the free heterocyclic amine was carried out with little modification to the already established procedure.¹¹⁸ In this reaction

compounds bearing N² alkyl and phenylethyl group (**81-84**) were dispersed in toluene and treated with two equivalents of benzoyl chloride and substituted benzoyl chlorides (**Scheme 2**) to obtain the mono-benzoyl derivatives (**101-116**) and phenyl acetyl derivatives (**121-124**), respectively. Di-substituted benzoyl derivatives (**117-120**) of analogues **81-84** were prepared under this standard condition using 4 equivalents of the benzoyl chloride and DIPEA. The solvent was removed under reduced pressure and subjected to column chromatography to obtain desired compounds **101-124**. In addition, the amide formation was confirmed by observing the absence of NH₂ peak between 6.1 to 7.2 ppm in ¹H NMR and presence of amide (CONH) peak between 11.1 to 11.7 ppm in the ¹H NMR spectra. Further, CONH formation was confirmed by observing (C=O) carbonyl peak between 166 to 169 ppm in ¹³C NMR. HMQC and ¹³C NMR analysis were performed for one compound in each N-alkyl (ar-alkyl) substituted and C⁶ acylated derivatives.

3.3.2 Experimental Methods

3.3.2.1 Chemistry

Reactions were routinely monitored by thin-layer chromatography (TLC) on silica gel plate (precoated 60 F₂₅₄ Merck plate). Column chromatographies were performed using silica gel 60 (Merck, 70-230 mesh). Melting points were determined on a Gallenkamp instrument and were uncorrected. Compounds were dissolved in HPLC (high performance liquid chromatography) grade methanol for determination of mass to charge *m/z* on a LCQ Finnigan MAT mass spectrometer (source of ionization: Electron spin ionization (ESI) probe). Purity of the compounds were determined by HPLC using HITACHI, *version 3.1.8b*. ¹H and ¹³C NMR spectra were determined in the deuterated dimethylsulfoxide (DMSO-*d*₆) solutions on Bruker DPX ultrashield NMR (400 MHz) spectrometers, with chemical shifts given in parts per million (δ) downfield relative to tetramethylsilane (TMS) as internal standard, and *J* values (coupling constants) given in hertz. The following abbreviations were used: s, singlet; d, doublet; t, triplet; sep, septet; m, multiplet; br, broad.

HPLC Studies. The purity of the compounds were determined using analytical HPLC using HITACHI, *version 3.1.8b* on a Phenomenex Gemini

5U C18 (5 μ M, 110 Å, 150mm \times 4.60 mm i.d.) column at room temperature at a flow rate of 1.0 mL/min with two different mobile phase eluent systems at 254 nm UV detection. The isocratic elution was followed and the analysis was carried out using two different mobile phase systems, eluent 1; ACN(60%): H₂O, eluent 2; MeOH (50%): H₂O.

3.3.2.2 General procedure for the synthesis of 3-amino-1-alkyl or aralkyl-1H-pyrazole-4- carbonitriles (65-68). To a solution of 3-amino-1H-pyrazole-4-carbonitrile (1.08 g, 0.01 mol) in anhydrous DMF (5 mL), anhydrous potassium carbonate (1.65 g, 0.012 mol, 1.2 equiv) was added at 0°C and the resulting mixture was stirred at the same temperature for 45 min. Appropriate (ar) alkyl iodide or bromide (0.012 mol, 1.2 equiv) was added slowly over 15 min and the reaction mixture was heated at 90°C for 10 h. Then the resulting reaction mixture was cooled, poured over ice cold water and the aqueous phase was extracted with EtOAc (3x10 mL), the combined organic layers were dried over Na₂SO₄, filtered, and the solvent was removed under reduced pressure to give a oily residue which was purified via column chromatography eluting with a mixture of hexane/ethylacetate (1:1) to obtain the desired products (65-68) as solids.

3-amino-1-methyl-1H-pyrazole-4-carbonitrile (65): Yield: 67%; pale yellow solid, mp 125-127 °C; ¹H NMR (400 MHz, DMSO-*d*₆): δ 3.52 (s, 3H, N-CH₃), 6.53 (s, 2H, NH₂), 7.51 (s, 1H, pyrazole-H). ¹³C NMR (400 MHz, DMSO-*d*₆): δ 35.0 (N-CH₃), 72.6 (C-CN), 115.7 (CN), 140.3 (CH), 151.9 (C-NH₂). LC-MS (ESI) analysis (*m/z*) calcd for C₅H₆N₄ (122.13): found 122.8 [M+H]⁺.

3-amino-1-isopropyl-1H-pyrazole-4-carbonitrile (66):Yield : 69%; pale yellow solid, mp 120-122 °C; ¹H NMR (400 MHz, DMSO- *d*₆): δ 1.33 (d, *J*= 6.64 Hz, 6H, 2CH₃), 4.24 (sep, *J*=6.64 Hz, 1H, CH), 5.52 (s, 2H, NH₂), 8.10 (s, 1H, pyrazole-H). LC-MS (ESI) analysis (*m/z*) calcd for C₇H₁₀N₄ (150.18): found 151.0 [M+H]⁺.

3-amino-1-neopentyl-1H-pyrazole-4-carbonitrile (67): Yield: 71%; pale yellow solid, mp 123-125 °C; ¹H NMR (400 MHz, DMSO- *d*₆): δ 0.89 (s, 9H, 3CH₃), 3.67 (s, 2H, CH₂), 5.50 (s, 2H, NH₂), 8.04 (s, 1H, pyrazole-H). LC-MS (ESI) analysis (*m/z*) calcd for C₉H₁₄N₄ (178.23): found 179.2 [M+H]⁺.

3-amino-1-phenethyl-1H-pyrazole-4-carbonitrile (68): Yield: 76%; pale yellow solid, m.p 132-134 °C; ¹H NMR (400 MHz, DMSO- *d*₆): δ 3.03 (t, *J*=7.16 Hz, 2H, CH₂), 4.11 (t, *J*=7.12 Hz, 2H, CH₂), 5.57 (s, 2H, NH₂), 7.13-7.29 (m, 5H, Ar-H), 7.92 (s, 1H, pyrazole-H). LC-MS (ESI) analysis (*m/z*) calcd for C₁₂H₁₂N₄ (212.25): found 213.0 [M+H]⁺, 235.0 [M+Na]⁺.

3.3.2.3 General procedure for synthesis of methyl 3-amino-1-(alkyl or aralkyl)-1H-pyrazole-4-carbimides hydrochloride (69-72). Dry hydrogen chloride was bubbled for an about 60 min through a solution of carbonitriles **65-68** (0.005 mol) in 4 ml anhydrous methanol at 0°C. The mixture was then stirred for 18 h at the same temperature. After flushing with N₂, the reaction mixture was dried under vacuum. The unstable carbimides were used for the next reaction without further purification.

Methyl 3-amino-1-methyl-1H-pyrazole-4-carbimide hydrochloride (69): Yield : 52%; White solid.

Methyl 3-amino-1-isopropyl-1H-pyrazole-4-carbimide hydrochloride (70): Yield : 49%; White solid.

Methyl 3-amino-1-neopentyl-1H-pyrazole-4-carbimide hydrochloride (71): Yield : 53%; White solid.

Methyl 3-amino-1-phenethyl-1H-pyrazole-4-carbimide hydrochloride (72): Yield: 57%; White solid.

3.3.2.4 General procedure for synthesis of ethyl 2-(alkyl or aralkyl)-4-oxo-4,5-dihydro-2H-pyrazolo[3,4-*d*]pyrimidin-6-ylcarbamates (73-76). A suspension of carbimides **69-72** (0.01mol) in 10 ml of anhydrous DMF under nitrogen was treated with ethoxy carbonylthiocyanate (0.011 mol, 1.1 equiv). The reaction mixture was stirred for an hour under N₂ and then triethylamine (0.01 mol) was added to it and stirring was continued for another 1 h. After that dicyclohexylcarbodiimide (0.013 mol, 1.3 equiv) was added to the mixture and stirred for 18 h. After flushing with N₂, the reaction mixture was dried under vacuum and the crude residue was purified by column chromatography (hexane/EtOAc, 1:1) to obtain the desired product (**73-76**) as white solid.

6-(ethoxymethylamino)-2-methyl-2H-pyrazolo[3,4-d]pyrimidin-4(5H)-one (73): Yield: 19%; white solid, mp 191-193 °C; ¹H NMR (400 MHz, DMSO-*d*₆): δ 1.20 (t, *J*=6.64 Hz, 3H, CH₃), 3.57 (s, 3H, N-CH₃), 4.08-4.10 (m, 2H, CH₂), 7.79 (s, 1H, pyrazole-H), 10.45 (s, 1H, NH). LC-MS (ESI) analysis (*m/z*) calcd for C₉H₁₁N₅O₃ (237.22): found 238.2 [M+H]⁺.

6-(ethoxymethylamino)-2-isopropyl-2H-pyrazolo[3,4-d]pyrimidin-4(5H)-one (74): Yield: 15%; white solid, mp 180-182 °C; ¹H NMR (400 MHz, DMSO-*d*₆): δ 1.25 (t, *J*= 7.12 Hz, 3H, CH₃), 1.40 (d, *J*= 6.64 Hz, 6H, 2CH₃), 4.18 (q, *J*₁= 7.04 Hz, *J*₂= 14.16 Hz, 2H, CH₂), 4.46 (sep, *J*= 6.64 Hz, 1H, CH), 8.54 (s, 1H, pyrazole-H), 9.89 (s, 1H, NH), 10.56 (s, 1H, NHCO). LC-MS (ESI) analysis (*m/z*) calcd for C₁₁H₁₅N₅O₃ (265.27): found 266.2 [M+H]⁺, 288.0 [M+Na]⁺.

6-(ethoxymethylamino)-2-neopentyl-2H-pyrazolo[3,4-d]pyrimidin-4(5H)-one (75): Yield: 20%; white solid, mp 210-212 °C; ¹H NMR (400 MHz, DMSO-*d*₆): δ 0.90 (s, 9H, 3CH₃), 1.25 (t, *J*= 7.04 Hz, 3H, CH₃), 3.88 (s, 9H, CH₂), 4.19 (q, *J*₁= 7.1 Hz, *J*₂= 14.24 Hz, 2H, CH₂), 8.46 (s, 1H, pyrazole-H), 9.89 (s, 1H, NH), 10.55 (s, 1H, NHCO). LC-MS (ESI) analysis (*m/z*) calcd for C₁₃H₁₉N₅O₃ (293.32): found 293.2 [M]⁺.

6-(ethoxymethylamino)-2-phenethyl-2H-pyrazolo[3,4-d]pyrimidin-4(5H)-one (76): Yield: 18%; white solid, mp 193-195 °C; ¹H NMR (400 MHz, DMSO-*d*₆): δ 1.28 (t, *J*=7.16 Hz, 3H, CH₃), 3.12 (t, *J*=7.28 Hz, 2H, CH₂), 4.22 (q, *J*₁= 7.1 Hz, *J*₂= 14.24 Hz, 2H, CH₂), 4.34 (t, *J*=7.16 Hz, 2H, CH₂), 7.19-7.34 (m, 5H, Ar-H), 8.37 (s, 1H, pyrazole-H), 9.95 (s, 1H, NH), 10.60 (s, 1H, NHCO). LC-MS (ESI) analysis (*m/z*) calcd for C₁₆H₁₇N₅O₃ (327.34): found 328.1 [M+H]⁺, 350.0 [M+Na]⁺.

3.3.2.5 General procedure for synthesis of 6-amino-2-(alkyl or aralkyl)-2H-pyrazolo[3,4-d]pyrimidin-4(5H)-one (77-80). To a solution of ethyl 2-(alkyl or aralkyl)-4-oxo-4,5-dihydro-2H-pyrazolo[3,4-d]pyrimidin-6-ylcarbamates **73-76** (0.0012 mol) in 4 mL of methanol, 2M sodium hydroxide solution (4 mL) was added. The reaction mixture was heated with stirring at 60°C for 12 h. The mixture was cooled and acidified at pH 6 with acetic acid. The solid was collected by filtration, washed with water and recrystallized from methanol to obtain the desired products (**77-80**) as solids.

6-amino-2-methyl-2H-pyrazolo[3,4-d]pyrimidin-4(5H)-one (77): Yield: 24%; white solid, mp >300 °C; ¹H NMR (400 MHz, DMSO-*d*₆): δ 3.69 (s, 3H, N-CH₃), 6.69 (s, 2H, NH₂), 7.73 (s, 1H, pyrazole-H), 10.58 (s, 1H, NHCO). LC-MS (ESI) analysis (*m/z*) calcd for C₆H₇N₅O (165.16): found 166.1 [M+H]⁺.

6-amino-2-isopropyl-2H-pyrazolo[3,4-d]pyrimidin-4(5H)-one (78): Yield: 28%; white solid, mp >300 °C; ¹H NMR (400 MHz, DMSO-*d*₆): δ 1.42 (d, *J*= 6.52 Hz, 6H, 2CH₃), 4.50 (sep, *J*= 6.52 Hz, 1H, CH), 7.64 (s, 2H, NH₂), 8.11 (s, 1H, pyrazole-H), 10.61 (s, 1H, NHCO). LC-MS (ESI) analysis (*m/z*) calcd for C₈H₁₁N₅O (193.21): found 194.2 [M+H]⁺, 216.0 [M+Na]⁺.

6-amino-2-neopentyl-2H-pyrazolo[3,4-d]pyrimidin-4(5H)-one (79): Yield: 24%; white solid, mp >300 °C; ¹H NMR (400 MHz, DMSO-*d*₆): δ 0.97 (s, 9H, 3CH₃), 3.96 (s, 2H, CH₂), 6.18 (s, 2H, NH₂), 8.23 (s, 1H, pyrazole-H), 10.40 (s, 1H, NHCO). LC-MS (ESI) analysis (*m/z*) calcd for C₁₀H₁₅N₅O (221.26): found 222.3 [M+H]⁺, 244.3 [M+Na]⁺.

6-amino-2-phenethyl-2H-pyrazolo[3,4-d]pyrimidin-4(5H)-one (80): Yield: 27%; white solid, mp >300 °C; ¹H NMR (400 MHz, DMSO-*d*₆): δ 3.13 (t, *J*=7.12 Hz, 2H, CH₂), 4.35 (t, *J*=7.12 Hz, 2H, CH₂), 6.17 (s, 2H, NH₂), 7.15-7.29 (m, 5H, Ar-H), 8.07 (s, 1H, pyrazole-H), 10.33 (s, 1H, NHCO). LC-MS (ESI) analysis (*m/z*) calcd for C₁₃H₁₃N₅O (255.28): found 256.0 [M+H]⁺, 278.0 [M+Na]⁺.

3.3.2.6 General procedure for synthesis of 3-amino-1-(alkyl or aralkyl)-1H-pyrazole-4-carboxamide (85-88). Carbonitriles **65-68** (0.03 mol) were dissolved in 7 mL conc.H₂SO₄ at 0°C and stirred at room temperature for 5 h. Then the reaction mixture was poured into ice cold water and neutralized to pH 7 with 28% NH₃ solution. The white precipitate was formed which was further washed with cold water and dried under vacuum to obtain the desired products (**85-88**) as solids.

3-amino-1-methyl-1H-pyrazole-4-carboxamide (85): Yield: 83%; white solid, mp 155-157 °C; ¹H NMR (400 MHz, DMSO-*d*₆): δ 3.50 (s, 3H, N-CH₃), 6.12 (s, 2H, NH₂), 6.64 (br s, 1H, NH), 7.16 (br s, 1H, NH), 7.60 (s, 1H, pyrazole-H). LC-MS (ESI) analysis (*m/z*) calcd for C₅H₈N₄O (140.14): found 140.9 [M+H]⁺.

3-amino-1-isopropyl-1H-pyrazole-4-carboxamide (86): Yield: 85%; white solid, mp 159-161 °C; ¹H NMR (400 MHz, DMSO-*d*₆): δ 1.34 (d, *J*= 6.52 Hz, 6H, 2CH₃), 4.18 (sep, *J*=6.64 Hz, 1H, CH), 5.33 (s, 2H, NH₂), 6.69 (br s, 1H, NH), 7.16 (br s, 1H, NH), 7.94 (s, 1H, pyrazole-H). LC-MS (ESI) analysis (*m/z*) calcd for C₇H₁₂N₄O (168.20): found 169.0 [M+H]⁺.

3-amino-1-neopentyl-1H-pyrazole-4-carboxamide (87): Yield: 78%; white solid, mp 161-163 °C; ¹H NMR (400 MHz, DMSO-*d*₆): δ 0.90 (s, 9H, 3CH₃), 3.64 (s, 2H, CH₂), 5.32 (s, 2H, NH₂), 6.72 (br s, 1H, NH), 7.21 (br, 1H, NH), 7.85 (s, 1H, pyrazole-H). LC-MS (ESI) analysis (*m/z*) calcd for C₉H₁₆N₄O (196.25): found 197.1 [M+H]⁺.

3-amino-1-phenethyl-1H-pyrazole-4-carboxamide (88): Yield: 90%; white solid, mp 166-168 °C; ¹H NMR (400 MHz, DMSO-*d*₆): δ 3.08 (t, *J*=7.16 Hz, 2H, CH₂), 4.12 (t, *J*=7.16 Hz, 2H, CH₂), 5.44 (s, 2H, NH₂), 6.24 (br s, 1H, NH), 6.73 (br s, 1H, NH), 7.19-7.35 (m, 5H, Ar-H), 7.80 (s, 1H, pyrazole-H). LC-MS (ESI) analysis (*m/z*) calcd for C₁₂H₁₄N₄O (230.27): found 231.0 [M+H]⁺, 254.3[M+Na]⁺.

3.3.2.7 General procedure for synthesis of 3-(3-benzoylthioureido)-1-(alkyl or aralkyl)-1H-pyrazole-4-carboxamide (89-92). To a solution of carboxamides **85-88** (0.015 mol) in dry acetone (10 mL), benzoyl isothiocyanate (0.0165 mol, 1.1 equiv) was added and refluxed at 60°C for 12 h. The reaction mixture was cooled. The resulting yellow solid was filtered, washed with acetone and dried under vacuum. The crude product was further recrystallized from methanol to obtain the desired products (**89-92**) as solids.

3-(3-benzoylthioureido)-1-methyl-1H-pyrazole-4-carboxamide (89): Yield: 61%; yellow solid, mp 218-220 °C; ¹H NMR (400 MHz, DMSO-*d*₆): δ 3.61 (s, 3H, N-CH₃), 7.17 (br s, 1H, NH), 7.46-7.60 (m, 5H, Ar-H), 7.73 (d, *J*= 7.04 Hz, 2H, CONH₂), 7.78 (s, 1H, pyrazole-H), 11.47 (br s, 1H, NH). LC-MS (ESI) analysis (*m/z*) calcd for C₁₃H₁₃N₅O₂S (303.34): found 304.0 [M+H]⁺.

3-(3-benzoylthioureido)-1-isopropyl-1H-pyrazole-4-carboxamide (90): Yield: 63%; yellow solid, mp 212-214 °C; ¹H NMR (400 MHz, DMSO-*d*₆): 1.42 (d, *J*= 5.76 Hz, 6H, 2CH₃), 4.44-4.50 (m, 1H, CH), 7.07 (br, 1H, NH), 7.58-7.68 (m, 5H, Ar-H), 8.00 (d, *J*=6.8 Hz, 2H, CONH₂), 8.31 (s, 1H,

pyrazole-H), 11.06 (br s, 1H, NH). LC-MS (ESI) analysis (m/z) calcd for $C_{15}H_{17}N_5O_2S$ (331.39): found 332.0 $[M+H]^+$.

3-(3-benzoylthioureido)-1-neopentyl-1H-pyrazole-4-carboxamide (91):

Yield: 60%; yellow solid, mp 215-217 °C; 1H NMR (400 MHz, DMSO- d_6): δ 0.91 (s, 9H, 3CH₃), 3.91 (s, 2H, CH₂), 7.09 (br s, 1H, NHCO), 7.57-7.70 (m, 5H, Ar-H), 8.00 (d, $J= 7.52$ Hz, 2H, CONH₂), 8.18 (br s, 1H, pyrazole-H). LC-MS (ESI) analysis (m/z) calcd for $C_{17}H_{21}N_5O_2S$ (359.45): found 360.2 $[M+H]^+$.

3-(3-benzoylthioureido)-1-phenethyl-1H-pyrazole-4-carboxamide (92):

Yield: 71%; yellow solid, mp 208-210 °C; 1H NMR (400 MHz, DMSO- d_6): δ 3.11 (br s, 2H, CH₂), 4.34 (br s, 2H, CH₂), 7.08-7.27 (m, 5H, Ar-H), 7.37-7.69 (m, 5H, Ar-H), 7.99 (d, $J= 7.04$ Hz, 2H, CONH₂), 8.01 (s, 1H, pyrazole-H), 11.51 (br s, 1H, NHCO), 12.7 (br s, 1H, NH). LC-MS (ESI) analysis (m/z) calcd for $C_{20}H_{19}N_5O_2S$ (393.46): found 393.9 $[M+H]^+$.

3.3.2.8 General procedure for synthesis of (E)-methyl N'-benzoyl-N-(4-carbamoyl-1-(alkyl or aralkyl)-1H-pyrazol-3-yl) carbamimidothioate (93-96). To a solution of benzoylthioureidos **89-92** (0.003 mol) in 10 mL of 0.1 N NaOH, methyl iodide (0.0036 mol, 1.2 equiv) was added at room temperature and the resulting mixture was stirred for 3 h. The white suspension was observed and it was adjusted to pH 6 with glacial acetic acid. The white precipitate was obtained, which was filtered and washed with cold water and finally dried under vacuum to obtain the desired products (**93-96**) as solids.

(E)-methyl-N'-benzoyl-N-(4-carbamoyl-1-methyl-1H-pyrazol-3-yl)

carbamimidothioate (93): Yield: 75%; white solid, mp 196-198 °C; 1H NMR (400 MHz, DMSO- d_6): δ 2.44 (s, 3H, SCH₃), 3.57 (s, 3H, N-CH₃), 6.99-7.52 (m, 5H, Ar-H), 7.70 (br s, 1H, pyrazole-H), 7.78 (d, $J= 4.76$ Hz, 2H, CONH₂), 11.52 (br s, 1H, NH). LC-MS (ESI) analysis (m/z) calcd for $C_{14}H_{15}N_5O_2S$ (317.37): found 318.1 $[M+H]^+$.

(E)-methyl-N'-benzoyl-N-(4-carbamoyl-1-isopropyl-1H-pyrazol-3-yl)

carbamimidothioate (94): Yield: 67%; white solid, mp 223-225 °C; 1H NMR (400 MHz, DMSO- d_6): 1.45 (d, $J=6.52$ Hz, 6H, 2CH₃), 2.42 (s, 3H, SCH₃), 4.59 (br s, 1H, CH), 7.39-7.91(m, 5H, Ar-H), 8.02 (d, $J= 5.92$ Hz, 2H,

CONH₂), 8.25 (s, 1H, pyrazole-H), 13.09 (br s, 1H, NH). LC-MS (ESI) analysis (*m/z*) calcd for C₁₆H₁₉N₅O₂S (345.42): found 346.0 [M+H]⁺.

(E)-methyl-N'-benzoyl-N-(4-carbamoyl-1-neopentyl-1H-pyrazol-3-yl)

carbamimidothioate (95) : Yield: 56%; white solid, mp 219-221 °C; ¹H NMR (400 MHz, DMSO-*d*₆): δ 0.89 (s, 9H, 3CH₃), 2.42 (s, 3H, SCH₃), 4.02 (s, 2H, CH₂), 7.40-7.95 (m, 5H, Ar-H), 8.02 (d, *J*= 7.40 Hz, 2H, CONH₂), 8.17 (s, 1H, pyrazole-H). LC-MS (ESI) analysis (*m/z*) calcd for C₁₈H₂₃N₅O₂S (373.47): found 374.1 [M+H]⁺, 396.2 [M+Na]⁺.

(E)-methyl-N'-benzoyl-N-(4-carbamoyl-1-phenethyl-1H-pyrazol-3-yl)

carbamimidothioate (96) : Yield: 63%; white solid, mp 235-237 °C; ¹H NMR (400 MHz, DMSO-*d*₆): δ 2.42 (s, 3H, SCH₃), 3.13 (t, *J*=7.04 Hz, 2H, CH₂), 4.45 (t, *J*=6.64 Hz, 2H, CH₂), 7.12-7.25 (m, 5H, Ar-H), 7.40-7.88 (m, 5H, acyl-H), 8.03 (d, *J*= 7.16 Hz, 2H, CONH₂), 8.14 (s, 1H, pyrazole-H), 13.12 (br s, 1H, NH). LC-MS (ESI) analysis (*m/z*) calcd for C₂₁H₂₁N₅O₂S (407.49): found 408.2 [M+H]⁺, 430.2 [M+Na]⁺.

3.3.2.9 General procedure for synthesis of (Z)-3-(2-benzoylguanidino)-1-(alkyl or aralkyl)-1H-pyrazole-4-carboxamide (97-100).

Carbamimidothioate derivatives **93-96** (0.003 mol) were dissolved in dry DMF (5 mL) containing 2% ammonia (5 ml) and heated to 120°C for 3 h in a sealed tube. At the end of the reaction the odor of methyl mercaptan was recognized, cooled and poured over ice water mixture. The resulting white precipitate was washed with water and dried under vacuum to obtain the desired products (**97-100**) as solids.

(Z)-3-(2-benzoylguanidino)-1-methyl-1H-pyrazole-4-carboxamide (97):

Yield: 53%; white solid, mp >300 °C; Insoluble.

(Z)-3-(2-benzoylguanidino)-1-isopropyl-1H-pyrazole-4-carboxamide (98):

Yield: 62%; white solid, mp >300 °C; Insoluble.

(Z)-3-(2-benzoylguanidino)-1-neopentyl-1H-pyrazole-4-carboxamide (99):

Yield: 56%; white solid, mp >300 °C; Insoluble.

(Z)-3-(2-benzoylguanidino)-1-phenethyl-1H-pyrazole-4-carboxamide

(100): Yield: 53%; white solid, mp >300 °C; Insoluble.

3.3.2.10 General procedure for synthesis of 6-amino-2-(alkyl or aralkyl)-2H-pyrazolo[3,4-d]pyrimidin-4(5H)-one (77-80). A suspension of benzoylguanidino derivatives **97-100** (0.0035 mol) in 1N NaOH (10 mL) was refluxed at 110°C for 12 h. The resulting milky white mixture was adjusted to pH 6 with acetic acid. A mixture of benzoic acid and free amine derivatives were obtained which was washed with water and dried. Finely divided powder was suspended in hot ethanol with stirring to remove benzoic acid and filtered hot. The resulting ethanolic portion was evaporated to dryness to obtain a pure desired product (**77-80**) as white solid.

6-amino-2-methyl-2H-pyrazolo[3,4-d]pyrimidin-4(5H)-one (77): Yield: 72%; white solid. ¹H NMR (400 MHz, DMSO-*d*₆): δ 3.69 (s, 3H, N-CH₃), 6.64 (s, 2H, NH₂), 7.73 (s, 1H, pyrazole-H), 10.49 (s, 1H, NHCO).

6-amino-2-isopropyl-2H-pyrazolo[3,4-d]pyrimidin-4(5H)-one (78): Yield: 75%; white solid. ¹H NMR (400 MHz, DMSO-*d*₆): δ 1.45 (d, *J*= 6.52 Hz, 6H, 2CH₃), 4.53 (sep, *J*= 6.52 Hz, 1H, CH), 7.66 (s, 2H, NH₂), 8.13 (s, 1H, pyrazole-H), 10.63 (s, 1H, NHCO).

6-amino-2-neopentyl-2H-pyrazolo[3,4-d]pyrimidin-4(5H)-one (79): Yield: 68%; white solid. ¹H NMR (400 MHz, DMSO-*d*₆): δ 0.97 (s, 9H, 3CH₃), 3.71 (s, 2H, CH₂), 6.25 (s, 2H, NH₂), 7.68 (s, 1H, pyrazole-H).

6-amino-2-phenethyl-2H-pyrazolo[3,4-d]pyrimidin-4(5H)-one (80): Yield: 81%; white solid. ¹H NMR (400 MHz, DMSO-*d*₆): δ 3.13 (t, *J*=6.92 Hz, 2H, CH₂), 4.35 (t, *J*=7.16 Hz, 2H, CH₂), 6.15 (s, 2H, NH₂), 7.16-7.29 (m, 5H, Ar-H), 8.07 (s, 1H, pyrazole-H), 10.30 (s, 1H, NHCO).

3.3.2.11 General procedure for synthesis of 4-chloro-2-(alkyl or aralkyl)-2H-pyrazolo[3,4-d]pyrimidin-6-amine (81-84). A mixture of 6-amino-2-(alkyl or aralkyl)-2H-pyrazolo[3,4-d]pyrimidin-4(5H)-ones (**77-80**) (0.005 mol), phosphoryl trichloride (0.1 mol, 20 equiv) and N-N dimethylamine (0.005 mol, 1 equiv) was refluxed at 110°C for 24 h. Then the reaction mixture was cooled and the excess phosphoryl chloride was removed under reduced pressure. The resulting red oil was poured onto ice mixture slowly, stirred for 10 min. The aqueous part was extracted with EtOAc (3x10ml). The combined organic layers were dried over Na₂SO₄, filtered, and the solvent was removed under reduced pressure to give a oily residue which was purified by

column chromatography eluting with a mixture of hexane/ethyl acetate (5:5) to obtain pale yellow solids as desired products (**81-84**).

4-chloro-2-methyl-2H-pyrazolo[3,4-d]pyrimidin-6-amine (81): Yield: 65%; pale yellow solid, mp 247-249 °C; ¹H NMR (400 MHz, DMSO-*d*₆): δ 3.99 (s, 3H, N-CH₃), 6.91 (s, 2H, NH₂), 8.43 (s, 1H, pyrazole-H). ¹³C NMR (400 MHz, DMSO-*d*₆): δ 33.9 (N-CH₃), 106.5(C), 132.2 (CH-pyrazole), 153.9(C-Cl), 156.1(C-NH₂), 161.8(N-C-N). LC-MS (ESI) analysis (*m/z*) calcd for C₆H₆ClN₅ (183.60): found 184.3 [M+H]⁺, 206.1 [M+Na]⁺. HPLC purity (254 nm); eluent 1: 98.2%, ^tR = 2.2 min, eluent 2: 99.6%, ^tR = 2.5 min.

4-chloro-2-isopropyl-2H-pyrazolo[3,4-d]pyrimidin-6-amine (82): Yield: 67%; pale yellow solid, mp 151-153 °C; ¹H NMR (400 MHz, DMSO-*d*₆): δ 1.48 (d, *J* = 6.64 Hz, 6H, 2CH₃), 4.53 (sep, *J* = 6.52 Hz, 1H, CH), 6.19 (s, 2H, NH₂), 8.30 (s, 1H, pyrazole-H). ¹³C NMR (400 MHz, DMSO-*d*₆): δ 22.0 (CH₃), 48.5 (CH-alkyl), 106.7 (C), 132.1 (CH-pyrazole), 153.8 (C-Cl), 155.2 (C-NH₂), 166.6 (N-C-N-). LC-MS (ESI) analysis (*m/z*) calcd for C₈H₁₀ClN₅ (211.65): found 212.1 [M+H]⁺, HPLC purity (254 nm); eluent 1: 96.8%, ^tR = 3.3min, eluent 2: 99.5%, ^tR = 3.2 min.

4-chloro-2-neopentyl-2H-pyrazolo[3,4-d]pyrimidin-6-amine (83): Yield: 77%; pale yellow solid, mp 154-156 °C; ¹H NMR (400 MHz, DMSO-*d*₆): δ 0.96 (s, 9H, 3CH₃), 4.01 (s, 2H, CH₂), 7.29 (s, 2H, NH₂), 8.02 (s, 1H, pyrazole-H). ¹³C NMR (400 MHz, DMSO-*d*₆): δ 28.2 (CH₃), 33.8 (C-alkyl), 57.4 (CH₂), 106.2 (C), 132.2 (CH-pyrazole), 153.9 (C-Cl), 156.9 (C-NH₂), 161.9 (N-C-N-). LC-MS (ESI) analysis (*m/z*) calcd for C₁₀H₁₄ClN₅ (239.70): found 240.0[M+H]⁺. HPLC purity (254 nm); eluent 1: 100%, ^tR = 6.0 min, eluent 2: 99.5%, ^tR = 6.3 min.

4-chloro-2-phenethyl-2H-pyrazolo[3,4-d]pyrimidin-6-amine (84): Yield: 72%; pale yellow solid, mp 146-148 °C; ¹H NMR (400 MHz, DMSO-*d*₆): δ 3.13 (t, *J* = 5.56 Hz, 2H, CH₂), 4.40 (t, *J* = 6.04 Hz, 2H, CH₂), 7.13 - 7.26 (m, 5H, Ar-H), 7.28 (s, 2H, NH₂), 7.99 (s, 1H, pyrazole-H). ¹³C NMR (400 MHz, DMSO-*d*₆): δ 35.0(CH₂), 47.9 (N-CH₂), 106.5 (C), 126.8 (CH), 128.8 (CH), 129.0 (CH), 132.5 (CH-pyrazole), 138.6 (CH), 153.8 (C-Cl), 156.1 (C-NH₂), 161.8 (N-C-N-). LC-MS (ESI) analysis (*m/z*) calcd for C₁₃H₁₂ClN₅ (273.72): found 272.0 [M-H]⁺. HPLC purity (254 nm); eluent 1: 99.3%, ^tR = 5.5 min, eluent 2: 99.5%, ^tR = 5.8 min.

3.3.2.12 General procedure for synthesis of N-(4-chloro-2(alkyl or aralkyl)-2H-pyrazolo[3,4-*d*]pyrimidin-6-yl) benzamide (101-104, 105-108, 109-112, 113-116). To a suspension of 4-chloro-2-(alkyl or aralkyl)-2H-pyrazolo[3,4-*d*]pyrimidin-6-amines **81-84** (0.001 mol) in toluene, diisopropylethylamine (0.002 mol, 2 equiv) and benzoyl chloride or substituted benzoyl chlorides (0.002 mol, 2 equiv) were added. The mixture was heated under reflux at 120°C for 24 hours. The solvent was removed under reduced pressure and the resulting residue was purified by column chromatography (hexane: EtOAc, 5:5) to obtain the desired products (**101-104, 105-108, 109-112, 113-116**) as solids.

N-(4-chloro-2-methyl-2H-pyrazolo[3,4-*d*]pyrimidin-6-yl)benzamide (101): Yield: 36%; White solid, mp 165-167 °C; ¹H NMR (400 MHz, DMSO-*d*₆): δ 3.99 (s, 3H, N-CH₃), 7.51-7.64 (m, 3H, Ar-H), 7.99 (d, *J*= 7.52 Hz, 2H, Ar-H), 8.34 (s, 1H, pyrazole-H), 11.42 (s, 1H, NH). ¹³C NMR (400 MHz, DMSO-*d*₆): δ 34.6 (N-CH₃), 103.2 (C), 129.0 (CH), 129.7 (CH), 132.6 (CH-pyrazole), 133.3 (CH), 134.9 (C), 150.2 (C-Cl), 152.5 (N-C-N), 156.6 (C-NH), 169.8 (CO). LC-MS (ESI) analysis (*m/z*) calcd for C₁₃H₁₀ClN₅O (287.70): found 288.1 [M+H]⁺, 310.1 [M+Na]⁺. HPLC purity (254 nm); eluent 1: 97.8 %, ^tR = 2.9 min, eluent 2: 100 %, ^tR = 3.0 min.

N-(4-chloro-2-methyl-2H-pyrazolo[3,4-*d*]pyrimidin-6-yl)-4-fluorobenzamide (102): Yield: 43%; White solid, mp 140-142 °C; ¹H NMR (400 MHz, DMSO-*d*₆): δ 3.99 (s, 3H, N-CH₃), 7.33-7.37 (m, 2H, Ar-H), 8.05-8.09 (m, 2H, Ar-H), 8.35 (s, 1H, pyrazole-H), 11.46 (s, 1H, NH). LC-MS (ESI) analysis (*m/z*) calcd for C₁₃H₉ClFN₅O (305.69): found 306.1 [M+H]⁺, 328.3 [M+Na]⁺. HPLC purity (254 nm); eluent 1: 99.4%, ^tR = 3.3 min, eluent 2: 96.6%, ^tR = 3.7 min.

N-(4-chloro-2-methyl-2H-pyrazolo[3,4-*d*]pyrimidin-6-yl)-4-(trifluoromethyl)benzamide (103): Yield: 57%; White solid, mp 145-147 °C; ¹H NMR (400 MHz, DMSO-*d*₆): δ 3.98 (s, 3H, N-CH₃), 7.88-7.91 (m, 2H, Ar-H), 8.15-8.17 (m, 2H, Ar-H), 8.35 (s, 1H, pyrazole-H), 11.67 (s, 1H, NH). LC-MS (ESI) analysis (*m/z*) calcd for C₁₄H₉ClF₃N₅O (355.70): found 356.2 [M+H]⁺, 378.2 [M+Na]⁺. HPLC purity (254 nm); eluent 1: 99.8%, ^tR = 5.7 min, eluent 2: 99.6%, ^tR = 5.6 min.

N-(4-chloro-2-methyl-2H-pyrazolo[3,4-d]pyrimidin-6-yl)-4-

methylbenzamide (104): Yield: 42%; White solid, mp 149-151 °C; ¹H NMR (400 MHz, DMSO-*d*₆): δ 2.39 (s, 3H, CH₃), 3.99 (s, 3H, N-CH₃), 7.31-7.93 (m, 4H, Ar-H), 8.33 (s, 1H, pyrazole-H), 11.32 (s, 1H, NH). LC-MS (ESI) analysis (*m/z*) calcd for C₁₄H₁₂ClN₅O (301.73): found 302.0 [M+H]⁺. HPLC purity (254nm); eluent 1: 99.4 %, ^tR = 3.8 min, eluent 2: 99.5 %, ^tR = 3.7 min.

N-(4-chloro-2-isopropyl-2H-pyrazolo[3,4-d]pyrimidin-6-yl)benzamide

(105): Yield: 28%; White solid, mp 151-153 °C; ¹H NMR (400 MHz, DMSO-*d*₆): δ 1.50 (d, *J* = 6.76 Hz, 6H, 2CH₃), 5.01 (sep, *J* = 6.52 Hz, 1H, CH), 7.51-7.99 (m, 5H, Ar-H), 8.35 (s, 1H, pyrazole-H), 11.39 (s, 1H, NH). LC-MS (ESI) analysis (*m/z*) calcd for C₁₅H₁₄ClN₅O (315.76): found 316.2 [M+H]⁺, 338.3 [M+Na]⁺. HPLC purity (254nm); eluent 1: 100%, ^tR = 4.2, eluent 2: 100.0%, ^tR = 4.6 min.

N-(4-chloro-2-isopropyl-2H-pyrazolo[3,4-d]pyrimidin-6-yl)-4-

fluorobenzamide (106): Yield: 40%; White solid, mp 120-122 °C; ¹H NMR (400 MHz, DMSO-*d*₆): δ 1.51 (d, *J* = 6.76 Hz, 6H, 2CH₃), 5.02 (sep, *J* = 6.76Hz, 1H, CH), 7.48-7.85 (m, 4H, Ar-H), 8.37 (s, 1H, pyrazole-H), 11.49 (s, 1H, NH). ¹³C NMR (400 MHz, DMSO-*d*₆): δ 22.0 (CH₃), 48.5 (CH-alkyl), 106.8 (C), 116.2 (CH), 132.1 (CH), 132.5 (C), 134.3 (CH-pyrazole), 153.8 (C-Cl), 154.9 (N-C-N), 158.2 (C-NH), 161.6 (C-F), 166.8 (CO). LC-MS (ESI) analysis (*m/z*) calcd for C₁₅H₁₃ClFN₅O (333.75): found 334.2 [M+H]⁺, 356.3 [M+Na]⁺. HPLC purity (254 nm); eluent 1: 95.5%, ^tR = 4.2 min, eluent 2: 95.1%, ^tR = 4.7 min.

N-(4-chloro-2-isopropyl-2H-pyrazolo[3,4-d]pyrimidin-6-yl)-4-

(trifluoromethyl)benzamide (107): Yield: 38%; White solid, mp 146-148 °C; ¹H NMR (400 MHz, DMSO-*d*₆): δ 1.47 (d, *J* = 6.8 Hz, 6H, 2CH₃), 4.96 (sep, *J* = 6.64 Hz, 1H, CH), 7.86-8.15 (m, 4H, Ar-H), 8.35 (s, 1H, pyrazole-H), 11.65 (s, 1H, NH). LC-MS (ESI) analysis (*m/z*) calcd for C₁₆H₁₃ClF₃N₅O (383.76): found 384.2 [M+H]⁺, 406.2 [M+Na]⁺. HPLC purity (254nm); eluent 1: 99.6 %, ^tR = 7.3 min, eluent 2: 99.4%, ^tR = 7.2 min.

N-(4-chloro-2-isopropyl-2H-pyrazolo[3,4-d]pyrimidin-6-yl)-4-

methylbenzamide (108): Yield: 34%; White solid, mp 131-133 °C; ¹H NMR (400 MHz, DMSO-*d*₆): δ 1.50 (d, *J* = 6.64 Hz, 6H, 2CH₃), 2.39 (s, 3H, CH₃),

5.00 (sep, $J = 6.64$ Hz, 1H, CH), 7.32 (d, $J = 8.04$ Hz, 2H, Ar-H), 7.91 (d, $J = 8.12$ Hz, 2H, Ar-H), 8.34 (s, 1H, pyrazole-H), 11.31 (s, 1H, NH). LC-MS (ESI) analysis (m/z) calcd for $C_{16}H_{16}ClN_5O$ (329.78): found 330.2 $[M+H]^+$, 352.1 $[M+Na]^+$. HPLC purity (254 nm); eluent 1: 95.7%, $t_R = 5.2$ min, eluent 2: 95.1%, $t_R = 5.9$ min.

N-(4-chloro-2-neopentyl-2H-pyrazolo[3,4-d]pyrimidin-6-yl)benzamide

(109): Yield : 44%; White solid, mp 135-137 °C; 1H NMR (400 MHz, DMSO- d_6): δ 0.95 (s, 9H, 3CH₃), 4.16 (s, 2H, CH₂), 7.51-8.0 (m, 5H, Ar-H), 8.38 (s, 1H, pyrazole-H), 11.38 (s, 1H, NH). ^{13}C NMR (400 MHz, DMSO- d_6): δ 28.1(CH₃), 33.8 (C-alkyl), 58.2 (CH₂), 110.0 (C), 128.8 (CH), 128.9 (CH), 132.5 (CH-pyrazole), 132.7 (CH), 134.5 (C), 154.1 (C-Cl), 155.2 (N-C-N), 155.3 (C-NH), 166.2 (CO). LC-MS (ESI) analysis (m/z) calcd for $C_{17}H_{18}ClN_5O$ (343.81): found 344.2 $[M+H]^+$, 366.3 $[M+Na]^+$. HPLC purity (254 nm); eluent 1: 97.8%, $t_R = 7.2$ min, eluent 2: 97.4%, $t_R = 7.9$ min.

N-(4-chloro-2-neopentyl-2H-pyrazolo[3,4-d]pyrimidin-6-yl)-4-

fluorobenzamide (110): Yield: 54%; White solid, mp 132-134 °C; 1H NMR (400 MHz, DMSO- d_6): δ 0.95 (s, 9H, 3CH₃), 4.15 (s, 2H, CH₂), 7.33-8.05 (m, 4H, Ar-H), 8.37 (s, 1H, pyrazole-H), 11.42 (s, 1H, NH). LC-MS (ESI) analysis (m/z) calcd for $C_{17}H_{17}ClFN_5O$ (361.80): found 362.2 $[M+H]^+$, 384.2 $[M+Na]^+$. HPLC purity (254nm); eluent 1: 98.3%, $t_R = 8.0$ min, eluent 2: 99.6%, $t_R = 8.4$ min.

N-(4-chloro-2-neopentyl-2H-pyrazolo[3,4-d]pyrimidin-6-yl)-4-

(trifluoromethyl)benzamide (111): Yield: 39%; White solid, mp 129-131 °C; 1H NMR (400 MHz, DMSO- d_6): δ 0.92 (s, 9H, 3CH₃), 4.10 (s, 2H, CH₂), 7.87-8.13 (m, 4H, Ar-H), 8.38 (s, 1H, pyrazole-H), 11.63 (s, 1H, NH). LC-MS (ESI) analysis (m/z) calcd for $C_{18}H_{17}ClF_3N_5O$ (411.81): found 412.3 $[M+H]^+$, 434.3 $[M+Na]^+$. HPLC purity (254 nm); eluent 1: 95.4%, $t_R = 10.9$ min, eluent 2: 98.1%, $t_R = 11.5$ min.

N-(4-chloro-2-neopentyl-2H-pyrazolo[3,4-d]pyrimidin-6-yl)-4-

methylbenzamide (112): Yield: 35%; White solid, mp 134-136 °C; 1H NMR (400 MHz, DMSO- d_6): δ 0.94 (s, 9H, 3CH₃), 2.36 (s, 3H, CH₃), 4.15 (s, 2H, CH₂), 7.28-7.91 (m, 4H, Ar-H), 8.34 (s, 1H, pyrazole-H), 11.28 (s, 1H, NH). LC-MS (ESI) analysis (m/z) calcd for $C_{18}H_{20}ClN_5O$ (357.84): found 358.3

[M+H]⁺, 380.2 [M+Na]⁺. HPLC purity (254 nm); eluent 1: 98.4%, ^tR = 8.3 min, eluent 2: 97.8%, ^tR = 8.5 min.

N-(4-chloro-2-phenethyl-2H-pyrazolo[3,4-d]pyrimidin-6-yl)benzamide

(113): Yield: 45%; White solid, mp 140-142 °C; ¹H NMR (400 MHz, DMSO-*d*₆): δ 3.23 (t, *J*= 7.28 Hz, 2H, CH₂), 4.60 (t, *J*= 7.04 Hz, 2H, CH₂), 7.17-7.26 (m, 5H, Ar-H), 7.51-7.99 (m, 5H, acyl-H), 8.34 (s, 1H, pyrazole-H), 11.39 (s, 1H, NH). ¹³C NMR (400 MHz, DMSO-*d*₆): δ 35.3 (CH₂), 48.3 (CH₂), 103.2 (C), 126.9 (CH), 128.8 (CH), 128.9 (CH), 129.03 (CH), 129.08 (CH), 132.6 (C), 133.7 (CH), 135.1 (CH-pyrazole), 138.6 (C), 150.1 (C-Cl), 152.4 (N-C-N), 156.6 (C-NH), 169.8(CO). LC-MS (ESI) analysis (*m/z*) calcd for C₂₀H₁₆ClN₅O (377.83): found 378.3 [M+H]⁺, 400.2 [M+Na]⁺. HPLC purity (254 nm); eluent 1: 99.7%, ^tR = 6.7 min, eluent 2: 99.5%, ^tR = 6.4 min.

N-(4-chloro-2-phenethyl-2H-pyrazolo[3,4-d]pyrimidin-6-yl)-4-

fluorobenzamide (114): Yield: 37 %; White solid, mp 127-129 °C; ¹H NMR (400 MHz, DMSO-*d*₆): δ 3.23 (t, *J*=7.44 Hz, 2H, CH₂), 4.61 (t, *J*= 7.04 Hz, 2H, CH₂), 7.15-7.19 (m, 5H, Ar-H), 7.22-7.26 (m, 2H, acyl-H), 8.05-8.08 (m, 2H, acyl-H), 8.35 (s, 1H, pyrazole-H), 11.43 (s, 1H,NH). LC-MS (ESI) analysis (*m/z*) calcd for C₂₀H₁₅ClFN₅O (395.82): found 396.3 [M+H]⁺, 418.3 [M+Na]⁺. HPLC purity (254nm); eluent 1: 99.6%, ^tR = 7.3 min, eluent 2: 95.8%, ^tR = 7.5 min.

N-(4-chloro-2-phenethyl-2H-pyrazolo[3,4-d]pyrimidin-6-yl)-4-

(trifluoromethyl)benzamide (115): Yield: 51%; White solid, mp 137-139 °C; ¹H NMR (400 MHz, DMSO-*d*₆): δ 3.20 (t, *J*= 7.28 Hz, 2H, CH₂), 4.59 (t, *J*= 7.16 Hz, 2H, CH₂), 7.16-7.25 (m, 5H, Ar-H), 7.86-8.15 (m, 4H, acyl-H), 8.34 (s,1H, pyrazole-H), 11.64 (s, 1H, NH). LC-MS (ESI) analysis (*m/z*) calcd for C₂₁H₁₅ClF₃N₅O (445.82): found 446.3 [M+H]⁺, 468.2 [M+Na]⁺. HPLC purity (254nm); eluent 1: 98.7%, ^tR = 9.2 min, eluent 2: 96.3%, ^tR = 9.0 min.

N-(4-chloro-2-phenethyl-2H-pyrazolo[3,4-d]pyrimidin-6-yl)-4-

methylbenzamide (116): Yield: 40 %; White solid, mp 131-133 °C; ¹H NMR (400 MHz, DMSO-*d*₆): δ 2.39 (s, 3H, CH₃), 3.22 (t, *J*= 7.16 Hz, 2H, CH₂), 4.60 (t, *J*= 7.04 Hz, 2H, CH₂), 7.17-7.25 (m, 5H, Ar-H), 7.31-7.91 (m, 4H, acyl-H), 8.33 (s, 1H, pyrazole-H), 11.29 (s, 1H,NH). LC-MS (ESI) analysis (*m/z*) calcd for C₂₁H₁₈ClN₅O (391.85): found 392.0 [M+H]⁺. HPLC purity (254 nm); eluent 1: 97.6%, ^tR = 6.9 min, eluent 2: 95.0%, ^tR = 6.9 min.

3.3.2.13 General procedure for synthesis of N-benzoyl-N-(4-chloro-2-(alkyl or aralkyl)-2H-pyrazolo[3,4-d]pyrimidin-6-yl) benzamide (117-120).

To a suspension of 4-chloro-2-(alkyl or aralkyl)-2H-pyrazolo[3,4-d]pyrimidin-6-amines **81-84** (0.001 mol) in toluene, diisopropylethylamine (0.004 mol, 4 equiv) and benzoyl chloride (0.004 mol, 4 equiv) were added. The mixture was heated under reflux for 18 hours. The solvent was removed under reduced pressure and the resulting residue was purified by column chromatography (hexane:EtOAc, 5:5) to obtain the desired products (**117-120**) as solids.

N-benzoyl-N-(4-chloro-2-methyl-2H-pyrazolo[3,4-d]pyrimidin-6-yl)benzamide (117): Yield : 61%; White solid, mp 163-165 °C; ¹H NMR (DMSO-*d*₆): δ 3.88 (s, 3H, N-CH₃), 7.53-7.89 (m, 10H, Ar-H), 8.53 (s, 1H, pyrazole-H). LC-MS (ESI) analysis (*m/z*) calcd for C₂₀H₁₄ClN₅O₂ (391.81): found 392.1 [M+H]⁺. HPLC purity (254 nm); eluent 1: 99.9%, ^tR = 4.5 min, eluent 2: 98.4%, ^tR = 4.8 min.

N-benzoyl-N-(4-chloro-2-isopropyl-2H-pyrazolo[3,4-d]pyrimidin-6-yl)benzamide (118): Yield : 57%; White solid, mp 153-155 °C; ¹H NMR (DMSO-*d*₆): δ 1.22 (d, *J*= 6.8 Hz, 6H, 2CH₃), 4.71 (sep, *J*= 6.64 Hz, 1H, CH), 7.48-7.83 (m, 10H, Ar-H), 8.45 (s, 1H, pyrazole-H). LC-MS (ESI) analysis (*m/z*) calcd for C₂₂H₁₈ClN₅O (419.86): found 421.3 [M+H]⁺, 442.3 [M+Na]⁺. HPLC purity (254nm); eluent 1: 99.4%, ^tR = 7.2 min, eluent 2: 97.6%, ^tR = 6.9 min.

N-benzoyl-N-(4-chloro-2-neopentyl-2H-pyrazolo[3,4-d]pyrimidin-6-yl)benzamide (119):Yield: 52%; White solid, mp 161-162 °C; ¹H NMR (400 MHz, DMSO-*d*₆): δ 0.61 (s, 9H, 3CH₃), 4.01 (s, 2H, CH₂), 7.48-7.83 (m, 10H, Ar-H), 8.52 (s, 1H, pyrazole-H). LC-MS (ESI) analysis (*m/z*) calcd for C₂₄H₂₂ClN₅O₂ (447.92): found 448.1[M+H]⁺, 470.1[M+Na]⁺. HPLC purity (254 nm); eluent 1: 100.0%, ^tR = 11.6 min, eluent 2: 99.1%, ^tR = 10.9 min.

N-benzoyl-N-(4-chloro-2-phenethyl-2H-pyrazolo[3,4-d]pyrimidin-6-yl)benzamide (120): Yield: 46%; White solid, mp 134-135 °C; ¹H NMR (400 MHz, DMSO-*d*₆): δ 2.79 (t, 7.0Hz, 3H, CH₃), 4.45 (t, *J*= 7.04 Hz, 2H, CH₂), 6.86-7.20 (m, 5H, Ar-H), 7.49-7.82 (m, 10H, acyl-H), 8.41 (s, 1H, pyrazole-H). LC-MS (ESI) analysis (*m/z*) calcd for C₂₇H₂₀ClN₅O₂ (481.93): found 482.1[M+H]⁺, 504.1[M+Na]⁺. HPLC purity (254 nm); eluent 1: 98.6%, ^tR = 12.3 min, eluent 2: 97.5%, ^tR = 11.6 min.

3.3.2.14 General procedure for synthesis of N-(4-chloro-2-(alkyl or aralkyl)-2H-pyrazolo[3,4-d]pyrimidin-6-yl)-2-phenylacetamide (121-124).

To a suspension of 4-chloro-2-(alkyl or aralkyl)-2H-pyrazolo[3,4-d]pyrimidin-6-amines **81-84** (0.001 mol) in toluene, diisopropylethylamine (0.002 mol, 2 equiv) and phenyl acetyl chloride (0.002 mol, 2 equiv) were added. The mixture was heated under reflux for 12 h. Subsequently, another 0.001 mol equivalent of diisopropylethylamine and phenyl acetyl chloride were added and refluxing continued for 12 h again. The solvent was then removed under reduced pressure and the resulting residue was purified by column chromatography (hexane: EtOAc, 5:5) to obtain the desired products (**121-124**) as solids.

N-(4-chloro-2-methyl-2H-pyrazolo[3,4-d]pyrimidin-6-yl)-2-phenylacetamide (121). Yield : 42%; White solid, mp 147-149 °C; ¹H NMR (DMSO-*d*₆): δ 3.83 (s, 2H, CH₂), 3.94 (s, 3H, N-CH₃), 7.25-7.34 (m, 5H, Ar-H), 8.29 (s, 1H, pyrazole-H), 11.23 (s, 1H, NH). LC-MS (ESI) analysis (*m/z*) calcd for C₁₄H₁₂ClN₅O (301.73): found 302.0 [M+H]⁺, 324.1 [M+Na]⁺. HPLC purity (254 nm); eluent 1: 96.2%, ^tR = 4.2 min, eluent 2: 99.4%, ^tR = 4.9 min.

N-(4-chloro-2-isopropyl-2H-pyrazolo[3,4-d]pyrimidin-6-yl)-2-phenylacetamide (122). Yield: 43%; White solid, mp 146-148 °C; ¹H NMR (DMSO-*d*₆): δ 1.47 (d, *J*= 6.76 Hz, 6H, 2CH₃), 3.84 (s, 2H, CH₂), 4.98 (sep, *J*= 6.64 Hz, 1H, CH), 7.25-7.34 (m, 5H, Ar-H), 8.30 (s, 1H, pyrazole-H), 11.21 (s, 1H, NH). LC-MS (ESI) analysis (*m/z*) calcd for C₁₆H₁₆ClN₅O (329.78): found 330.0 [M+H]⁺, 352.3 [M+Na]⁺. HPLC purity (254 nm); eluent 1: 99.5%, ^tR = 5.3 min, eluent 2: 95.1%, ^tR = 6.0 min.

N-(4-chloro-2-neopentyl-2H-pyrazolo[3,4-d]pyrimidin-6-yl)-2-phenylacetamide (123). Yield: 45%; White solid, mp 155-157 °C; ¹H NMR (DMSO-*d*₆): δ 0.93 (s, 9H, 3CH₃), 3.85 (s, 2H, aryl-CH₂), 4.12 (s, 2H, alkyl-CH₂), 7.24-7.34 (m, 5H, Ar-H), 8.33 (s, 1H, pyrazole-H), 11.19 (s, 1H, NH). LC-MS (ESI) analysis (*m/z*) calcd for C₁₈H₂₀ClN₅O (357.84): found 358.1 [M+H]⁺, 380.5 [M+Na]⁺. HPLC purity (254 nm); eluent 1: 98.3%, ^tR = 10.0 min, eluent 2: 99.3%, ^tR = 10.6 min.

N-(4-chloro-2-phenethyl-2H-pyrazolo[3,4-d]pyrimidin-6-yl)-2-phenylacetamide (124). Yield: 39%; White solid, mp 141-143 °C; ¹H NMR

(DMSO-*d*₆): δ 3.20 (t, J = 7.16 Hz, 2H, CH₂), 3.85 (s, 2H, CH₂), 4.57 (t, J = 6.88 Hz, 2H, CH₂), 7.12-7.22 (m, 5H, Ar-H), 7.25-7.35 (m, 5H, acyl-H), 8.30 (s, 1H, pyrazole-H), 11.17 (s, 1H, NH). LC-MS (ESI) analysis (m/z) calcd for C₂₁H₁₈ClN₅O (391.85): found 392.3 [M+H]⁺, 414.0 [M+Na]⁺. HPLC purity (254 nm); eluent 1: 99.5%, t_R = 7.9 min, eluent 2: 97.4%, t_R = 8.4 min.

3.3.3 X-ray crystallographic studies

Further, in order to confirm the N² alkyl(ar-alkyl) substitution, crystals of the compound **81** were grown by vapor diffusion of diethyl ether into a saturated solution of MeOH. The detailed key crystallographic parameters can be found in **Table A1 & A2** under Appendix. The X-ray crystallographic results confirmed the successful substitution of the substituent (methyl group) at N² position (**Figure 22**).

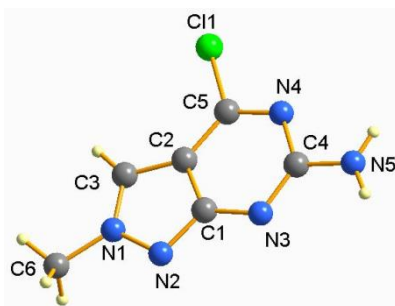


Figure 22. X-ray crystal structure of compound **81** (CCDC-937929). All the atoms are represented by spheres of arbitrary radii.

X-ray data were collected from Bruker AXS SMART APEX diffractometer using Mo-K α radiation at 223(2) K with the SMART suite of Programs.^[30] Lorentz and polarization effects and absorption effects of data were processed and corrected using softwares SAINT,^[31] SADABS^[32] respectively. Further SHELXTL suite of programs^[33] were used to carry out structural solution and refinement. The structure was solved by Direct Methods. Non-hydrogen atoms were located using difference maps and were given anisotropic displacement parameters in the final refinement. All H atoms were put at calculated positions using the riding model. **CCDC-937929** contains the supplementary crystallographic data.

3.3.4 Conclusion

The synthesis of 28 new 4-chloro-pyrazolopyrimidine derivatives was successfully achieved using optimized synthetic procedures as described above. All the final compounds and derivatives were confirmed by ^1H NMR, ^{13}C NMR and mass spectrometry (ESI). Additionally, final compounds **81-84** and derivatives **101, 106, 109 & 113** were confirmed by 2D NMR (HMQC). The purity of the compounds was determined by HPLC analysis (HPLC data of newly synthesized compounds **81-124** were tabulated in **Table A3** under appendix), and all of the compounds showed the purity of 95% and above, which were considered to be pure for biological evaluation.

3.4 Pharmacological Evaluation of a Novel Series of 4-Chloro-PyrazoloPyrimidine Derivatives

3.4.1 Introduction

The binding affinities of the novel series of pyrazolo[3,4-*d*]pyrimidines at the human A_1 , A_{2A} and A_3 adenosine receptor subtypes and the adenylyl cyclase activity of the derivatives at the human A_{2B} receptor are described in this chapter. In addition, the selectivities were also assessed by comparing the binding affinity values (K_i) against the hA_3 receptor with K_i values against the hA_1 and hA_{2A} receptors.

3.4.2 Binding affinity towards human A_1 , A_{2A} and A_3 adenosine receptors

The displacement of selective radioligands towards respective adenosine receptors (expressed in Chinese Hamster Ovary cells (CHO) for hA_1 , hA_{2A} , hA_3 receptors),¹⁵⁸⁻¹⁶⁰ was measured to evaluate the binding affinities of the synthesized compounds. There is inverse proportion for the amount of tested compounds against affinity of the compound for a particular receptor subtype (i.e. the lower is the amount of a compound required to displace the radioligands, the higher is the affinity of the compound). In this assay, the displacement of: (i) specific [^3H]CCPA ([^3H]-2-chloro-6-cyclopentyl adenosine) binding at the hA_1 receptors; (ii) specific [^3H]NECA ([^3H]-N-ethylcarboxamido adenosine) binding at the hA_{2A} receptors; (iii) [^3H]HEMADO ([^3H]-2-hexyn-1-yl-N(6)-methyl adenosine) at the hA_3

receptors were evaluated. The K_i (dissociation constant) value of the data was calculated from the Cheng and Prusoff equation ($K_i = IC_{50} / (1 + [C^*] / K_D^*)$), where $[C^*]$ denotes the concentration of the radioligand and K_D^* indicates the dissociation constant of the radio ligand),¹⁶¹ with the geometric means of at least 3 experiments, including 95% confidence intervals.

3.4.3 Adenylyl cyclase activity at human A_{2B} adenosine receptors

The potency of compounds **81-84 & 101-124** at the hA_{2B} receptor (expressed in CHO cells) was determined in adenylyl cyclase experiments, because of the lack of a suitable radioligand for hA_{2B} receptor in binding assay. The experiment was carried out through the procedure reported previously by Klotz *et al.* with some modifications.^{158, 159} In this assay, a known concentration of non-selective adenosine agonist, NECA, was subjected to inhibitory effect of tested compounds. Consequently, the activation of hA_{2B} receptor led to stimulation of adenylyl cyclase, followed by conversion of ATP into cAMP. When the antagonists bind to the hA_{2B} receptor, the stimulation of adenylyl cyclase induced by the agonist NECA is blocked, resulting in decrease of the cAMP production. Similarly, different levels of cAMP accumulation were obtained based on the different concentrations of tested compound. As mentioned earlier, Cheng and Prusoff equation was used to calculate the K_i values, which corresponded to the IC_{50} for each compound by applying geometric means of at least three experiments, including 95% confidence intervals.

3.4.4 Experimental Methods

3.4.4.1 Preparation of CHO membrane

The procedures for radioligand binding experiments, which involve pharmacological methods with membrane preparation, were performed as described in Klotz *et al.*¹⁵⁸ A two-step procedure was employed to prepare a membrane for radioligand binding from cells stably transfected with the human adenosine receptor subtypes (hA₁, hA_{2A}, hA_{2B} and hA₃ expressed on CHO cells). Firstly, using the low-speed step (1,000 x g for 4 min), the cell fragments and nuclei were removed, and then crude membrane fraction from the supernatant was sedimented at 100,000 x g for 30 min. Subsequently, the

membrane pellet was resuspended in the specific buffer, frozen in liquid nitrogen and stored at -80°C . However, one step centrifugation method was used for the measurement of the adenylyl cyclase activity, in which the homogenate was sedimented for about 30 min at $54,000 \times g$. Finally, the obtained crude membrane pellet was resuspended in 50 mM Tris/HCl, pH 7.4 and used for the adenylyl cyclase assay immediately.

3.4.4.2 Binding assay of human cloned A_1 , A_{2A} , A_3 adenosine receptor

Klotz *et al.* and Lohse *et al.* described the binding of [^3H]-CCPA to CHO cells transfected with the human recombinant A_1 adenosine receptors and subsequent binding assay was performed as reported.^{158, 159, 162} As per the procedure, displacement experiments were carried out for 3 h at 25°C in 200 μL of buffer containing 1 nM [^3H] CCPA, 0.2 U/mL adenosine deaminase, 20 μL of diluted membranes (50 μg of protein/assay) in 50 mM Tris/HCl, pH 7.4 and tested compounds in different concentrations. Similarly, 1 mM theophylline was used to determine the nonspecific binding. In the same manner, binding of [^3H]-NECA to CHO cells transfected with the human recombinant A_{2A} adenosine receptors was performed.^{158, 159} In this experiments, samples containing a protein concentration of 50 μg /assay in buffer, 30 nM [^3H]-NECA and assayed compound in different concentrations were incubated for 3 h at 25°C . Likewise, 100 μM R-PIA (R- N^6 -phenyl isopropyl adenosine) was used to determine the nonspecific binding.¹⁶⁰ Additionally, binding of [^3H]HEMADO to CHO cells transfected with the human recombinant A_3 adenosine receptors was carried out as described earlier.^{158, 159, 163} The displacement experiment was carried out for 3 h at 25°C in buffer solution containing 10 nM [^3H]-NECA, 20 μg membrane protein in 50mM Tris-HCl, 1 mM EDTA(ethylene diamino tetraacetate), 10 mM MgCl_2 , pH 8.25 and tested compound in different concentrations and non specific binding was determined in the presence of 100 μM R-PIA((R)- N^6 -phenyl isopropyl adenosine).¹⁶⁰ Moreover, filtration of assay mixture was carried out to separate bound and free radioactivity, through Whatman GF/B glass-fiber filters using a Micro-Mate 196-cell harvester (Packard Instrument Company). The filter bound radioactivity was calculated on Top Count (efficiency of 57%) with Micro-Scint 20. Lastly, the Bio-Rad method¹⁶⁴ using

bovine albumin as a reference standard was employed to measure the protein concentration.

3.4.4.3 Adenylyl cyclase activity assay

The potency of the compounds at hA_{2B} receptor (expressed in CHO cells) was determined in adenylyl cyclase experiments. All these experiments were performed as described previously with minor modifications.^{158, 159}

In this assay, the hA_{2B} receptor transfected with membranes were incubated with 100 nM NECA, followed by 150,000 cpm of [α -³²P]ATP and tested compounds in different concentrations were treated for 20 min in the incubation mixture as described^{158, 159} without EGTA (ethylene glycol tetraacetic acid) and NaCl. The IC₅₀ values were calculated for concentration-dependent inhibition of NECA-mediated adenylyl cyclase activity caused by antagonists.

3.4.4.4 Data analysis

In the assay, a non-linear curve fitting method implemented in the SCT-FIT program was used to calculate the 50% inhibition of binding of [³H]-CCPA and [³H]-NECA (IC₅₀) produced by concentration of the tested compounds, as described by De Lean *et al.*¹⁶⁰ This assay was performed with different concentrations of tested compounds, as triplicate experiment. In addition, the dissociation constant (K_i) values were calculated from IC₅₀ as per the Cheng and Prusoff equation.¹⁶¹ Moreover, a non-linear regression analysis using the equation for sigmoidal concentration-response curve was applied to calculate the IC₅₀ values of adenylyl cyclase activity assay. This experiment was performed with different concentrations of tested compounds, each performed in triplicate.

3.4.5 Results and Discussion

3.4.5.1 Structure-affinity relationships

Pharmacological evaluation was performed for the novel series of pyrazolo[3,4-*d*]pyrimidine to examine their binding affinities at all the four adenosine receptors. The receptor binding affinities of compounds **81-84** & **101-124** were determined at the human A₁, A_{2A}, A₃ receptors and the

corresponding adenylyl cyclase activity in CHO cells which expressed the human A_{2B} receptors are summarized in **Table 3**.

In this work, we proposed to modify our previously synthesized tricyclic pyrazolo[4,3-*e*]-1,2,4-triazolo-[1,5-*c*]-pyrimidines (PTPs)¹¹⁸ into a bicyclic pyrazolo[3,4-*d*]pyrimidine (PP) scaffold by considering the significance of simplified structures^{107, 145, 146} that can act as promising antagonists, hopefully with similar or even improved affinity and selectivity at the hA₃ receptor. Towards that purpose, a new series of 2-(alkyl and aralkyl substituted)-2*H*-pyrazolo[3,4-*d*]pyrimidines derivatives substituted at N², C⁶ and C⁴ position were successfully synthesized and characterized. The binding assay results indicated that the reported molecular simplification of the PTP structure, although with a remarkable drop (10000 fold decrease) in the K_i values, still enabled the binding at the hARs (**Table 3**). This result seems very promising, considering that the PP represents a much smaller scaffold which possesses low molecular weight (183-420) as compared to PTP (265-552) for the hA₃AR (The smaller scaffold compounds into a better range of mol.wt for an orally available compound). Indeed, most of the pyrazolo[3,4-*d*]pyrimidines were able to maintain moderate affinity at hA₃ receptors as indicated by the low micromolar range (1.5-33.5 μM) of K_i values but showed significant drop in selectivity towards the other receptor subtypes.

Effect of N² substitution on affinity of PP scaffold

To examine the impact of the alkyl group substitutions at N² position towards the pharmacological profile, we compared the binding assay results of the analogues bearing various alkyl substitutions (i.e. R= methyl, isopropyl & neopentyl) or a phenylethyl at this position. The alkyl substituents (methyl, isopropyl & neopentyl) at N² position (**Table 3**) of the pyrazolo ring were found to modulate the affinity at hA₃AR to a certain extent. Among them, N² isopropyl substituted analogues showed the lowest binding affinity (**105-108, 118 & 122**, with K_i hA₃ values between 6.7 and 27.1 μM, although with a few exceptions showing K_i hA₃>100 μM) towards A₃AR, followed by N² methyl substituted ligands (**101-104, 117 & 121**, with K_i hA₃ values in the 6.6-33.5 μM range).

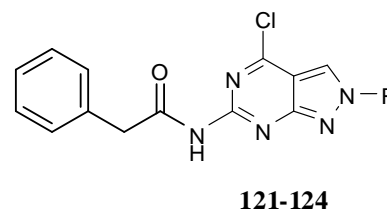
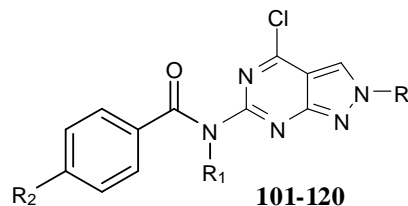
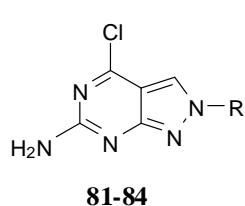
In contrast, N² isopropyl presented better hA_{2A} affinity (**105-108, 118 & 122**, with K_i hA_{2A} values between 0.8 and 4.7 μ M and K_i hA₃ values between 6.7 and >100 μ M). Interestingly, neopentyl substituted analogues (**109-112 & 119, 123**) exerted a relatively more favourable effect at the hA₃AR receptor, and also displayed a 6-7 fold increased affinity in comparison with the N² methyl derivatives. Among all the N² alkyl substituted derivatives, compound **112** showed the best affinity at the hA₃AR (K_i hA₃ = 5 μ M). Moreover, derivative **111 & 119** of the same series exhibited equal potency (**111**, K_i hA₃ = 6.6 μ M and **119**, K_i hA₃ = 6.5 μ M) and the highest selectivity towards other receptor subtypes (**hA₁/A₃>15; hA_{2A}/A₃ >15**).

In addition, the presence of a phenyl ethyl group at N² position resulted in a significant (8-10 fold) increase of hA₃ affinity (**113-116, 120 & 124**, K_i hA₃ values between 1.5 and 8.6 μ M) and better selectivity in comparison to the other N² alkyl counterparts (**101-112, 117-118 & 121-122**, K_i hA₃ = 5.0 - <100 μ M). This result indicates that the phenylethyl group at N² position played a more essential role in the binding at the hA₃ receptor; in fact, it suggests that the steric hindrance far from N² position is more favourable for the bulky phenylethyl group to orient itself inside the binding cavity, in comparison with steric hindrance in close proximity of N² position (i.e. methyl **81** & isopropyl **82**). However, these findings are in contrast with the PTP scaffold, where small substituents (e.g., CH₃) at N⁸ position are preferable than larger alkyl and arsubstituents.²⁷

Effect of C⁶ substitution on affinity of PP scaffold

Analogues bearing a free amino group at C⁶ position (**81-84**) showed no measurable affinity towards the hA₃ receptor (K_i hA₃ >100 μ M), while they showed better affinity towards the hA_{2A} (K_i hA_{2A} = 3.3-9.1 μ M) and the hA₁ receptor (K_i hA₁ = 4.3 - 29.7 μ M) subtypes. This was somehow expected, as it was already observed that PTPs with a free amino group at C⁵ position are able to bind A₁ and A_{2A} ARs better than A₃ARs. Therefore, further studies will assess the influence of acyl substitutions at the C⁶ position of PP to improve the hA₃ affinity.

Table 3. Binding affinity (K_i) of synthesized compounds at hA_1 , hA_{2A} , and hA_3 adenosine receptors^[a] and selectivity against hA_1 and hA_{2A} receptors (R denote N^2 position)



Com pound	R	R ₁	R ₂	K_i , μM (95% CI)				Selectivity	
				hA_1 ^[a]	hA_{2A} ^[c]	hA_{2B} ^[a]	hA_3 ^[c]	hA_1/A_3	hA_{2A}/A_3
81	CH ₃	-	-	29.7 (28.6-30.7)	9.1 (4.4-19.1)	>20	>100	> 0.29	>0.09
82	CH(CH ₃) ₂	-	-	9.0 (6.4-12.5)	3.3 (1.5-7.2)	>10	>100	>0.09	0.03
83	CH ₂ C(CH ₃) ₃	-	-	12.0 (10.6-13.7)	4.1 (2.2-7.6)	>10	>60	>0.2	>0.6
84	CH ₂ CH ₂ C ₆ H ₅	-	-	4.3 (2.9-6.4)	3.7 (3.4-4.1)	>20	>100	>0.04	>0.03
101	CH ₃	H	H	>100	24.2 (7.7-76.5)	>20	23.6 (15.8-35.4)	> 4.2	1.0
102	CH ₃	H	F	>100	20.5 (12.7-33.2)	>20	31.9 (25.7-39.6)	>3.1	0.6
103	CH ₃	H	CF ₃	>100	25.6 (16-41)	>20	33.5 (28.2-39.7)	>2.9	0.7
104	CH ₃	H	CH ₃	>100	12.0 (6.6-21.8)	>20	13.5 (5.8-31.2)	7.4	0.8

Com pound	R	R ₁	R ₂	K _i , μM (95% CI)				Selectivity	
				hA ₁ ^[b]	hA _{2A} ^[c]	hA _{2B} ^[d]	hA ₃ ^[e]	hA ₁ /A ₃	hA _{2A} / A ₃
105	CH(CH ₃) ₂	H	H	19.6 (19.3-20)	4.6 (1.8-11.8)	>20	12.8 (6.9-23)	1.5	0.3
106	CH(CH ₃) ₂	H	F	3.4 (3.41-3.47)	1.6 (0.85-3.29)	>20	>60	>0.05	> 0.02
107	CH(CH ₃) ₂	H	CF ₃	13.8 (9.3-20.3)	2.7 (1.8-4.1)	>20	10.3 (6.0-17.6)	1.3	0.2
108	CH(CH ₃) ₂	H	CH ₃	4.1 (2.3-7.4)	1.1 (0.66-2.0)	>20	>100	>0.04	0.01
109	CH ₂ C(CH ₃) ₃	H	H	11.0 (5.7-20.0)	3.5 (2.9-4.3)	≥10	30.3 (17.4-52.7)	0.3	0.1
110	CH ₂ C(CH ₃) ₃	H	F	16.5 (6.8-39.8)	2.2 (1.6-3.1)	>10	5.9 (3.0-11.4)	2.7	0.3
111	CH ₂ C(CH ₃) ₃	H	CF ₃	>100	>100	>20	6.6 (3.6-12.1)	>15	>15
112	CH ₂ C(CH ₃) ₃	H	CH ₃	11.1 (7.3-16.6)	2.1 (1.8-2.4)	>10	5.0 (4.6-5.4)	2.2	0.4
113	CH ₂ CH ₂ C ₆ H ₅	H	H	3.8 (2.2-6.5)	3.1 (2.3-4.3)	>20	8.6 (3.3-21.9)	0.4	0.3
114	CH ₂ CH ₂ C ₆ H ₅	H	F	2.7 (2.1-3.4)	2.06 (0.83-5.06)	>20	>100	0.02	0.02
115	CH ₂ CH ₂ C ₆ H ₅	H	CF ₃	>60	16.4 (8.3-32.6)	>20	2.8 (1.7-4.5)	>21.4	5.8
116	CH ₂ CH ₂ C ₆ H ₅	H	CH ₃	10.8 (9.5-12.1)	9.9 (9.3-15.5)	>20	1.5 (0.71-3.2)	7.2	6.6

Compound	R	R ₁	R ₂	K _i , μM (95% CI)				Selectivity	
				hA ₁ ^[b]	hA _{2A} ^[c]	hA _{2B} ^[d]	hA ₃ ^[e]	hA ₁ /A ₃	hA _{2A} /A ₃
117	CH ₃	C ₆ H ₅ CO	H	>60	17.5 (10.5-29.4)	>20	7.1 (6.2-8.1)	8.4	2.4
118	CH(CH ₃) ₂	C ₆ H ₅ CO	H	7.9 (7.6-8.1)	0.8 (0.61-1.2)	>20	6.7 (2.2-20.5)	1.1	0.1
119	CH ₂ C(CH ₃) ₃	C ₆ H ₅ CO	H	>100	~100	>100	6.5	>15.3	>15.3
120	CH ₂ CH ₂ C ₆ H ₅	C ₆ H ₅ CO	H	>100	5.4	>100	2.9	>34.5	2
121	CH ₃	-	-	16.3 (14-18.9)	29.9 (13-69.2)	>20	6.6 (2.6-16.9)	2.4	4.5
122	CH(CH ₃) ₂	-	-	1.9 (1.0-3.6)	4.7 (3.7-5.9)	>10	27.1 (18.5-39.7)	0.07	0.17
123	CH ₂ C(CH ₃) ₃	-	-	31.9 (26.4-38.6)	23.6 (9.5-58.2)	>20	10.9 (4.3-27.6)	2.9	2.1
124	CH ₂ CH ₂ C ₆ H ₅	-	-	6.5 (3.9-10.7)	8.6 (5.0-14.9)	>20	11.4 (7.4-17.5)	0.5	0.7

[a] Adenylyl cyclase activity of synthesized compounds at the hA_{2B}AR. [b] Displacement of specific [³H]-CCPA binding at human A₁ receptors expressed in Chinese hamster ovary (CHO) cells (n=3–6). [c] Displacement of specific [³H]-5'-Nethylcarboxamido adenosine (NECA) binding at human A_{2A} receptors expressed in CHO cells (n=3–6). [d] K_i values for inhibition of NECA-stimulated adenylyl cyclase activity in CHO cells (n=3–6). [e] Displacement of specific [³H]-2-(1-hexynyl)-N⁶-methyl adenosine (HEMADO) binding at human A₃ receptors expressed in CHO cells (n=3-6).

In addition, analogue **117**, bearing a dibenzoyl group at C⁶ position, displayed a moderate affinity at the hA₃ subtype (K_i hA₃=7.1 μM) and a 3 fold improvement in comparison with the mono-acylated analogue (**101**, with K_i hA₃=23.6 μM) and also retained the selectivity against the hA₁AR as compound **101**.

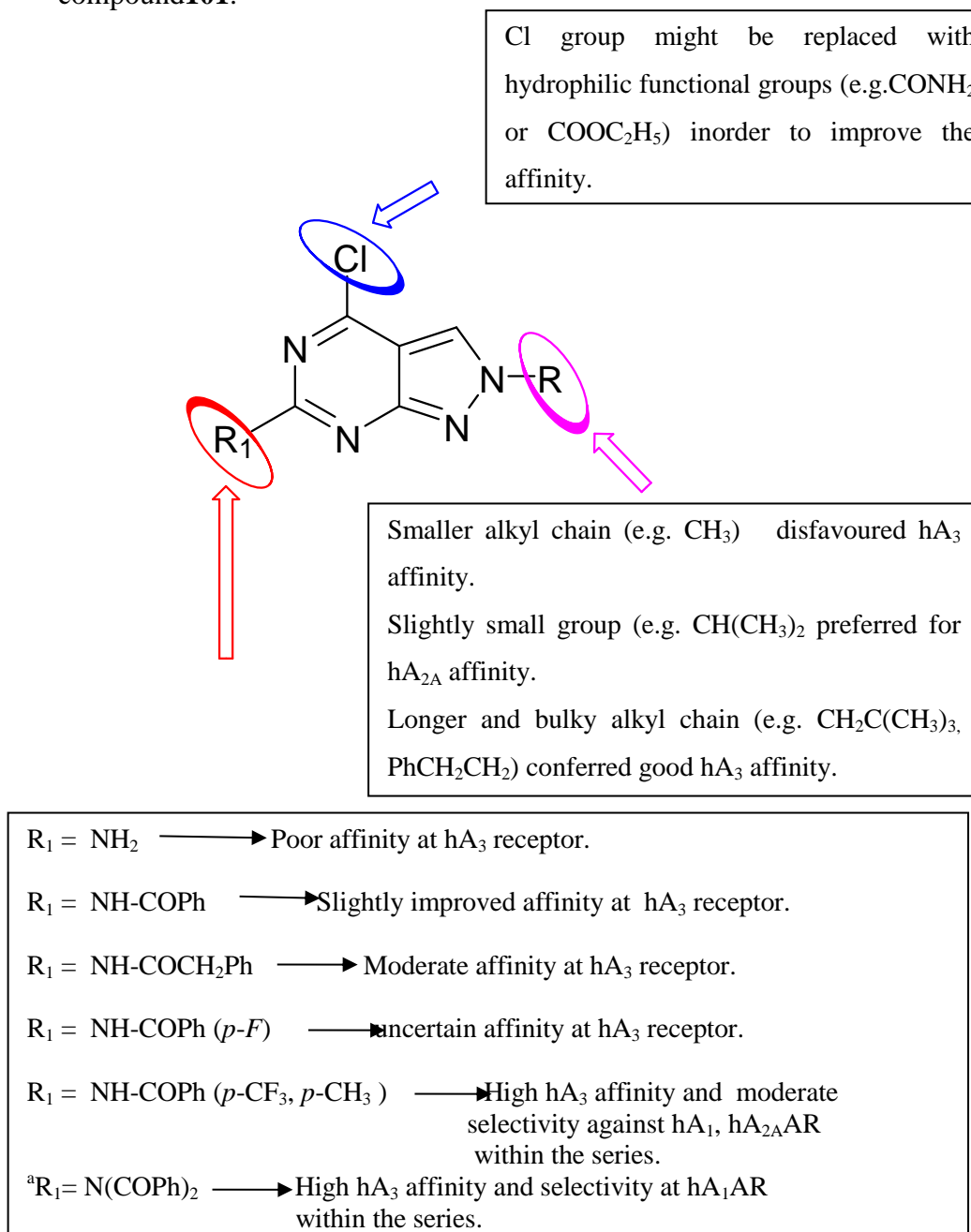


Figure 23. Overview of structure-affinity relationship (SAR) profile for the new series of 4-Chloro-PP derivatives **81-84 & 101-124**. ^aSpecific for N² phenylethyl substitution

This affinity was maintained when the C⁶ group was replaced by a slightly longer phenyl acetyl group (**121**, with K_i hA₃=6.6 μM). This indicates that binding cavity is spacious enough to accommodate the bulky diacyl group and longer phenylacetyl group at C⁶ position. In contrast, shorter chains like single benzoyl groups seemed less favourable.

As seen in **Table 3**, C⁶ acyl substituents of N²-isopropyl derivatives (**105-108**, **118** & **122**) shifted the affinity towards the hA_{2A} receptor; in fact the best result was observed for the di-acylated analogue (**118**, with K_i hA_{2A}=0.8 μM). This derivative was also about 7-8 times more selective towards the other receptor subtypes. Also, the presence of an additional electron donating methyl group at the *para* position of the C⁶-benzoyl substituent maintained the affinity (**108**, with K_i hA_{2A}=1.1 μM) and remarkably increased the selectivity against the hA₃ receptor subtype (hA₃/hA_{2A}=91). Likewise, electron withdrawing groups (e.g. *para*-F as in **106**, with K_i hA_{2A}=1.6 μM, and hA₃/hA_{2A}>37) were more favourable towards hA_{2A}AR than hA₃AR. Moreover, it was noted that high affinity towards the hA_{2A} subtype was reflected in the whole N² isopropyl series. Nevertheless, affinity switched towards hA₃AR for the neopentyl series. Although the free amino group of neopentyl prompted a better affinity at the hA_{2A}AR (**83**, with K_i hA_{2A}=4.1 μM and K_i hA₃>60 μM), corresponding acyl substitution improved the affinity at hA₃ ARs (e.g. **109**, with K_i hA₁=11.0 μM; K_i hA_{2A}=3.5 μM and K_i hA₃=30 μM). This indicates the importance of an acyl group at C⁶ position for hA₃ affinity profile. Notably, *para* substitutions (e.g., F, CF₃) at C⁶ benzoyl groups slightly ameliorated the affinity towards the hA₃AR (e.g. **110**, with K_i hA₃=5.9 μM & **111**, with K_i hA₃=6.6 μM). Interestingly, compound **112** (with an electron donating *p*-toluoyl group) showed the best affinity at the hA₃AR (K_i hA₃=5.0 μM) in the neopentyl series, its *para*-CF₃ analogue **111** displayed the highest selectivity (hA₁/A₃>15, hA_{2A}/A₃>15). This indicates the different contributions of electron donating and electron withdrawing groups at the *para* position of the benzoyl group at C⁶. Similarly, compound **119** with dibenzoyl substitution displayed the highest selectivity (hA₁/A₃>15.3, hA_{2A}/A₃>15.3) in the among the N² alkyl series derivatives.

In the N²-phenylethyl series, *para* unsubstituted benzoyl (**113**, with K_i hA₃ = 8.6 μM) and chain lengthened phenylacetyl (**124**, with K_i hA₃ = 11.4 μM) at the C⁶ position, appeared to reduce moderately the affinity of the PP scaffold at the hA₃ receptor in comparison with the *para* substituted benzoyl derivatives. Similarly, *para*-F group (**114**, with K_i hA₃ = 100 μM) in the acyl chain diminished affinity to a great extent at the hA₃AR, however, it showed good affinity towards hA_{2A} receptor subtype (K_i hA_{2A} = 2.06 μM). On the other hand, analogue **116**, with the electron donating *p*-toluoyl substituent at C⁶ position displayed substantial increase of the affinity towards the hA₃AR (K_i hA₃ = 1.5 μM) and it also imparted a 6 to 8 fold increment in affinity in comparison with corresponding C⁶ unsubstituted and C⁶ lengthy phenylacetyl compounds **113** & **122**, respectively. Further, *p*-CH₃ substituted compound (**116**) displayed almost 4 fold increment in the affinity as compared to N²-neopentyl counterpart (**112**, with K_i hA₃ = 5.0 μM). Similarly, analogue **115**, with electron withdrawing *para*-CF₃ benzoyl group, also exhibited comparable affinity at the hA₃ receptor (K_i hA₃ = 2.8 μM). Interestingly, a 36 fold increase in affinity was observed for the derivative with *para*-CF₃ substituent in comparison to the *para*-F analogue, overall indicating that bulky, either electron-donating or electron acceptor functional groups, are preferred over less bulky groups for a better affinity at the hA₃AR. SAR on the fluoro derivatives at R₂ seems to be reversed when R is changes from isopropyl to phenylethyl. When R was Isopropyl, R₂ seems to have no activity, when R group was replaced by less rotatable neopentyl the activity was reversed. In contrast, another rotatable phenylethyl at R₂ showed no activity, this again explains that multiple rotatable bonds not preferred for the activity. Interestingly, compound **120** with dibenzamide chain at C⁶ position displayed the potency which is comparable to that of compound **115**. In addition, compound **120** was around 35 fold selective towards the hA₁AR and 2 fold selective towards hA_{2A}AR.

Comparison of binding affinity PP to PTP

Figure 23 summarizes the structure-affinity relationship (SAR) profiles observed in this new series of 4-Chloro-pyrazolopyrimidine derivatives (**81-84** & **101-124**). We noticed a slightly different trend of

hA₃ affinity and selectivity in the new series of PP with C⁶, C⁴ and N² substitution. Despite the fact that these compounds still maintained good hA₃ affinity in the low micromolar range (1.5-33.5 μM), it was found that the molecular simplification from the tricyclic PTP to bicyclic PP resulted in several logs decrease of affinity and selectivity towards the hA₃ receptor. Moreover, it was noticed that N² substituents in the main scaffold caused a somehow opposite binding affinity for PP and PTP. In PTP, non bulky methyl group at N⁸ position displayed higher affinity than N⁸ phenyl ethyl substituted derivatives. On the contrary, lengthy and bulky groups such as neopentyl and phenylethyl at N² position of PP showed high binding affinity than methyl substitution. Considering the wide space of the hA₃ receptor, the complex PTP structure occupied the most of the space in the receptor centre and needed sterically less constraints methyl group in order to accommodate the whole PTP structure within the binding cavity, whereas simpler PP analogues, which localize at the centre of the binding pocket, needed lengthy bulky groups to make potential interaction with the corresponding residues. In addition, the C⁶ substitution in PP (corresponding to N⁵ substitution in PTP) showed a lot of difference in the affinity between PTP and PP derivatives. Generally, in PP scaffolds substituted benzamide chain displayed stronger activity than unsubstituted benzamide and the lengthy phenylacetamide chain, whereas in PTP scaffold benzamide chain showed weaker activity than phenylacetamide chain.

3.4.6 Conclusion

In summary, structure-affinity relationship analysis showed that both substituents at N² and C⁶ positions play a key role in modulating the binding affinity at the adenosine receptors. First, at the N² position, lengthy and bulky groups such as neopentyl and phenylethyl substitution showed favourable effect on the affinity at hA₃ receptor. In addition, we also evaluated the electronic effect of *para*-substituents on the acyl chain towards the affinity profile at the hA₃ receptors. Based on the binding results, it was confirmed that the substituents (e.g., F, CF₃, CH₃) at the *para*-position of the C⁶-benzamide chain were found to modulate the affinity at hA₃AR to a great extent. In particular, among the substituents introduced at the *para*-position of the

phenyl ring, both the CF₃ and CH₃ groups have exerted relatively more favourable effect on the affinity at hA₃ receptor.

Overall, our results demonstrated the importance of the contemporary introduction in the PP system of a) large lipophilic substituents (e.g., neopentyl and phenylethyl) at N² position to maintain the potency at hA₃ receptor; b) sterically bulky electron donating or electron withdrawing *para* substituted acyl chains at C⁶ position to increase the affinity and selectivity towards hA₃ receptor; c) a slightly smaller chain (i.e. isopropyl) at N² to confer the affinity towards the hA_{2A} receptor, if further study is intended on hA_{2A} receptor; d) Electron deficient functional groups (e.g., CF₃, Cl, Br, etc.) substituted acyl chains at C⁶ position to increase the selectivity at hA₃ receptor.

Among the newly synthesized PP derivatives, analogue **116**, with a phenyl ethyl substitution at N² position and a *para*-methylbenzamide at C⁶ position, possessed the best hA₃ affinity profile (K_i hA₃ = 1.5 μM) and about 7 fold selectivity at the hA₁ and hA_{2A} ARs. Instead analogues **115** & **120** of the same series emerged for their high selectivity (**115**, hA₁/A₃ = 21, hA_{2A}/A₃ = 6 and **120**, hA₁/A₃ = 35, hA_{2A}/A₃ = 2) against the other adenosine receptors, while displaying almost equal (**115**, K_i hA₃ = 2.8 μM & **120**, K_i hA₃ = 2.9 μM) affinity at the hA₃AR. Similarly, in the N² alkyl series, compound **112** with N² neopentyl, and C⁶ *p*-toluamide substituents showed the best affinity at the hA₃AR (K_i hA₃ = 5.0 μM) and its *para*-CF₃ analogue **111** displayed the highest selectivity (hA₁/A₃ >15, hA_{2A}/A₃ >15) in the whole series. Compound **111**, which has a CF₃ at the 4th position of the benzamide chain, showed high selectivity towards other receptor subtypes. A similar trend is also observed with compound **115**, also bearing a *para* CF₃ substitution at position 4 as well. The presence of sterically bulky (high ClogP, **Table A4, Appendix**) electron withdrawing groups at the *para* position shifted the affinity towards the hA₃AR. However, compound **112**, having *para*-CH₃ in the benzamide ring, is sterically weaker (low ClogP) than *para*-CF₃ and showed less selectivity towards other receptor subtypes. This trend is observed clearly only in the N² neopentyl and phenylethyl series because the bulky group at N² position favoured the hA₃ affinity. Hence, it is concluded that such electron withdrawing group with high ClogP, together with neopentyl or phenyl

moieties at N², is needed at the *para* position of C⁶ benzamide to improve the selectivity.

The molecular simplification of the tricyclic pyrazolo-triazolo-pyrimidine has led to the identification of a novel series of bicyclic pyrazolo[3,4-*d*]pyrimidine derivatives as hA₃AR antagonists. The present study has highlighted that the pyrazolopyrimidine moiety is an potential scaffold and suggest ways to progress it for obtaining novel hA₃AR antagonists. Although there is a remarkable drop in the affinity, still it could be considered as a starting point for further investigations. Consequently, the affinity and selectivity could be enhanced to a certain extent, upon analyzing the structural features responsible for the drop in affinity by molecular modeling studies.

From the comparison of SAR of PP analogues with PTP analogues, the following features are derived.

N² position long chain such as neopentyl and phenylethyl are favourable in PP analogues, whereas in PTP analogues at N² position small alkyl groups are prefferable(e.g. CH₃) than longer bulky group.

Similalry, at C⁶ position acylaated group favoured for affinity at hA₃AR for both PTP and PP analogues.

In addition, the steric chloro group didnot show much impact on the affinity apart from providing some lipophilicity to the scaffold. Hence, the C⁴ position could be substituted by some rotatable hydrogen bond donor or acceptor group in opposite to steric group to explore more about this position.

3.5 Quantitative Structure-Activity Relationship (QSAR) Study on a New Series of PyrazoloPyrimidine Derivatives

3.5.1 Introduction

In this chapter, Topomer CoMFA study has been performed to identify pharmacophoric units and to establish the contributions of each of the identified R groups in the data set. Topomer CoMFA is a 3D-QSAR tool that automatically generates a model for predicting the biological activity or properties of compounds.¹⁶⁵ Similarly, topomer CoMFA differs from conventional CoMFA by using topomers, which are molecular fragments with

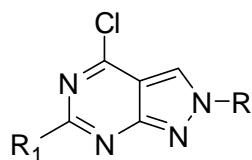
standardized internal geometries. This enables the topomer CoMFA methodology to do away with structural alignments, which is the most difficult and subjective step of the conventional CoMFA methodology. Mostly, all the steps in topomer CoMFA are automated and thus the methodology is entirely objective. In addition, conformation and orientation of a molecular fragment were described by a topomer and it was generated based on 2D structure without any involvement of a receptor site or other ligands. The SAR of the new series of 4-chloro-pyrazolopyrimidine derivatives was quantitatively elucidated and the structural features essential for the inhibition of hA₃AR particularly at the N² & C⁶ position of the bicyclic nucleus was proposed. Topomer 3D models are constructed for each fragment automatically, using a probe atom around the 3D grid. Subsequently, the steric and electrostatic fields (“CoMFA column”) are generated for each set of topomers. Therefore, the corresponding biological activity was correlated with both the steric and electrostatic properties of a derivative’s chemical structure.

3.5.2 Experimental Methods

3.5.2.1 Selection and preparation of dataset

The structures of the 6 amino-4chloro-pyrazolo[3,4-*d*]pyrimidine derivatives (26 compounds) and their respective biological data are given in **Table 3** (see **chapter 4**). SYBYL-X 1.3 program (Tripos Associates Inc.)¹⁶⁶ was used to perform the QSAR experiment using windows operating system version. A molecule sketch program was used for the molecule building. All ionisable groups were drawn in their uncharged forms. Derivatives with K_i hA₃ >60 μ M or >100 μ M were assigned an arbitrary high K_i of 1000 μ M for topomer CoMFA.¹³² Firstly, a standard Tripos molecular mechanics force field of 0.05 kcal/ (mol·Å) was used to minimize the molecular geometry of each compound. In addition, Gasteiger-Huckel MMFF method was used to compute the charges.^{167, 168} Powell Method of 100 iterations were used for energy minimization of the atom and prior to that, atomic charges were assigned to each atom.

Training set structures were separated into two sets of fragments (also referred as R-groups) as shown in **Table 4**, before the job submission for Topomer CoMFA analysis.



R	R ₁
CH ₃	NH ₂
CH(CH ₃) ₂	NHCOPh
CH ₂ C(CH ₃) ₃	NHCOPh (<i>p</i> -F)
CH ₂ CH ₂ C ₆ H ₅	NHCOPh (<i>p</i> -CF ₃)
	NHCOPh (<i>p</i> -CH ₃)
	N(CO-Ph) ₂
	NHCOCH ₂ Ph

Table 4. Fragments of training sets of 4-chloro-pyrazolopyrimidine derivatives

This was achieved by specifying multiple acyclic single bonds to cut within each complete structure, since they all shared identical substructure (i.e., constant core). Subsequently, after the fragmentation, the input structures were standardized, normalized and the topomers generated. After the model was created, the following values were reported in the Topomer CoMFA dialog: number of components that provided the highest q^2 results; crossvalidated r^2 (q^2) value for the specified number of components; conventional r^2 value; y-intercept for the PLS analysis; fragment contributions of R-group to the predicted activity (adding the sum of the fragment contributions with the PLS intercept value gives the predicted activity value). These results are summarized in **Table 5**. The model generated was successful (since $q^2 > 0.2$), and it was therefore used to predict the activity of other structures.

3.5.3 Results and discussion

The final topomer CoMFA model had a q^2 of 0.325 and r^2 of 0.561 using two components. These results are comparable to those for some of the datasets used to assess the topomer CoMFA methodology.¹³² The topomer CoMFA model had an intercept of 2.85 and the contributions of the different substituents for R and R₁ are given in **Table 6**.

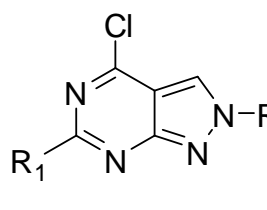
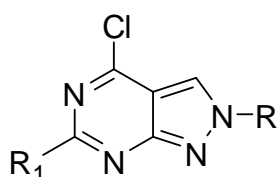
	Parameters	value
	q^2	0.325
	r^2	0.561
	N	2
	y intercept	2.85

Table 5. Results of the Topomer CoMFA analysis.

It can be seen that substituents at $R_1(C^6)$ position had a much larger effect on the activities of the compounds than substituents at $R(N^2)$ position.



R	pIC_{50} Contribution	R_1	pIC_{50} Contribution
CH ₃	-0.03	NH ₂	0.04
CH(CH ₃) ₂	-0.22	NHCOPh	1.69
CH ₂ C(CH ₃) ₃	0.17	NHCOPh (<i>p</i> -F)	1.66
CH ₂ CH ₂ C ₆ H ₅	0.04	NHCOPh(<i>p</i> CF ₃)	2.04
		NHCOPh(<i>p</i> CH ₃)	1.78
		N(CO-Ph) ₂	1.80
		NHCOCH ₂ Ph	1.94

Table 6. Average pIC_{50} value contributions of different substituents for R and R_1 group at pyrazolopyrimidine derivatives in topomer CoMFA with an intercept of 2.85.

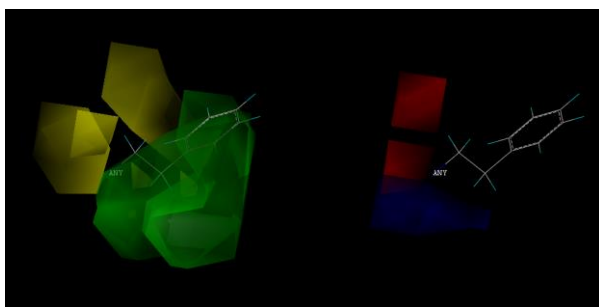


Figure 24. The steric and electrostatic effects at the N² position in compound **116** (green region denote the bulky substituents).

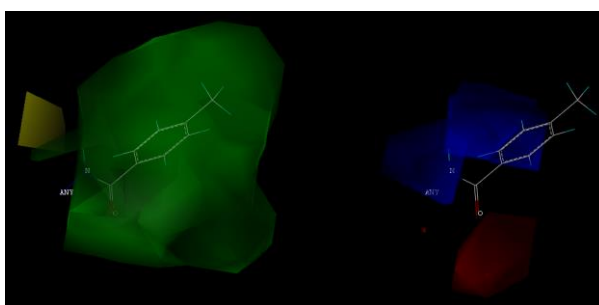
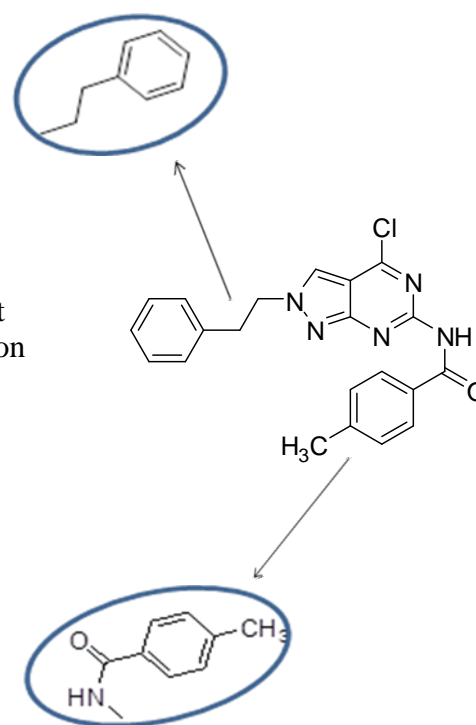


Figure 25. The steric and electrostatic effects at the C⁶ position in compound **116** (green region denotes steric effects, blue and red regions denotes electrostatic effects).



N² Substitution

Topomer CoMFA produced large green contours around N² position (phenyl ethyl group of compound **116** as representative example), as shown in **Figure 24**, indicating that presence of a bulky lengthy chain was needed for biological activities. Similarly, pIC₅₀ value seems to be correlating with contour plots analysis, as hydrophobic neopentyl groups displayed the highest pIC₅₀ followed by phenyl ethyl groups. Subsequently, the negative pIC₅₀ value obtained for the methyl and isopropyl derivatives proves the less importance of non bulky groups. The electrostatic map around the N² position was not as informative as all the substituents do not contain polar atoms.

C⁶ substitution

As shown in the **table 6**, free amino groups at C⁶ position showed lowest pIC₅₀ value, which in turn was indicated by the absence of contour plot surrounding this region. When the free amino group was acylated, pIC₅₀ values seemed to be increasing and there is a pattern observed between the

SAR of the compounds and pIC₅₀ values: as the hydrophobicity increases, pIC₅₀ value also increases. SAR showed that limited activity for the C⁶ benzamide analogues followed by *para*-F benzamide derivatives. The same trend was observed for pIC₅₀ value of corresponding substitutions. Similarly, electron withdrawing substitution such as at *para*-CH₃ group possessed maximum activity followed by *para*-CF₃ substitution, as seen in the **Table 3**. Moreover, chain elongated phenylactyl and bulky dibenzoyl groups displayed almost equal pIC₅₀ and the same trend was followed for the binding affinity of the compounds.

Similarly, the contour map analysis of R¹ groups showed that there is also a large green region around the phenyl ring of acyl chain at C⁶ position (**Figure 25**), indicating that the presence of bulky substituents should improve the biological activities. Similarly, the presence of both blue and red contours signifies the necessity of having electronic properties substituents at the *para* position of the acyl chain. This was indicated by the electrostatic maps, in which substituents with both positive and negative groups near to the C⁶ position are deemed vital for activity.

3.5.4 Conclusion

Topomer CoMFA has been established as a 3D QSAR tool that creates the model for bio activity prediction of compounds. The 3D QSAR model exposed the important sites for chemical modifications to improve the affinity. The new insights on the steric and electrostatic factors that are important in modulating the hA₃ affinity for the new series of 4-chloro-PP derivatives, at the N² position and N⁶ position of the bicyclic nucleus, were obtained from the topomer CoMFA methodology. From QSAR analysis, it was noticed that the large green region around N² position favoured bulky substituents (e.g., neopentyl, phenyl ethyl). Similarly, a large green region around the C⁶ position suggests that bulky acyl substituents (e.g., substituted benzoyl groups) are favoured at this position. The electrostatic map at C⁶ position shows that substituents with both positive and negative groups in *para* (e.g. *para*-CF₃, *para*-F, *para*-CH₃) at the C⁶ position are important for activity. These results additionally support the SAR fact that N² bulky groups (e.g. neopentyl and phenylethyl) and C⁶ benzoyl with different *para*

and *meta* substituted electronic groups (e.g. CF₃, CH₃, Br, Cl etc.) are needed to improve the affinity. Overall, the hA₃ receptor antagonistic activity has been optimized by the contribution of the steric effects around the N² and C⁶ positions.

3.6 Homology modeling of human A₃ adenosine receptor and molecular docking evaluation of 4-chloro-pyrazolopyrimidine derivatives

3.6.1 General Introduction

In this chapter, homology modeling of human A₃ adenosine receptor was carried out and using the built homology based human A₃ model, a molecular docking simulation on PP derivatives was further carried out to examine the binding modes and vital interactions between the ligands and specific amino acid residues.¹⁶⁹

3.6.2 Homology Modeling of Human A₃ Adenosine Receptor

3.6.2.1 Introduction

Recently, the crystal structure of hA_{2A}AR, bound with a selective and potent antagonist (ZM241385) was identified¹⁶⁹ and it shares moderate sequence identity of about 43% with the hA₃AR. Moreover, this structure serves as an alternate template for the construction of hA₃ homology model applied for docking studies.^{77, 107, 140} In the present study, we have developed the single template-based homology modeling of A₃ receptor.

3.6.2.2 Experimental Methods

Construction of hA₃ homology model

The high affinity antagonist ZM-241385 (PDB code: 3EML),¹⁶⁹ which are complexed with humanA_{2A} adenosine receptor crystallographic structure, was recently resolved and a new alternative template to perform homology modeling of other GPCRs, especially the adenosine receptors, was provided. The template of the human hA_{2A}AR¹⁶⁹ protein sequence (PDB code: 3EML) was obtained from PDB, whereas the protein sequence of hA₃ receptor (Accession no. P33765, Gene name ADORA3 UNQ1931/PRO4406) was

and visualizations were performed by means of PyMOL Molecular Graphics System.¹⁷⁷ **Figure 26** depicts the general steps involved in the homology modeling.

3.6.2.3 Results and Discussion

Evaluation of hA₃ homology models

The overall sequence identity between the hA_{2A} template and the target sequence of hA₃AR was found to be ~43%. Consistently, the model based on the hA_{2A}AR (**Figure A1 in Appendix**) has shown better parameters (% of residues in the most favoured regions = 93.9%, G factor = 0.34, **Table 7**) in the Ramachandran Plot (**Figure A2 in Appendix**) than previous results from our lab.¹¹⁸ Moreover, none of the residues were observed in the generously allowed and disallowed regions. As described by the previous

Table 7. Ramachandran Plot Summary from Procheck

Homology Model	Most favoured regions		Additionally allowed regions		Generously allowed regions		Disallowed regions		G-factor
	n	%	n	%	n	%	n	%	
hA ₃ Model	278	93.9%	18	6.1%	0	0.0%	0	0.0%	0.48 (<i>phi-psi</i>)
									0.34 (all)

Table 8. Ramachandran Plot Summary from Richardson Lab's Molprobity

	Most favoured regions	Additionally allowed regions	Generously allowed regions	Disallowed regions
hA ₃ Model	96.5%	3.5%	0.0%	0.0%

Table 9. Global quality scores

Program	Verify3D	ProsaII (-ve)	Procheck (<i>phi-psi</i>)	Procheck (all)	MolProbity Clashscore
Raw Score	-0.17	-0.04	0.48	0.34	90.72
Z-Score	-4.65	-2.85	2.20	2.01	-14.04

Table 10. RMS deviations of hA₃ Model and its respective templates

	Number of close contacts (within 2.2 Å)	RMS deviation for bond angles:	RMS deviation for bond lengths:
hA ₃ Model	0	2.1 °	0.019 Å

findings, 80% of C α -atoms can be expected to be within 3.5 Å of their true position, for 30-50% of sequence identity, whereas significant errors are expected for less than 30% sequence identity.^{177,178} In addition, 96.5% of residues was observed in the Richardson Lab's Molprobit analysis (**Table 8**). Interestingly, observations of current study were in agreement with previous studies.^{118, 140} All of these findings proposed that the hA₃ model based on hA_{2A}AR was stereochemically more precise and accurate.

After a model building, it was checked for possible errors. Mainly, the quality of the model is predicted by the sequence similarity between the target and the template (**Figure A1 in Appendix**). Above 30% of sequence identity is deemed as a predictor of the model accuracy. Evaluation is usually performed by two types. “Internal” evaluation of self-consistency is able to confirm whether a model meets the restraints used to calculate it.

“External” evaluation depends on information which are not used in the calculation of the model. Programs such as PROCHECK¹⁷⁹ (internal evaluation) is often used to assess the stereochemistry of models (e.g. bonds, dihedral angles, bond angles, and non-bonded atom lengths). Main advantage of PROCHECK is that a large error such as alignment errors are easily detected by cluster of stereochemical errors obtained from the evaluation. A small RMSD (< 2.5 Å) value of bond length and bond angles of binding pocket residues were observed between A₃AR model and hA_{2A} template (**Table 10**). This indicates that hA₃ homology model closely resembles hA_{2A} template in terms of binding pocket. Hence, this model could be deduced as efficient model for the prediction of ligand binding. However, the molecular docking study will be further investigated (**Section 6.3**) to identify the predictive comparable binding modes and interactions ability of the hA_{2A}-based model with ligands.

3.6.3 Molecular Docking Simulations

3.6.3.1 Introduction

This section describes the hypothetical binding interactions of newly synthesized 4-Chloro-PPs (**81-84** & **101-124**) through the hA₃ ‘hybrid’ homology model. The derivatives were docked through the hA_{2A}AR-based hA₃ model (**Figure 27**). Binding interaction of N² alkyl, C⁶ substituted derivatives are compared with N² aralkyl, C⁶ substituted derivatives. Moreover, the binding modes and interactions of the most potent 2-aryl-PTP and the potent PP analogues (**116**) inside the hA₃AR were also evaluated to compare the binding pose with PTP analogues and rationalize the results.

A molecular docking study was performed on the novel 2-(alkyl and aralkyl substituted)-2*H*-pyrazolo[3,4-*d*]pyrimidine derivatives (**81-84** & **101-124**) to identify the hypothetical binding mode at the hA₃ adenosine receptor and to rationalize the results obtained from the pharmacological evaluation.



Figure 27. General topology of the hA₃ ‘hybrid’ homology model

Especially, molecular docking studies were carried out on both hA₃ and hA_{2A} adenosine receptors. Different docking softwares have been evaluated for their ability to reproduce the crystallographic pose of ZM241385 inside the binding cavity of hA_{2A} receptor. Among the different programme, MOE gave the lowest RMSD value, hence we decided to use MOE as a docking programme for the pose inspection of the novel pyrazolo[3,4-*d*]pyrimidine derivatives in both hA_{2A} and hA₃ receptors. All the newly synthesized pyrazolo[3,4-

d]pyrimidine derivatives were docked into the orthosteric trans-membrane (TM) binding cavities of both adenosine receptors. On top of that, ligand-receptor interactions were analysed using ligand vs receptor residues binding interaction energy calculation.

Ligands were energy minimized to obtain highly populated docked conformations and used for interpretation of binding mode inside the binding cavity of hA₃ homology models as well as hA_{2A}AR. Subsequently, docking results were analyzed and the results of the pharmacological evaluation were correlated to the binding assay results.

Generally, this section emphasized on the binding orientation of the new 4-chloro PP derivatives within the binding pocket of homology hA₃ model and hA_{2A}AR. Concomitantly, it allowed us to: (i) explore the amino acid residues involved in the binding interactions, which are essential for the hA₃ antagonist recognition; (ii) investigate the factors responsible for the difference in the activity between the 4-chloro-PP derivatives and the corresponding 2-aryl-PTP analogues. Therefore, the key residues and physicochemical properties at N², C⁶ and at C⁴-positions of the bicyclic nucleus could be delineated via docking study.

3.6.3.2 Experimental Methods

Computational Methodologies

All modeling studies were carried out on a Intel(R) Core(TM) 2 Quad CPU Q9550, 2.83 GHz, 3.25 GB RAM system. Docking simulation, energy calculation and the analyses of docking poses were performed using the Molecular Operating Environment (MOE, version 2010.10) suite.¹⁸⁰ The software package Hooman's IF-E 6.0¹⁸¹ implemented in the MOE suite, was utilized to calculate all interaction energy. PyMOL molecular Graphics system was used for graphical visualizations and manipulations.¹⁷⁷

MOE-builder tool as a part of the MOE suite was used to build a ligand structures¹⁸⁰ and were subjected to MMFF94x energy minimization until the rms of conjugate gradient was <0.05 kcal mol⁻¹ Å⁻¹.

The docking protocols were calibrated using three different programs, such as MOE-Dock,¹⁸⁰ AutoDock,^{182, 183 184} and PLANTS.¹⁸⁵ Using different docking algorithms and scoring functions, ZM-241385 was redocked into the

crystal structure of the hA_{2A} adenosine receptor (PDB code:3EML). Considering the lowest rmsd value, the lowest mean rmsd value and the highest number of poses with rmsd value <2.5 Å, the MOE-Dock was chosen as docking programme (**Figure 28**).

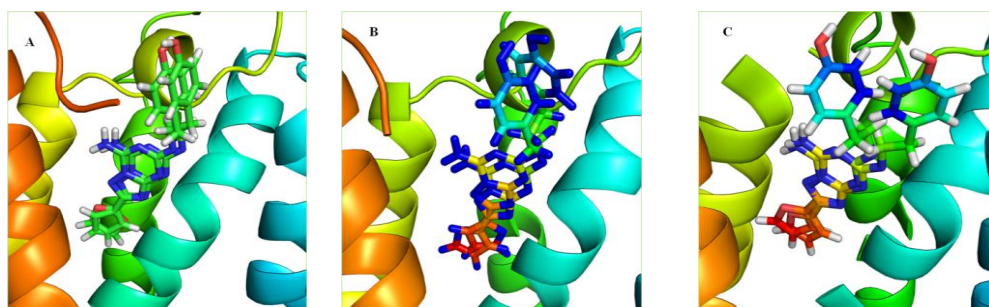


Figure 28. The crystallographic pose of ZM241385 inside the binding cavity of hA_{2A} receptor reproduced using different docking programmes A. MOE-Dock (rmsd 2.25) B. PLANTS (rmsd 2.48) C. Autodock (rmsd 2.94).

On the basis of the best docking performance, all ligands were docked into the hypothetical TM binding site of the hA₃AR model and that of the hA_{2A}AR crystal structure by using the docking tool of the MOE suite.¹⁸⁰ In the MOE-Dock, the Alpha PMI placement method, followed by force field refinement and london dG scoring, were used for the docking runs. MOE-Dock performed an independent docking runs (100 for our specific case) and wrote the resulting conformations and their energies in a molecular database file. The resulting docked complexes were subjected to MMFF94x energy minimization until the rms of conjugate gradient was <0.1 kcal mol⁻¹ Å⁻¹. Prediction of antagonist-receptor complex stability (in terms of corresponding pK_i value) and the quantitative analysis for non bonded intermolecular interactions (H-bonds, hydrophobic, electrostatic) were calculated and visualized using several tools implemented in MOEsuite.¹⁸⁰ Electrostatic contributions to the binding energy of individual amino acids have been calculated using software package Hooman's IF-E 6.0 as implemented in MOE suite.

3.6.3.3 Results and Discussion

From the docking simulation analysis, the synthesized derivatives were mostly seen to share a slightly similar binding pose in the TM region of the hA₃AR. Moreover, the ligand-recognition occurred in the upper region of

the TM bundle, and the pyrazolo[3,4-*d*]pyrimidine scaffold was surrounded by TMs 2, 3, 5, 6, 7 with the benzamide ring at the C⁶ position located towards the intracellular environment.

Common binding interactions at the bicyclic nucleus and C⁴-position

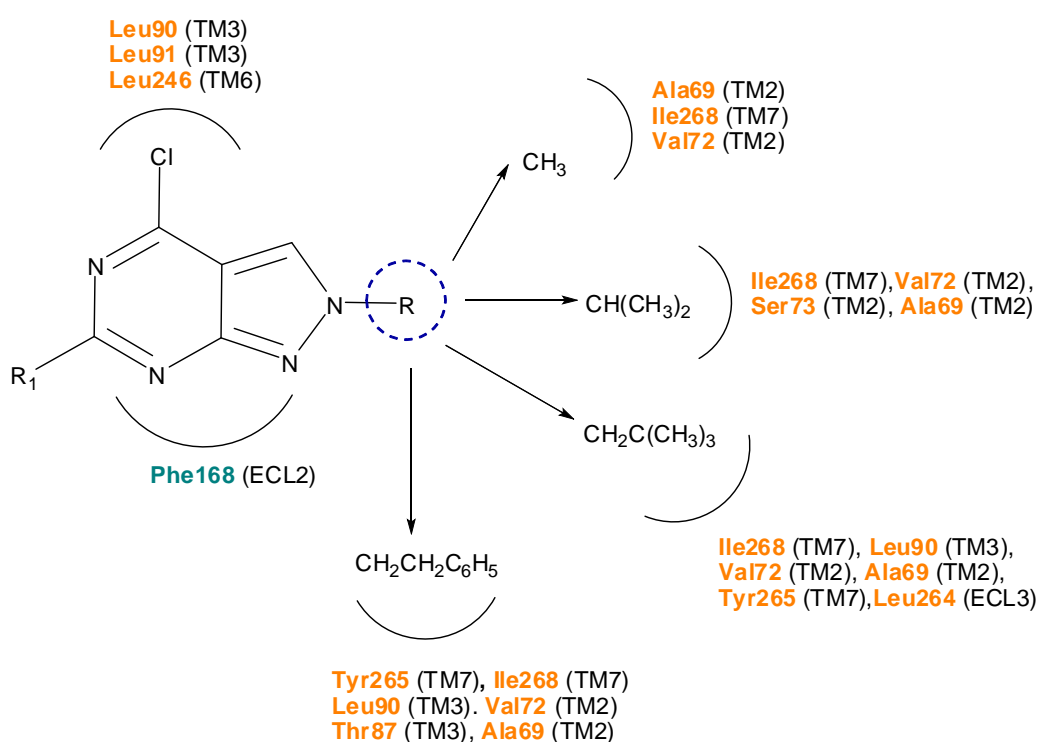
In the molecular docking studies on the pyrazolo[3,4-*d*]pyrimidine derivatives, four main interactions were involved in the binding of the ligands to the hA₃AR, namely hydrophobic interactions, hydrogen bonding, π - π stacking and dipole-dipole interactions. Among these interactions, the hydrogen bonding and hydrophobic interactions appeared to be vital for ligand affinity and stability.

In all ligands, π - π stacking interaction of the planar bicyclic nucleus with the phenyl ring of Phe168 (ECL2) was observed. Notably, this interaction was also present in the binding modes of other classes of hA₃AR antagonists, including the pyrazolo-triazolo-pyrimidines (PTP).¹¹⁸ Data from literature and docking studies on PTP analogues suggested the importance of the binding of the Phe168 for the hA₃ antagonistic activity. Moreover, the mutagenesis analyses conducted at the A_{2A}AR demonstrated the importance of Phe168 for antagonist binding.¹⁸⁶ Thus, as this residue was conserved in both the A_{2A}AR and A₃AR, it was deduced that Phe168 could be implicated in antagonist affinity at the latter receptor.¹⁸⁷

Similarly, C⁴ chloro group was found to interact with some hydrophobic leucine based residues such as Leu90 (TM3), Leu91 (TM3) and leu246 (TM6). However, these residues do not seem to be recognized for an antagonistic activity. Therefore, from the binding study, the contribution of chloro functional group present in the simplified PP structures seems to be negligible, as it did not make an impact on potential interaction with some conserved residues which are essential for the antagonist recognition. Considering its lower importance towards binding, it is worth to mention that chloro group was mainly assigned because it could be easily substituted and subsequently could help in improving the affinity by further functionalization of the ligand.

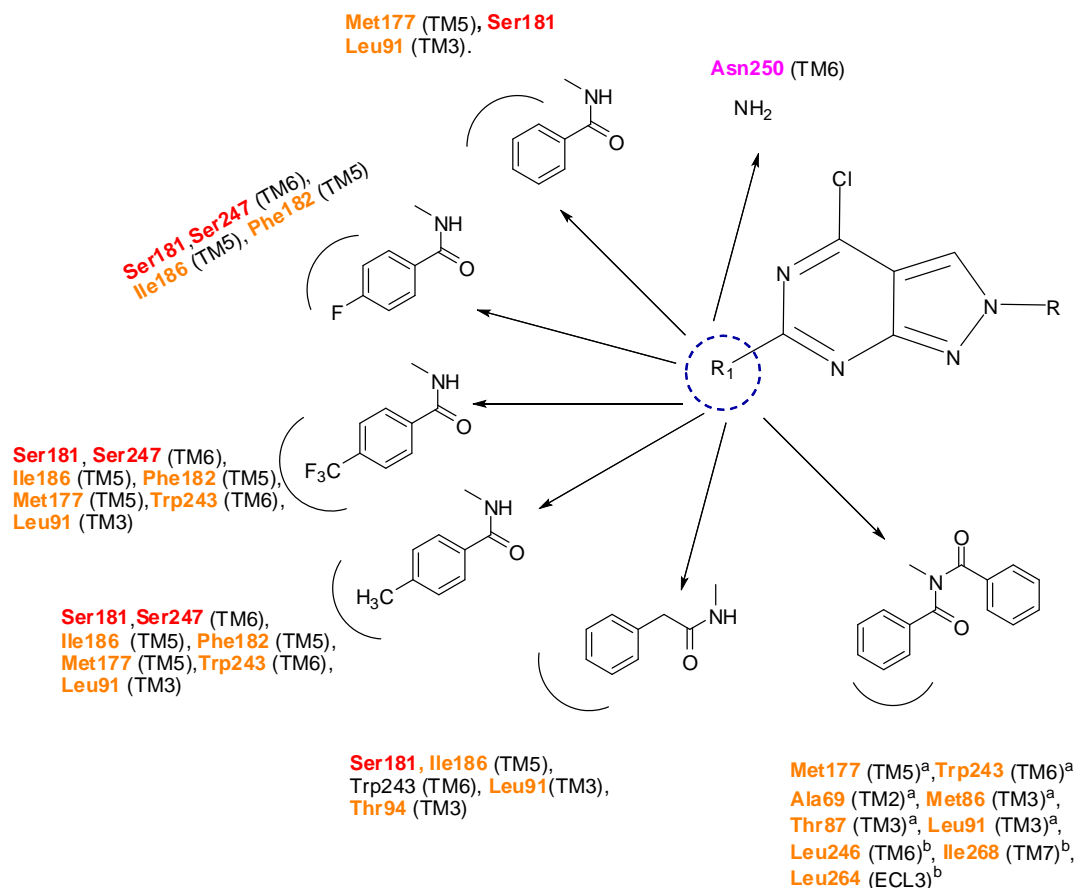
Common binding interaction of N² and C⁶ substituents with residues

All the important binding interactions between the substituents at N² positions of new 4-Chloro-PPs (**81-84** & **101-124**) and the corresponding residues in hA₃ receptor were summarized in **Figure 29**. As seen in the **Figure 29**, less bulky groups such as methyl and isopropyl, bound with some common hydrophobic residues such as Ala69 (TM2), Ile268 (TM7) and Val72 (TM2). Similarly, lengthy bulky substituents such as neopentyl and phenylethyl, shared the common interaction with hydrophobic residues such as Ala69 (TM2), Val72 (TM2), Leu90 (TM3), Tyr265 (TM7) and Ile268 (TM7).



Residue: Involved in π - π interaction, Residue: Involved in hydrophobic interaction

Figure 29. Common binding interactions of new series of 4-Chloro PPs (**81-84** & **101-124**) at N² & C⁴ position with residues at hA₃AR.



Residue: Involved in H-bonding, **Residue:** Involved in hydrophobic interaction, **Residue:** Involved in van der Waals interaction

Figure 30. Common binding interactions of new series of 4-Chloro PPs (**81-84 & 101-124**) at C^6 position with respective residues in hA_3AR . ^aResidues found to interact with N^2 methyl substitution only, ^bResidues found to interact with N^2 isopropyl substitution only.

Among the different residues, Tyr 265 (TM7) and Leu90 (TM3) which are not observed with small substituents, seem to be essential for the antagonist binding, as the lengthy bulky groups in turn showed high affinity (**Table 3**). Moreover, previous binding interaction of PTP analogues showed that these two residues were essential for the antagonistic recognition (**Figure 20**).

In addition, common binding interaction involved between C^6 substituents and crucial residues are summarized in **Figure 30**. Notably, residues such as Ser181 (TM5), Ser247 (TM6), made van der Waals interactions with ligands, whereas residues such as Ile186 (TM5), Phe182 (TM5) and Leu91 (TM3) seem to make hydrophobic interactions with phenyl

ring of C⁶ benzamide substituents. However, few residues such as Met177 (TM5), Trp243 (TM6) are observed in *para*-CF₃ and *para*-CH₃ benzamide substituents only. Moreover, compounds with these two substituents displayed the highest binding affinity towards the hA₃ receptor in the whole series (**Table 3**). Interestingly, similar type of hydrophobic interactions were observed for the PTP analogues, where binding interactions with Met177 (TM5) and Trp243 (TM6) were deemed vital for the adenosine receptor activation and antagonistic recognition.¹⁴²

Binding interactions of non bulky group substituted derivatives at N² position

In this section, binding interactions of analogues of N² alkyl series (especially N² methyl and isopropyl) is evaluated by comparing its binding mode with the binding pattern of the most potent compound, **116**, inside the hA₃AR. **Figure 31** (panel A) presents the hypothetical binding pose of compound **116** at the hA₃AR, which possesses the highest hA₃ affinity among all the newly synthesized derivatives (*K_i* hA₃=1.5 μM). It appeared that the bicyclic pyrazolo[3,4-*d*]pyrimidine core was anchored within the binding cleft through an aromatic π-π stacking interaction with Phe168 (EL2). Moreover, the carbonyl group of the exocyclic acyl chain at the bicyclic core interacted with polar residue Asn250 (TM6), forming a lone stabilizing H-bonding interaction. The N² phenylethyl chain of the ligand was directed towards the TM2 and TM3. In addition, the phenyl ring of the acyl chain was located deep within the ligand binding cavity and formed hydrophobic interactions with the highly conserved Trp243 (TM6), an important residue in receptor activation and antagonist binding. Compound **116** also formed hydrophobic interaction with several residues in the binding cleft such as Leu90 (TM3), Leu91 (TM3), Met177 (TM5), Trp243 (TM6), Leu246 (TM6), Tyr265 (TM7), Leu264 (EL3) and Ile268 (TM7).

N²-methyl & N²-isopropyl derivatives, displayed slightly different binding pose as compared to **116**. However, as an exception, compound **117** in the N² methyl series and compound **118** in the isopropyl series showed a similar pattern as compound **116**, which in turn was reflected in the high binding activity of these compounds. The pyrazolo ring of these compounds is

directed towards the extracellular environment rather than towards TM2 and TM3, and also the main nucleus pyrazolo[3,4-*d*]pyrimidine was rotated of about 45° compared to the binding pose of compound **116**.

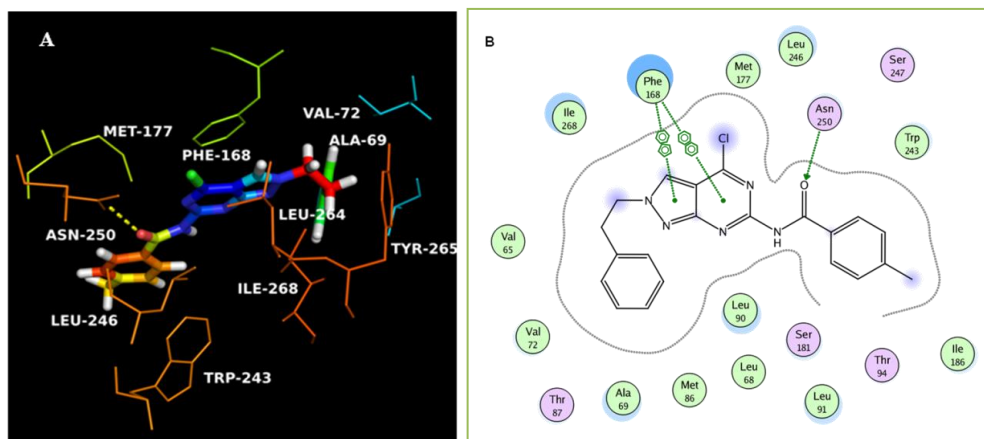


Figure 31. A. Hypothetical binding mode of compound **116** obtained after docking simulations inside the hA₃AR binding site. Poses are viewed from the membrane side facing TM6, TM7, and TM1. The view of TM7 is omitted. B. 2D view of binding residue with ligand **116** inside hA₃AR binding site.

In contrast, the binding pattern of compounds bearing non bulky substituents, such as N²-methyl & N²-isopropyl derivatives, displayed slightly different binding pose as compared to **116**. However, as an exception, compound **117** in the N² methyl series and compound **118** in the isopropyl series showed a similar pattern as compound **116**, which in turn was reflected in the high binding activity of these compounds. The pyrazolo ring of these compounds is directed towards the extracellular environment rather than towards TM2 and TM3, and also the main nucleus pyrazolo[3,4-*d*]pyrimidine was rotated of about 45° compared to the binding pose of compound **116**. Because of this different orientation of the molecule inside the binding cleft, derivatives of N² methyl and isopropyl (**101-104**, **105-108** & **122**) might have lost the H-bonding interaction with Asn250 (TM6). The lack of these important interactions resulting from different orientation seems to be responsible for the lower binding affinity.

Binding interactions of bulky group substituted derivatives at N² position

Interestingly, the pyrazolo[3,4-*d*]pyrimidine derivatives bearing lipophilic moieties at N² position, such as phenylethyl and neopentyl derivatives, shared similar binding patterns, which accounted for high binding affinity of the compounds in these series. In fact, for all these derivatives, the pyrazolo[3,4-*d*]pyrimidine scaffold is utterly aligned inside the TM region of hA₃ receptor with the exception of compound **109** in the neopentyl series and compound **114** in the phenylethyl series. In particular, the aromatic stacking interaction with Phe168 (EL2), a lone H-bonding interaction with Asn250 (TM6) and the hydrophobic interaction with Try243 (TM6) are conserved among these derivatives. As seen in **Table 3**, compounds **115 & 116** of the N² phenylethyl series and compounds **110, 111 & 112** of the N² neopentyl series showed close binding affinity value, which is reflected in the overlapping binding pattern with one another inside the binding cleft. Notably, due to the flexible nature of the neopentyl and phenylethyl substituents, which possess lengthy and multiple rotatable bonds (2 for neopentyl and 3 for phenylethyl), enabled the scaffold to obtain a different conformation to fit into the binding cleft. Therefore, it is deduced that the presence of sterically bulky but lengthy chains at N² position ensures high binding affinity of the derivatives at the hA₃AR.

Binding interactions of PP analogues at hA_{2A} AR

As shown in **Figure 32** (panel B), the hypothetical binding pose of compound **116**, obtained after docking inside the hA_{2A} receptor crystal structure (**Figure 32, panel B**), is quite different compared to its pose inside the hA₃ subtype. However, the same region of the TM bundle is involved in the ligand recognition. Particularly, the phenylethyl ring points toward EL2 and the pyrimidine nucleus is oriented towards the intra cellular environment. The ligand formed an aromatic π - π stacking interaction with Phe168 (EL2), however it lost the H-bonding interaction with Asn253 (TM6) and the hydrophobic interaction with Try243 (TM6). Most of the newly synthesized derivatives showed slightly different binding orientation (except N² isopropyl analogues) inside the hA_{2A} receptor pocket as compared to hA₃ receptor pocket. Interestingly, it made weak interaction with Glu169 (ECL2), which is

essential for hA_{2A} affinity. All the isopropyl derivatives **105-108**, **118** & **120** showed this same binding mode inside the hA_{2A} receptor pocket. Moreover, comparing the docking pose of compound **116** on the hA_{2A} receptor with the crystallographic pose of the antagonist ZM-241385 (**Figure 32, panel A**) we noted that the bicyclic core of the pyrazolo[3,4-*d*]pyrimidine derivative was aligned opposite in comparison with the bicyclic region of ZM-241385.

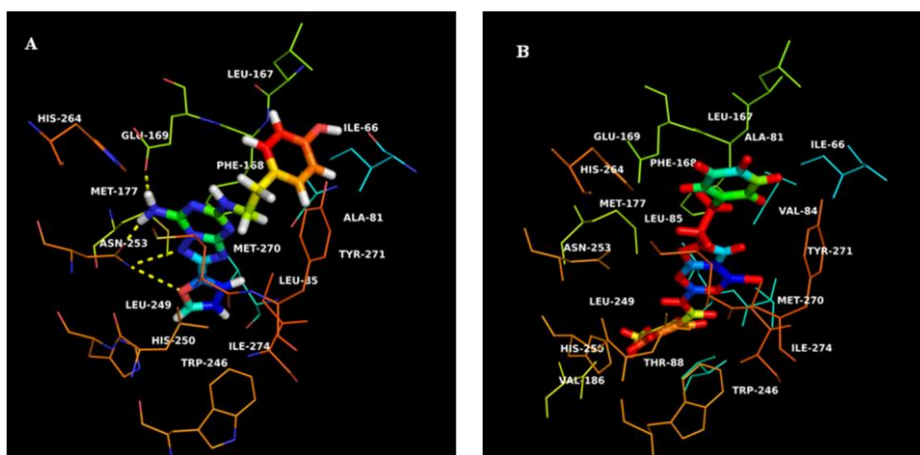


Figure 32. A. Crystallographic binding mode of ZM-241385 inside the hA_{2A} receptor (PDB code 3EML) and hypothetical binding mode of compound **116** obtained after docking simulations B. inside the hA_{2A}AR binding site and poses are viewed from the membrane side facing TM6, TM7, and TM1. The view of TM7 is omitted.

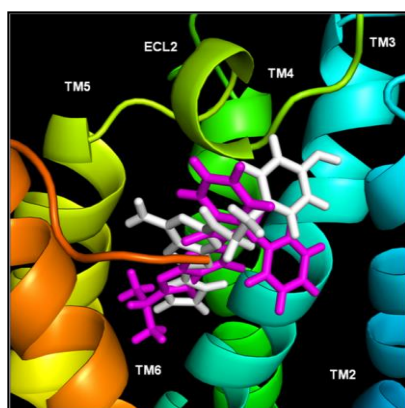


Figure 33. Binding orientation of ZM-241385 (grey) and analogue **118** (magenta) inside the hA_{2A}AR binding site. The view of TM7 is voluntarily omitted.

In contrast, N² isopropyl derivatives (**105-108**, **118** & **122**) showed slightly similar binding pattern as compared to ZM-241385. Among the isopropyl derivatives, compound **118**, with diacyl substitution at C⁶ position and with the highest hA_{2A} affinity ($K_i = 0.8 \mu\text{M}$) among all the isopropyl derivatives, showed a binding pattern close to ZM-241385 (**Figure 33**). Notably, impeded free rotation of isopropyl group due to ring constraints directed the ligand to obtain a fixed conformation and this accounted for the shifting of affinity towards the hA_{2A} receptor. The isopropyl substituents of the main scaffold are located towards the TM2, one of the diacyl chains pointing towards the EL2, whereas other acyl chains pointed towards the TM6. This result indicates that the receptor pocket, where the C⁶ appended moiety of these derivatives is accommodated, is roomy enough to hold the

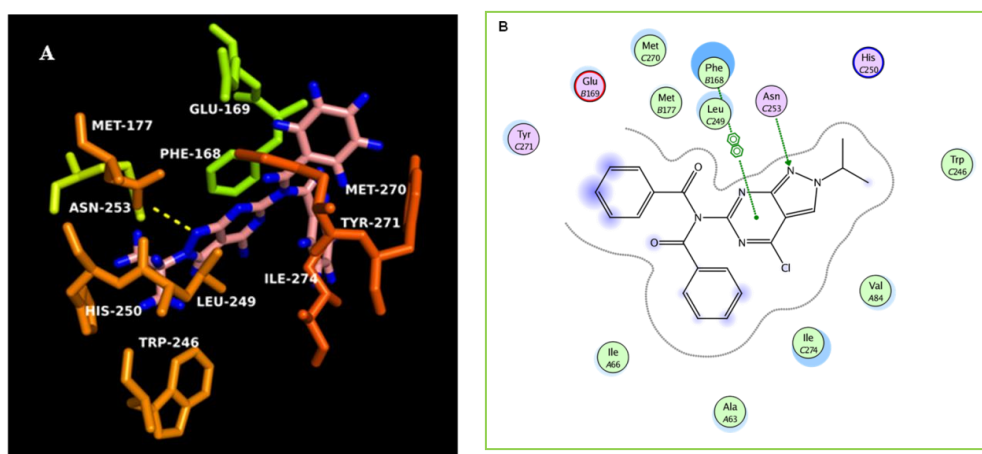


Figure 34. A. Hypothetical binding mode of analogue **118** inside the hA_{2A}AR binding site. The view of TM7 is voluntarily omitted. B. 2D view of binding residue with ligand **118** inside hA_{2A} AR binding site.

rather bulky and broadened diacyl chain. In addition, N¹ of the pyrazole ring formed a H-bonding interaction with Asn253 (TM6) and a stable interaction with Glu169 (EL2), which is considered to be vital for ligand binding at the hA_{2A}AR (**Figure 34, Panel A**). Similarly, compound **108**, with a *para*-toluoyl group of the C⁶-benzoyl substituent, bound to hA_{2A} receptor in a similar fashion as compound **118**, thus justifying an equally potent affinity at this receptor subtype. To analyze the possible ligand-receptor recognition mechanism in a quantitative way an individual electrostatic contribution ($\Delta E_{\text{int}}^{\text{el}}$) to the interaction energy (ΔE_{int}) of each receptor residue was

calculated (**Figure A3 in appendix**). The calculated electrostatic contribution per residue to the whole interaction energy for both the complexes between compound **116** and two adenosine receptor subtypes were analysed. The pattern showed stronger per residue contributions for hA₃AR-ligand complexes compared to the ones at the hA_{2A} AR. From this analysis, it was found that one of the most critical residues affecting the affinity at ARs seems to be the asparagine 6.55 (Asn 253 in hA_{2A} and Asn 250 in hA₃) due to the H-bonding interactions with the ligand mentioned above. It is evidenced that calculated electrostatic contribution of Asn (6.55) is moderate and more stabilizing for hA₃AR complex (-5 kcal/mol, **Figure A3-C in appendix**) due to a different orientations of ligand **116** inside the hA₃AR, as compared to Asn 253 (< -2 kcal/mol, **Figure A3-B in appendix**) in hA_{2A}AR complex (no hydrogen bonding interactions). Similarly, the hydrophobic interaction score pattern showed that one of the strong stabilizing contributions corresponded to the bicyclic core interactions with Phe168 (EL2) and the moderate stabilizing contributions of Leu246 (6.51). Both of these residues are essential for the hA₃AR affinity, however, one of the main residues, Phe168, showed weaker interactions at hA_{2A}AR and resulted in lower affinity towards the same receptor.

Comparison of binding interactions of PP analogues with PTP analogues in hA₃ binding site

Eventually, we compared the binding pose of the analogue **116** with the most potent **PTP** analogue, bearing a methyl group at N⁸ position, phenylacetyl moiety at C⁵ position and phenyl group at C² position.¹¹⁸ As expected, both these analogues showed similar binding patterns.

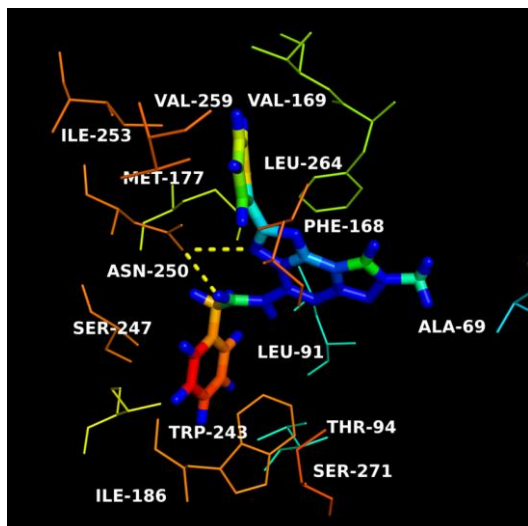


Figure 35. Hypothetical binding mode of PTP inside the hA₃AR binding site. The view of TM7 is voluntarily omitted.

Moreover, most of the compounds in the N² neopentyl and N² phenylethyl series shared almost similar binding pattern as PTP scaffold.

Generally, the main scaffold pyrazolopyrimidine aligned exactly over the pyrazolopyrimidine moiety of the PTP scaffold (**Figure 36**). In addition, the triazole ring of the PTP aligned over Cl functional group of PP. Coherently, these compounds displayed similar interactions, such as, aromatic π - π stacking interaction with Phe168, and hydrophobic interaction with residues

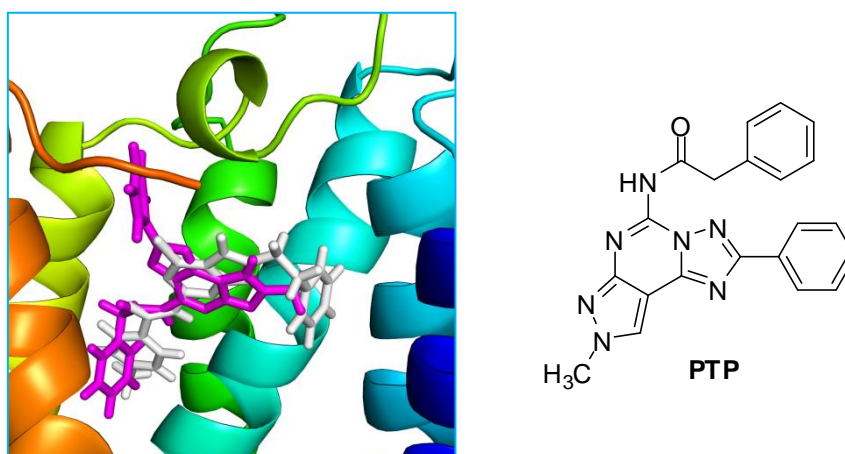


Figure 36. Binding orientation of **PTP** (magenta) and analogue **116** (grey) inside the hA₃AR binding site. The view of TM7 is voluntarily omitted.

including Met177 (TM5), Leu246 (TM6) and Leu264 (EL3), which are crucial for hA₃ affinity. Moreover, the phenyl ring of the C⁶ phenyl acetamide chain of the PTP made strong aromatic π - π stacking interaction with Trp243(TM6) (**Figure 35**).

In contrast, PP analogue made a weak hydrophobic interaction with Trp243 (TM6). Additionally, the PTP scaffold formed two stabilizing H-bonding interactions (one with the carbonyl oxygen atom and other one with N of triazole ring) with Asn250 (TM6) residue. On the contrary, the PP analogues of bulky series formed only a lone stabilizing hydrogen bonding interaction with Asn250 (TM6). Consequently, missing one H-bonding interaction of PP scaffold along with weak aromatic interaction with Trp243 (TM6) seem to explain the decrease in the binding affinity of PP analogues as compared to the PTP analogues.

3.6.3.4 Conclusion

A homology model for the hA₃ receptor has been constructed using a single-template homology modeling approach based on hA_{2A}AR crystal structure. Improved stereochemistry parameters were obtained for the hA₃ 'hybrid' model as compared to the previous study (as evidenced from Ramachandran Plot). These observations suggest that the ligand binding modes and interactions within the 'hybrid' model might be efficient, which could be further justified by the docking studies.

Indeed, through our molecular modeling investigation, the experimental findings have been rationalized by depicting the hypothetical binding mode between these newly synthesized derivatives and the specific amino acid residues within the binding site of hA₃ and hA_{2A} receptors. Overall, the molecular docking studies provided new useful insights about the steric, lipophilic, and electrostatic requirements that are important for the optimal anchoring of these derivatives to the hA₃AR recognition site. Generally, the binding pattern of the PP analogues varied depending on the length of substituents at the N²- and / or C⁶-positions of the PP. As mentioned earlier, the binding pattern of compounds bearing non bulky substituents, such as N²-methyl & N²-isopropyl derivatives, displayed slightly different binding

pose as compared to lengthy bulky substituents (neopentyl and phenylethyl) at N² position inside the hA₃ model and hA_{2A}AR.

Overall, the ligands and the residues have made the following interaction at hA₃ model: (i) hydrophobic interactions of N²-substituents with non-polar residues, which are crucial for conferring hA₃ affinity; (ii) hydrophobic interactions of phenyl ring of benzamide chain at C⁶-position, vital for affinity; (iii) van der Waals interactions of steric electron donor and or electron acceptor groups at *para* position of the benzamide chain, essential for affinity. (iv) aromatic planar bicyclic moiety like pyrazolopyrimidine ring involved in π - π interaction with the nearby aromatic residues, essential for antagonistic activity; (iv) van der Waals interactions (e.g. dipole-dipole) between the polar moiety at amidic group at C⁶ position and polar residues.

For the binding interactions of ligands at hA_{2A}AR, a restricted rotation of isopropyl group at N² position is needed along with benzamide moiety at C⁶ position to make potential interaction with Glu169. As discussed in the above section, most of the compounds of PP lost the potential H bonding interaction with Asn250 (TM6), and displayed weak hydrophobic interactions with Trp243 (TM6). However, the potent compounds of PP series still enabled the other essential hydrophobic binding interactions as PTP derivatives. This seems to explain why PP derivatives showed inferior activity to PTP scaffold. Moreover, a chloro group at C⁴ position is in close vicinity to polar residues such as Asn250 (TM6). Consequently, further structural modification such as replacing the chloro functional group at the C⁴ position with some hydrogen bond donor (CONH₂) or acceptor groups (COOC₂H₅) could potentially improve the binding affinity at hA₃ receptor and selectivity at other receptor subtypes towards new potential candidates.

Chapter 4 Rationale of further ligand modification

The SAR and the molecular modeling studies of the previously synthesized 4-chloro-pyrazolo[3,4-*d*]pyrimidine derivatives provided useful information about the relevant structural features of PP scaffold and essential amino acid interaction at the receptor's binding site required for the improvement of affinity and selectivity of PPs at the hA₃AR. Following that study, we aimed to improve the potency and selectivity of 4-chloro pyrazolo[3,4-*d*]pyrimidines, by modifying certain structural features in the previously synthesized PP derivatives.

Towards that purpose, we speculated that the following features could be vital for the hA₃ receptor antagonistic activity:

- I. C⁶ substituents with benzamide chain with different electronic properties seem crucial for good affinity at the hA₃AR. Hence benzamide chain with different substituents at *para* position will be introduced in the new series of derivatives (**Chart 4**).
- II. Electron withdrawing bulky groups at *para* position of C⁴ benzamide are essential for the selectivity, hence more bulky groups with electronic properties will be introduced (e.g. 3,4-F, 3,4-Cl, 4-Br, 3,4-Br).
- III. Considering the wide space of the A₃ binding pocket, which can accommodate relatively bulky size substituents, more C⁶ diacylated compounds will be introduced in order to determine the maximum spatial tolerability at the receptor pocket.
- IV. Upon analyzing docking results of molecular modeling studies, it was noticed that PP scaffold lacks one of the two hydrogen bonding interactions with Asn250, which was deemed essential for hA₃AR affinity as in the PTP series. Therefore, it was decided to replace the chloro group with hydrogen bond donor or hydrogen bond acceptor groups such as ester or amide groups in the new series (**Chart 4**).
- V. N² substituents with lipophilic groups such as neopentyl and phenylethyl are essential for affinity. Therefore, in the new derivatives, neopentyl and phenyl ethyl groups will be retained. In addition, some

of the N² methyl and isopropyl substituted derivatives will also be synthesized to observe the impact of hydrophilic ester substituents on the small alkyl chain derivatives and also to derive a detailed comparative structure activity relationship analysis.

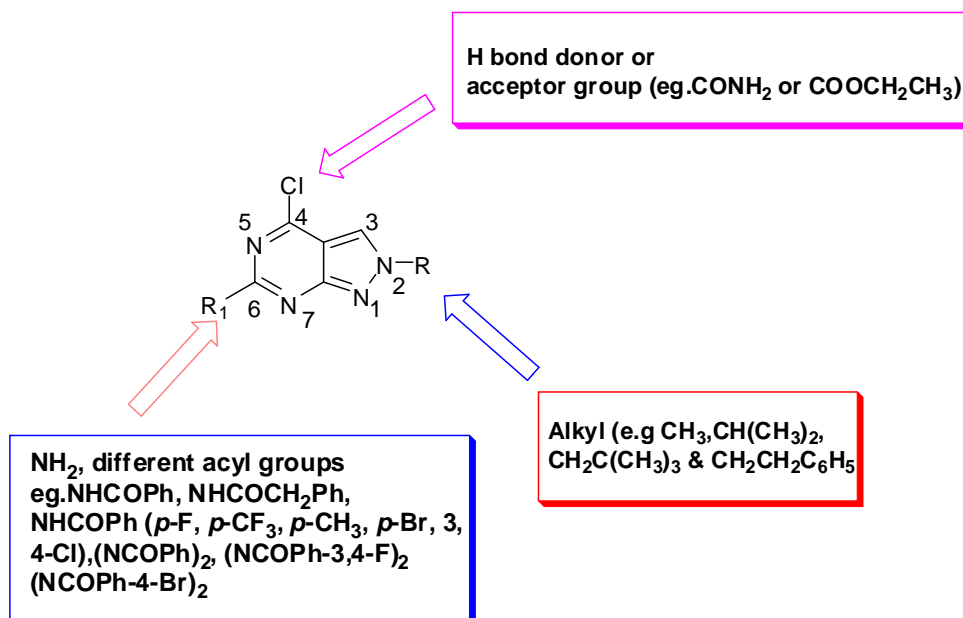


Chart 4. Structural features of pyrazolo[3,4-*d*]pyrimidines and proposed changes (R denotes N² position, R₁ denotes C⁶ position).

Hypothesis 1:

Based on the above mentioned structural limitations of the chloro group and advantages of different substituents introduced in the original PP scaffold, it is therefore hypothesized that the replacement of chloro group by ester substituents at C⁴ position, together with other substitutions at the N² and C⁶ positions, will improve the hA₃AR affinity and selectivity.

Hypothesis 2:

It is also hypothesized that pertinent molecular docking investigations will successfully rationalize the experimental data, particularly structural features at C⁴ & N⁶ position of bicyclic nucleus, towards the design of more potent and selective PP derivatives.

Main objectives:

To test these hypotheses, the following investigations were planned and carried out:

- a) Design, synthesis and characterization of a new series of pyrazolo[3,4-*d*]pyrimidine-4-carboxylate derivatives bearing an ester functional group at the C⁴-position, in conjunction with various substituents at N²- and C⁶-positions of the bicyclic scaffold.
- b) Pharmacological investigation of the new series of compounds to assess the importance of different structural parameters at each position of PP bicyclic nucleus towards the affinity and selectivity profile at the hA₃AR. This is achieved through binding affinity assays at the hA₁, hA_{2A} and hA₃ receptors as well as functional assays at the hA_{2B}AR.
- c) Detailed analyses of the SAR for the new series of pyrazolo[3,4-*d*]pyrimidines-4-carboxylate towards hA₃AR subtype.
- d) Rationalization of the experimental binding affinity data through molecular docking simulations for the new series of pyrazolo[3,4-*d*]pyrimidines-4-carboxylate derivatives.

Chapter 5 Design, Synthesis, Pharmacological and Molecular Docking Evaluation of Pyrazolo[3,4-*d*]Pyrimidine-4-carboxylate derivatives

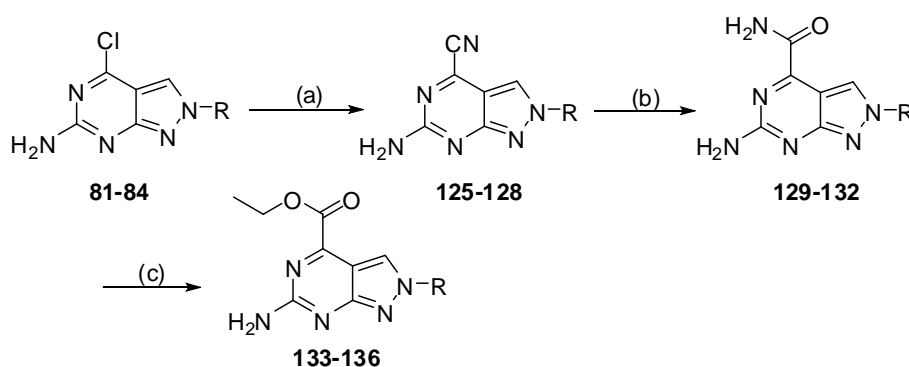
*Pharmacological assays were performed by our collaborator, Professor Karl-Norbert Klotz, at the Institute for Pharmacology and Toxicology, University of Würzburg, Germany.

5.1 Introduction

This section describes the design and synthesis of a new series of pyrazolo[3,4-*d*]pyrimidine-4-carboxylate bearing ester substituents at C⁶-position (based on the proposed structural modification as mentioned in **Chapter 7**) concurrently with different substituents at the N²- and C⁶-positions of the bicyclic nucleus. The discussion will first elaborate the synthetic schemes followed by details of the reaction and mechanism.

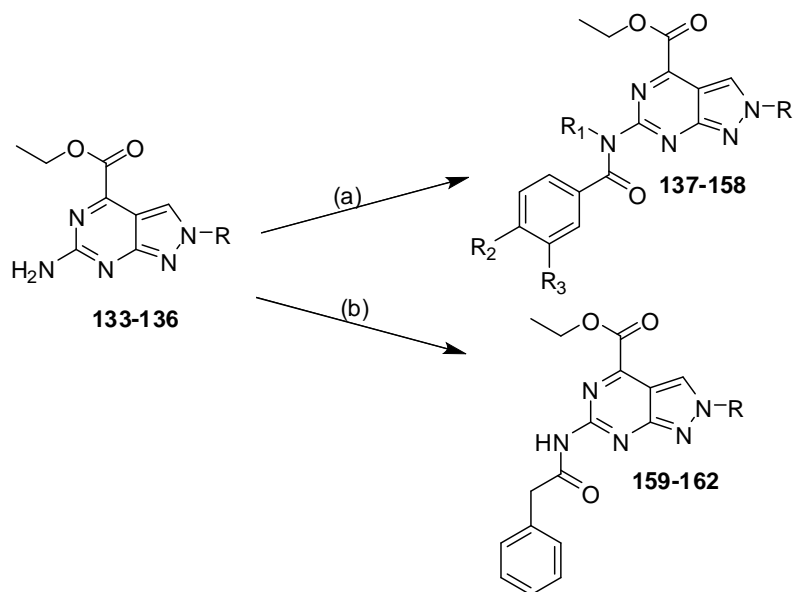
5.2 Chemical considerations

The new series of 6-amino-2-(alkyl or aralkyl)-2*H*-pyrazolo[3,4-*d*]pyrimidine-4-carboxylates **133-136** and its derivatives **137-162** were synthesized as summarized in **Schemes 3 & 4**, respectively. **Scheme 3** shows the synthesis of compounds **133-136** and **Scheme 4** depicts the synthesis of derivatives **137-162**.



Compound	R
133	CH ₃
134	CH (CH ₃) ₂
135	CH ₂ C(CH ₃) ₃
136	CH ₂ CH ₂ C ₆ H ₅

Scheme 3. Reagents : (a) NaCN / *p*-toluene sulfinate sodium / DMF, 80°C, 2h; (b) K₂CO₃ / 30% H₂O₂, rt, 1h; (c) ethanol / conc. H₂SO₄, reflux, 12 h.



No	R	R ₁	R ₂	R ₃		R	R ₁	R ₂	R ₃
133	CH ₃	-	-	-	148	CH ₂ CH ₂	H	H	H
134	CH (CH ₃) ₂	-	-	-	149	C ₆ H ₅	H	F	H
135	CH ₂ C(CH ₃) ₃	-	-	-	150	CH ₂ CH ₂	H	CF ₃	H
136	CH ₂ CH ₂	-	-	-	151	C ₆ H ₅	H	CH ₃	H
137	CH ₃	H	H	H	152	CH ₂ CH ₂ C ₆ H ₅	H	Br	H
138	CH ₃	H	F	H	153	CH ₂ CH ₂ C ₆ H ₅	H	Cl	Cl
139	CH ₃	H	CF ₃	H	154	CH ₃	C ₆ H ₅ CO	H	H
140	CH ₃	H	CH ₃	H	155	CH ₃	4-Br-C ₆ H ₅ CO	Br	H
141	CH (CH ₃) ₂	H	H	H	156	CH ₃	3,4-F-C ₆ H ₅ CO	F	F
142	CH (CH ₃) ₂	H	F	H	157	CH (CH ₃) ₂	C ₆ H ₅ CO	H	H
143	CH (CH ₃) ₂	H	CF ₃	H	158	CH ₂ CH ₂ C ₆ H ₅	C ₆ H ₅ CO	H	H
144	CH (CH ₃) ₂	H	CH ₃	H	159	CH ₃	-	-	-
145	CH ₂ C(CH ₃) ₃	H	F	H	160	CH (CH ₃) ₂	-	-	-
146	CH ₂ C(CH ₃) ₃	H	CF ₃	H	161	CH ₂ C(CH ₃) ₃	-	-	-
147	CH ₂ C(CH ₃) ₃	H	CH ₃	H	162	CH ₂ CH ₂ C ₆ H ₅	-	-	-

Scheme 4. Reagents : (a) substituted benzoyl chloride/ DIPEA/ toluene, 120°C, reflux, 24 h ; (b) phenylacetyl chloride / DIPEA/ toluene, 120°C, reflux, 24 h.

5.2.1 Synthesis of ethyl 6-amino-2-(alkyl or aralkyl)-2*H*-pyrazolo[3,4-*d*]pyrimidine-4-carboxylate (133-136), ethyl 6-benzamido-(alkyl or aralkyl)-2*H*-pyrazolo[3,4-*d*]pyrimidine-4-carboxylate (137-153), ethyl 6-(*N*-benzoylbenzamido)-2-methyl-2*H*-pyrazolo[3,4-*d*]pyrimidine-4-carboxylate (154-158), ethyl 2-(alkyl or aralkyl)-6-(2-phenylacetamido)-2*H*-pyrazolo[3,4-*d*]pyrimidine-4-carboxylate (159-162)

Nucleophilic substitution of chloro group by cyanide ion for heterocycles (e.g. purine, pyrimidine etc.) was reported by various research groups.¹⁸⁸⁻¹⁹⁰ Among them, cross coupling reaction involving KCN and palladium complex such as Pd(PPh₃)₂Cl₂ or Pd (PPh₃)₄ and Zn(CN)₂ in NMP were the most commonly used reaction conditions for the preparation of heteroarylnitriles from chloro heteroarenes.¹⁹⁰⁻¹⁹² The method from literature was followed for the cyanation; however, the reaction did not progress as expected. Subsequently, we also attempted to prepare heterocarbonitriles analogues by treatment of halohetero compounds with tetraethyl ammonium cyanide (TEACN) in the presence of base, as reported for the synthesis of purine-6-carbonitriles.¹⁹² However, the reaction was not successful. It was noticed that, in order to substitute the cyanide group, the less active chloro atom needed to be activated or replaced by other active groups.¹⁹³

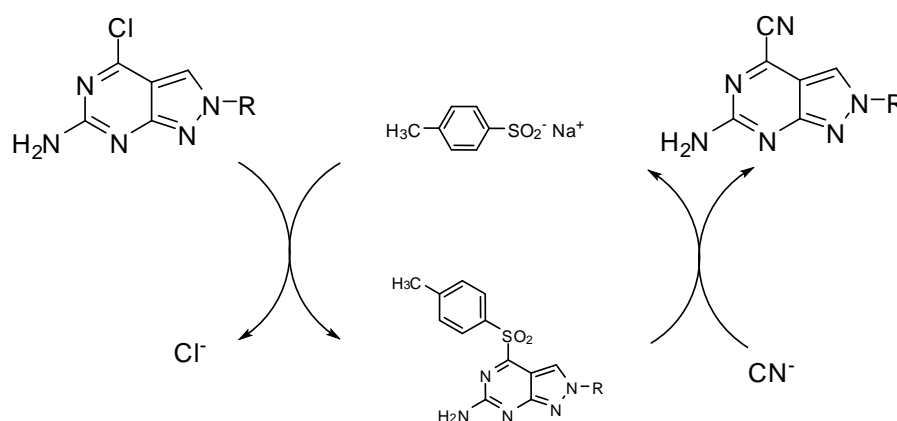


Chart 5. Proposed mechanism of formation of **125-128**

It is well known that if sulfonyl group attached with the heteroarenes, the electrophilicity of the heteroarene would be increased and subsequent nucleophilic substitution with cyanide ion will occur easily. Hence, we used

catalytic amount of sulfinate for the cyanation of chloroheteroarenes with sodium or potassium cyanide through formation of sulfonylheteroarenes.

(Chart 5)

Compounds **125-128** were prepared by treating sodium cyanide in the presence of *p*-toluene sulfinate sodium as catalyst in dry DMF at 80°C for 2 h. The nitrile groups were detected by the presence of CN peak at 115 ppm at ¹³C NMR and also confirmed by presence of CN peak between 2250-2260 cm⁻¹ in IR spectroscopy.

Hydrolysis of nitrile group was reported by several groups.^{189, 190, 194} Nitrile group can be hydrolysed by acidic or basic condition. Initially, we tried this hydrolysis using 98% H₂SO₄ in both cold and hot condition, however the reaction was not progressed. Then the reaction was carried out using literature method called “Radziszewski reaction” using aqueous hydrogen peroxide and aqueous potassium carbonate in cold or hot condition.¹⁹⁵ However, the product was obtained with low yield in cold and hot condition. Hence, with the slight modification to reported procedure, the reaction was carried out at a room temperature to obtain carbamides (**129-132**) with good yield. Mechanism related to the hydrolysis of CN to CONH₂ is depicted in the **Chart 6**.

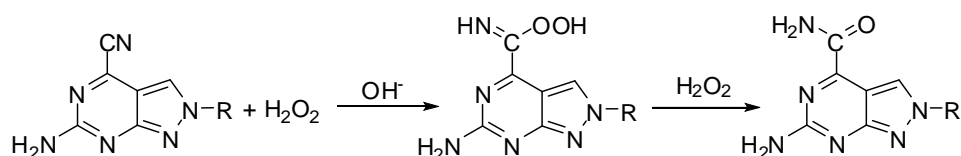


Chart 6. Proposed mechanism of formation of **129-132**

Esterification of heterocyclic amide was a straightforward reaction.¹⁵¹ Subsequently, these intermediate compounds (**129-132**) were esterified in the presence of conc.H₂SO₄ with absolute ethanol under reflux condition to obtain the corresponding carboxylates **133-136** as solid (**Chart 7**). All the corresponding final compounds **81-84** were confirmed by ¹H NMR,¹³C NMR, HMQC and mass spectra (ESI) analysis.

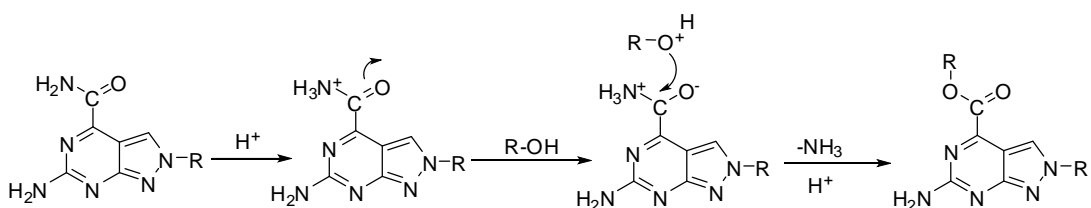


Chart 7. Proposed mechanism of formation of **133-136**

Acylation of compounds **133-136** was carried out as reported in **Scheme 4**. With a slight modification to previous 4-chloro substituted pyrazolopyrimidines, 3 equivalents of substituted benzoyl chlorides and diisopropylethylamine were used to obtain monoacylated compounds **137-153**. Disubstituted derivatives were prepared under standard conditions, using 6 equivalents of substituted benzoyl chlorides and DIPEA (compounds **154-158**). Similarly, compounds **159-162** (with phenylacetyl substitutions) were synthesized under similar conditions as compounds **137-153**. In addition, similar to C⁶ acylated 4-chloro PP derivatives, the amide formation in the ester series was confirmed by observing the absence of NH₂ peak between 7.1 to 7.5 ppm in ¹H NMR and the presence of amide (CONH) peak between 11.1 to 11.7 ppm in the ¹H NMR spectra. Further, CONH formation was confirmed by observing (C=O) carbonyl peak around 163 ppm in ¹³C NMR and HMQC NMR analysis and these NMR analysis were performed for one compound in each N-alkyl (ar-alkyl) substituted and C⁶ acylated derivatives.

5.2.2 Experimental section

5.2.2.1 Chemistry

Reactions were routinely monitored by thin-layer chromatography (TLC) on silica gel plate (precoated 60 F₂₅₄ Merck plate). Column chromatographies were performed using silica gel 60 (Merck, 70-230 mesh). Melting points were determined on a Gallenkamp instrument and were uncorrected. Compounds were dissolved in HPLC (high performance liquid chromatography) grade methanol for determination of mass to charge *m/z* on a LCQ Finnigan MAT mass spectrometer (source of ionization: Electron spin ionization (ESI) probe). ¹H and ¹³C NMR spectra were determined in the deuterated dimethylsulfoxide (DMSO-*d*₆) solutions on Bruker DPX

ultrashield NMR (400 MHz) spectrometers, with chemical shifts given in parts per million (δ) downfield relative to tetramethylsilane (TMS) as internal standard, and J values (coupling constants) given in hertz. The following abbreviations were used: s, singlet; d, doublet; t, triplet; sep, septet; m, multiplet; br, broad.

HPLC Studies. The purity of the compounds were determined using analytical HPLC using HITACHI, *version* 3.1.8b on a Phenomenex Gemini 5U C18 (5 μ M, 110 \AA , 150mm \times 4.60 mm i.d.) column at room temperature at a flow rate of 1.0 mL/min with two different mobile phase eluent systems at 254 nm UV detection. The isocratic elution was followed and analysis was carried out using two different mobile phase eluent systems such as, Eluent 1; ACN (65%): H₂O, Eluent 2; MeOH (55%): H₂O.

5.2.2.2 General procedure for synthesis of 6-amino-2-(alkyl or aralkyl)-2H-pyrazolo[3,4-*d*]pyrimidine-4-carbonitrile (125-128). A mixture of 4-chloro-2-(alkyl or aralkyl)-2H-pyrazolo[3,4-*d*]pyrimidin-6-amines **81-84** (0.00054 mol), sodium cyanide (0.0011 mol, 2 equiv), sodium *p*-toluene sulfinate (0.00016 mol, 0.3 equiv) in 5 mL of anhydrous DMF was heated on an oil bath at 80 °C for 2 h. The resultant mixture was cooled, poured into ice water mixture and stirred for 10 min. The solid was collected by filtration, washed with water and recrystallized from dimethylformamide and methanol mixture to obtain the desired products (**125-128**) as solids.

6-amino-2-methyl-2H-pyrazolo[3,4-*d*]pyrimidine-4-carbonitrile (125): Yield: 65%; pale yellow solid, mp 131-133 °C; ¹H NMR (400 MHz, DMSO-*d*₆): δ 3.88 (s, 3H, N-CH₃), 7.51 (s, 2H, NH₂), 8.24 (s, 1H, pyrazole-H). ¹³C NMR (400 MHz, DMSO-*d*₆): δ 33.7 (N-CH₃), 108.7 (C), 115.1 (CN), 131.9 (CH-pyrazole), 135.3 (C-CN), 155.7 (C-NH₂), 162.2 (N-C-N). LC-MS (ESI) analysis (m/z) calcd for C₇H₆N₆ (174.16): found 173.1 [M-H]⁺.

6-amino-2-isopropyl-2H-pyrazolo[3,4-*d*]pyrimidine-4-carbonitrile (126): Yield: 77%; pale yellow solid, mp 125-127 °C; ¹H NMR (400 MHz, DMSO-*d*₆): δ 1.47 (d, J = 6.64 Hz, 6H, 2CH₃), 4.91 (sep, J =6.40 Hz, 1H, CH), 7.46 (s, 2H, NH₂), 8.23 (s, 1H, pyrazole-H). ¹³C NMR (400 MHz, DMSO-*d*₆): δ 21.9 (CH₃), 48.3 (CH-alkyl), 109.1 (C), 115.1 (CN), 131.8 (CH-pyrazole), 135.3

(C-CN), 154.8 (C-NH₂), 162.0 (N-C-N-). LC-MS (ESI) analysis (*m/z*) calcd for C₉H₁₀N₆ (202.22): found 201.1 [M-H]⁺.

6-amino-2-neopentyl-2H-pyrazolo[3,4-*d*]pyrimidine-4-carbonitrile (127):

Yield: 62%; pale yellow solid, mp 148-150 °C; ¹H NMR (400 MHz, DMSO-*d*₆): δ 0.98 (s, 9H, 3CH₃), 4.06 (s, 2H, CH₂), 7.48 (s, 2H, NH₂), 8.27 (s, 1H, pyrazole-H). ¹³C NMR (400 MHz, DMSO-*d*₆): δ 28.1 (CH₃), 33.7 (C), 57.2 (CH₂), 108.5 (C), 115.1 (CN), 131.8 (CH-pyrazole), 135.4 (C-CN), 156.6 (C-NH₂), 162.3 (N-C-N-). LC-MS (ESI) analysis (*m/z*) calcd for C₁₁H₁₄N₆ (230.27): found 229.2 [M-H]⁺.

6-amino-2-phenethyl-2H-pyrazolo[3,4-*d*]pyrimidine-4-carbonitrile (128):

Yield: 81%; pale yellow solid, mp 135-137 °C; ¹H NMR (400 MHz, DMSO-*d*₆): δ 3.14 (t, *J* = 7.16 Hz, 2H, CH₂), 4.44 (t, *J* = 7.16 Hz, 2H, CH₂), 7.12-7.26 (m, 5H, Ar-H), 7.43 (s, 2H, NH₂), 8.21 (s, 1H, pyrazole-H). ¹³C NMR (400 MHz, DMSO-*d*₆): δ 34.9 (CH₂), 47.6 (N-CH₂), 108.8 (C), 115.0 (CN), 126.9 (CH), 128.8 (CH), 129.0 (CH), 132.1 (CH), 135.3 (C-CN), 138.5 (CH-pyrazole), 155.8 (C-NH₂), 162.2 (N-C-N-). LC-MS (ESI) analysis (*m/z*) calcd for C₁₄H₁₂N₆ (264.29): found 263.4 [M-H]⁺.

5.2.2.3 General procedure for synthesis of 6-amino-2-(alkyl or aralkyl)-2H-pyrazolo[3,4-*d*]pyrimidine-4-carboxamide (129-132). To a stirred solution of 6-amino-2-(alkyl or aralkyl)-2H-pyrazolo[3,4-*d*] pyrimidine-4-carbonitriles **125-128** (0.00057 mol) in DMSO (3 mL) at cold condition, 30% H₂O₂ (0.0023 mol, 4 equiv) and anhydrous K₂CO₃ (0.0011 mol, 2 equiv) were added. The mixture was stirred at room temperature for one hour. Then the resultant mixture was poured into ice water mixture and stirred for 10 min. The solid was collected by filtration, washed with water and recrystallized from methanol to obtain the desired products (**129-132**) as solids.

6-amino-2-methyl-2H-pyrazolo[3,4-*d*]pyrimidine-4-carboxamide (129):

Yield: 78%; White solid, mp >300 °C; ¹H NMR (DMSO-*d*₆): δ 3.83 (s, 3H, CH₃), 7.03 (s, 2H, NH₂), 7.84 (br s, 1H, NH), 7.96 (br s, 1H, NH), 8.16 (s, 1H, pyrazole-H). LC-MS (ESI) analysis (*m/z*) calcd for C₇H₈N₆O (192.18): found 191.4 [M-H]⁺.

6-amino-2-isopropyl-2H-pyrazolo[3,4-*d*]pyrimidine-4-carboxamide (130):

Yield : 70%; White solid, mp 177-179 °C; ¹H NMR (DMSO-*d*₆): δ 1.48 (d,

$J=6.8$ Hz, 6H, 2CH₃), 4.93 (sep, $J=6.52$ Hz, 1H, CH), 7.03 (s, 2H, NH₂), 7.90 (br s, 1H, NH), 7.98 (br s, 1H, NH), 8.23 (s, 1H, pyrazole-H). LC-MS (ESI) analysis (m/z) calcd for C₉H₁₂N₆O (220.23): found 219.0 [M-H]⁺.

6-amino-2-neopentyl-2H-pyrazolo[3,4-*d*]pyrimidine-4-carboxamide

(131): Yield: 79%; White solid, mp 174-176 °C; ¹H NMR (DMSO- *d*₆): δ 0.99 (s, 9H, 3CH₃), 4.07 (s, 2H, CH₂), 7.03 (s, 2H, NH₂), 7.89 (br s, 1H, NH), 8.00 (br s, 1H, NH), 8.24 (s, 1H, pyrazole-H). LC-MS (ESI) analysis (m/z) calcd for C₁₁H₁₆N₆O (248.28) : found 247.0 [M-H]⁺.

6-amino-2-phenethyl-2H-pyrazolo[3,4-*d*]pyrimidine-4-carboxamide (132):

Yield: 84%; pale yellow solid, mp 182-184 °C; ¹H NMR (400 MHz, DMSO- *d*₆): δ 3.16 (br s, 2H, CH₂), 4.44 (br s, 2H, CH₂), 7.00 (s, 2H, NH₂), 7.16-7.25 (m, 5H, Ar-H), 7.85 (br s, 1H, NH), 7.96 (br s, 1H, NH), 8.19 (s, 1H, pyrazole-H). LC-MS (ESI) analysis (m/z) calcd for C₁₄H₁₄N₆O (282.30): found 281.3 [M-H]⁺.

5.2.2.4 General procedure for synthesis of ethyl 6-amino-2-(alkyl or aralkyl)-2H-pyrazolo[3,4-*d*]pyrimidine-4-carboxylate (133-136). To a solution of 6-amino-2-(alkyl or aralkyl)-2H-pyrazolo[3,4-*d*]pyrimidine-4-carboxamides **129-132** (0.00052 mol) in absolute ethanol (30 mL), conc. H₂SO₄ (3 mL) was added slowly and the resulting mixture was refluxed at 80 °C for 12h. The reaction mixture was cooled and excess ethanol was evaporated and the resulting oily residue was poured into ice water mixture, stirred for 10 min. The solid was collected by filtration, washed with water and recrystallized from methanol to obtain the desired products (**133-136**) as solids.

Ethyl-6-amino-2-methyl-2H-pyrazolo[3,4-*d*]pyrimidine-4-carboxylate

(133): Yield : 72%; pale brown, mp 155-156 °C; ¹H NMR (DMSO- *d*₆): δ 1.37 (t, $J=7.16$ Hz, 3H, CH₃), 3.83 (s, 3H, N-CH₃), 4.42 (q, $J_1=7.10$ Hz, $J_2=14.20$ Hz, 2H, COOCH₂), 7.26 (s, 2H, NH₂), 8.09 (s, 1H, pyrazole-H). ¹³C NMR (400 MHz, DMSO-*d*₆): δ 14.5 (CH₃), 33.6 (CH₃), 62.3 (COO-CH₂), 106.4 (C), 133.9 (CH-pyrazole), 150.8 (C-COO), 156.9 (C-NH₂), 162.4 (N-C-N-), 163.8 (COO). LC-MS (ESI) analysis (m/z) calcd for C₉H₁₁N₅O₂ (221.22) : found 222.1 [M+H]⁺, 244.1 [M+Na]⁺. HPLC purity (254 nm); eluent 1: 99.7%, ^tR = 2.8 min and eluent 2: 99.7%, ^tR = 2.9 min.

Ethyl-6-amino-2-isopropyl-2H-pyrazolo[3,4-d]pyrimidine-4-carboxylate

(134): Yield: 75%; pale yellow solid, mp. 139-141 °C; ¹H NMR (DMSO-*d*₆): δ 1.37 (t, *J*= 7.16 Hz, 3H, CH₃), 1.43 (d, *J*= 6.76 Hz, 6H, 2CH₃), 4.42 (q, *J*₁= 7.16Hz, *J*₂= 14.16Hz, 2H, COOCH₂), 4.89 (sep, *J*=6.64 Hz, CH), 7.22 (s, 2H, NH₂), 8.11 (s, 1H, pyrazole-H). ¹³CNMR (400 MHz, DMSO-*d*₆): δ 14.5 (CH₃), 22.0 (CH₃), 47.9 (CH-alkyl), 62.3 (CH₂), 106.6 (C), 133.7 (CH-pyrazole), 151.0 (C-COO), 155.9 (C-NH₂), 162.4 (N-C-N-), 163.9 (COO). DEPT (400 MHz, DMSO-*d*₆): δ 14.5(CH₃), 22.0 (CH₃), 47.9 (CH-alkyl), 62.3 (CH₂), 133.7 (CH-pyrazole). LC-MS (ESI) analysis (*m/z*) calcd for C₁₁H₁₅N₅O₂ (249.27) : found 250.1 [M+H]⁺. HPLC purity (254 nm); eluent 1: 100%, ^tR = 2.7 min and eluent 2: 99.1%, ^tR = 3.2 min.

Ethyl-6-amino-2-neopentyl-2H-pyrazolo[3,4-d]pyrimidine-4-carboxylate

(135): Yield: 84%; pale yellow solid, mp. 120-122 °C; ¹H NMR (DMSO- *d*₆): δ 0.99 (s, 9H, 3CH₃), 1.43 (t, *J*= 7.0 Hz, 3H,CH₃), 4.07 (s, 2H, CH₂), 4.47 (q, *J*₁= 7.0Hz, *J*₂= 14.18 Hz, 2H, COOCH₂), 7.27 (s, 2H, NH₂), 8.18 (s, 1H, pyrazole-H). ¹³CNMR (400 MHz, DMSO-*d*₆): δ 14.5 (CH₃), 28.2 (CH₃)₃, 33.8 (C), 57.0 (CH₂), 62.3 (COOCH₂), 106.0 (C), 133.7 (CH-pyrazole), 151.0 (C-COO), 157.7 (C-NH₂), 162.7 (N-C-N-), 163.9 (COO). LC-MS (ESI) analysis (*m/z*) calcd for C₁₃H₁₉N₅O₂ (277.32) : found 278.3 [M+H]⁺, 300.2 [M+Na]⁺. HPLC purity (254 nm); eluent 1: 97.9 %, ^tR = 3.6 min and eluent 2: 100.0 %, ^tR = 3.5 min.

Ethyl-6-amino-2-phenethyl-2H-pyrazolo[3,4-d]pyrimidine-4-carboxylate

(136): Yield: 88%; yellowish brown solid, mp 131-132 °C; ¹H NMR (400 MHz, DMSO-*d*₆): δ 1.37 (t, *J*= 6.96 Hz, 3H, CH₃), 3.15 (t, *J*= 6.84 Hz, 2H, CH₂), 4.39-4.46 (m, 4H, COOCH₂, CH₂), 7.14-7.24 (m, 7H, Ar-H), 8.11 (s, 1H, pyrazole-H). ¹³C NMR (400 MHz, DMSO-*d*₆): δ 14.5 (CH₃), 35.1 (CH₂), 47.5 (N-CH₂), 62.3 (COOCH₂), 106.4 (C), 126.8 (CH-Ar), 128.8 (CH), 129.1 (CH), 133.9 (CH-pyrazole), 138.7 (C), 151.0 (C-COO), 156.9 (N-C-N-), 162.6 (C-NH₂), 163.9 (COO). LC-MS (ESI) analysis (*m/z*) calcd for C₁₆H₁₇N₅O₂ (311.34): found 312.0 [M+H]⁺. HPLC purity (254 nm); eluent 1: 100 %, ^tR = 3.1 min and eluent 2: 99.4 %, ^tR = 3.5 min.

5.2.2.5 General procedure for synthesis of ethyl 6-benzamido-(alkyl or aralkyl)-2H-pyrazolo[3,4-*d*]pyrimidine-4-carboxylate (137-151). To a suspension of ethyl 6-amino-2-(alkyl or aralkyl)-2H-pyrazolo[3,4-*d*]pyrimidine-4-carboxylates **133-136** (0.00045 mol) in anhydrous toluene (5 mL), diisopropylethylamine (0.00135 mol, 3 equiv) and substituted benzoyl chlorides (0.00135 mol, 3 equiv) were added. The mixture was heated under reflux for 24 hours. The solvent was removed under reduced pressure and the resulting residue was purified by column chromatography (hexane: EtOAc, 4:6) to obtain the desired products (**137-151**) as solids.

Ethyl-6-benzamido-2-methyl-2H-pyrazolo[3,4-*d*]pyrimidine-4-carboxylate (137): Yield : 51%; White solid, mp 107-109 °C; ¹H NMR (DMSO- *d*₆): δ 1.42 (t, *J* = 7.16 Hz, 3H, CH₃), 4.03 (s, 3H, N-CH₃), 4.50 (q, *J*₁ = 7.20 Hz, *J*₂ = 14.22 Hz, 2H, COOCH₂), 7.51-8.03 (m, 5H, Ar-H), 8.45 (s, 1H, pyrazole-H), 11.47 (s, 1H, NH). ¹³C NMR (400 MHz, DMSO-*d*₆): δ 14.5 (CH₃), 34.2 (CH₃), 62.8 (COO-CH₂), 109.9 (C), 128.8 (CH), 128.9 (CH), 129.7 (CH-pyrazole), 132.7 (CH), 134.0 (C), 150.8 (C-COO), 155.6 (C-NH), 156.2 (N-C-N), 163.4 (CO), 166.3 (COO). LC-MS (ESI) analysis (*m/z*) calcd for C₁₆H₁₅N₅O₃ (325.32) : found 326.1 [M+H]⁺, 348.2 [M+Na]⁺. HPLC purity (254 nm); eluent 1: 100%, ^tR = 3.0 min and eluent 2: 96.5%, ^tR = 3.4 min.

Ethyl-6-(4-fluorobenzamido)-2-methyl-2H-pyrazolo[3,4-*d*]pyrimidine-4-carboxylate (138): Yield: 53%; White solid, mp 103-105 °C; ¹H NMR (DMSO- *d*₆): δ 1.42 (t, *J* = 7.04 Hz, 3H, CH₃), 4.03 (s, 3H, N-CH₃), 4.50 (q, *J*₁ = 7.08 Hz, *J*₂ = 14.24 Hz, 2H, COOCH₂), 7.34-8.11 (m, 4H, Ar-H), 8.45 (s, 1H, pyrazole-H), 11.52 (s, 1H, NH). LC-MS (ESI) analysis (*m/z*) calcd for C₁₆H₁₄FN₅O₃ (343.31) : found 344.2 [M+H]⁺. HPLC purity (254 nm); eluent 1: 95.6%, ^tR = 3.0 min and eluent 2: 95.8%, ^tR = 3.5 min.

Ethyl-2-methyl-6-(4-(trifluoromethyl)benzamido)-2H-pyrazolo[3,4-*d*]pyrimidine-4-carboxylate (139): Yield : 55%; White solid. mp. 114-116 °C; ¹H NMR (DMSO- *d*₆): δ 1.42 (t, *J* = 7.16 Hz, 3H, CH₃), 4.02 (s, 3H, N-CH₃), 4.50 (q, *J*₁ = 7.14 Hz, *J*₂ = 14.24 Hz, 2H, COOCH₂), 7.89-8.18 (m, 4H, Ar-H), 8.46 (s, 1H, pyrazole-H), 11.75 (s, 1H, NH). LC-MS (ESI) analysis (*m/z*) calcd for C₁₇H₁₄F₃N₅O₃ (393.32) : found 394.2 [M+H]⁺, 416.1 [M+Na]⁺. HPLC purity (254 nm); eluent 1: 98.4%, ^tR = 5.9 min and eluent 2: 99.2%, ^tR = 5.8 min.

Ethyl-2-methyl-6-(4-methylbenzamido)-2H-pyrazolo[3,4-d]pyrimidine-4-carboxylate (140): Yield: 58%; White solid, mp. 109-111 °C; ¹H NMR (DMSO- *d*₆): δ 1.42 (t, *J* = 7.16 Hz, 3H, CH₃), 2.40 (s, 3H, CH₃), 4.03 (s, 3H, N-CH₃), 4.50 (q, *J*₁ = 7.08 Hz, *J*₂ = 14.24 Hz, 2H, COOCH₂), 7.33-7.95 (m, 4H, Ar-H), 8.44 (s, 1H, pyrazole-H), 11.38 (s, 1H, NH). LC-MS (ESI) analysis (*m/z*) calcd for C₁₇H₁₇N₅O₃ (339.35): found 340.1 [M+H]⁺, 362.1 [M+Na]⁺. HPLC purity (254 nm); eluent 1: 100.0%, ^tR = 3.7 min and eluent 2: 100%, ^tR = 3.8 min.

Ethyl-6-benzamido-2-isopropyl-2H-pyrazolo[3,4-d]pyrimidine-4-carboxylate (141): Yield : 49%; White solid, mp 115-117 °C; ¹H NMR (DMSO- *d*₆): δ 1.42 (t, *J* = 7.12 Hz, 3H, CH₃), 1.51 (d, *J* = 6.64 Hz, 6H, 2CH₃), 4.50 (q, *J*₁ = 7.10 Hz, *J*₂ = 14.26 Hz, 2H, COOCH₂), 5.07 (sep, *J* = 6.64 Hz, 1H, CH), 7.51-8.02 (m, 5H, Ar-H), 8.45 (s, 1H, pyrazole-H), 11.44 (s, 1H, NH). LC-MS (ESI) analysis (*m/z*) calcd for C₁₈H₁₉N₅O₃ (353.38): found 354.3 [M+H]⁺, 376.3 [M+Na]⁺. HPLC purity (254 nm); eluent 1: 100%, ^tR = 4.0 min and eluent 2: 100%, ^tR = 4.6 min.

Ethyl-6-(4-fluorobenzamido)-2-isopropyl-2H-pyrazolo[3,4-d]pyrimidine-4-carboxylate (142): Yield : 42%; White solid, mp 107-109 °C; ¹H NMR (DMSO- *d*₆): δ 1.41 (t, *J* = 7.12 Hz, 3H, CH₃), 1.51 (d, *J* = 6.64 Hz, 6H, 2CH₃), 4.50 (q, *J*₁ = 7.08 Hz, *J*₂ = 14.24 Hz, 2H, COOCH₂), 5.07 (sep, *J* = 6.64 Hz, 1H, CH), 7.33-8.10 (m, 4H, Ar-H), 8.45 (s, 1H, pyrazole-H), 11.49 (s, 1H, NH). ¹³CNMR (400 MHz, DMSO-*d*₆): δ 14.5 (CH₃), 22.1 (CH₃), 49.3 (CH-alkyl), 62.7 (COOCH₂), 110.2 (C), 115.6 (CH), 115.8 (CH), 131.6 (C-F), 131.7 (C), 133.9 (CH-pyrazole), 150.8 (N-C-N), 154.5 (C-COO), 155.8 (C-NH), 163.4 (CO), 165.3 (COO). LC-MS (ESI) analysis (*m/z*) calcd for C₁₈H₁₈FN₅O₃ (371.37): found 372.1 [M+H]⁺, 394.1 [M+Na]⁺. HPLC purity (254 nm); eluent 1: 97.7%, ^tR = 4.3 min and eluent 2: 97.8%, ^tR = 4.7 min.

Ethyl-2-isopropyl-6-(4-(trifluoromethyl)benzamido)-2H-pyrazolo[3,4-d]pyrimidine-4-carboxylate (143): Yield : 53%; White solid, mp 128-130 °C; ¹H NMR (DMSO- *d*₆): δ 1.41 (t, *J* = 7.04 Hz, 3H, CH₃), 1.49 (d, *J* = 6.68 Hz, 6H, 2CH₃), 4.49 (q, *J*₁ = 7.16 Hz, *J*₂ = 14.20 Hz, 2H, COOCH₂), 5.01 (sep, *J* = 6.04 Hz, 1H, CH), 7.88-8.15 (m, 4H, Ar-H), 8.46 (s, 1H, pyrazole-H), 11.72 (s, 1H, NH). LC-MS (ESI) analysis (*m/z*) calcd for C₁₉H₁₈F₃N₅O₃

(421.37) : found 422.2 [M+H]⁺, 444.2 [M+Na]⁺. HPLC purity (254 nm); eluent 1: 98.1%, ^tR = 6.9 min and eluent 2: 98.8%, ^tR = 7.3 min.

Ethyl-2-isopropyl-6-(4-methylbenzamido)-2H-pyrazolo[3,4-d]pyrimidine-4-carboxylate (144): Yield : 51%; White solid. mp. 131-133 °C; ¹H NMR (DMSO- *d*₆): δ 1.42 (t, *J*= 7.16 Hz, 3H, CH₃), 1.51 (d, *J*= 6.76 Hz, 6H, 2CH₃), 2.40 (s, 3H, CH₃), 4.50 (q, *J*₁= 7.14Hz, *J*₂= 14.18Hz, 2H, COOCH₂), 5.08 (sep, *J*= 6.76 Hz, 1H, CH), 7.32-7.94 (m, 4H, Ar-H), 8.45 (s, 1H, pyrazole-H), 11.36 (s, 1H, NH). LC-MS (ESI) analysis (*m/z*) calcd for C₁₉H₂₁N₅O₃ (367.40): found 390.3 [M+Na]⁺. HPLC purity (254 nm); eluent 1: 98.1%, ^tR = 5.0 min and eluent 2: 99.1%, ^tR = 5.4 min.

Ethyl-6-(4-fluorobenzamido)-2-neopentyl-2H-pyrazolo[3,4-d]pyrimidine-4-carboxylate (145): Yield: 57%; pale yellow solid, mp 112-114 °C; ¹H NMR (400 MHz, DMSO-*d*₆): δ 0.96 (s, 9H, 3CH₃), 1.43 (t, *J*= 7.16 Hz, 3H, CH₃), 4.21 (s, 2H, CH₂), 4.49 (q, *J*₁= 7.14 Hz, *J*₂= 14.18 Hz, 2H, CH₂), 7.33-8.09 (m, 4H, Ar-H), 8.48 (s, 1H, pyrazole-H), 11.49 (s, 1H, NH). LC-MS (ESI) analysis (*m/z*) calcd for C₂₀H₂₂FN₅O₃ (399.42): found 400.3 [M+H]⁺, 422.2 [M+Na]⁺. HPLC purity (254 nm); eluent 1: 98.9%, ^tR= 6.6 min and eluent 2: 96.3%, ^tR = 6.7 min.

Ethyl-2-neopentyl-6-(4-(trifluoromethyl)benzamido)-2H-pyrazolo[3,4-d]pyrimidine-4-carboxylate (146): Yield: 61%; pale yellow solid, mp 116-118 °C; ¹H NMR (400 MHz, DMSO-*d*₆): δ 0.99 (s, 9H, 3CH₃), 1.47 (t, *J*= 7.0 Hz, 3H, CH₃), 4.20 (s, 2H, CH₂), 4.55 (q, *J*₁= 7.02 Hz, *J*₂= 14.18 Hz, 2H, CH₂), 7.93-8.20 (m, 4H, Ar-H), 8.53 (s, 1H, pyrazole-H), 11.76 (s, 1H, NH). LC-MS (ESI) analysis (*m/z*) calcd for C₂₁H₂₂F₃N₅O₃ (449.43) : found 450.4 [M+H]⁺, 472.2 [M+Na]⁺. HPLC purity (254 nm); eluent 1: 100%, ^tR = 8.0 min and eluent 2: 97.4%, ^tR = 7.9 min.

Ethyl-6-(4-methylbenzamido)-2-neopentyl-2H-pyrazolo[3,4-d]pyrimidine-4-carboxylate (147): Yield: 48%; pale yellow solid, mp 97- 99 °C; ¹H NMR (400 MHz, DMSO-*d*₆): δ 1.01 (s, 9H, 3CH₃), 1.48 (t, *J*= 7.16 Hz, 3H, CH₃), 2.45 (s, 3H, CH₃), 4.25 (s, 2H, CH₂), 4.55 (q, *J*₁= 7.16 Hz, *J*₂ = 14.16 Hz, 2H, CH₂), 7.36-7.98 (m, 4H, Ar-H), 8.51 (s,1H, pyrazole-H), 11.39 (s, 1H, NH). ¹³C NMR (400 MHz, DMSO-*d*₆): δ 14.5 (CH₃), 21.5 (CH₃), 28.1 (CH₃)₃, 33.8 (C-alkyl), 57.8 (CH₂), 62.7 (COOCH₂), 109.4 (C), 128.9 (CH), 129.3 (CH), 129.9 (C), 131.7 (C), 133.9 (CH-pyrazole), 142.8 (N-C-N), 150.9 (C-

COO), 156.3 (C-NH), 163.5 (CO), 166.3 (COO). LC-MS (ESI) analysis (m/z) calcd for $C_{21}H_{25}N_5O_3$ (395.45) : found 396.3 $[M+H]^+$, 418.3 $[M+Na]^+$. HPLC purity (254 nm); eluent 1: 100%, t_R = 7.1 min and eluent 2: 98.4%, t_R = 7.1 min.

Ethyl-6-benzamido-2-phenethyl-2H-pyrazolo[3,4-d]pyrimidine-4-

carboxylate (148): Yield: 57%; pale yellow solid, mp 106-108 °C; 1H NMR (400 MHz, DMSO- d_6): δ 1.48 (t, J = 7.16 Hz, 3H, CH₃), 3.34 (t, J = 7.28 Hz, 2H, CH₂), 4.56 (q, J_1 = 7.10 Hz, J_2 = 14.26 Hz, 2H, CH₂), 4.72 (t, J = 7.0 Hz, 2H, CH₂), 7.22-7.32 (m, 5H, Ar-H), 7.57-8.08 (m, 5H, acyl-H), 8.49 (s, 1H, pyrazole-H), 11.51 (s, 1H, NH). LC-MS (ESI) analysis (m/z) calcd for $C_{23}H_{21}N_5O_3$ (415.44) : found 416.3 $[M+H]^+$, 438.3 $[M+Na]^+$. HPLC purity (254 nm); eluent 1: 99.7%, t_R = 3.3 min and eluent 2: 99.7%, t_R = 3.1 min.

Ethyl-6-(4-fluorobenzamido)-2-phenethyl-2H-pyrazolo[3,4-d]pyrimidine-

4-carboxylate (149): Yield: 56%; pale yellow solid, mp 112-113 °C; 1H NMR (400 MHz, DMSO- d_6): δ 1.42 (t, J = 7.12 Hz, 3H, CH₃), 3.25 (t, J = 7.24 Hz, 2H, CH₂), 4.49 (q, J_1 = 7.08 Hz, J_2 = 14.24 Hz, 2H, CH₂), 4.65 (t, J = 7.4 Hz, 2H, CH₂), 7.16-7.25 (m, 5H, Ar-H), 7.33-8.10 (m, 4H, acyl-H), 8.42 (s, 1H, pyrazole-H), 11.49 (s, 1H, NH). LC-MS (ESI) analysis (m/z) calcd for $C_{23}H_{20}FN_5O_3$ (433.44) : found 434.4 $[M+H]^+$, 456.3 $[M+Na]^+$. HPLC purity (254 nm); eluent 1: 100%, t_R = 6.5 min and eluent 2: 97.3%, t_R = 6.1 min.

Ethyl-2-phenethyl-6-(4-(trifluoromethyl)benzamido)-2H-pyrazolo[3,4-

d]pyrimidine-4-carboxylate (150): Yield: 52%; pale yellow solid, mp 105-107 °C; 1H NMR (400 MHz, DMSO- d_6): δ 1.48 (t, J = 7.16 Hz, 3H, CH₃), 3.31 (t, J = 7.16 Hz, 2H, CH₂), 4.56 (q, J_1 = 7.10 Hz, J_2 = 14.22 Hz, 2H, CH₂), 4.72 (t, J = 7.0 Hz, 2H, CH₂), 7.24-7.31 (m, 5H, Ar-H), 7.39-8.16 (m, 4H, acyl-H), 8.49 (s, 1H, pyrazole-H), 11.56 (s, 1H, NH). LC-MS (ESI) analysis (m/z) calcd for $C_{24}H_{20}F_3N_5O_3$ (483.44): found 483.3 $[M]^+$, 484.3 $[M+H]^+$. HPLC purity (254 nm); eluent 1: 100%, t_R = 6.7 min and eluent 2: 99.6%, t_R = 6.9 min.

Ethyl-6-(4-methylbenzamido)-2-phenethyl-2H-pyrazolo[3,4-d]pyrimidine-

4-carboxylate (151): Yield: 50%; pale yellow solid, mp 143-144 °C; 1H NMR (400 MHz, DMSO- d_6): δ 1.47 (t, J = 7.16 Hz, 3H, CH₃), 2.45 (s, 3H, CH₃), 3.30 (t, J = 7.28 Hz, 2H, CH₂), 4.54 (q, J_1 = 7.10 Hz, J_2 = 14.26 Hz, 2H, CH₂), 4.71 (t, J = 7.0 Hz, 2H, CH₂), 7.21-7.30 (m, 5H, Ar-H), 7.37-7.99

(m, 4H, Acyl-H), 8.47 (s, 1H, pyrazole-H), 11.40 (s, 1H, NH). LC-MS (ESI) analysis (m/z) calcd for $C_{24}H_{23}N_5O_3$ (429.47) : found 430.3 $[M+H]^+$, 452.2 $[M+Na]^+$. HPLC purity (254 nm); eluent 1: 100%, t_R = 7.2 min and eluent 2: 100%, t_R = 7.8 min.

Ethyl-6-(4-bromobenzamido)-2-phenethyl-2H-pyrazolo[3,4-*d*]pyrimidine-4-carboxylate (152): Yield: 67%; pale yellow solid, mp 139-141 °C; 1H NMR (400 MHz, DMSO- d_6): δ 1.42 (t, J = 7.04 Hz, 3H, CH₃), 3.25 (t, J = 7.28 Hz, 2H, CH₂), 4.49 (q, J_1 = 7.08 Hz, J_2 = 14.24 Hz, 2H, CH₂), 4.65 (t, J = 7.16 Hz, 2H, CH₂), 7.16-7.52 (m, 5H, Ar-H), 7.81-8.19 (m, 4H, acyl-H), 8.43 (s, 1H, pyrazole-H), 11.59 (s, 1H, NH). LC-MS (ESI) analysis (m/z) calcd for $C_{23}H_{20}BrN_5O_3$ (494.34) : found 494.1 $[M]^+$, 496.1 $[M+2H]^+$, 516.2 $[M+Na-H]^+$, 518.1 $[M+Na+H]^+$. HPLC purity (254 nm); eluent 1: 97.9%, t_R = 10.3 min and eluent 2: 100%, t_R = 9.1 min.

Ethyl-6-(3,4-dichlorobenzamido)-2-phenethyl-2H-pyrazolo[3,4-*d*]pyrimidine-4-carboxylate (153): Yield: 64%; pale yellow solid, mp 147-149 °C; 1H NMR (400 MHz, DMSO- d_6): δ 1.42 (t, J = 7.16 Hz, 3H, CH₃), 3.25 (t, J = 7.28 Hz, 2H, CH₂), 4.49 (q, J_1 = 7.10 Hz, J_2 = 14.26 Hz, 2H, CH₂), 4.65 (t, J = 7.16 Hz, 2H, CH₂), 7.14-7.25 (m, 5H, Ar-H), 7.77-8.26 (m, 3H, acyl-H), 8.43 (s, 1H, pyrazole-H), 11.66 (s, 1H, NH). ^{13}C NMR (400 MHz, DMSO- d_6): δ 14.5 (CH₃), 34.9 (CH₂), 48.3 (CH₂), 62.8 (COOCH₂), 110.0 (C), 126.9 (CH-Ar), 128.8 (CH), 129.1 (CH), 130.9 (C), 131.1 (CH), 131.4 (CH), 131.7 (C-Cl), 134.2 (CH-pyrazole), 135.0 (C-Cl), 138.4 (C), 150.8 (C-NH), 155.4 (C-COO), 155.7 (N-C-N-), 163.3 (CO), 164.3 (COO). LC-MS (ESI) analysis (m/z) calcd for $C_{23}H_{19}Cl_2N_5O_3$ (484.33) : found 484.2 $[M]^+$, 506.0 $[M+Na]^+$. HPLC purity (254 nm); eluent 1: 97.7%, t_R = 11.1 min and eluent 2: 100.0%, t_R = 12.0 min.

5.2.2.6 General procedure for synthesis of ethyl 6-(N-benzoylbenzamido)-2-methyl-2H-pyrazolo[3,4-*d*]pyrimidine-4-carboxylate (154-158). To a suspension of ethyl 6-amino-2-(alkyl or aralkyl)-2H-pyrazolo[3,4-*d*]pyrimidine-4-carboxylates **133-136** (0.00045 mol) in anhydrous toluene (5 mL), diisopropylethylamine (0.0027 mol, 6 equiv) and benzoyl chloride or substituted benzoyl chlorides (0.0027 mol, 6 equiv) were added. The mixture was heated under reflux for 24 hours. The solvent was removed under

reduced pressure and the resulting residue was purified by column chromatography (hexane: EtOAc, 4:6).

Ethyl-6-(N-benzoylbenzamido)-2-methyl-2H-pyrazolo[3,4-*d*]pyrimidine-4-carboxylate (154): Yield: 56%; White solid, mp. 105-107 °C; ¹H NMR (DMSO- *d*₆): δ 1.36 (t, *J*= 7.16 Hz, 3H, CH₃), 3.87 (s, 3H, N-CH₃), 4.43 (q, *J*₁= 7.16 Hz, *J*₂= 14.16 Hz, 2H, COOCH₂), 7.47-7.83 (m, 10H, Ar-H), 8.53 (s, 1H, pyrazole-H). LC-MS (ESI) analysis (*m/z*) calcd for C₂₃H₁₉N₅O₄ (429.43): found 430.2 [M+H]⁺, 452.2 [M+Na]⁺. HPLC purity (254 nm); eluent 1: 98.0%, ^tR = 5.4 min and eluent 2: 97.8%, ^tR = 5.4 min.

Ethyl-6-(4-bromo-N-(4-bromobenzoyl)benzamido)-2-methyl-2H-pyrazolo[3,4-*d*]pyrimidine-4-carboxylate (155): Yield: 53%; White solid, mp. 128-130 °C; ¹H NMR (DMSO- *d*₆): δ 1.36 (t, *J*= 7.0 Hz, 3H, CH₃), 3.92 (s, 3H, N-CH₃), 4.43 (q, *J*₁= 7.08 Hz, *J*₂= 14.24 Hz, 2H, COOCH₂), 7.40-8.05 (m, 8H, Ar-H), 8.56 (s, 1H, pyrazole-H). LC-MS (ESI) analysis (*m/z*) calcd for C₂₃H₁₇Br₂N₅O₄ (587.22): found 587.1 [M]⁺, 610.2 [M+Na]⁺. HPLC purity (254 nm); eluent 1: 95.5%, ^tR = 13.0 min and eluent 2: 13.7%, ^tR = 99.5 min.

Ethyl-6-(N-(3,4-difluorobenzoyl)-3,4-difluorobenzamido)-2-methyl-2H-pyrazolo[3,4-*d*]pyrimidine-4-carboxylate (156): Yield: 59%; White solid, mp. 169-171 °C; ¹H NMR (DMSO- *d*₆): δ 1.36 (t, *J*= 7.16 Hz, 3H, CH₃), 3.92 (s, 3H, N-CH₃), 4.43 (q, *J*₁ = 7.16 Hz, *J*₂ = 14.20 Hz, 2H, COOCH₂), 7.52-8.00 (m, 6H, Ar-H), 8.55 (s, 1H, pyrazole-H). LC-MS (ESI) analysis (*m/z*) calcd for C₂₃H₁₅F₄N₅O₄ (501.39) : found 502.1 [M+H]⁺, 524.2 [M+Na]⁺. HPLC purity (254 nm); eluent 1: 100.0%, ^tR = 11.6 min and eluent 2: 100.0%, ^tR = 13.0 min.

Ethyl-6-(N-benzoylbenzamido)-2-isopropyl-2H-pyrazolo[3,4-*d*]pyrimidine-4-carboxylate (157): Yield: 53%; White solid, mp 140-142 °C; ¹H NMR (DMSO- *d*₆): δ 1.25 (d, *J*= 6.64 Hz, 6H, 2CH₃), 1.37 (t, *J*= 7.04 Hz, 3H, CH₃), 4.45 (q, *J*₁= 7.04 Hz, *J*₂= 14.04 Hz, 2H, COOCH₂), 4.79 (sep, *J*= 6.52 Hz, 1H, CH), 7.47-7.97 (m, 10H, Ar-H), 8.51 (s, 1H, pyrazole-H). LC-MS (ESI) analysis (*m/z*) calcd for C₂₅H₂₃N₅O₄. (457.48) : found 458.3 [M+H]⁺, 480.2 [M+Na]⁺. HPLC purity (254 nm); eluent 1: 99.7%, ^tR = 8.0 min and eluent 2: 99.3%, ^tR = 8.3 min.

Ethyl-6-(N-benzoylbenzamido)-2-phenethyl-2H-pyrazolo[3,4-*d*]pyrimidine-4-carboxylate (158): Yield: 55%; pale yellow solid, mp 157-

159 °C; ¹H NMR (400 MHz, DMSO-*d*₆): δ 1.41 (t, *J*= 7.04 Hz, 3H, CH₃), 2.87 (t, *J*= 6.92 Hz, 2H, CH₂), 4.48 (q, *J*₁= 7.08 Hz, *J*₂= 14.12 Hz, 2H, CH₂), 4.57 (t, *J*= 6.92 Hz, 2H, CH₂), 6.92-7.25 (m, 5H, Ar-H), 7.54-8.02 (m, 10H, acyl-H), 8.50 (s, 1H, pyrazole-H), LC-MS (ESI) analysis (*m/z*) calcd for C₃₀H₂₅N₅O₄ (519.55): found 520.1 [M+H]⁺, 542.3 [M+Na]. HPLC purity (254 nm); eluent 1: 95.8%, *t*_R = 9.4 min and eluent 2: 97.9%, *t*_R = 9.3 min.

5.2.2.7 General procedure for synthesis of ethyl 2-(alkyl or aralkyl)-6-(2-phenylacetamido)-2*H*-pyrazolo[3,4-*d*]pyrimidine-4-carboxylate (159-162).

To a suspension of ethyl-6-amino-2-(alkyl or aralkyl)-2*H*-pyrazolo[3,4-*d*]pyrimidine-4-carboxylates **133-136** (0.00045 mol) in anhydrous toluene (5 mL), diisopropylethylamine (0.00135 mol, 3 equiv) and phenylacetyl chloride (0.00135 mol, 3 equiv) were added. The mixture was heated under reflux for 24 hours. The solvent was removed under reduced pressure and the resulting residue was purified by column chromatography (hexane: EtOAc, 4:6)

Ethyl-2-methyl-6-(2-phenylacetamido)-2*H*-pyrazolo[3,4-*d*]pyrimidine-4-carboxylate (159): Yield: 49%; White solid, mp. 168-170 °C; ¹H NMR (DMSO- *d*₆): δ 1.42 (t, *J*= 7.16 Hz, 3H, CH₃), 3.87 (s, 2H, CH₂), 3.98 (s, 3H, N-CH₃), 4.49 (q, *J*₁=7.10 Hz, *J*₂=14.26 Hz, 2H, COOCH₂), 7.24-7.38 (m, 5H, Ar-H), 8.39 (s, 1H, pyrazole-H), 11.29 (s, 1H, NH). LC-MS (ESI) analysis (*m/z*) calcd for C₁₇H₁₇N₅O₃ (339.35) : found 340.3 [M+H]⁺, 362.3 [M+Na]⁺. HPLC purity (254 nm); eluent 1: 100%, *t*_R = 3.8 min and eluent 2: 99.3%, *t*_R = 3.6 min.

Ethyl-2-isopropyl-6-(2-phenylacetamido)-2*H*-pyrazolo[3,4-*d*]pyrimidine-4-carboxylate (160): Yield: 45%; White solid, mp. 120-122 °C; ¹H NMR (DMSO- *d*₆): δ 1.41 (t, *J*= 7.16 Hz, 3H, CH₃), 1.49 (d, *J*= 6.64 Hz, 6H, 2CH₃), 3.87 (s, 2H, CH₂), 4.49 (q, *J*₁= 7.16 Hz, *J*₂= 14.20 Hz, 2H, COOCH₂), 5.04 (sep, *J*= 6.52 Hz, 1H, CH), 7.25-7.37 (m, 5H, Ar-H), 8.39 (s, 1H, pyrazole-H), 11.28(s, 1H, NH). LC-MS (ESI) analysis (*m/z*) calcd for C₁₉H₂₁N₅O₃ (367.40) : found 368.3[M+H]⁺, 390.2[M+Na]⁺. HPLC purity (254 nm); eluent 1: 100%, *t*_R = 4.1 min and eluent 2: 99.7%, *t*_R = 4.2 min.

Ethyl-2-neopentyl-6-(2-phenylacetamido)-2*H*-pyrazolo[3,4-*d*]pyrimidine-4-carboxylate (161): Yield: 47%; pale yellow solid, mp 112-114 °C; ¹H NMR (400 MHz, DMSO-*d*₆): δ 0.97 (s, 9H, 3CH₃), 1.46 (t, *J*= 7.16 Hz, 2H,

CH₂), 3.92 (s, 2H, CH₂), 4.21 (s, 2H, Ar-CH₂), 4.53 (q, *J*₁= 7.08 Hz, *J*₂= 14.24 Hz, 2H, COOCH₂), 7.28 -7.41 (m, 5H, Ar-H), 8.45 (s, 1H, pyrazole-H), 11.30 (s, 1H, NH). LC-MS (ESI) analysis (*m/z*) calcd for C₂₁H₂₅N₅O₃ (395.45) : found 396.1 [M+H]⁺, 418.2 [M+Na]⁺. HPLC purity (254 nm); eluent 1: 99.9%, *t*_R = 5.7 min and eluent 2: 97.2%, *t*_R = 5.5 min.

Ethyl-2-phenethyl-6-(2-phenylacetamido)-2*H*-pyrazolo[3,4-*d*]pyrimidine-4-carboxylate (162): Yield: 53%; pale yellow solid, mp 141-143 °C; ¹H NMR (400 MHz, DMSO-*d*₆): δ 1.44 (t, *J*= 7.16 Hz, 3H, CH₃), 3.26 (t, *J*= 7.16 Hz, 2H, CH₂), 3.92 (s, 2H, CH₂), 4.51 (q, *J*₁= 7.08 Hz, *J*₂= 14.24 Hz, 2H, CH₂), 4.65 (t, *J*= 7.0 Hz, 2H, CH₂), 7.16-7.31 (m, 5H, Ar-H), 7.35-7.41 (m, 5H, acyl-H), 8.41 (s, 1H, pyrazole-H), 11.28 (s, 1H, NH). LC-MS (ESI) analysis (*m/z*) calcd for C₂₄H₂₃N₅O₃ (429.47) : found 430.2 [M+H]⁺, 452.3 [M+Na]⁺. HPLC purity (254 nm); eluent1: 100%, *t*_R = 7.7 min and eluent 2: 100%, *t*_R = 7.5 min.

5.2.3 Conclusion

The synthesis of 34 new pyrazolopyrimidine-4-carboxylates derivatives was successfully achieved using optimized synthetic procedures as described above. All the final compounds and derivatives were confirmed by ¹H NMR, ¹³C NMR and mass spectrometry (ESI). Additionally, final compounds **135**, **136** and derivatives **137**, **142**, **147** & **153** were confirmed by 2D NMR (HMQC). The purity of the compounds was determined by HPLC analysis (HPLC data of newly synthesized compounds **129-136** were tabulated in **Table A5** under appendix) and all of the compounds showed purity of 95% and above, which were considered to be pure for biological evaluation.

5.3 Pharmacological Evaluation of a Novel Series of PyrazoloPyrimidine-4-Carboxylate Derivatives

5.3.1 Introduction

Binding affinities of the novel series of pyrazolo[3,4-*d*]pyrimidine-4-carboxylates at the human A₁, A_{2A} and A₃ adenosine receptor subtypes and the adenylyl cyclase activity of the derivatives at the human A_{2B} receptor are described in this chapter. In addition, the selectivities were also assessed by comparing the binding affinity values (K_i) against the hA₃ receptor with K_i values against the hA₁ and hA_{2A} receptors. This section also describes the docking studies of pyrazolo[3,4-*d*]pyrimidine-4-carboxylate derivatives performed on hA_{2A}AR based on hA₃AR homology model and crystal structure of hA_{2A}AR, to rationalize the predicted binding affinity with experimental binding affinities.

5.3.2 Experimental Methods

The displacement of selective radioligands towards respective adenosine receptors (expressed in Chinese Hamster Ovary cells (CHO) for hA₁, hA_{2A}, hA₃ receptors), which were previously bound to cell surface expressed by receptors, was measured to evaluate the binding affinities of the new synthesized compounds. Binding experiments were carried out as reported in the **Chapter 4**. For more details on experimental methods which include, CHO membrane preparation, binding assay of human cloned A₁, A_{2A}, A₃ adenosine receptor and adenylyl cyclase assay, please refer **Chapter 4, Section 4.2**.

5.3.3 Results and discussion

5.3.3.1 Binding affinity towards human A₁, A_{2A} and A₃ adenosine receptors: Structure-affinity relationships

Pharmacological evaluation was performed for the novel series of pyrazolo[3,4-*d*]pyrimidine-4-carboxylate to examine their binding affinities at all four adenosine receptor subtypes. The receptor binding affinities of compounds **129-162** were determined at the human A₁, A_{2A}, A₃ receptors and the corresponding adenylyl cyclase activity in CHO cells which expressed the human A_{2B} receptors are summarized in **Table 11**.

In this project, ligand modification of 4-chloro-PP derivatives bearing pyrazolopyrimidine basic nucleus, C⁴ ester substituents (different to chloro group of previous PP series), various lipophilic N² alkyl and aralkyl substituents and different substituents with electronic properties at C⁶ benzamide chain, was carried out to improve the hA₃AR affinity and selectivity profile towards other receptor subtypes. Towards that purpose, a new series of 2-(alkyl and aralkyl substituted)-2*H*-pyrazolo[3,4-*d*]pyrimidine-4-carboxylate derivatives substituted at N², C⁶ and C⁴ positions, was successfully synthesized and characterized. The binding assay results indicated that the ligand modification increased the affinity and remarkably improved selectivity towards other receptor subtypes as compared to the 4-chloro-PP series. Indeed, most of the pyrazolo[3,4-*d*]pyrimidine-4-carboxylates improved the affinity at hA₃ receptors as indicated by the very low micromolar range (K_i hA₃ = 0.7-34 μM) and some of the compounds displayed high selectivity (>111 at hA₁ / hA₃ and hA_{2A} / hA₃) towards the other receptor subtypes.

Effect of C⁴ amide and C⁴ ester with C⁶ free amino substitution on affinity of PP scaffold

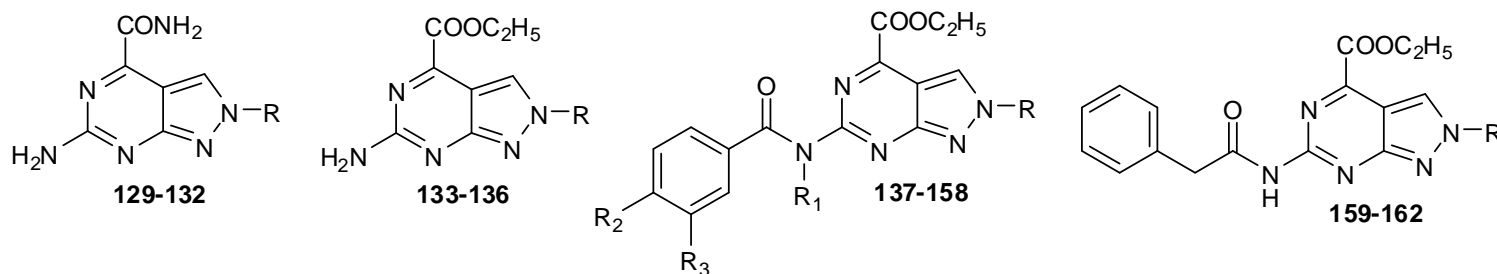
The binding assay results of the analogues bearing various alkyl substitutions (i.e. methyl, isopropyl & neopentyl) or a phenylethyl group at N² position were compared to examine the impact of the alkyl group substitutions at N² on the pharmacological profile. Based on the bioassay results, the alkyl substituents (methyl, isopropyl & neopentyl) at N² position of the pyrazolo ring seemed to modulate the affinity at hA₃AR to a considerable level. In

addition, binding affinity of C⁴ amide substituents (**129-132**) with free amino groups was compared with C⁴ ester substituted compounds (**133-136**). All of the C⁴ amide substituted compounds exhibited a weak affinity towards the hA₃AR (K_i hA₃ = 16.9 - >100 μM) as compared to the C⁴ ester compounds (K_i hA₃ = 0.7 - 30 μM). However, these C⁴-amide derivatives propelled the affinity towards hA_{2A}AR and hA₁AR and displayed 13-15 times selectivity over hA₃AR. Conversely, among the compounds with C⁶ free amino substituents but with an ester group at C⁴ (**133-136**), compound **133**, with a methyl group at N² displayed the best affinity at the hA₃AR (K_i hA₃ = 0.7 μM) in the whole series and also exhibited moderate affinity towards other receptor subtypes (K_i hA_{2A} = 2 μM and K_i hA₁ = 9.3 μM). In addition, compound **134**, with a N² isopropyl group, displayed a sub micromolar affinity towards the hA₁AR (K_i hA₁ = 0.9 μM), with 35 times selectivity over the hA₃AR.

Effect of C⁶ acyl substitution on affinity of PP scaffold

N²-methyl: Substitution of benzamide or substituted benzamide groups at C⁶ position and a methyl group at N² gave rise to compounds with drastically decreased affinity towards the hA₃AR (**137-140, 154&156**, K_i hA₃ = >100 μM), with the only exception of compound **155**, with a dibenzamide substitution along with *para*-Br group at C⁶: this compound, in fact, presented the best combined affinity and selectivity profile in N² small alkyl substituted derivatives (**155**, K_i hA₃ = 2.9 μM, hA₁/A₃ >34, hA_{2A}/A₃ >34). The reason behind such affinity profile is still unclear, since similar dibenzamide substituted compounds **154** and **156** with 3,4-F group at *para* position (K_i hA₃ = >100 μM) were inactive at hA₃AR (K_i hA₃ >100 μM). This emphasize the fact that steric group (Br) at *para* position of dibenzoyl chain might have played a role essential for the improvement of affinity at hA₃AR. Interestingly, similar trend was also observed with the other receptor subtypes (**137-140, 154-156**; K_i hA₁ = 21.5 - >100 μM, K_i hA_{2A} = 14 - >100 μM) throughout the series. However, this is in contrast with previous findings of 4-chloro-PP and PTP derivatives,¹¹⁸ where corresponding benzamide substitution ameliorated the affinity towards hA₃AR.

Table 11. Binding affinity (K_i) of synthesized compounds at hA₁, hA_{2A}, and hA₃ adenosine receptors^[a] and selectivity against hA₁ and hA_{2A} receptors (R denotes N² position)



Compound	R	R ¹	R ²	R ³	K_i / IC ₅₀ (μM)				Selectivity	
					A ₁ (K_i) ^[b]	A _{2A} (K_i) ^[c]	A _{2B} (IC ₅₀) ^[d]	A ₃ (K_i) ^[e]	hA ₁ /h ₃	hA _{2A} /h ₃
129	CH ₃	-	-	-	8.3	3.8	>100	>100	>0.08	>0.04
130	CH(CH ₃) ₂	-	-	-	8.4	9.3	>100	>100	>0.08	>0.09
131	CH ₂ C(CH ₃) ₃	-	-	-	~80	~80	>100	16.9	4.7	4.7
132	CH ₂ CH ₂ C ₆ H ₅	-	-	-	43	12.5	>100	34.4	1.2	0.4
133	CH ₃	-	-	-	9.3	2.0	>100	0.7	13.2	2.9
134	CH(CH ₃) ₂	-	-	-	0.9	2.7	~80	30.0	0.03	0.09
135	CH ₂ C(CH ₃) ₃	-	-	-	4.0	5.3	~80	18.6	0.2	0.3
136	CH ₂ CH ₂ C ₆ H ₅	-	-	-	3.7	4.9	~60	17.0	0.2	0.3
137	CH ₃	H	H	-	21.5	16.1	>100	>100	>0.2	>0.1
138	CH ₃	H	F	-	>100	14.0	>100	>100	>1	>1
139	CH ₃	H	CF ₃	-	>100	>100	>100	>100	>1	>1

Compound	R	R ¹	R ²	R ³	K _i / IC ₅₀ (μM)				Selectivity	
					A ₁ (K _i) ^[b]	A _{2A} (K _i) ^[c]	A _{2B} (K _i) ^[d]	A ₃ (K _i) ^[e]	hA ₁ / hA ₃	hA _{2A} / h ₃
140	CH ₃	H	CH ₃	-	>100	12	>100	~100	>1	>1
141	CH(CH ₃) ₂	H	H	-	4.8	3.3	~100	5.3	0.9	0.6
142	CH(CH ₃) ₂	H	F	-	2.9	3.1	>100	5.7	0.5	0.5
143	CH(CH ₃) ₂	H	CF ₃	-	>100	>100	>100	>100	>1	>1
144	CH(CH ₃) ₂	H	CH ₃	-	0.7	3.1	~100	28.7	0.02	0.1
145	CH ₂ C(CH ₃) ₃	H	F	-	2.7	5.9	>100	4.5	0.6	1.3
146	CH ₂ C(CH ₃) ₃	H	CF ₃	-	>100	>100	>100	1.3	>77	>77
147	CH ₂ C(CH ₃) ₃	H	CH ₃	-	>100	>100	>100	0.9	>111	>111
148	CH ₂ CH ₂ C ₆ H ₅	H	H	-	5.2	3.7	~80	7.4	0.7	0.5
149	CH ₂ CH ₂ C ₆ H ₅	H	F	-	5.2	6.1	>100	7.0	0.7	0.8
150	CH ₂ CH ₂ C ₆ H ₅	H	CF ₃	-	2.7	7.5	~100	9.0	0.3	0.8
151	CH ₂ CH ₂ C ₆ H ₅	H	CH ₃	-	>100	6.0	>100	3.0	>33	2
152	CH ₂ CH ₂ C ₆ H ₅	H	Br	-	2.6	4.5	~100	3.6	0.7	1.2
153	CH ₂ CH ₂ C ₆ H ₅	-	Cl	Cl	>100	>100	>100	2.2	>46	>46
154	CH ₃	C ₆ H ₅ CO	H	-	>100	>100	>100	>100	>1	>1
155	CH ₃	(4Br)C ₆ H ₅ CO	Br		>100	>100	>100	2.9	>34	>34

Compound	R	R ¹	R ²	R ³	K _i / IC ₅₀ (μM)				Selectivity	
					A ₁ (K _i) ^[b]	A _{2A} (K _i) ^[c]	A _{2B} (K _i) ^[d]	A ₃ (K _i) ^[e]	hA ₁ /hA ₃	hA _{2A} /h ₃
156	CH ₃	(3,4F)C ₆ H ₅ CO	F	F	>100	>100	>100	>100	>1	>1
157	CH(CH ₃) ₂	C ₆ H ₅ CO	H		17.7	>100	>100	5.4	3.2	>19
158	CH ₂ CH ₂ C ₆ H ₅	C ₆ H ₅ CO	H		>100	>100	>100	>100	>1	>1
159	CH ₃	-	-	-	5.9	7.3	>100	15.2	0.3	0.5
160	CH(CH ₃) ₂	-	-	-	0.7	8.8	~80	9.5	0.07	0.9
161	CH ₂ C(CH ₃) ₃	-	-	-	6.0	8.3	>100	8.1	0.7	1.0
162	CH ₂ CH ₂ C ₆ H ₅	-	-	-	0.6	1.8	~30	7.1	0.08	0.2

[a] Adenylyl cyclase activity of synthesized compounds at the hA_{2B}AR. [b] Displacement of specific [³H]-CCPA binding at human A₁ receptors expressed in Chinese hamster ovary (CHO) cells (n=3–6). [c] Displacement of specific [³H]-5'-ethyl carboxamido adenosine (NECA) binding at human A_{2A} receptors expressed in CHO cells (n=3–6). [d] K_i values for inhibition of NECA-stimulated adenylyl cyclase activity in CHO cells (n=3–6). [e] Displacement of specific [³H]-2-(1-hexynyl)-N⁶-methyl adenosine (HEMADO) binding at human A₃ receptors expressed in CHO cells (n=3-6).

N²-isopropyl: On the other hand, benzamide substitution of N² isopropyl derivatives (**141-144**) showed much improved affinity (K_i hA₃ = 5.4-28.7 μM) as compared to its N²-methyl counterpart derivatives, with the exception of compound **143**, which was inactive at all the receptor subtypes. Similarly, these derivatives (**141-144**) showed a comparable or even better affinity at hA_{2A}AR and hA₁AR, thus determining a weak selectivity of the compounds. Compound **157**, with C⁶-dibenzamide substitution, displayed good affinity (K_i hA₃=5.4 μM) and high selectivity (hA_{2A}/A₃ = >19) towards the hA_{2A}AR subtype. Moreover, its selectivity towards the hA_{2A}AR subtype is improved 190 fold as compared to similar substitution with 4-chloro PP derivatives (Compound **120** in **Table 3**). In contrast, compound **144** (K_i hA₁ = 0.7 μM) with *para*-CH₃ benzamide chain at C⁶ position, was inactive at the hA₃AR and showed submicromolar affinity towards the hA₁AR.

N²-neopentyl: Similarly, C⁶-benzamide substitution of N² neopentyl analogues displayed the overall best affinity (K_i hA₃ = 0.9-8.1 μM) and selectivity among the different N² alkyl and phenylethyl substituted derivatives. Presence of *para*-F group in the benzamide chain led to compound **145** with improved affinity (K_i hA₃ = 4.5 μM) as compared to its N² isopropyl counterpart (**142**). When the *para*-F group of benzamide was replaced by electron withdrawing steric CF₃ group, the activity was increased by 4 fold (**146**, K_i hA₃ = 1.3 μM). as compared to **145**. In addition, the selectivity was remarkably improved to large extent by 77 fold towards both hA_{2A}AR and hA₁AR. Interestingly, the same C⁶ substituted compound of the previous chloro series (Compound **111** in **Table 3**) displayed only 15 fold selectivity towards the hA_{2A}AR and hA₁AR. Similarly, when *para*-CH₃ group was introduced at the benzamide chain, the affinity was further improved (**147**, K_i hA₃ = 0.9 μM) to 5 fold as compared to compound **145**. Moreover, this compound (**147**) showed second best affinity and the best overall selectivity (111 fold *versus* hA_{2A}AR and hA₁AR) in the whole series. This strongly suggests that both electron withdrawing CF₃ and electron donating CH₃ groups are highly essential for the affinity at hA₃AR and selectivity towards the other receptor subtypes. Moreover, this compound (**147**) displayed 6 fold increment in the hA₃AR affinity and over 50 fold

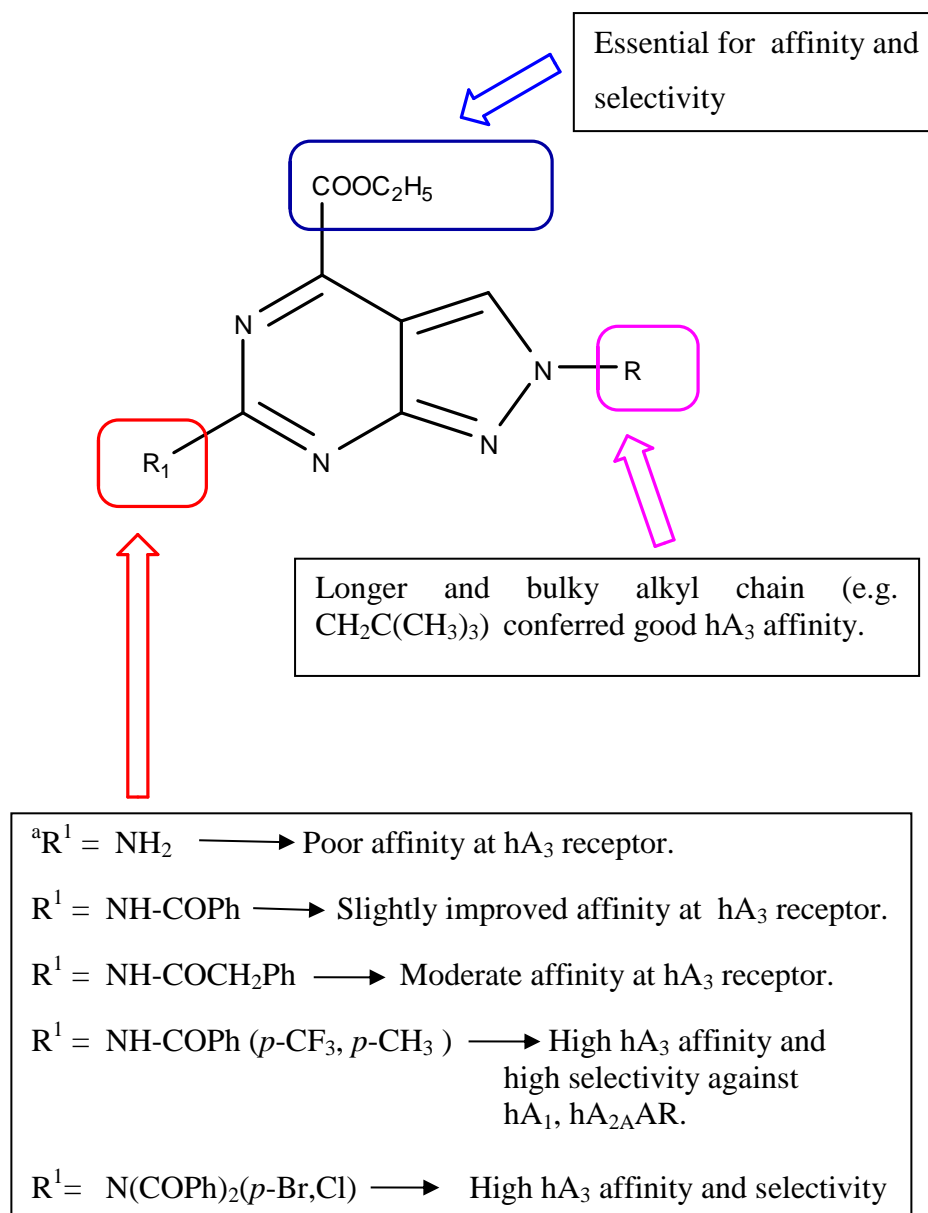


Figure 37. Overview of structure-affinity relationship (SAR) profile for the new series of PP-4-carboxylate derivatives **129-162**. ${}^a\text{N}^2$ -methyl group favoured high hA_3 affinity.

versus hA_1AR and 278 fold *versus* hA_{2A}AR enhancement in the selectivity as compared to its N^2 -chloro-PP counterpart compound (**112**).

N^2 phenylethyl: Benzamide substitution in the N^2 phenylethyl derivatives (**148-153 & 162**) further improved the affinity ($K_i \text{ hA}_3 = 2.2\text{-}9.0 \mu\text{M}$) as compared to free amino compound **136**, with the exception of compound **158**, which was not active at any of the receptor subtypes. Among these derivatives, unsubstituted benzamide (**148**) showed moderate affinity ($K_i \text{ hA}_3 = 7.4 \mu\text{M}$).

Surprisingly, electron withdrawing substitution such as F (**149** K_i hA₃ = 7.0) and CF₃ (**150**, K_i hA₃ = 9.0 μM) failed to make any additional impact on the affinity at hA₃AR. Conversely, *para*-CH₃ benzamide (**151**, K_i hA₃ = 3.0 μM) improved affinity around 2.5 fold as compared to unsubstituted benzamide derivative (**148**) and also strengthened the selectivity against hA₁AR by 33 fold. In addition, introduction of a bulky Br group at the *para* position of benzamide (**152**) led to a 2 fold improvement in the affinity (K_i hA₃ = 3.6 μM) as compared to **148**. Similarly, steric dichloro substitution at 3&4 positions of benzamide (**153**) ameliorated the affinity by >3 fold as compared to **148**. This compound (**153**) was 46 times more selective for hA₃AR against the hA_{2A}AR and hA₁AR.

This signifies the necessity of having a steric electronwithdrawing chloro group at the *para* position of benzamide. Surprisingly, dibenzoyl substitution (**158**, K_i hA₃ = >100 μM) made the compound inactive. This is in contrast to the dibenzoyl substitution of the chloro series, where the compound (compound **120** in **Table 3**) displayed comparable affinity and selectivity to monoacylated compounds.

Throughout the series, a lengthy phenylacetamide substitution (**159-162**) at the C⁶ position did not improve the affinity (K_i hA₃ = 7.1-15.2 μM) and selectivity at hA₃AR significantly. This could be due to the steric hindrance of the phenylacetamide chain at the C⁶ position. However, compounds **160** (K_i hA₁ = 0.7 μM), and **162** (K_i hA₁ = 0.6 μM), showed high potent affinity towards the hA₁AR. This could promote further investigations on hA₁AR.

5.3.3.2 Comparison of SAR of PP-4-carboxylate with 4-chloro-PP derivatives

Figure 37 summarizes the structure-affinity relationship (SAR) profiles observed in this new series of pyrazolopyrimidine-4-carboxylate derivatives (**129-162**). Overall, the C⁶ free amino group with N² substituents in the 4-chloro-PP and PP-4-carboxylate derivatives displayed similar affinity at the hA₃AR with the exception of compound **133** of PP-4-carboxylate, which was remarkably (143 fold) more potent than its 4-chloro counterpart (Compound **81** in **Table 3**). Similarly, the C⁶ benzamide chain substitution in

the N² methyl compound series displayed entirely a different affinity profile as compared to the chloro series. In the ester series, N² isopropyl derivatives were non selective whereas in the chloro series, N² isopropyl derivatives were significantly selective towards the hA_{2A}AR. Similarly, neopentyl derivatives in the ester series showed much superior affinity as compared to the chloro series derivatives. Particularly, *para*-F substituted compound (**145**) was 22 times more potent than that of its chloro counterpart towards hA₃AR. In contrast, compound **150**, with N² phenylethyl and C⁶ *para*-CF₃ benzamide chain of the ester series displayed 3 fold decrease in affinity as compared to the chloro series analogue. Similarly, *para*-CH₃ group (compound **151**) showed a slight decreased affinity and an increase in selectivity against the hA₁AR by 5 times as compared to the chloro series compounds.

PP-4-Carboxylate	4-Chloro-PP
N ² neopentyl derivatives showed 5 fold improvement in affinity and 50 fold improvement in selectivity.	N ² neopentyl derivatives showed moderate affinity.
N ² Phenyl ethyl derivatives affinity was maintained but the selectivity was improved by 5 fold.	N ² Phenyl ethyl derivatives showed good affinity.
N ² methyl derivatives totally lost the affinity at all four receptor subtypes, except the diacyl (<i>p</i> -Br)substituted compounds.	N ² methyl derivatives showed weak affinity.
N ² isopropyl derivatives showed affinity towards the hA ₁ AR	N ² isopropyl derivatives showed affinity to hA _{2A} AR.

Table. 12 Comparison of affinity of 4-Chloro-PP derivatives with PP-4-Carboxylate derivatives.

In summary, ligand modification of the 4-chloro-pyrazolopyrimidine led to the derivatives with improved affinity at hA₃AR and selectivity over hA₁AR and hA_{2A}AR. Based on the binding assay results, the hypothesis of replacing chloro group by ester substituents at C⁴ position and introducing

electron withdrawing and electron donating substituents (e.g. CF₃, CH₃, Br, Cl) at the *para* position of the C⁶ benzamide chain have been successfully proven. In addition, the structure-affinity relationship analysis showed that substituents at N², C⁴ & C⁶ positions play a key role in modulating the binding affinity at the hA₃AR. In particular, at the N² position, neopentyl substitution showed favourable effect on the affinity at hA₃ receptor (**147**, K_i hA₃ = 0.9 μM). Similarly, *para*-CF₃ and *para*-CH₃ groups of the same series were proven to be important for selectivity (**147**; hA₁/A₃ = >111, hA_{2A}/A₃ = >111 and **146**; hA₁/A₃ = >77, hA_{2A}/A₃ = >77. Additionally, C⁶-free amino group with N² methyl substitution was proven to be vital for affinity (**133**, K_i hA₃ = 0.7 μM), whereas subsequent acylation was detrimental for the affinity for methyl derivatives (**137**, K_i hA₃ = >100 μM). In contrast, dibenzamide substituents with steric groups at the *para* position in the N² methyl series was essential for affinity (**155**, K_i hA₃ = 2.9 μM) and selectivity (hA₁/A₃ = >34, hA_{2A}/A₃ = >34), Similarly, additional substitution at the aromatic ring such as 3,4-Cl as in compound **153** (**155**, K_i hA₃ = 2.2 μM, hA₁/A₃ = >46, hA_{2A}/A₃ = >46) was also important for affinity and selectivity.

From this new design, we conclude that the simplified bicyclic pyrazolopyrimidines have partially overcome some of the limitations of the PTP analogues, as described in the **Table 13**.

Phycochemical Properties	PTP	PP
Mol. Wt range	265-552 (g/mol)	183-420 (g/mol)
ClogP	2.8-4.9	1.0-3.5
Yield	Low (15-17%), difficult purification (column)	High (72-88%), mostly precipitation reactions
Synthesis difficulties	High temperature and longer reaction time required	Reflux conditions and straight forward reactions
Polar groups	Less	More

Table. 13 Comparison of physicochemical properties of PP-4-Carboxylate derivatives with PTP derivatives.

Although the new PP-4 carboxylate derivatives showed better affinity and selectivity profile than 4-chloro PP series derivatives (**Table 12**), these compounds are still inferior in affinity as compared to the parent PTP derivatives. Further, to improve the affinity and selectivity, it is deduced that, benzamide chain could be replaced by steric and lengthy aralkyl or substituted phenyl groups, since lengthy steric groups are favoured at the C⁶ position. Additionally, electron withdrawing and /or electron donating groups such as Cl, Br, CF₃, CH₃ etc., could be substituted at the *para* position of phenyl groups. Moreover, considering the potent affinity of neopentyl groups at N² position, various bulky alkyl chains (e.g. *tert*-butyl) or halide substituted alkyl chain could also be introduced at this position to improve the affinity further. In addition, the ester group might be substituted by some bioisosteres (oxazole or ketoxime ether) or a free amino group.

5.4. Docking Evaluation of a Novel Series of PyrazoloPyrimidine-4-Carboxylate Derivatives

5.4.1 Introduction

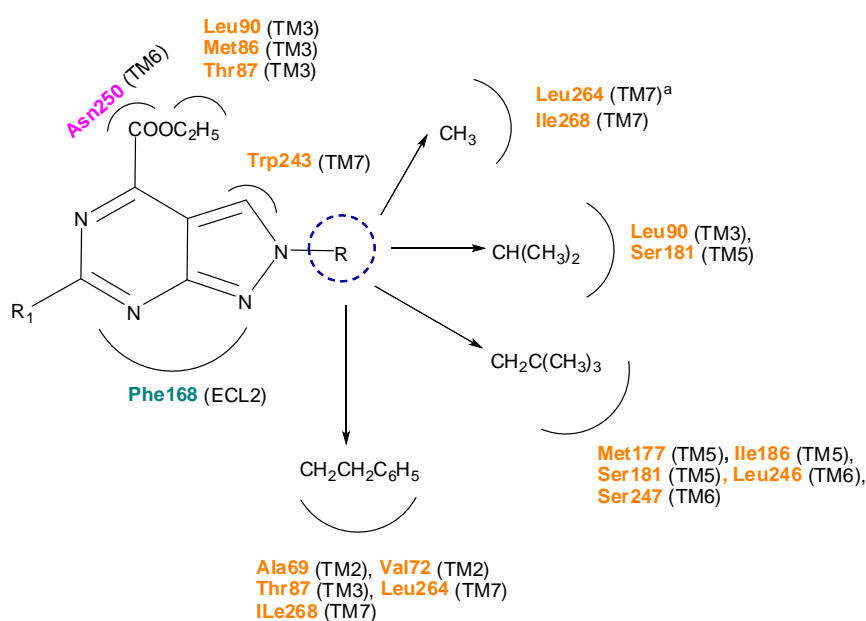
This section describes the docking studies of pyrazolo[3,4-*d*]pyrimidine-4-carboxylate derivatives performed on hA_{2A}AR based on hA₃AR homology model and crystal structure of hA_{2A}AR, to rationalize the predicted binding affinity with experimental binding affinities.

5.4.2 Results and Discussion

The molecular docking studies were performed on newly synthesized pyrazolopyrimidine-4-carboxylate derivatives (**129-162**) to identify hypothetical binding mode and interaction at the hA₃AR and also to rationalize the results of the binding data. Docking studies were performed using molecular operating environment (MOE) programme and all new pyrazolo[3,4-*d*]pyrimidine-4-carboxylate derivatives were docked into the orthosteric trans-membrane (TM) binding cavities of both hA₃ and hA_{2A} adenosine receptors and the binding interaction of N² alkyl, C⁶ substituted

derivatives are compared with N² aralkyl, C⁶ substituted derivatives. Similarly, the binding modes and interactions of the potent compound of the new PP-4-carboxylate series was compared with the potent compounds of both 4-chloro-PP (**116**) and PTP series.

Docking simulation demonstrated that binding pattern of the derivatives varied depending on the substituents at N² & C⁶ position in the whole series. Ligand-recognition occurred in the upper region of the TM bundle, and the pyrazolo[3,4-*d*]pyrimidine scaffold was surrounded by TMs 3, 5, 6, 7. As seen with the 4-chloro PP compounds, 4 different types of interactions were observed and among them hydrophobic interactions and hydrogen bonding interaction seemed to play an essential role.

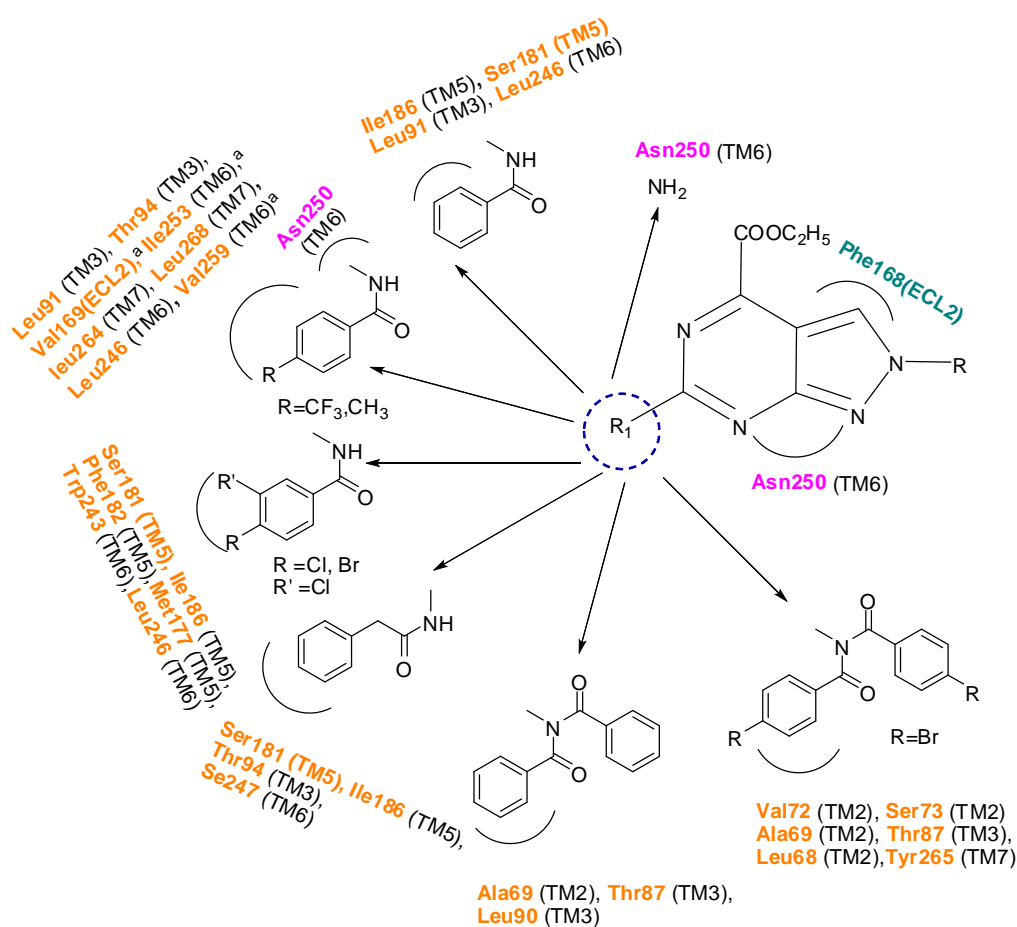


Residue: Involved in π - π interaction, **Residue:** Involved in hydrogen bonding interaction, **Residue:** Involved in hydrophobic interaction

Figure 38. Common binding interactions of new series of PP-4-carboxylates (**133-162**) with N² substitution ^aResidues found to interact with C⁶ free amino substitution only.

Figures 38 & 39 summarize the binding interactions of the pyrazolo[3,4-*d*]pyrimidine-4-carboxylate derivatives. Among the C⁶ free amino group compounds, compound **133** was positioned at the centre of the binding pocket on the top of the TM helix (**Figure 40**). This could be due to

the unrotatable nature of the N²-methyl group, which assisted ligand to obtain a stable confirmation at the centre of the binding pocket.



Residue: Involved in π - π interaction, **Residue:** Involved in hydrogen bonding interaction, **Residue:** Involved in hydrophobic interaction

Figure 39. Common binding interactions of new series of PP-4-carboxylates (133-162) with C⁶ substitution. ^aResidues found to interact with N² neopentyl substitution only.

Although the binding orientation is same as the potent compound of the chloro series (**116** in **Table 3**), the ligand was inverted to about 180° and preserved the important hydrophobic interactions with Tyr265, Ile268, Leu264, Leu246, Leu90 and Thr87. Moreover, compound **133** also made the lone stabilizing hydrogen bonding interaction with Asn250 and pyrimidine ring of the PP scaffold made π - π stacking interaction with Phe168. On the other hand, other

compounds (**134-136**) with bulky chains at N² position, due to steric hindrance, orientated in different fashion and they were oriented away from

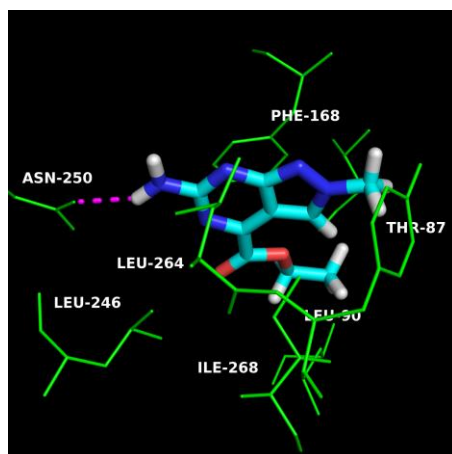


Figure 40. Hypothetical binding mode of compound **133** obtained after docking simulations inside the hA₃AR binding site. Poses are viewed from the membrane side facing TM6, TM7, and TM1. The view of TM7 is omitted.

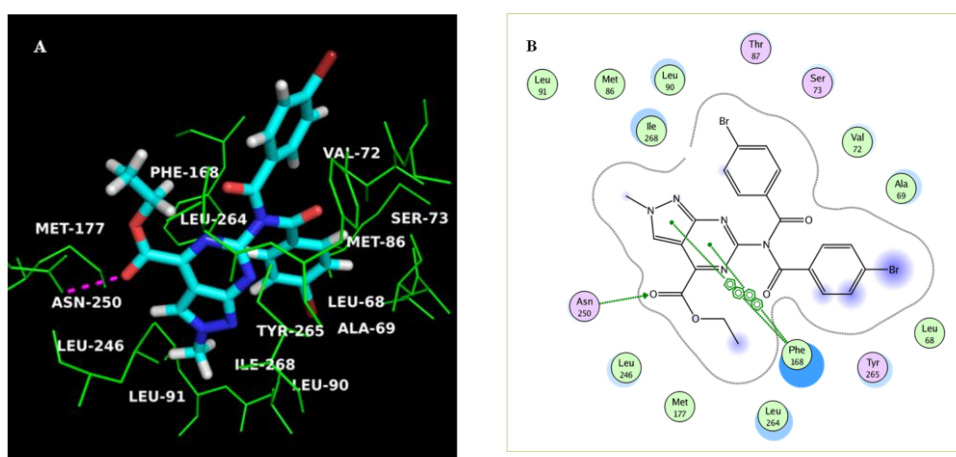


Figure 41. A. Hypothetical binding mode of compound **155** obtained after docking simulations inside the hA₃AR binding site. Poses are viewed from the membrane side facing TM6, TM7, and TM1. The view of TM7 is omitted. B. 2D view of binding residue with ligand **155** inside hA₃AR binding site.

the centre and moved towards the TM 4. The binding mode of compound **133** inside the hA_{2A}AR was also analysed. Interestingly, the compound occupied the same position as hA₃AR and it retained the vital hydrogen bonding interaction with Asn253 and other hydrophobic interactions with hA_{2A}AR. This led to the poor selectivity of compound **133**. It is to be noted that the same N² methyl substituted compound (**81** in **Table 3**) with a chloro group at C⁴ (instead of the ester group of derivative **133**) was inactive at hA₃AR. This

could be due to the rotatable nature of the hydrophilic ester group in **133**, which assisted the ligand to obtain a suitable confirmation to make a potential hydrogen bonding and hydrophobic interaction.

In contrast, acylated compounds of N² methyl derivatives (**137-140**, **154**) displayed different binding pose as compared to compound **133**. The extra benzamide linkage of the analogues caused the ligands to move away from the centre, and to orient slightly to the interior towards TM4. This caused the ligands to lose an essential hydrogen bonding interaction with Asn250 and also a π - π stacking interaction with Phe168. Whereas compound **159**, with lengthy phenylacetamide chain at C⁶ position, was able to interact with some of the hydrophobic residues because of the rotatable methylene group, which assisted the ligand to attain a slightly different binding pattern.

In addition, compound **155**, with *para*-Br dibenzamide substituent at C⁶ position, was positioned at the centre, due to the broaden and rotatable nature of the dibenzamide chain (**Figure 41**). Moreover, this substituted dibenzamide chain interacted with hydrophobic residues such as Val72, Ser73, Leu68 and Tyr265. Interestingly, these interactions were not seen with the *para* unsubstituted dibenzamide derivatives (compound **154**), due to absence of steric Br group. Similarly, the ethyl group of the C⁴-ester chain interacted with Met177, Leu246, and Leu264, while basic nucleus PP made π - π stacking interaction with Phe168. Most importantly, carbonyl group of the ester substituents made hydrogen bonding interactions with Asn250. This proven the speculation that hA₃AR binding site possesses the maximum spatial tolerability, which can accommodate the broaden diacyl chain with even stronger steric group (Br).

Generally, acylated N² isopropyl ligands moved towards the centre of the binding pocket due to the steric hindrance produced by the isopropyl group, which extended towards the TM4. Ligands were bound in a vertical direction at the centre of the binding pocket. These binding poses are quite different from the ones observed for the benzamide derivatives (**137-140**) of N² methyl group series. The basic scaffold was situated at the centre of the binding pocket and the benzamide chains are extended towards the TM6 and

TM7. Due to this close contact with TM helix, the carbonyl group of the ester chains were able to make a hydrogen bonding interaction with Asn250, with

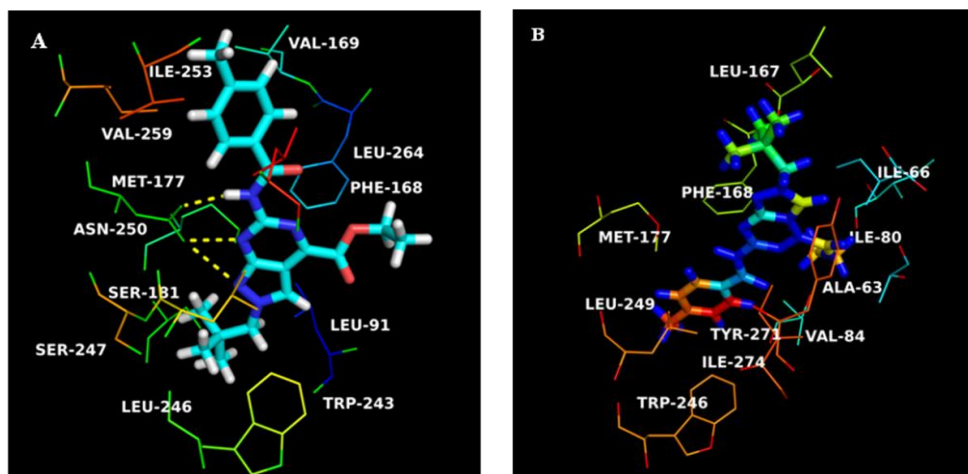


Figure 42. **A.** Hypothetical binding mode of compound **147** obtained after docking simulations inside the hA₃AR binding site. **B.** Compound **147** inside the hA_{2A}AR binding site. Poses are viewed from the membrane side facing TM6, TM7, and TM1. The view of TM7 is omitted.

exception of compound **143** with steric CF₃ group that created a steric hindrance and made the chain unavailable for the interaction with Asn 250 residue.

Interestingly, N² neopentyl substituted benzamide compounds displayed a slightly different binding pose in comparison to compound **133**. Among them, compound **147** (**Figure 42-A**), which was the most potent analogue of the C⁴-ester series, was placed little away from the centre of the binding pocket towards the TM5. In addition, the ester group was oriented towards the TM2 and the phenyl ring of the benzamide pointed towards the ECL2. Due to this reason, it was able to make a potential hydrogen bonding interaction with Asn250. Surprisingly, three stabilizing hydrogen bonding interactions were observed between ligand **147** and Asn250. Among them, one of the hydrogen bonding was seen with NH of the amide chain, and other two bondings were observed with the N-1 of the pyrazole and N-2 of pyrimidine, respectively. Similarly, another potent and selective compound of the series, compound **146**, also shared a close resemblance of the binding pose and was

noticed that, due to the highly steric Cl group, the compound made some additional hydrophobic interactions with Ile186, which is not observed with other benzamide substituted compounds (**148-152**).

Generally, dibenzamide substituted compounds (**154, 156 &158**) moved away from the binding site, oriented deeply into the intracellular loop and the ligands were flipped to opposite direction as of ligand **153**, i.e. the pyrazole towards the TM6 (instead of TM3) and the pyrimidine towards the TM3 (instead of TM 6). Due to the irregular orientation, phenyl ring of the dibenzamide made stacking interactions with Phe168.

We also docked the newly synthesized compounds inside the hA_{2A} binding pocket. We noticed that most of the compounds shared similar binding pose inside the binding pocket. In addition, the most potent and selective compound of the series, compound **147**, showed quite a opposite binding orientation inside the hA_{2A} binding pocket (**Figure 42-B**) as compared to hA_{3AR} and failed to make hydrophobic interaction with essential residue such as Glu169 and barely made contact with Asn253 which is essential for the Some of the common hydrophobic residues observed around the ligands are Ala63, Ile80, Val84, Leu85, Trp246 and Tyr271.

Finally, we compared the binding pose of the most potent compounds of both chloro (**116**) and ester series (**147**) inside the hA_{3AR}. It was observed that compound **147** was oriented in a different pattern from compound **116** of the chloro series. It is speculated that rotatable ester chain at C⁴ position caused the ligand to attain different confirmation. However, compound **147** retained all essential hydrophobic interactions with residues such as Met177, Leu246 and Leu264 and Trp243. As seen earlier, compound **147** gained extra stabilizing hydrogen bonding interaction with Asn250, whereas with

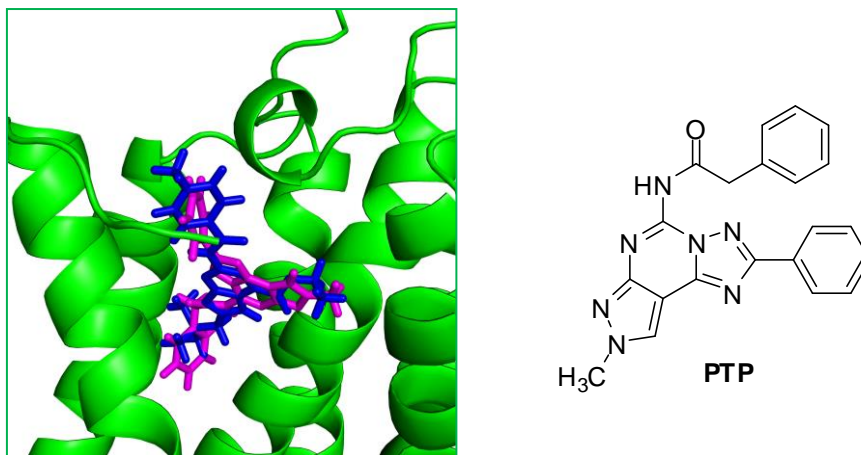


Figure 44. Binding orientation of **PTP** (magenta) and analogue **147** (blue) inside the hA₃AR binding site. The view of TM7 is voluntarily omitted. receptor affinity.

compound **116**, a lone hydrogen bonding interaction was observed (**Figure 31-A in Chapter 6**). These findings substantiate the experimental results of increased affinity and selectivity for compound **147** over compound **116**.

The docking pose of the compound **147** was also compared with the most potent PTP compound **125**. As seen in the **Figure 44**, the binding orientations of both the ligands are slightly different. However, compound **147** is oriented in same plane as PTP. Interestingly, there is a trend observed between the binding pose of the PTP and compound **147**. Phenyl ring of the benzamide linkage in the PP is aligned over the phenyl ring of the PTP, thereby the PP has retained the essential hydrophobic interactions with residues such as Met177, Leu246 and Leu264 and Trp243, which are observed at the phenyl ring of PTP. Moreover, the ester chain of **147** was aligned over N² methyl group of the PTP counterpart, thus retaining interaction with residues associated with N² methyl of PTPs. Finally, the N²-neopentyl group was aligned over phenylacetamide chain of the PTP and involved in the hydrophobic interactions common to the phenylacetamide chain of **PTP**. These findings signify that most of the hydrophobic interactions associated with PTP are retained in the PP ligand as well.

5.4.3 Conclusion

Generally, binding assay results exemplified that C⁴ ester substituted derivatives (**129-162**) are more potent than that of C⁴ chloro substituted compounds (**81-124**). The structure-affinity relationship analysis showed that substituents at N², C⁴ & C⁶ positions play a key role in modulating the binding affinity at the hA₃AR.

Overall, SAR results confirmed the importance of the following features;

- i) lipophilic neopentyl group at N² position for favouring affinity,
- ii) N² methyl with free amino group at C⁶ for favouring affinity,
- iii) *para*-substitution at the aromatic ring of the benzamide in C⁶ for favouring selectivity,
- iv) dibenzamide substitution with steric groups (e.g.Br) at C⁶ for favouring affinity.

In addition, docking evaluations were carried out on both homology based hA₃ receptors and hA_{2A} receptors. Slightly different binding orientation was observed for the ligands in the both binding pockets, which differ based on the substituents at C⁶ and N² positions. The predicted binding affinity has successfully rationalized the experimental SAR data of newly synthesized derivatives. Docking analysis gave the essential interactions involved between the ligand and residues. As seen with chloro compounds, the binding pattern of the new PP analogues varied depending on the length of substituents at the N²- and / or C⁶-positions of the PP. As mentioned earlier, the binding pattern of compounds bearing N²-neopentyl derivatives are slightly different from the other N² substituted analogues because of the steric hindrance produced by the neopentyl groups inside the hA₃ model and hA_{2A}AR.

Overall, the following interactions were observed between the ligands and the residues at hA₃ model, (i) hydrophobic interactions of N²-substituents with non-polar residues, which are crucial for conferring hA₃ affinity; (ii) hydrophobic interactions of phenyl ring of benzamide chain at C⁶-position, vital for affinity; (iii) van der Waals interactions of steric electron donor and or electron acceptor groups at *para* position of the benzamide chain, essential for the selectivity. (iv) aromatic planar bicyclic moiety like pyrazolo-pyrimidine ring involved in π - π interaction with the nearby aromatic residues,

essential for antagonistic activity; (v) hydrogen bonding interactions of the ester group, amide chain and 'N' of pyrimidine and pyrazole ring essential for affinity and more precisely selectivity.

Generally, most of the newly synthesized derivatives showed a common binding orientation pattern throughout the series inside the hA_{2A}AR, with exception of some compounds, which were bound in the quite a different fashion due to the substituents effects such as electronic properties, positional effects and rotatable nature. This resulted in compounds to obtain a common interactions which include the hydrogen bonding interactions with Asn253 and other hydrophobic interaction essential for hA_{2A}AR activation. Thus some compounds showed the good affinity towards the hA_{2A}AR as well.

Docking evaluation confirmed that newly synthesized PP-4-carboxylate derivatives, are better than the 4-chloro PP derivatives. Apparently, some of the compounds of the new PP series made a additional stabilizing hydrogen bonding interactions with the Asn250, which was not found with previous PP-chloro series derivatives. In addition most potent compounds of the series displayed some specific hydrophobic interactions with Val169, Val259 and Ile253. These hydrogen bonding and hydrophobic interactions have contributed for the affinity and selectivity to a considerable extent.

Overall, the hypothesis of ligand modification which includes the introduction of the ester group and other bulky groups at the *para* position of the benzamide chain have been successfully proven.

Chapter 6 Pharmacological evaluation and docking studies of pyrazolopyrimidine derivatives as adenosine deaminase inhibitors

*Pharmacological assays were performed by our collaborator La Motta *et. al* at the Dept of Pharmacy, University of Pisa, Italy.

6.1 Introduction

This chapter describes the pharmacological and docking evaluation of pyrazolopyrimidine derivatives as adenosine deaminase (ADA) inhibitors. Generally, adenosine deaminase (ADA) catalyzes the deamination of adenosine and 2'-deoxyadenosine to form inosine and 2'-deoxyinosine, respectively. This enzyme is largely present in mammalian cells and plays a significant role in human pathological conditions, which include severe immunodeficiency diseases, leukaemia diseases, lymphoproliferative disorders, inflammatory diseases etc. Therefore, modulation of ADA activity is in great demand.

As described in the Chapter 1, section 1.3.6, various heterocyclic scaffolds which include natural products such as (+)-EHNA, deoxycoformycin and synthetic ligands such as pyrazolo[3,4-*d*]pyrimidine-4-one, imidazo[4,5-*d*]pyridazine-7-one etc, have been tested as ADA inhibitors. However, potent inhibitors such as EHNA, and deoxycoformycin are clinically unsuccessful because of the toxicities. Therefore, several research groups have involved in the identification of the synthetic lead compounds as ADA antagonists without toxicity. Among them, pyrazolo[3,4-*d*]pyrimidine-4-one with different structural nature is one of the compound to be identified as potent ADA inhibitor.

Considering all these aspects and the role of pyrazolopyrimidine scaffold on ADA modulation, we have attempted to test our pyrazolopyrimidine derivatives as new enzyme ADA inhibitors, with the aim of providing new therapeutic molecules/options. For achieving that purpose, a total of 20 compounds from both chloro PP and ester PP series were investigated for their ADA inhibitory activity in an attempt to draw the SAR profile based on the functional properties.

6.1.1 Experimental Methods

Materials and Methods. Adenosine deaminase (ADA) type IX from bovine spleen (150-200 U/mg) and adenosine were purchased from Sigma Chemical Co. All other chemicals were of reagent grade.

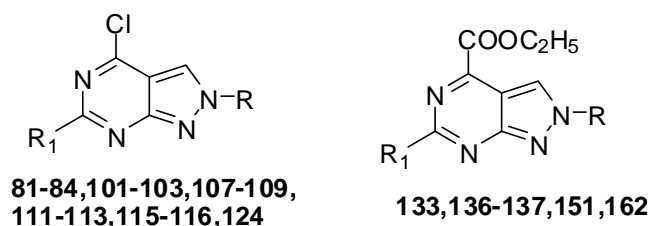
Enzymatic Assay.¹¹⁹ The activity of the test enzyme was determined spectrophotometrically by monitoring for 2 min the change in absorbance at 262 nm, which is due to the deamination of adenosine catalyzed by ADA. The change in adenosine concentration/min was determined using a Beckman DU-64 kinetics software program (Solf Pack TM Module). ADA activity was assayed at 30 °C in a reaction mixture containing 50 mM adenosine, 50 mM potassium phosphate buffer pH 7.2, and 0.3 nM enzyme solution in a total volume of 500 μ L. The inhibitory activity of the newly synthesized compounds was assayed by adding 100 μ L of the inhibitor solution to the reaction mixture described above. All the inhibitors were dissolved in water, and the solubility was facilitated by using DMSO, whose concentration never exceeded 4% in the final reaction mixture. To correct for the nonenzymatic changing in adenosine concentration and the absorption by the test compounds, a reference blank containing all the above assay components except the substrate were prepared. The inhibitory effect of the new derivatives was routinely estimated at a concentration of 10^{-5} M. Those compounds found to be active were tested at additional concentrations between 10^{-5} and 10^{-11} M. Each inhibitor concentration was tested in triplicate and the determination of the IC_{50} values was performed by using linear regression analysis of the log-dose response curve. The K_i values were calculated from IC_{50} s by using the Cheng and Prusoff equation.¹⁶¹

6.1.2 Results and Discussion

6.1.2.1 Biological Evaluation

The % inhibition of bovine spleen ADA at 100 μ M by pyrazolopyrimidine derivatives is presented in **Table 14** and (+)-EHNA was used as the reference standard. Twenty compounds from the derivatives of 4-chloro-PP and PP-4-carboxylate series were selected based on the different electronic

Table 14. ADA inhibition data of pyrazolo[3,4-*d*]pyrimidine derivatives (R denotes N² position, R₁ denotes C⁶ position)



Compound	R	R ₁	% inhibition at 100 μM ^a
81	CH ₃	NH ₂	n.a. ^b
82	CH(CH ₃) ₂	NH ₂	n.a
83	CH ₂ C(CH ₃) ₃	NH ₂	7±3
84	CH ₂ CH ₂ C ₆ H ₅	NH ₂	9±1
101	CH ₃	NHCOPh	51±1
103	CH ₃	NHCOPh (<i>p</i> -CF ₃)	53±7
107	CH(CH ₃) ₂	NHCOPh (<i>p</i> -CF ₃)	48±7
108	CH(CH ₃) ₂	NHCOPh (<i>p</i> -CH ₃)	39±3
109	CH ₂ C(CH ₃) ₃	NHCOPh	6±2
111	CH ₂ C(CH ₃) ₃	NHCOPh (<i>p</i> -CF ₃)	45±4
112	CH ₂ C(CH ₃) ₃	NHCOPh (<i>p</i> -CH ₃)	37±5
113	CH ₂ CH ₂ C ₆ H ₅	NHCOPh	19±6
115	CH ₂ CH ₂ C ₆ H ₅	NHCOPh (<i>p</i> -CF ₃)	34±4
116	CH ₂ CH ₂ C ₆ H ₅	NHCOPh (<i>p</i> -CH ₃)	27±1
124	CH ₂ CH ₂ C ₆ H ₅	NHCOCH ₂ Ph	65±1
133	CH ₃	NH ₂	n.a
136	CH ₂ CH ₂ C ₆ H ₅	NH ₂	n.a
137	CH ₃	NHCOPh	49±1
151	CH ₂ CH ₂ C ₆ H ₅	NHCOPh (<i>p</i> -CH ₃)	65±5
162	CH ₂ CH ₂ C ₆ H ₅	NHCOCH ₂ Ph	64±4
(+)EHNA			1.20±0.15 (<i>K_i</i> , nM)

^a Means±SEM of three determinations, performed in duplicate. ^bNot active, inhibition occurred at concentration higher than 100 μM.

properties including electron withdrawing (e.g. CF₃) and electron donating (e.g. CH₃) nature of the substituents, and they were tested for their ADA inhibitory activity. As shown in **Table 14**, some of the novel compounds were able to inhibit the *in vitro* activity of ADA, exhibiting high % inhibition.

Generally, the PP-4-carboxylate derivatives showed better inhibitory activity as compared to the 4 chloro-PP derivatives. Free amino group compounds **81 & 82** in the chloro series and compounds **133 & 136** in the

ester series did not show any activity at ADA. Similarly, compound **83 & 84**, with bulky chain at N² position, displayed poor inhibition. Generally, the benzamide substitution increased the inhibitory effect to a certain extent, with the only exception of compound **109**, with *para* unsubstituted benzamide, which displayed the least activity in the whole series (6%), and very close to that of the C⁶ unsubstituted parent compound **83**. Interestingly, compounds of the chloro series with less steric groups (e.g. methyl) at N² position (**101**, with 51 % and **103**, with 53%) showed moderate activity at ADA. In addition, compound **107 & 108**, with a N² isopropyl group, were less active at the ADA as compared to N² methyl derivatives. Generally, in the N² methyl and isopropyl series, the insertion of benzamide chains at the C⁶ position improved the activity at ADA (**101-108**, 39-53 %). Among the various substituted benzamide chains, insertion of both electron withdrawing (*para*-CF₃) or electron donating (*para*-CH₃) groups at the *para* position of the distal phenyl ring did not affect the inhibitory potency significantly. Indeed, compounds **103 & 107**, bearing a CF₃ function, were almost as potent (53 % & 48 %) as the *para* unsubstituted compound **101** (51%). On the other hand, substitution of benzamide chains at C⁶ position led to detrimental effects for N² neopentyl series (**109**, with 6%). Interestingly, the insertion of a *para*-CF₃ group in the same series, as in **111** (45 %), made a 8-fold increase in inhibitory potency with respect to **109**. Conversely, the same substitution in the phenyl ethyl series led to only 5 fold improvement in the potency as compared to N² neopentyl counterpart. Similarly, electron donating *para*-CH₃ substituted analogues of both N² neopentyl (**112**, 37 %) and phenylethyl (**116**, 27 %) displayed diminished potency than electron withdrawing substituents (*para*-CF₃).

In the chloro series, the insertion of a phenylethyl chain at N² position led to the detrimental effect in the inhibitory potency. The only exception was for compound **124**, which has a rotatable methylene containing lengthy benzamide chain; this compound showed best inhibitory activity of 65%, with an increase of 7 fold as compared to the parent compound **84**. Similarly, its N² phenyl ethyl counterpart with C⁴-ester substituted compound (**162**) also showed similar inhibitory potency.

As mentioned above, *para* substituted benzamide chain of the compounds in the N² neopentyl and phenylethyl series displayed 7-9 times more potency than that of free amino group or *para* unsubstituted benzamide group compounds, indicating that presence of bulky groups are needed at the *para* position of the benzamide chain.

As compared to the chloro series, ester series compounds with both *para* unsubstitution (**137,162**) and *para* substitution (**151**) showed much superior activity (49-65 %). This proves that hydrophilic ester group at C⁴ is more essential than the steric chloro group. This fact was again supported by compound **151**, where its chloro counterpart **116** exhibited 3 times lower potency than that of **151**. Additionally, longer phenyl acetamide chain compounds in both chloro and ester series displayed similar activity and the highest profile among the whole series. This in turn indicates that the presence of lengthy chains at C⁶ and at N² are suitable for the activity.

All these above reported observations, despite the low potency of our compounds, are somehow in agreement with the findings of Da Settimo¹¹⁹ where 2 amino pyrazolopyrimidine derivatives with N² alkyl substituents up to n=9 showed potent activity in the nM range, whereas, shorter alkyl chain showed loss of activity, indicating that the activity is totally depend upon the length of the substitution at the N² position.

On the whole, from the SAR of PP derivatives, the following features are deduced:

1. As lengthy chains are preferred at the N² position, the activity could be enhanced by increasing the length of the alkyl and aryl chain at N² position. (e.g n = 4-9). Various substituted alkyl or aryl chains could also be helpful.
2. C⁴ ester group is preferred than the C⁴ chloro group for maintaining ADA's inhibitory activity.
4. Since a hydrophilic group is preferred at the C⁴ position, the ester group could be replaced by other polar functional groups (e.g. NH₂, CONH₂) to improve the activity.
5. Considering the poor activity of free amino group analogues at the C⁶ position, acyl substitution at C⁶ could be vital for the inhibitory activity.

6.2 Docking Studies

Molecular docking studies were carried out using X-ray crystal structure of ADA (**Figure 45**) complexed with the highly potent non-nucleoside inhibitor (PDB code 1O5R),¹⁹⁶ to rationalize the hypothetical binding data with results of SARs and to understand the inhibitory potency of synthesized compounds at a molecular level.

Various potent inhibitors with different chemical structures have been deposited in the PDB database (PDB IDs: 1VFL, 3IAR, 2Z7G, 3OU8, 1NDV, 1NDW, 1NDY, 1NDZ, 3KM8, 1WXY, 1KRM, 1QXL, 3PAN, 3PBM, 1FKW, 1O5R, 1FKX, 3OCQ, 3PAO, 1 UML). La Motta *et al.* described that the active site of ADA adopts two distinct conformations: a closed and an open one.¹⁹⁷ In the closed form, the active site consists of a hydrophobic subsite F0, and hydrophilic area (S0).

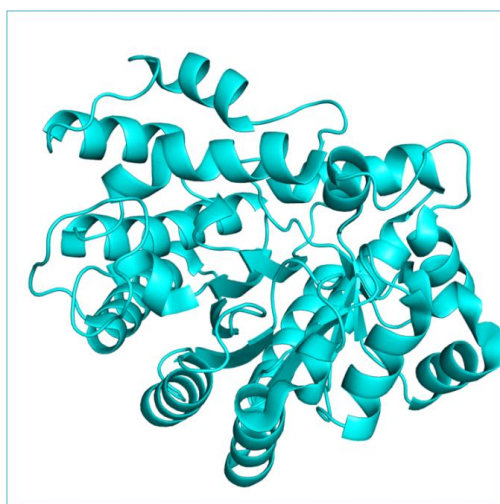


Figure 45. Crystal structure of Adenosine deaminase.

Moreover, it was demonstrated that S0 subsite is enclosed within a structural gate comprising the β -strand (Leu182-Asp185) and R-helix (Thr57-Ala73) with two leucine side chains (Leu58 and Leu62). From the overlay of the open and closed ADA structures it was confirmed that the shape of the active site in the closed form is entirely preserved in the open conformation of the enzyme. Considering all the above facts, open structure form of crystal structure 1O5R was chosen for docking studies.¹⁹⁶

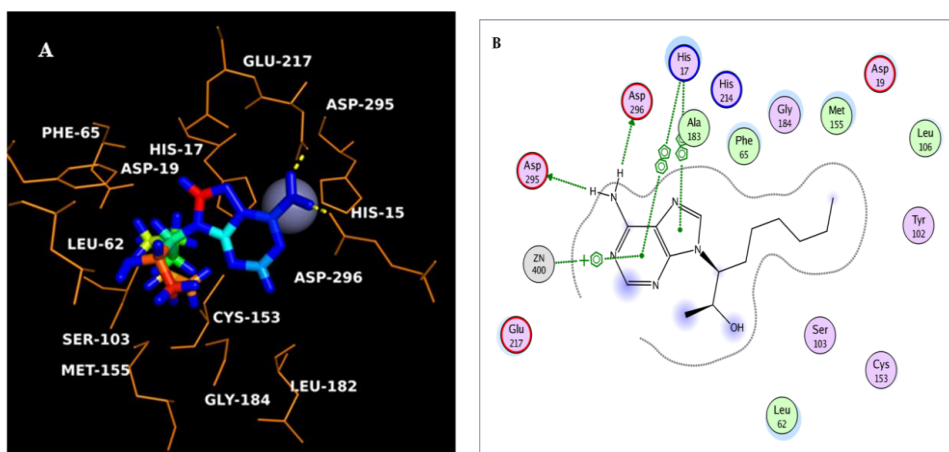


Figure 46. A. Binding mode of reference ligand (+)-EHNA into the ADA binding cavity. B. 2D view of the reference compound (+)-EHNA inside the ADA.

Docking investigations were focused on the most active inhibitors **124**, **151** & **162**, using the MOE docking programme. The most active reference compound 2'S, 3'R-*erythro*-enantiomer of EHNA, (+)-EHNA, was also docked into the catalytic site of the enzyme for a proper comparison to delineate the SARs of synthesized compounds.

From the docking studies it was noticed that the ligand EHNA was localized in the same active site as the inhibitor in the crystal structure (1O5R). As illustrated in **Figure 46-A**, the NH₂ group of adenine formed hydrogen bonds with the Asp295 and the Asp296. Similarly, Zn atom coordinating His17 residue was making π - π stacking interactions with main scaffold adenine moiety. The hydrophobic alkyl chain was located at the entrance of the binding pocket and formed numerous favorable lipophilic interactions with residues such as Asp19, Phe65, Tyr102, Ser103, Leu106, Gly184, Met155 and His 214.

One of the most active compounds, **151**, was found to be binding in the known active binding site as that of (+)-EHNA, with the long lipophilic phenylethyl chain localized in a deep and narrow channel at the entrance of the enzyme. In addition, NH proton at C⁶ position was involved in a hydrogen bond with the Asp295. Moreover, the phenyl ring of the benzamide of the

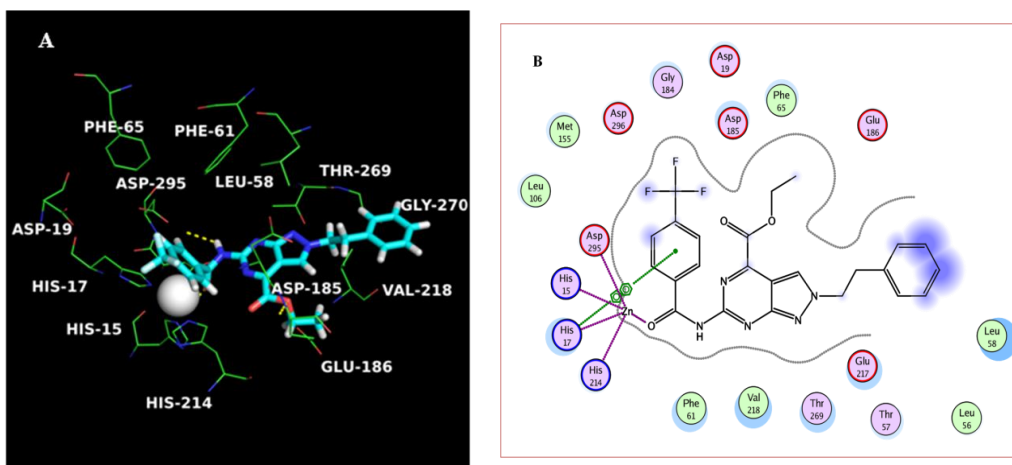


Figure 47. A. Binding mode of compound **151** inside the ADA binding cavity. B. 2D view of the compound **151** inside the ADA binding cavity.

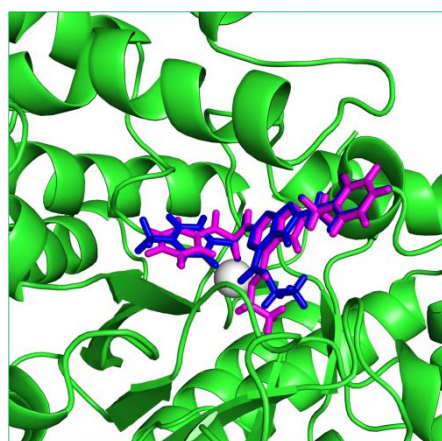


Figure 48. Superimposition of ligand **151** (blue) & **162** (magenta) inside ADA binding cavity.

pyrazolopyrimidine system made a hydrophobic bond with Zn atom coordinating the histidine residues such as His15, His17 and His 214.

As shown in Figure 47-A, the binding orientation of **151** inside ADA is slightly different to that observed for (+)-EHNA binding. Hence, the pyrimidine ring of PP nucleus displaced little away towards the upper side of the enzyme. This caused the ligand to lose one of the strong stabilizing hydrogen bonding interactions with Asp296, which was deemed essential for the inhibitory activity at the receptor pocket. In addition, lipophilic phenylethyl group was surrounded by a small hydrophobic pocket, which consisted of residues such as Leu56, Leu58, Thr57, Glu217 and Glu186. Due

to the shorter chain of phenylethyl as compared to the (+)-EHNA, the ligand **151** lost some of the essential lipophilic interactions including those with Phe65, Tyr102, and Ser103 which were observed with (+)-EHNA and other potent inhibitors. As shown in **Table 12**, inhibitory activities varied significantly due to change in n-alkyl substituent.

Moreover, another potent compound **162**, also showed similar binding orientation as compound **151** (**Figure 48**). This superimposed binding orientation led to similar types of hydrogen bonding and hydrophobic interactions with residues as those of compound **151**. Interestingly, compound **124** (counter part of the compound **162**) of the chloro series, which showed equal potency as compound **151**, shared similar binding mode and interactions as compound **151 & 162**.

The docking was also performed for less active or inactive compounds, in an effort to elucidate the reasons behind the reduced biological activity of PP derivatives bearing the free amino (**81-84**) and unsubstituted benzamide chain at position C⁶ position (**109 & 113**). It was found that the ligands occupied a different space at the binding site. Thus lost the essential hydrogen bonding with Asp 295 & Asp 296 and hydrophobic interactions with other residues. From a visual inspection of the free amino group compounds and ADA complex, it seems obvious that the absence of phenylacetamide chain caused the pyrazolopyrimidine system to attain a reduced rotation and thereby changes the optimal binding mode of the ligand significantly.

Similarly, compounds with C⁴ chloro substitution (**101, 103, 107-109, 111-113 & 115-116**) exhibited a slightly different binding mode as compared to compound **151**, which in turn mirrored the moderate ADA inhibitory potency of these chloro derivatives. Although these compounds showed some common hydrophobic interactions with Ala183, Met155, Asp19, yet they lacked the essential hydrogen bonding interactions with Asp295 & Asp296. Additionally, a hydrophobic residue Phe61, which was surrounding the ester atom of the compound **151**, was missing in the chloro series analogues. Consequently, the loss of binding interaction could be due to the presence of sterically hindered, unrotatable chloro group. This aspect has resulted in loss of essential hydrophobic and hydrogen bonding interactions with Phe61 and Asp295 & Asp296. respectively. These observations plainly explain the loss in the

inhibitory potency of chloro series in comparison with the ester series analogues.

6.2.1 Conclusion

The docking simulation performed on the PP derivatives into the ADA binding site successfully rationalized the SARs of these inhibitors. Docking analysis highlighted key pharmacophoric elements which are essential for hydrophobic, hydrogen and π - π stacking interactions. From the SAR and docking studies of pyrazolopyrimidine derivatives, it is deduced that compounds with lengthy substitutions at N² substitution and electron donating bulky benzamide chains at C⁶ position are essential for ADA inhibitory potency. In addition, considering the importance of hydrogen bonding properties of ester substituents at C⁴ position, other hydrogen bond donors including amide(CONH) or amine(NH₂) or substituted amine (N(CH₃)₂) could be replaced to improve the potency. Moreover, as mentioned in the SAR section, lengthy alkyl chain or substituted alkyl chain at N² position could improve the inhibitory potency of compounds.

Chapter 7 Concluding Remarks and Future Perspective

In this thesis, we tested the hypothesis that molecular simplification of PTP structure to PP, together with other substituents at N², C⁶ and C⁴ positions of the PP scaffold, could maintain the affinity and selectivity at the hA₃AR. To test this hypothesis, we

- 1) designed simplified analogues of previously synthesized PTPs in the form of bicyclic pyrazolopyrimidines (PPs), with the rationale of improving the physico chemical properties, to reduce the synthetic procedures associated with the complex PTP structures and retain the affinity and selectivity
- 2) synthesized and characterized 2 libraries of PP compounds and we tested them for their ability to bind the hA₃AR subtype through relevant pharmacological assays;
- 3) rationalized the experimental results from the initial pharmacological evaluation with theoretical studies (i.e. QSAR, homology modeling and molecular docking studies), by identifying the essential structural features and binding interactions able to guarantee the affinity at the hA₃AR.

To achieve these objectives, a new series of pyrazolopyrimidines with C⁴ chloro, N² alkyl & aralkyl, and C⁶ free amino and benzamide substituents were designed and synthesized successfully (**CHAPTER 3**). The molecular simplification of the tricyclic PTP resulted in the identification of 4-chloro-PP derivatives with moderate hA₃AR affinity and selectivity towards other receptor subtypes. Especially, some of the N² neopentyl derivatives displayed a good affinity and moderate selectivity, for example compound **112** with N² neopentyl, and C⁶ *para*-toluamide substituents showed affinity in low micromolar (μM) range and its *para*-CF₃ analogue **111** displayed the highest selectivity (hA₁/A₃ >15, hA_{2A}/A₃ >15) in the series. On the other hand, analogue **116**, a N²phenyl ethyl counterpart of compound **112**, displayed the best hA₃ affinity profile with 5 fold increase in the affinity as compared to **112**. Further, analogues **115** & **120** of the same series emerged for their high

selectivity at hA₁AR, (**115 & 120**, 21 & 35 fold, respectively, more selective) and displayed almost equal affinity at the hA₃AR, which are anyhow 2 fold better than that of compound **112** (**CHAPTER 4**).

In addition, the SAR of the new series of 4-chloro-pyrazolopyrimidine derivatives was quantitatively elucidated by 3D-QSAR methodology such as Topomer CoMFA (**CHAPTER 5**). The structural features essential for the inhibition of hA₃AR, particularly at the N² & C⁶ position of the pyrazolopyrimidine nucleus was proposed. Notably, the steric effect around the N² position and the electrostatic effect at C⁶ position seemed to play an essential role on the antagonistic activity of the PP scaffold. Such a 3D QSAR based model exposed the important sites for chemical modifications and further improvement of the affinity.

The receptor-driven computational approach, such as molecular docking simulations was performed using a hA_{2A} based hA₃ homology model (**CHAPTER 6**). This study was able to predict comparable binding modes and interactions for the 4-chloro-PP derivatives. Through a molecular modeling investigation, the experimental findings have been rationalized. Docking analysis suggested that hydrophobic interactions with N² & C⁶ phenyl position, π - π stacking interaction with pyrazolopyrimidine nucleus and hydrogen bonding with C⁶amide are essential for hA₃ affinity. Further, derivatives of 4-chloro-PP's lost one of the potential H-bonding interaction with Asn250 (TM6), which was deemed essential for hA₃AR affinity. Hence, the PP derivatives showed inferior activity to PTP scaffold.

Hence, to improve the affinity and selectivity of PP ligands, further structural modification was carried out to obtain pyrazolopyrimidine-4-carboxylate derivatives (**CHAPTERS 7&8**). In this new work, C⁴ chloro group was substituted by ester group to make potential hydrogen bonding interactions with Asn 250 and various lipophilic groups (e.g. CF₃, CH₃, Cl, Br) were also introduced to improve the affinity and selectivity.

A new series of pyrazolo[3,4-*d*]pyrimidine-4-carboxylates has been designed and synthesized successfully in the new project. A replacement of chloro group by ester group and additional hydrophobic substituents at the *para* position of C⁶ benzamide linkage led to the identification of a new series of PP-4-carboxylate derivatives as hA₃AR antagonists with better hA₃

affinity and improved selectivity profile towards the other adenosine receptor subtypes in comparison to the 4-chloro-PP derivatives (**CHAPTER 9**). Particularly, compound **133**, bearing N² methyl and C⁶ amino groups, showed >142 fold increment in affinity as compare to its counterpart compound **81** and 2 fold increment as compared to the potent compound (**116**) of the chloro series. Similarly, compound **147**, bearing N² neopentyl and C⁶ *para*-toluamide substitution, showed 2 fold increase in the affinity and 15-17 fold increase in the selectivity against other adenosine receptor subtypes. In addition, another compound (**146**) as part of the N² neopentyl series, displayed almost equal affinity and selectivity profile as **147**. Subsequently, steric *para*-substituted benzamide compounds **153** and **155** displayed comparable affinity and selectivity as compound **147**.

Through docking evaluations, the experimental SAR data and selectivity over hA_{2A}AR were successfully rationalized (**CHAPTER 9**). Specifically, an additional hydrogen bonding interaction at N of pyrimidine & pyrazole and amide of C⁶ was identified, which was not found with previous PP-chloro series derivatives. This additional hydrogen bonding interaction led to a significant improvement in the selectivity and moderate improvement in affinity at hA₃AR. In addition, some specific hydrophobic interactions of *para* substituted C⁶ benzamide with Val169, Val259 and Ile253 are proven to be essential for selectivity. Moreover, a loss of hydrogen bonding interaction and hydrophobic interaction with Glu169, which is due to the steric hindrance caused by the N²-neopentyl group towards TM3 and TM4, are speculated to be reason for the decrease in affinity towards the hA_{2A}AR.

In addition, new PP derivatives were also tested for their ADA inhibitory activity (**CHAPTER 10**). Some of the compounds showed promising inhibitory potency, which could be further improved by the additional substitution as recommended in the section 9.4 in Chapter 4.

In summary, the molecular simplification of PTP ligands and further ligand modification of 4-chloro-PPs to pyrazolo[3,4-*d*]pyrimidine-4-carboxylates have given rise to a new class of potent and selective hA₃AR antagonists. Molecular modeling evaluation employed in our study has provided new perspectives on the structural features and binding interactions responsible for the hA₃ affinity of new PP derivatives.

In addition, the most potent compounds of the series will be tested for functional assays and in the future the most promising compounds could be biologically tested for anticancer activity.

Although the new PP-4-carboxylate derivatives improved the affinity and selectivity significantly as compared to the 4-chloro-PP derivatives, yet these compounds seem to be inferior to the parent PTP analogues in terms of pharmacological profile. Considering the novelty of this bicyclic scaffold, it can be considered as a promising starting point for developing more potent and selective PP antagonists towards the hA₃AR. It is emphasized that further studies on this scaffold could enhance the pharmacological profile comparable to parent PTP analogues. Therefore, in order to further improve the affinity and selectivity, following features can be considered, which are derived from the SAR and molecular modeling studies of the new PP-4-carboxylate derivatives. Those are as follows:

(i) Neopentyl substitution at the N² position for retaining the activity. Additionally, steric groups such as *tert*-butyl and lengthy halide substituted alkyl groups could be substituted at N² position to optimize the substituents at this position.

(ii) Various mono substituted and disubstituted electron withdrawing groups other than CF₃ (e.g. Cl, Br, OCF₃, SF₅, NO₂, CF₃SO₂) could be substituted at the 4 or 3,4 position of the benzamide chain for improving affinity and selectivity.

(iii) Various mono substituted and disubstituted electron donating groups other than CH₃ (e.g. N(CH₃)₂, NHC₄H₉, OCH(CH₃)₂) could be substituted at the 4 or 3,4 position of the benzamide chain for improving affinity and selectivity.

(iv) The ester substituents at the C⁴ position could be retained for the affinity. In addition, the length of the alkyl substituents in the ester chain could be enhanced (e.g. Isopropyl ester). Alternatively, the ester group may be substituted by thioester (C=OSCH₃) or bioisosteres such as oxazole, oxadiazole and ketoxime ether to optimize the groups at the C⁴ position.

In addition, further QSAR study on newly synthesized PP-4-carboxylate derivatives could also be carried out to derive a detailed

quantitative SAR and to evaluate the structural features essential at N², C⁶ & C⁴ positions of these ligands for the antagonistic interaction at the hA₃AR.

Bibliography

1. Moro, S.; Deflorian, F.; Spalluto, G.; Pastorin, G.; Cacciari, B.; Kim, S. K.; Jacobson, K. A. Demystifying the three dimensional structure of G protein-coupled receptors (GPCRs) with the aid of molecular modeling. *Chem Commun* **2003**, 2949-2956.
2. Ralevic, V.; Burnstock, G. Receptors for purines and pyrimidines. *Pharmacol Rev* **1998**, 50, 413-492.
3. Pierce, K. L.; Premont, R. T.; Lefkowitz, R. J. Seven-transmembrane receptors. *Nat Rev Mol Cell Bio* **2002**, 3, 639-650.
4. Jacobson, K. A.; Gao, Z. G. Adenosine receptors as therapeutic targets. *Nat Rev Drug Discov* **2006**, 5, 247-264.
5. Fredholm, B. B.; Arslan, G.; Halldner, L.; Kull, B.; Schulte, G.; Wasserman, W. Structure and function of adenosine receptors and their genes. *N-S Arch Pharmacol* **2000**, 362, 364-374.
6. Sun, D. Q.; Samuelson, L. C.; Yang, T. X.; Huang, Y. N.; Paliege, A.; Saunders, T.; Briggs, J.; Schnermann, J. Mediation of tubuloglomerular feedback by adenosine: Evidence from mice lacking adenosine 1 receptors. *P Natl Acad Sci USA* **2001**, 98, 9983-9988.
7. Fredholm, B. B.; Ijzerman, A. P.; Jacobson, K. A.; Klotz, K. N.; Linden, J. International Union of Pharmacology. XXV. Nomenclature and classification of adenosine receptors. *Pharmacol Rev* **2001**, 53, 527-552.
8. Fredholm, B. B.; Ijzerman, A. P.; Jacobson, K. A.; Linden, J.; Muller, C. E. International Union of Basic and Clinical Pharmacology. LXXXI. Nomenclature and Classification of Adenosine Receptors-An Update. *Pharmacol Rev* **2011**, 63, 1-34.
9. Corvol, J. C.; Studler, J. M.; Schonn, J. S.; Girault, J. A.; Herve, D. G alpha(olf) is necessary for coupling D1 and A2a receptors to adenylyl cyclase in the striatum. *J Neurochem* **2001**, 76, 1585-1588.
10. Kull, B.; Svenningsson, P.; Fredholm, B. B. Adenosine A(2A) receptors are colocalized with and activate G(olf) in rat striatum. *Mol Pharmacol* **2000**, 58, 771-777.
11. Eltzschig, H. K.; Sitkovsky, M. V.; Robson, S. C. MECHANISMS OF DISEASE Purinergic Signaling during Inflammation. *New Engl J Med* **2012**, 367, 2322-2333.
12. Eckle, T.; Grenz, A.; Laucher, S.; Eltzschig, H. K. A2B adenosine receptor signaling attenuates acute lung injury by enhancing alveolar fluid clearance in mice. *J Clin Invest* **2008**, 118, 3301-3315.
13. Grenz, A.; Bauerle, J. D.; Dalton, J. H.; Ridyard, D.; Badulak, A.; Tak, E.; McNamee, E. N.; Clambey, E.; Moldovan, R.; Reyes, G.; Klawitter, J.; Ambler, K.; Magee, K.; Christians, U.; Brodsky, K. S.; Ravid, K.; Choi, D. S.; Wen, J. M.; Lukashev, D.; Blackburn, M. R.; Osswald, H.; Coe, I. R.; Nurnberg, B.; Haase, V. H.; Xia, Y.; Sitkovsky, M.; Eltzschig, H. K. Equilibrative nucleoside transporter 1 (ENT1) regulates postischemic blood flow during acute kidney injury in mice. *J Clin Invest* **2012**, 122, 693-710.
14. Grenz, A.; Kim, J. H.; Bauerle, J. D.; Tak, E.; Eltzschig, H. K.; Clambey, E. T. Adora2b Adenosine Receptor Signaling Protects during Acute Kidney Injury via Inhibition of Neutrophil-Dependent TNF-alpha Release. *J Immunol* **2012**, 189, 4566-4573.

15. Cheong, S. L.; Federico, S.; Venkatesan, G.; Mandel, A. L.; Shao, Y. M.; Moro, S.; Spalluto, G.; Pastorin, G. The A₃ adenosine receptor as multifaceted therapeutic target: pharmacology, medicinal chemistry, and in silico approaches. *Med Res Rev* **2013**, *33*, 235-335.
16. Baraldi, P. G.; Cacciari, B.; Romagnoli, R.; Merighi, S.; Varani, K.; Borea, P. A.; Spalluto, G. A₃ adenosine receptor ligands: History and perspectives. *Med Res Rev* **2000**, *20*, 103-128.
17. Zhou, Q. Y.; Li, C. Y.; Olah, M. E.; Johnson, R. A.; Stiles, G. L.; Civelli, O. Molecular-Cloning and Characterization of an Adenosine Receptor - the A₃ Adenosine Receptor. *P Natl Acad Sci USA* **1992**, *89*, 7432-7436.
18. Salvatore, C. A.; Jacobson, M. A.; Taylor, H. E.; Linden, J.; Johnson, R. G. Molecular-Cloning and Characterization of the Human-a₃ Adenosine Receptor. *P Natl Acad Sci USA* **1993**, *90*, 10365-10369.
19. Baraldi, P. G.; Borea, P. A. New potent and selective human adenosine A₃ receptor antagonists. *Trends Pharmacol Sci* **2000**, *21*, 456-459.
20. Germack, R.; Dickenson, J. M. Adenosine triggers preconditioning through MEK/ERK1/2 signalling pathway during hypoxia/reoxygenation in neonatal rat cardiomyocytes. *J Mol Cell Cardiol* **2005**, *39*, 429-442.
21. Haas, H. L.; Selbach, O. Functions of neuronal adenosine receptors. *N-S Arch Pharmacol* **2000**, *362*, 375-381.
22. Mozzicato, S.; Joshi, B. V.; Jacobson, K. A.; Liang, B. T. Role of direct RhoA-phospholipase D interaction in mediating adenosine-induced protection from cardiac ischemia. *Faseb J* **2003**, *17*, 406-408.
23. Shryock, J. C.; Belardinelli, L. Adenosine and adenosine receptors in the cardiovascular system: Biochemistry, physiology, and pharmacology. *Am J Cardiol* **1997**, *79*, 2-10.
24. Jacobson, K. A. Adenosine A₃ receptors: novel ligands and paradoxical effects. *Trends Pharmacol Sci* **1998**, *19*, 184-191.
25. Merighi, S.; Mirandola, P.; Varani, K.; Gessi, S.; Leung, E.; Baraldi, P. G.; Tabrizi, M. A.; Borea, P. A. A glance at adenosine receptors: novel target for antitumor therapy. *Pharmacol Therapeut* **2003**, *100*, 31-48.
26. Sei, Y.; vonLubitz, D. K. J. E.; Abbracchio, M. P.; Ji, X. D.; Jacobson, K. A. Adenosine A₂ receptor agonist-induced neurotoxicity in rat cerebellar granule neurons. *Drug Develop Res* **1997**, *40*, 267-273.
27. von Lubitz, D. K. J. E.; Ye, W.; McClellan, J.; Lin, R. C. S. Stimulation of adenosine A₃ receptors in cerebral ischemia - Neuronal death, recovery, or both? *Ann Ny Acad Sci* **1999**, *890*, 93-106.
28. Von Lubitz, D. K. J. E.; Lin, R. C. S.; Boyd, M.; Bischofberger, N.; Jacobson, K. A. Chronic administration of adenosine A₃ receptor agonist and cerebral ischemia: neuronal and glial effects. *Eur J Pharmacol* **1999**, *367*, 157-163.
29. Abbracchio, M. P.; Rainaldi, G.; Giammarioli, A. M.; Ceruti, S.; Brambilla, R.; Cattabeni, F.; Barbieri, D.; Franceschi, C.; Jacobson, K. A.; Malorni, W. The A₃ adenosine receptor mediates cell spreading, reorganization of actin cytoskeleton, and distribution of Bcl-x(L): Studies in human astrogloma cells. *Biochem Bioph Res Co* **1997**, *241*, 297-304.
30. Chen, G. J.; Harvey, B. K.; Shen, H.; Chou, J.; Victor, A.; Wang, Y. Activation of adenosine A₃ receptors reduces ischemic brain injury in rodents. *J Neurosci Res* **2006**, *84*, 1848-1855.

31. Boison, D. Adenosine as a modulator of brain activity. *Drug News Perspect* **2007**, 20, 607-611.
32. Von Lubitz, D. K. J. E.; Simpson, K. L.; Lin, R. C. S. Right thing at a wrong time? Adenosine A(3) receptors and cerebroprotection in stroke. *Neuroprotective Agents* **2001**, 939, 85-96.
33. Rivkees, S. A.; Thevananther, S.; Hao, H. P. Are A3 adenosine receptors expressed in the brain? *Neuroreport* **2000**, 11, 1025-1030.
34. Zhu, C. B.; Lindler, K. M.; Campbell, N. G.; Sutcliffe, J. S.; Hewlett, W. A.; Blakely, R. D. Colocalization and Regulated Physical Association of Presynaptic Serotonin Transporters with A(3) Adenosine Receptors. *Mol Pharmacol* **2011**, 80, 458-465.
35. Olanrewaju, H. A.; Qin, W.; Feoktistov, I.; Scemama, J. L.; Mustafa, S. J. Adenosine A(2A) and A(2B) receptors in cultured human and porcine coronary artery endothelial cells. *Am J Physiol-Heart C* **2000**, 279, H650-H656.
36. Armstrong, S.; Ganote, C. E. Adenosine Receptor Specificity in Preconditioning of Isolated Rabbit Cardiomyocytes - Evidence of a(3) Receptor Involvement. *Cardiovasc Res* **1994**, 28, 1049-1056.
37. Wang, J. X.; Drake, L.; Sajjadi, F.; Firestein, G. S.; Mullane, K. M.; Bullough, D. A. Dual activation of adenosine A(1) and A(3) receptors mediates preconditioning of isolated cardiac myocytes. *Eur J Pharmacol* **1997**, 320, 241-248.
38. Zhao, T. C.; Kukreja, R. C. Late preconditioning elicited by activation of adenosine A(3) receptor in heart: Role of NF-kappa B, iNOS and mitochondrial K-ATP channel. *J Mol Cell Cardiol* **2002**, 34, 263-277.
39. Leshem-Lev, D.; Hochhauser, E.; Chanyshv, B.; Isak, A.; Shainberg, A. Adenosine A(1) and A(3) receptor agonists reduce hypoxic injury through the involvement of P38 MAPK. *Mol Cell Biochem* **2010**, 345, 153-160.
40. Maddock, H. L.; Mocanu, M. M.; Yellon, D. M. Adenosine A(3) receptor activation protects the myocardium from reperfusion/reoxygenation injury. *Am J Physiol-Heart C* **2002**, 283, H1307-H1313.
41. Mahaffey, K. W.; Puma, J. A.; Barbagelata, N. A.; DiCarli, M. F.; Leesar, M. A.; Browne, K. F.; Eisenberg, P. R.; Bolli, R.; Casas, A. C.; Molina-Viamonte, V.; Orlandi, C.; Blevins, R.; Gibbons, R. J.; Califf, R. M.; Granger, C. B.; Investigators, A. Adenosine as an adjunct to thrombolytic therapy for acute myocardial infarction - Results of a multicenter, randomized, placebo-controlled trial: The Acute Myocardial Infarction Study of Adenosine (AMISTAD) Trial. *J Am Coll Cardiol* **1999**, 34, 1711-1720.
42. Kopecky, S. L.; Aviles, R. J.; Bell, M. R.; Lobl, J. K.; Tipping, D.; Frommell, G.; Ramsey, K.; Holland, A. E.; Midei, M.; Jain, A.; Kellett, M.; Gibbons, R. J. A randomized, double-blinded, placebo-controlled, dose-ranging study measuring the effect of an adenosine agonist on infarct size reduction in patients undergoing primary percutaneous,transluminal under coronary angioplasty: The ADMIRE (AmP579 Delivery for Myocardial Infarction REduction) study. *Am Heart J* **2003**, 146, 146-152.
43. Lusis, A. J. Atherosclerosis. *Nature* **2000**, 407, 233-241.
44. Gessi, S.; Fogli, E.; Sacchetto, V.; Merighi, S.; Varani, K.; Preti, D.; Leung, E.; MacLennan, S.; Borea, P. A. Adenosine Modulates HIF-1 alpha, VEGF, IL-8, and Foam Cell Formation in a Human Model of Hypoxic Foam Cells. *Arterioscl Throm Vas* **2010**, 30, 90-97.

45. Marquardt, D. L.; Gruber, H. E.; Wasserman, S. I. Adenosine Release from Stimulated Mast-Cells. *P Natl Acad Sci-Biol* **1984**, 81, 6192-6196.
46. Madara, J. L.; Patapoff, T. W.; Gillececastro, B.; Colgan, S. P.; Parkos, C. A.; Delp, C.; Mrsny, R. J. 5'-Adenosine Monophosphate Is the Neutrophil-Derived Paracrine Factor That Elicits Chloride Secretion from T84 Intestinal Epithelial-Cell Monolayers. *J Clin Invest* **1993**, 91, 2320-2325.
47. Resnick, M. B.; Colgan, S. P.; Patapoff, T. W.; Mrsny, R. J.; Awtrey, C. S.; Delparcher, C.; Weller, P. F.; Madara, J. L. Activated Eosinophils Evoke Chloride Secretion in Model Intestinal Epithelia Primarily Via Regulated Release of 5'-Amp. *J Immunol* **1993**, 151, 5716-5723.
48. Kreckler, L. M.; Wan, T. C.; Ge, Z. D.; Auchampach, J. A. Adenosine inhibits tumor necrosis factor-alpha release from mouse peritoneal macrophages via A(2A) and A(2B) but not the A(3) adenosine receptor. *J Pharmacol Exp Ther* **2006**, 317, 172-180.
49. Gessi, S.; Merighi, S.; Fazzi, D.; Stefanelli, A.; Varani, K.; Borea, P. A. Adenosine receptor targeting in health and disease. *Expert Opin Inv Drug* **2011**, 20, 1591-1609.
50. Gao, Z. H.; Li, B. S.; Day, Y. J.; Linden, J. A(3) adenosine receptor activation triggers phosphorylation of protein kinase B and protects rat basophilic leukemia 2H3 mast cells from apoptosis. *Mol Pharmacol* **2001**, 59, 76-82.
51. Gessi, S.; Varani, K.; Merighi, S.; Morelli, A.; Ferrari, D.; Leung, E.; Baraldi, P. G.; Spalluto, G.; Borea, P. A. Pharmacological and biochemical characterization of A(3) adenosine receptors in Jurkat T cells. *Brit J Pharmacol* **2001**, 134, 116-126.
52. Zhong, H.; Shlykov, S. G.; Molina, J. G.; Sanborn, B. M.; Jacobson, M. A.; Tilley, S. L.; Blackburn, M. R. Activation of murine lung mast cells by the adenosine A(3) receptor. *J Immunol* **2003**, 171, 338-345.
53. Walker, B. A. M.; Jacobson, M. A.; Knight, D. A.; Salvatore, C. A.; Weir, T.; Zhou, D. Y.; Bai, T. R. Adenosine A(3) receptor expression and function in eosinophils. *Am J Resp Cell Mol* **1997**, 16, 531-537.
54. Fan, M.; Qin, W. X.; Mustafa, S. J. Characterization of adenosine receptor(s) involved in adenosine-induced bronchoconstriction in an allergic mouse model. *Am J Physiol-Lung C* **2003**, 284, L1012-L1019.
55. Press, N. J.; Taylor, R. J.; Fullerton, J. D.; Tranter, P.; McCarthy, C.; Keller, T. H.; Brown, L.; Cheung, R.; Christie, J.; Habberthuer, S.; Hatto, J. D. I.; Keenan, M.; Mercer, M. K.; Press, N. E.; Sahri, H.; Tuffnell, A. R.; Tweed, M.; Fozard, J. R. A new orally bioavailable dual adenosine A(2B)/A(3) receptor antagonist with therapeutic potential. *Bioorg Med Chem Lett* **2005**, 15, 3081-3085.
56. Lee, J. Y.; Jhun, B. S.; Oh, Y. T.; Lee, J. H.; Choe, W.; Baik, H. H.; Ha, J. H.; Yoon, K. S.; Kim, S. S.; Kang, I. S. Activation of adenosine A(3) receptor suppresses lipopolysaccharide-induced TNF-alpha production through inhibition of PI 3-kinase/Akt and NF-kappa B activation in murine BV2 microglial cells. *Neurosci Lett* **2006**, 396, 1-6.
57. Madi, L.; Cohen, S.; Ochayin, A.; Bar-Yehuda, S.; Barer, F.; Fishman, P. Overexpression of A(3) adenosine receptor in peripheral blood mononuclear cells in rheumatoid arthritis: Involvement of nuclear factor-kappa B in mediating receptor level. *J Rheumatol* **2007**, 34, 20-26.

58. Bar-Yehuda, S.; Luger, D.; Ochaion, A.; Cohen, S.; Patokaa, R.; Zozulya, G.; Silver, P. B.; De Morales, J. M. G. R.; Caspi, R. R.; Fishman, P. Inhibition of experimental auto-immune uveitis by the A3 adenosine receptor agonist CF101. *Int J Mol Med* **2011**, *28*, 727-731.
59. Yang, H.; Avila, M. Y.; Peterson-Yantorno, K.; Coca-Prados, M.; Stone, R. A.; Jacobson, K. A.; Civan, M. M. The cross-species A(3) adenosine-receptor antagonist MRS 1292 inhibits adenosine-triggered human nonpigmented ciliary epithelial cell fluid release and reduces mouse intraocular pressure. *Curr Eye Res* **2005**, *30*, 747-754.
60. Wang, Z.; Do, C. W.; Avila, M. Y.; Peterson-Yantorno, K.; Stone, R. A.; Gao, Z. G.; Joshi, B.; Besada, P.; Jeong, L. S.; Jacobson, K. A.; Civan, M. M. Nucleoside-derived antagonists to A(3) adenosine receptors lower mouse intraocular pressure and act across species. *Exp Eye Res* **2010**, *90*, 146-154.
61. Schlotzer-Schrehardt, U.; Zenkel, M.; Hofmann-Rummelt, C.; Kruse, F. E.; Naumann, G. O. Functional significance of adenosine receptors in the eye and their dysregulation in pseudoexfoliation syndrome. *Ophthalmologie* **2005**, *102*, 1074-+.
62. Zhang, M.; Hu, H. L.; Zhang, X. L.; Lu, W. N.; Lim, J.; Eysteinnsson, T.; Jacobson, K. A.; Laties, A. M.; Mitchell, C. H. The A(3) adenosine receptor attenuates the calcium rise triggered by NMDA receptors in retinal ganglion cells. *Neurochem Int* **2010**, *56*, 35-41.
63. Peifer, M.; Polakis, P. Cancer - Wnt signaling in oncogenesis and embryogenesis - a look outside the nucleus. *Science* **2000**, *287*, 1606-1609.
64. Madi, L.; Ochaion, A.; Rath-Wolfson, L.; Bar-Yehuda, S.; Erlanger, A.; Ohana, G.; Harish, A.; Merimski, O.; Barer, F.; Fishman, P. The A(3) adenosine receptor is highly expressed in tumor versus normal cells: Potential target for tumor growth inhibition. *Clin Cancer Res* **2004**, *10*, 4472-4479.
65. Bar-Yehuda, S.; Stemmer, S. M.; Madi, L.; Castel, D.; Ochaion, A.; Cohen, S.; Barer, F.; Zabutti, A.; Perez-Liz, G.; Del Valle, L.; Fishman, P. The A(3) adenosine receptor agonist CF102 induces apoptosis of hepatocellular carcinoma via de-regulation of the Wnt and NF-kappa B signal transduction pathways. *Int J Oncol* **2008**, *33*, 287-295.
66. Merighi, S.; Benini, A.; Mirandola, P.; Gessi, S.; Varani, K.; Leung, E.; MacLennan, S.; Borea, P. A. Adenosine modulates vascular endothelial growth factor expression via hypoxia-inducible factor-1 in human glioblastoma cells. *Biochem Pharmacol* **2006**, *72*, 19-31.
67. Bar-Yehuda, S.; Madi, L.; Silberman, D.; Gery, S.; Shkapenuk, M.; Fishman, P. CF101, an agonist to the A(3) adenosine receptor, enhances the chemotherapeutic effect of 5-fluorouracil in a colon carcinoma murine model. *Neoplasia* **2005**, *7*, 85-90.
68. Fishman, P.; Bar-Yehuda, S.; Madi, L.; Cohn, I. A3 adenosine receptor as a target for cancer therapy. *Anti-Cancer Drug* **2002**, *13*, 437-443.
69. Madi, L.; Bar-Yehuda, S.; Barer, F.; Ardon, E.; Ochaion, A.; Fishman, P. A3 adenosine receptor activation in melanoma cells - Association between receptor fate and tumor growth inhibition. *J Biol Chem* **2003**, *278*, 42121-42130.
70. Ohana, G.; Bar-Yehuda, S.; Arich, A.; Madi, L.; Dreznick, Z.; Rath-Wolfson, L.; Silberman, D.; Slosman, G.; Fishman, P. Inhibition of primary colon carcinoma growth and liver metastasis by the A3 adenosine receptor agonist CF101. *Brit J Cancer* **2003**, *89*, 1552-1558.

71. Brandt, S. J.; Peters, W. P.; Atwater, S. K.; Kurtzberg, J.; Borowitz, M. J.; Jones, R. B.; Shpall, E. J.; Bast, R. C.; Gilbert, C. J.; Oette, D. H. Effect of Recombinant Human Granulocyte Macrophage Colony-Stimulating Factor on Hematopoietic Reconstitution after High-Dose Chemotherapy and Autologous Bone-Marrow Transplantation. *New Engl J Med* **1988**, 318, 869-876.
72. Harish, A.; Hohana, G.; Fishman, P.; Arnon, O.; Bar-Yehuda, S. A3 adenosine receptor agonist potentiates natural killer cell activity. *Int J Oncol* **2003**, 23, 1245-1249.
73. Gessi, S.; Merighi, S.; Varani, K.; Cattabriga, E.; Benini, A.; Mirandola, P.; Leung, E.; Mac Lennan, S.; Feo, C.; Baraldi, S.; Borea, P. A. Adenosine receptors in colon carcinoma tissues and colon tumoral cell lines: Focus on the A(3) adenosine subtype. *J Cell Physiol* **2007**, 211, 826-836.
74. Abbracchio, M. P.; Camurri, A.; Ceruti, S.; Cattabeni, F.; Falzano, L.; Giammarioli, A. M.; Jacobson, K. A.; Trincavelli, L.; Martini, C.; Malorni, W.; Fiorentini, C. The A(3) adenosine receptor induces cytoskeleton rearrangement in human astrocytoma cells via a specific action on Rho proteins. *Neuroprotective Agents* **2001**, 939, 63-73.
75. Merighi, S.; Benini, A.; Mirandola, P.; Gessi, S.; Varani, K.; Leung, E.; MacLennan, S.; Borea, P. A. A(3) adenosine receptor activation inhibits cell proliferation via phosphatidylinositol 3-kinase/Akt-dependent inhibition of the extracellular signal-regulated kinase 1/2 phosphorylation in A375 human melanoma cells. *J Biol Chem* **2005**, 280, 19516-19526.
76. Nakamura, K.; Yoshikawa, N.; Yamaguchi, Y.; Kagota, S.; Shinozuka, K.; Kunitomo, M. Antitumor effect of cordycepin (3'-deoxyadenosine) on mouse melanoma and lung carcinoma cells involves adenosine A(3) receptor stimulation. *Anticancer Res* **2006**, 26, 43-47.
77. Taliani, S.; La Motta, C.; Mugnaini, L.; Simorini, F.; Salerno, S.; Marini, A. M.; Da Settimo, F.; Cosconati, S.; Cosimelli, B.; Greco, G.; Limongelli, V.; Marinelli, L.; Novellino, E.; Ciampi, O.; Daniele, S.; Trincavelli, M. L.; Martini, C. Novel N-2-Substituted Pyrazolo[3,4-d]pyrimidine Adenosine A(3) Receptor Antagonists: Inhibition of A(3)-Mediated Human Glioblastoma Cell Proliferation. *J Med Chem* **2010**, 53, 3954-3963.
78. Tchilibon, S.; Joshi, B. V.; Kim, S. K.; Duong, H. T.; Gao, Z. G.; Jacobson, K. A. (N)-Methanocarba 2,N-6-disubstituted adenine nucleosides as highly potent and selective A(3) adenosine receptor agonists. *J Med Chem* **2005**, 48, 1745-1758.
79. Okamura, T.; Kurogi, Y.; Hashimoto, K.; Sato, S.; Nishikawa, H.; Kiryu, K.; Nagao, Y. Structure-activity relationships of adenosine A(3) receptor ligands: new potential therapy for the treatment of glaucoma. *Bioorg Med Chem Lett* **2004**, 14, 3775-3779.
80. Lloyd, H. G. E.; Fredholm, B. B. Involvement of Adenosine-Deaminase and Adenosine Kinase in Regulating Extracellular Adenosine Concentration in Rat Hippocampal Slices. *Neurochem Int* **1995**, 26, 387-395.
81. Cristalli, G.; Costanzi, S.; Lambertucci, C.; Lupidi, G.; Vittori, S.; Volpini, R.; Camaioni, E. Adenosine deaminase: Functional implications and different classes of inhibitors. *Med Res Rev* **2001**, 21, 105-128.
82. Cohen, A.; Hirschhorn, R.; Horowitz, S. D.; Rubinstein, A.; Polmar, S. H.; Hong, R.; Martin, D. W. Deoxyadenosine Triphosphate as a Potentially

Toxic Metabolite in Adenosine-Deaminase Deficiency. *P Natl Acad Sci USA* **1978**, 75, 472-476.

83. Resta, R.; Jiang, H.; Hooker, S. W.; Laurent, A. B.; Knudsen, T. B.; Thompson, L. F. 2'-deoxycoformycin blocks T cell differentiation in murine fetal thymic organ culture: A model for adenosine deaminase deficiency. *J Allergy Clin Immun* **1997**, 99, 1603-1603.

84. Sauter, C.; Lamanna, N.; Weiss, M. A. Pentostatin in chronic lymphocytic leukemia. *Expert Opin Drug Met* **2008**, 4, 1217-1222.

85. Blackburn, M. R.; Kellems, R. E. Adenosine deaminase deficiency: Metabolic basis of immune deficiency and pulmonary inflammation. *Adv Immunol* **2005**, 86, 1-41.

86. Hershfield, M. S. New insights into adenosine-receptor-mediated immunosuppression and the role of adenosine in causing the immunodeficiency associated with adenosine deaminase deficiency. *Eur J Immunol* **2005**, 35, 25-30.

87. Schaeffe.Hj; Schwende.Cf. Enzyme-Inhibitors .26. Bridging Hydrophobic and Hydrophilic Regions on Adenosine Deaminase with Some 9-(2-Hydroxy-3-Alkyl)Adenines. *J Med Chem* **1974**, 17, 6-8.

88. Agarwal, R. P.; Spector, T.; Parks, R. E. Tight-Binding Inhibitors .4. Inhibition of Adenosine Deaminases by Various Inhibitors. *Biochem Pharmacol* **1977**, 26, 359-367.

89. Choi, W. J.; Lee, H. W.; Kim, H. O.; Chinn, M.; Gao, Z. G.; Patel, A.; Jacobson, K. A.; Moon, H. R.; Jung, Y. H.; Jeong, L. S. Design and synthesis of N-6-substituted-4'-thioadenosine-5'-uronamides as potent and selective human A(3) adenosine receptor agonists. *Bioorgan Med Chem* **2009**, 17, 8003-8011.

90. Elzein, E.; Palle, V.; Wu, Y. Z.; Maa, T. N.; Zeng, D. W.; Zablocki, J. 2-pyrazolyl-N-6-substituted adenosine derivatives as high affinity and selective adenosine A3 receptor agonists. *J Med Chem* **2004**, 47, 4766-4773.

91. Muller, C. E. Medicinal chemistry of adenosine A(3) receptor ligands. *Curr Top Med Chem* **2003**, 3, 445-462.

92. Baraldi, P. G.; Preti, D.; Tabrizi, M. A.; Fruttarolo, F.; Romagnoli, R.; Zaid, N. A.; Moorman, A. R.; Merighi, S.; Varani, K.; Borea, P. A. New pyrrolo[2,1-f]purine-2,4-dione and imidazo[2,1-f]purine-2,4-dione derivatives as potent and selective human A(3) adenosine receptor antagonists. *J Med Chem* **2005**, 48, 4697-4701.

93. Jiang, J. L.; vanRhee, A. M.; Melman, N.; Ji, X. D.; Jacobson, K. A. 6-phenyl-1,4-dihydropyridine derivatives as potent and selective A(3) adenosine receptor antagonists. *J Med Chem* **1996**, 39, 4667-4675.

94. Li, A. H.; Moro, S.; Melman, N.; Ji, X. D.; Jacobson, K. A. Structure-activity relationships and molecular modeling of 3,5-diacyl-2,4-dialkylpyridine derivatives as selective A(3) adenosine receptor antagonists. *J Med Chem* **1998**, 41, 3186-3201.

95. Jung, K. Y.; Kim, S. K.; Gao, Z. G.; Gross, A. S.; Melman, N.; Jacobson, K. A.; Kim, Y. C. Structure-activity relationships of thiazole and thiadiazole derivatives as potent and selective human adenosine A(3) receptor antagonists. *Bioorgan Med Chem* **2004**, 12, 613-623.

96. Moro, S.; van Rhee, A. M.; Sanders, L. H.; Jacobson, K. A. Flavonoid derivatives as adenosine receptor antagonists: A comparison of the

hypothetical receptor binding site based on a comparative molecular field analysis model. *J Med Chem* **1998**, 41, 46-52.

97. van Muijlwijk-Koezen, J. E.; Timmerman, H.; Link, R.; van der Goot, H.; IJzerman, A. P. A novel class of adenosine A₃ receptor ligands. 1. 3-(2-pyridinyl)isoquinoline derivatives. *J Med Chem* **1998**, 41, 3987-3993.

98. Gao, Z. G.; Kim, S. K.; Biadatti, T.; Chen, W. Z.; Lee, K.; Barak, D.; Kim, S. G.; Johnson, C. R.; Jacobson, K. A. Structural determinants of A₃ adenosine receptor activation: Nucleoside ligands at the agonist/antagonist boundary. *J Med Chem* **2002**, 45, 4471-4484.

99. Jeong, L. S.; Choe, S. A.; Gunaga, P.; Kim, H. O.; Lee, H. W.; Lee, S. K.; Tosh, D. K.; Patel, A.; Palaniappan, K. K.; Gao, Z. G.; Jacobson, K. A.; Moon, H. R. Discovery of a new nucleoside template for human A₃ adenosine receptor ligands: D-4'-thioadenosine derivatives without 4'-hydroxymethyl group as highly potent and selective antagonists. *J Med Chem* **2007**, 50, 3159-3162.

100. Kim, Y. C.; de Zwart, M.; Chang, L.; Moro, S.; Kunzel, J. K. V. D.; Melman, N.; IJzerman, A. P.; Jacobson, K. A. Derivatives of the triazoloquinazoline adenosine antagonist (CGS 15943) having high potency at the human A_{2B} and A₃ receptor subtypes. *J Med Chem* **1998**, 41, 2835-2845.

101. Okamura, T.; Kurogi, Y.; Nishikawa, H.; Hashimoto, K.; Fujiwara, H.; Nagao, Y. 1,2,4-triazolo[5,1-i]purine derivatives as highly potent and selective human adenosine A₃ receptor ligands. *J Med Chem* **2002**, 45, 3703-3708.

102. Colotta, V.; Catarzi, D.; Varano, F.; Cecchi, L.; Filacchioni, G.; Martini, C.; Trincavelli, L.; Lucacchini, A. 1,2,4-triazolo[4,3-a]quinoxalin-1-one: A versatile tool for the synthesis of potent and selective adenosine receptor antagonists. *J Med Chem* **2000**, 43, 1158-1164.

103. Colotta, V.; Catarzi, D.; Varano, F.; Lenzi, O.; Filacchioni, G.; Martini, C.; Trincavelli, L.; Ciampi, O.; Traini, C.; Pugliese, A. M.; Pedata, F.; Morizzo, E.; Moro, S. Synthesis, ligand-receptor modeling studies and pharmacological evaluation of novel 4'-modified-2-aryl-1,2,4-triazolo[4,3-a]quinoxalin-1-one derivatives as potent and selective human A₃ adenosine receptor antagonists. *Bioorgan Med Chem* **2008**, 16, 6086-6102.

104. Colotta, V.; Catarzi, D.; Varano, F.; Cecchi, L.; Filacchioni, G.; Martini, C.; Trincavelli, L.; Lucacchini, A. Synthesis and structure-activity relationships of a new set of 2-arylpyrazolo[3,4-c]quinoline derivatives as adenosine receptor antagonists. *J Med Chem* **2000**, 43, 3118-3124.

105. Colotta, V.; Catarzi, D.; Varano, F.; Capelli, F.; Lenzi, O.; Filacchioni, G.; Martini, C.; Trincavelli, L.; Ciampi, O.; Pugliese, A. M.; Pedata, F.; Schiesaro, A.; Morizzo, E.; Moro, S. New 2-arylpyrazolo[3,4-c]quinoline derivatives as potent and selective human A₃ adenosine receptor antagonists. Synthesis, pharmacological evaluation, and ligand-receptor modeling studies. *J Med Chem* **2007**, 50, 4061-4074.

106. Baraldi, P. G.; Tabrizi, M. A.; Preti, D.; Bovero, A.; Fruttarolo, F.; Romagnoli, R.; Zaid, N. A.; Moorman, A. R.; Varani, K.; Borea, P. A. New 2-arylpyrazolo[4,3-c]quinoline derivatives as potent and selective human A₃ adenosine receptor antagonists. *J Med Chem* **2005**, 48, 5001-5008.

107. Lenzi, O.; Colotta, V.; Catarzi, D.; Varano, F.; Poli, D.; Filacchioni, G.; Varani, K.; Vincenzi, F.; Borea, P. A.; Paoletta, S.; Morizzo, E.; Moro, S. 2-Phenylpyrazolo[4,3-d]pyrimidin-7-one as a New Scaffold To Obtain Potent

and Selective Human A(3) Adenosine Receptor Antagonists: New Insights into the Receptor-Antagonist Recognition. *J Med Chem* **2009**, *52*, 7640-7652.

108. Morrone, F. B.; Jacques-Silva, M. C.; Horn, A. P.; Bernardi, A.; Schwartsmann, G.; Rodnight, R.; Lenz, G. Extracellular nucleotides and nucleosides induce proliferation and increase nucleoside transport in human glioma cell lines. *J Neuro-Oncol* **2003**, *64*, 211-218.

109. Biagi, G.; Bianucci, A. M.; Coi, A.; Costa, B.; Fabbrini, L.; Giorgi, I.; Livi, O.; Micco, I.; Pacchini, F.; Santini, E.; Leonardi, M.; Nofal, F. A.; Salerni, O. L.; Scartoni, V. 2,9-Disubstituted-N-6-(arylcarbamoyl)-8-azaadenines as new selective A(3) adenosine receptor antagonists: Synthesis, biochemical and molecular modelling studies. *Bioorgan Med Chem* **2005**, *13*, 4679-4693.

110. Baraldi, P. G.; Cacciari, B.; Spalluto, G.; Villatoro, M. J. P. D. I. Y.; Zocchi, C.; Dionisotti, S.; Ongini, E. Pyrazolo[4,3-e]-1,2,4-triazolo[1,5-c]pyrimidine derivatives: Potent and selective A(2A) adenosine antagonists. *J Med Chem* **1996**, *39*, 1164-1171.

111. Baraldi, P. G.; Cacciari, B.; Spalluto, G.; Ji, X. D.; Olah, M. E.; Stiles, G.; Dionisotti, S.; Zocchi, C.; Ongini, E.; Jacobson, K. A. Novel N-6-(substituted-phenylcarbamoyl)adenosine-5'-uronamides as potent agonists for A(3) adenosine receptors. *J Med Chem* **1996**, *39*, 802-806.

112. Baraldi, P. G.; Cacciari, B.; de Las Infantas, M. J. P.; Romagnoli, R.; Spalluto, G.; Volpini, R.; Costanzi, S.; Vittori, S.; Cristalli, G.; Melman, N.; Park, K. S.; Ji, X. D.; Jacobson, K. A. Synthesis and biological activity of a new series of N-6-arylcarbamoyl, 2-(Ar)alkynyl-N-6-arylcarbamoyl, and N-6-carboxamido derivatives of adenosine-5'-N-ethyluronamide as A(1) and A(3) adenosine receptor agonists. *J Med Chem* **1998**, *41*, 3174-3185.

113. Baraldi, P. G.; Cacciari, B.; Romagnoli, R.; Spalluto, G.; Klotz, K. N.; Leung, E.; Varani, K.; Gessi, S.; Merighi, S.; Borea, P. A. Pyrazolo[4,3-e]-1,2,4-triazolo[1,5-c]-pyrimidine derivatives as highly potent and selective human A(3) adenosine receptor antagonists. *J Med Chem* **1999**, *42*, 4473-4478.

114. Baraldi, P. G.; Cacciari, B.; Romagnoli, R.; Spalluto, G.; Moro, S.; Klotz, K. N.; Leung, E.; Varani, K.; Gessi, S.; Merighi, S.; Borea, P. A. Pyrazolo[4,3-e]1,2,4-triazolo[1,5-c]pyrimidine derivatives as highly potent and selective human A(3) adenosine receptor antagonists: Influence of the chain at the N-8 pyrazole nitrogen. *J Med Chem* **2000**, *43*, 4768-4780.

115. Moro, S.; Braiuca, P.; Deflorian, F.; Ferrari, C.; Pastorin, G.; Cacciari, B.; Baraldi, P. G.; Varani, K.; Borea, P. A.; Spalluto, G. Combined target-based and ligand-based drug design approach as a tool to define a novel 3D-pharmacophore model of human A(3) adenosine receptor antagonists: Pyrazolo[4,3-e]1,2,4-triazolo[1,5-c]pyrimidine derivatives as a key study. *J Med Chem* **2005**, *48*, 152-162.

116. Pastorin, G.; Da Ros, T.; Bolcato, C.; Montopoli, C.; Moro, S.; Cacciari, B.; Baraldi, P. G.; Varani, K.; Borea, P. A.; Spalluto, G. Synthesis and biological studies of a new series of 5-heteroarylcarbamoylaminopyrazolo[4,3-e]1,2,4-triazolo[1,5-c]pyrimidines as human A(3) adenosine receptor antagonists. Influence of the heteroaryl substituent on binding affinity and molecular modeling investigations. *J Med Chem* **2006**, *49*, 1720-1729.

117. Maconi, A.; Pastorin, G.; Da Ros, T.; Spalluto, G.; Gao, Z. G.; Jacobson, K. A.; Baraldi, P. G.; Cacciari, B.; Varani, K.; Moro, S.; Borea, P. A. Synthesis, biological properties, and molecular modeling investigation of the first potent, selective, and water-soluble human A(3) adenosine receptor antagonist. *J Med Chem* **2002**, *45*, 3579-3582.
118. Cheong, S. L.; Dolzhenko, A.; Katchler, S.; Paoletta, S.; Federico, S.; Cacciari, B.; Dolzhenko, A.; Klotz, K. N.; Moro, S.; Spalluto, G.; Pastorin, G. The Significance of 2-Furyl Ring Substitution with a 2-(para-substituted) Aryl Group in a New Series of Pyrazolo-triazolo-pyrimidines as Potent and Highly Selective hA(3) Adenosine Receptors Antagonists: New Insights into Structure-Affinity Relationship and Receptor-Antagonist Recognition. *J Med Chem* **2010**, *53*, 3361-3375.
119. Da Settimo, F.; Primofiore, G.; La Motta, C.; Taliani, S.; Simorini, F.; Marini, A. M.; Mugnaini, L.; Lavecchia, A.; Novellino, E.; Tuscano, D.; Martini, C. Novel, highly potent adenosine deaminase inhibitors containing the pyrazolo[3,4-d]pyrimidine ring system. Synthesis, structure-activity relationships, and molecular modeling studies. *J Med Chem* **2005**, *48*, 5162-5174.
120. Verheijen, J. C.; Richard, D. J.; Curran, K.; Kaplan, J.; Lefever, M.; Nowak, P.; Malwitz, D. J.; Brooijmans, N.; Toral-Barza, L.; Zhang, W. G.; Lucas, J.; Hollander, I.; Ayral-Kaloustian, S.; Mansour, T. S.; Yu, K.; Zask, A. Discovery of 4-Morpholino-6-aryl-1H-pyrazolo[3,4-d]pyrimidines as Highly Potent and Selective ATP-Competitive Inhibitors of the Mammalian Target of Rapamycin (mTOR): Optimization of the 6-Aryl Substituent. *J Med Chem* **2009**, *52*, 8010-8024.
121. Traxler, P.; Bold, G.; Frei, J.; Lang, M.; Lydon, N.; Mett, H.; Buchdunger, E.; Meyer, T.; Mueller, M.; Furet, P. Use of a pharmacophore model for the design of EGF-R tyrosine kinase inhibitors: 4-(Phenylamino)pyrazolo[3,4-d]pyrimidines. *J Med Chem* **1997**, *40*, 3601-3616.
122. Jorda, R.; Havlicek, L.; McNae, I. W.; Walkinshaw, M. D.; Voller, J.; Sturc, A.; Navratilova, J.; Kuzma, M.; Mistrik, M.; Bartek, J.; Strnad, M.; Krystof, V. Pyrazolo[4,3-d]pyrimidine Bioisostere of Roscovitine: Evaluation of a Novel Selective Inhibitor of Cyclin-Dependent Kinases with Antiproliferative Activity. *J Med Chem* **2011**, *54*, 2980-2993.
123. Ali, A.; Taylor, G. E.; Ellsworth, K.; Harris, G.; Painter, R.; Silver, L. L.; Young, K. Novel pyrazolo[3,4-d]pyrimidine-based inhibitors of Staphylococcus aureus DNA polymerase III: Design, synthesis, and biological evaluation. *J Med Chem* **2003**, *46*, 1824-1830.
124. Gonzalez, M. P.; Teran, C.; Teijeira, M. Search for new antagonist ligands for adenosine receptors from QSAR point of view. How close are we? *Med Res Rev* **2008**, *28*, 329-371.
125. Lewis, R. A. A general method for exploiting QSAR models in lead optimization. *J Med Chem* **2005**, *48*, 1638-1648.
126. Dudek, A. Z.; Arodz, T.; Galvez, J. Computational methods in developing quantitative structure-activity relationships (QSAR): A review. *Comb Chem High T Scr* **2006**, *9*, 213-228.
127. Tafi, A.; Bernardini, C.; Botta, M.; Corelli, F.; Andreini, M.; Martinelli, A.; Ortore, G.; Baraldi, P. G.; Fruttarolo, F.; Borea, P. A.; Tuccinardi, T. Pharmacophore based receptor modeling: The case of

adenosine A(3) receptor antagonists. An approach to the optimization of protein models. *J Med Chem* **2006**, 49, 4085-4097.

128. Cheong, S. L.; Federico, S.; Venkatesan, G.; Paira, P.; Shao, Y. M.; Spalluto, G.; Yap, C. W.; Pastorin, G. Pharmacophore elucidation for a new series of 2-aryl-pyrazolo-triazolo-pyrimidines as potent human A(3) adenosine receptor antagonists. *Bioorg Med Chem Lett* **2011**, 21, 2898-2905.

129. Hide, W.; Mizrahi, V.; Venkatesh, B.; Brenner, S.; Simpson, A.; Blatch, G.; Soodyall, H.; Denby, K.; Wingfield, M.; Wingfield, B.; van Helden, P.; Ramesar, R.; Dorrington, R.; Kelso, J.; Oppon, E.; Goyvaerts, E.; Ramsay, M.; de Villiers, E.; van Heerden, C.; Allsopp, B.; Seoighe, C. A platform for genomics in South Africa. *Samj S Afr Med J* **2001**, 91, 1006-1007.

130. Kubinyi, H.; Folkers, G.; Martin, Y. C. 3D QSAR in drug design: Ligand-protein interactions and molecular similarity - Preface. *Perspect Drug Discov* **1998**, 9-11, V-Vii.

131. Klebe, G.; Mietzner, T.; Weber, F. Different Approaches toward an Automatic Structural Alignment of Drug Molecules - Applications to Sterol Mimics, Thrombin and Thermolysin Inhibitors. *J Comput Aid Mol Des* **1994**, 8, 751-778.

132. Cramer, R. D. Topomer CoMFA: A design methodology for rapid lead optimization. *J Med Chem* **2003**, 46, 374-388.

133. Cramer, R. D.; Clark, R. D.; Patterson, D. E.; Ferguson, A. M. Bioisosterism as a molecular diversity descriptor: Steric fields of single "topomeric" conformers. *J Med Chem* **1996**, 39, 3060-3069.

134. Moro, S.; Guo, D. P.; Camaioni, E.; Boyer, J. L.; Harden, T. K.; Jacobson, K. A. Human P2Y(1) receptor: Molecular modeling and site-directed mutagenesis as tools to identify agonist and antagonist recognition sites. *J Med Chem* **1998**, 41, 1456-1466.

135. Hibert, M. F.; Trumppkallmeyer, S.; Bruinvels, A.; Hoflack, J. 3-Dimensional Models of Neurotransmitter G-Binding Protein-Coupled Receptors. *Mol Pharmacol* **1991**, 40, 8-15.

136. Cherezov, V.; Rosenbaum, D. M.; Hanson, M. A.; Rasmussen, S. G. F.; Thian, F. S.; Kobilka, T. S.; Choi, H. J.; Kuhn, P.; Weis, W. I.; Kobilka, B. K.; Stevens, R. C. High-resolution crystal structure of an engineered human beta(2)-adrenergic G protein-coupled receptor. *Science* **2007**, 318, 1258-1265.

137. Jones, M. E. E.; Thorburn, A. W.; Britt, K. L.; Hewitt, K. N.; Misso, M. L.; Wreford, N. G.; Proietto, J.; Oz, O. K.; Leury, B. J.; Robertson, K. M.; Yao, S. G.; Simpson, E. R. Aromatase-deficient (ArKO) mice accumulate excess adipose tissue. *J Steroid Biochem* **2001**, 79, 3-9.

138. Evers, A.; Klebe, G. Ligand-supported homology modeling of G-protein-coupled receptor sites: Models sufficient for successful virtual screening. *Angew Chem Int Edit* **2004**, 43, 248-251.

139. Moro, S.; Deflorian, F.; Bacilieri, M.; Spalluto, G. Ligand-based homology modeling as attractive tool to inspect GPCR structural plasticity. *Curr Pharm Design* **2006**, 12, 2175-2185.

140. Morizzo, E.; Federico, S.; Spalluto, G.; Moro, S. Human A(3) Adenosine Receptor as Versatile G Protein-Coupled Receptor Example to Validate the Receptor Homology Modeling Technology. *Curr Pharm Design* **2009**, 15, 4069-4084.

141. Yuzlenko, O.; Kiec-Kononowicz, K. Molecular Modeling of A(1) and A(2A) Adenosine Receptors: Comparison of Rhodopsin- and beta(2)-Adrenergic-Based Homology Models Through the Docking Studies. *J Comput Chem* **2009**, *30*, 14-32.
142. Martinelli, A.; Tuccinardi, T. Molecular Modeling of adenosine receptors: New results and trends. *Med Res Rev* **2008**, *28*, 247-277.
143. Lipinski, C. A.; Lombardo, F.; Dominy, B. W.; Feeney, P. J. Experimental and computational approaches to estimate solubility and permeability in drug discovery and development settings. *Adv Drug Deliver Rev* **1997**, *23*, 3-25.
144. Lipinski, C. A. Drug-like properties and the causes of poor solubility and poor permeability. *J Pharmacol Toxicol* **2000**, *44*, 235-249.
145. Morizzo, E.; Capelli, F.; Lenzi, O.; Catarzi, D.; Varano, F.; Filacchioni, G.; Vincenzi, F.; Varani, K.; Borea, P. A.; Colotta, V.; Moro, S. Scouting human A(3) adenosine receptor antagonist binding mode using a molecular simplification approach: From triazoloquinoxaline to a pyrimidine skeleton as a key study. *J Med Chem* **2007**, *50*, 6596-6606.
146. Poli, D.; Catarzi, D.; Colotta, V.; Varano, F.; Filacchioni, G.; Daniele, S.; Trincavelli, L.; Martini, C.; Paoletta, S.; Moro, S. The Identification of the 2-Phenylphthalazin-1(2H)-one Scaffold as a New Decorable Core Skeleton for the Design of Potent and Selective Human A(3) Adenosine Receptor Antagonists. *J Med Chem* **2011**, *54*, 2102-2113.
147. Paira, P.; Chow, M. J.; Venkatesan, G.; Kosaraju, V. K.; Cheong, S. L.; Klotz, K. N.; Ang, W. H.; Pastorin, G. Organoruthenium antagonists of human A(3) adenosine receptors. *Chemistry* **2013**, *19*, 8321-30.
148. Shenlin, H. *PCT Int. Appl. WO 2011025927* **2011**.
149. Srivastava, P. C.; Ivanovics, G. A.; Rousseau, R. J.; Robins, R. K. Nucleosides of 4-Substituted Imidazoles. *J Org Chem* **1975**, *40*, 2920-2924.
150. Groziak, M. P.; Chern, J. W.; Townsend, L. B. Heterocyclic Synthesis Via a 1,3-Dicyclohexylcarbodiimide-Mediated Cyclodesulfurative Annulation Reaction - New Methodology for the Preparation of Guanosine and Guanosine-Type Nucleoside Analogs. *J Org Chem* **1986**, *51*, 1065-1069.
151. Higashino, T.; Yoshida, S.; Hayashi, E. Purines .5. Reaction of 9-Phenyl-9h-Purine-6-Carbonitrile with Nucleophilic-Reagents. *Chem Pharm Bull* **1982**, *30*, 4521-4525.
152. Kazaoka, K.; Sajiki, H.; Hirota, K. Synthesis of 6-substituted 9-benzyl-8-hydroxypurines with potential interferon-inducing activity. *Chem Pharm Bull* **2003**, *51*, 608-611.
153. Qi, C. *PCT Int. Appl. WO 2012030924* **2012**.
154. Yamazaki, A.; Kumashir, I.; Takenish, T. Synthesis of Guanosine and Its Derivatives from 5-Amino-1-Beta-D-Ribofuranosyl-4-Imidazolecarboxamide .I. Ring Closure with Benzoyl Isothiocyanate. *J Org Chem* **1967**, *32*, 1825-1828.
155. Brown, R.; Joseph, M.; Leigh, T.; Swain, M. L. Synthesis and Reactions of 7,8-Dihydro-8-Methylpterin and 9-Methylguanine 7-Oxide. *J Chem Soc Perk T* **1977**, 1003-1009.
156. Robins, M. J.; Uznanski, B. Nucleic-Acid Related-Compounds .34. Non-Aqueous Diazotization with Tert-Butyl Nitrite - Introduction of Fluorine, Chlorine, and Bromine at C-2 of Purine Nucleosides. *Can J Chem* **1981**, *59*, 2608-2611.

157. Frank, S. H., S.; . Synthesis of 2'-Deoxyribofuranosides of 8-Aza-7-deazaguanine and Related Pyrazolo[3,4-d]pyrimidines. *Helv. Chim. Acta* **1986**, 69, 1602.
158. Klotz, K. N.; Hessling, J.; Hegler, J.; Owman, C.; Kull, B.; Fredholm, B. B.; Lohse, M. J. Comparative pharmacology of human adenosine receptor subtypes - characterization of stably transfected receptors in CHO cells. *N-S Arch Pharmacol* **1998**, 357, 1-9.
159. Klotz, K. N.; Cristalli, G.; Grifantini, M.; Vittori, S.; Lohse, M. J. Photoaffinity-Labeling of A1-Adenosine Receptors. *J Biol Chem* **1985**, 260, 4659-4664.
160. Delean, A.; Hancock, A. A.; Lefkowitz, R. J. Validation and Statistical-Analysis of a Computer Modeling Method for Quantitative-Analysis of Radioligand Binding Data for Mixtures of Pharmacological Receptor Subtypes. *Mol Pharmacol* **1982**, 21, 5-16.
161. Cheng, Y.; Prusoff, W. H. Relationship between Inhibition Constant (K₁) and Concentration of Inhibitor Which Causes 50 Per Cent Inhibition (I₅₀) of an Enzymatic-Reaction. *Biochem Pharmacol* **1973**, 22, 3099-3108.
162. Lohse, M. J.; Klotz, K. N.; Lindenbornfotinos, J.; Reddington, M.; Schwabe, U.; Olsson, R. A. 8-Cyclopentyl-1,3-Dipropylxanthine (Dpcpx) - a Selective High-Affinity Antagonist Radioligand for A1 Adenosine Receptors. *N-S Arch Pharmacol* **1987**, 336, 204-210.
163. Klotz, K. N.; Falgner, N.; Kachler, S.; Lambertucci, C.; Vittori, S.; Volpini, R.; Cristalli, G. [H-3]HEMADO - a novel tritiated agonist selective for the human adenosine A(3) receptor. *Eur J Pharmacol* **2007**, 556, 14-18.
164. Bradford, M. M. Rapid and Sensitive Method for Quantitation of Microgram Quantities of Protein Utilizing Principle of Protein-Dye Binding. *Anal Biochem* **1976**, 72, 248-254.
165. Cramer, R. D.; Cruz, P.; Stahl, G.; Curtiss, W. C.; Campbell, B.; Masek, B. B.; Soltanshahi, F. Virtual Screening for R-Groups, including Predicted pIC₅₀ Contributions, within Large Structural Databases, Using Topomer CoMFA. *J Chem Inf Model* **2008**, 48, 2180-2195.
166. Sybyl-X 1.3, St. Louis, 2010. <http://www.tripos.com>
167. Halgren, T. A. Merck molecular force field .1. Basis, form, scope, parameterization, and performance of MMFF94. *J Comput Chem* **1996**, 17, 490-519.
168. Halgren, T. A. Merck molecular force field .5. Extension of MMFF94 using experimental data, additional computational data, and empirical rules. *J Comput Chem* **1996**, 17, 616-641.
169. Jaakola, V. P.; Griffith, M. T.; Hanson, M. A.; Cherezov, V.; Chien, E. Y. T.; Lane, J. R.; IJzerman, A. P.; Stevens, R. C. The 2.6 Angstrom Crystal Structure of a Human A(2A) Adenosine Receptor Bound to an Antagonist. *Science* **2008**, 322, 1211-1217.
170. <http://www.uniprot.org/>. In.
171. Eswar, N. M.-R., M. A.; Webb, B.; Madhusudhan, M. S.; Eramian, D.; Shen, M.; Pieper, U.; Sali, A. Comparative protein structure modeling using MODELLER. 2007, . In *Curr Protoc Protein Sci.*, 2007; Vol. Chapter 2,.
172. Marti-Renom, M. A.; Stuart, A. C.; Fiser, A.; Sanchez, R.; Melo, F.; Sali, A. Comparative protein structure modeling of genes and genomes. *Annu Rev Bioph Biom* **2000**, 29, 291-325.

173. Sali, A.; Blundell, T. L. Comparative Protein Modeling by Satisfaction of Spatial Restraints. *J Mol Biol* **1993**, 234, 779-815.
174. Fiser, A.; Do, R. K. G.; Sali, A. Modeling of loops in protein structures. *Protein Sci* **2000**, 9, 1753-1773.
175. ClustalW; European Molecular Biology Laboratory-European Bioinformatics, Institute; <http://www.ebi.ac.uk/Tools/clustalw2/>.
176. http://psvs-1_4-dev.nesg.org/. In.
177. DeLano, W. L. The PyMOL Molecular Graphics System (2002) DeLano Scientific. (San Carlos, CA, USA); <http://www.pymol.org>. In.
178. Humphrey, W.; Dalke, A.; Schulten, K. VMD: Visual molecular dynamics. *J Mol Graph Model* **1996**, 14, 33-38.
179. Laskowski, R. A.; Macarthur, M. W.; Moss, D. S.; Thornton, J. M. Procheck - a Program to Check the Stereochemical Quality of Protein Structures. *J Appl Crystallogr* **1993**, 26, 283-291.
180. MOE (Molecular Operating Environment), version 2010.10; Chemical computing group Inc. (1010 Sherbrooke Street West, Suite 910, Montreal, Quebec H3A 2R7, Canada); <http://www.chemcomp.com>.
181. http://www.shadnia.com/H_IFE/.
182. Morris, G. M.; Goodsell, D. S.; Halliday, R. S.; Huey, R.; Hart, W. E.; Belew, R. K.; Olson, A. J. Automated docking using a Lamarckian genetic algorithm and an empirical binding free energy function. *J Comput Chem* **1998**, 19, 1639-1662.
183. Huey, R.; Morris, G. M.; Olson, A. J.; Goodsell, D. S. A semiempirical free energy force field with charge-based desolvation. *J Comput Chem* **2007**, 28, 1145-1152.
184. Sanner, M. F. Python: A programming language for software integration and development. *J Mol Graph Model* **1999**, 17, 57-61.
185. Korb, O.; Stutzle, T.; Exner, T. E. Empirical Scoring Functions for Advanced Protein-Ligand Docking with PLANTS. *J Chem Inf Model* **2009**, 49, 84-96.
186. Kim, E. J.; Zhen, R. G.; Rea, P. A. Site-Directed Mutagenesis of Vacuolar H⁺-Pyrophosphatase - Necessity of Cys(634) for Inhibition by Maleimides but Not Catalysis. *J Biol Chem* **1995**, 270, 2630-2635.
187. Gao, Z. G.; Chen, A.; Barak, D.; Kim, S. K.; Muller, C. E.; Jacobson, K. A. Identification by site-directed mutagenesis of residues involved in ligand recognition and activation of the human A(3) adenosine receptor. *J Biol Chem* **2002**, 277, 19056-19063.
188. Frohn, M.; Viswanadhan, V.; Pickrell, A. J.; Golden, J. E.; Muller, K. M.; Burli, R. W.; Biddlecome, G.; Yoder, S. C.; Rogers, N.; Dao, J. H.; Hungate, R.; Allen, J. R. Structure-guided design of substituted azabenzimidazoles as potent hypoxia inducible factor-1 alpha prolyl hydroxylase-2 inhibitors. *Bioorg Med Chem Lett* **2008**, 18, 5023-5026.
189. Sala, M.; De Palma, A. M.; Hrebabecky, H.; Dejmek, M.; Dracinsky, M.; Leyssen, P.; Neyts, J.; Mertlikova-Kaiserova, H.; Nencka, R. SAR studies of 9-norbornylpurines as Coxsackievirus B3 inhibitors. *Bioorg Med Chem Lett* **2011**, 21, 4271-4275.
190. Dolakova, P.; Masojidkova, M.; Holy, A. Efficient synthesis of pyrimidine carbonitriles and their derivatives. *Heterocycles* **2007**, 71, 1107-1115.

191. Sundermeier, U.; Dobler, C.; Mehlretter, G. M.; Baumann, W.; Beller, M. Synthesis of 9-N-cinchona alkaloid peptide hybrid derivatives: Preparation and conformational study of 9-N-acylamino(9-deoxy)cinchona alkaloids. *Chirality* **2003**, *15*, 127-134.
192. Tanji, K.; Higashino, T. Purines .9. Reaction of 9-Phenyl-9h-Purine-2-Carbonitriles with Grignard-Reagents. *Heterocycles* **1990**, *30*, 435-440.
193. Miyashita, A.; Suzuki, Y.; Ohta, K.; Higashino, T. Preparation of Heteroarene carbonitriles by Reaction of Haloheteroarenes with Potassium Cyanide Catalyzed by Sodium P-Toluenesulfinate. *Heterocycles* **1994**, *39*, 345-356.
194. Higashino, T.; Katori, T.; Yoshida, S.; Hayashi, E. Triazolo[4,5-D]Pyrimidines .6. 3-Phenyl-3h-1,2,3-Triazolo[4,5-D]-Pyrimidine-7-Carbonitrile and Related-Compounds. *Chem Pharm Bull* **1980**, *28*, 255-261.
195. Miyashita, A.; Sato, S.; Taido, N.; Tanji, K.; Oishi, E.; Higashino, T. Studies on Pyrazolo[3,4-D]Pyrimidine Derivatives .17. Reactions of 5-Benzoyl-4,5-Dihydro-6-Methyl-1-Phenyl-1h-Pyrazolo[3,4-D]Pyrimidine-4-Carbonitrile (the 6-Methylpyrazolopyrimidine Reissert Compound). *Chem Pharm Bull* **1990**, *38*, 230-233.
196. Terasaka, T.; Kinoshita, T.; Kuno, M.; Seki, N.; Tanaka, K.; Nakanishi, I. Structure-based design, synthesis, and structure-activity relationship studies of novel non-nucleoside adenosine deaminase inhibitors. *J Med Chem* **2004**, *47*, 3730-3743.
197. La Motta, C.; Sartini, S.; Mugnaini, L.; Salerno, S.; Simorini, F.; Taliani, S.; Marini, A. M.; Da Settinio, F.; Lavecchia, A.; Novellino, E.; Antonioli, L.; Fornai, M.; Blandizzi, C.; Del Tacca, M. Exploiting the Pyrazolo[3,4-d]pyrimidin-4-one Ring System as a Useful Template To Obtain Potent Adenosine Deaminase Inhibitors. *J Med Chem* **2009**, *52*, 1681-1692.

Appendix

- Table A1** Selected X-ray crystallographic data for **81**
- Table A2** Selected bond angles [°] and lengths [Å] for **81**
- Table A3** HPLC data of 4-chloro-pyrazolopyrimidine derivatives
- Table A4** C logP values of the pyrazolopyrimidine derivatives
- Table A5** HPLC data of pyrazolopyrimidine-4-carboxylate derivatives
- Figure A1** Sequence alignment used to build hA₃ based on hA_{2A} template retrieved by Modeller 9.11
- Figure A2** Ramachandran Plot for hA_{2A}AR-based hA₃ homology model [A,B,L (red)]:most favoured regions; [a,b,l,p (yellow)]: additional allowed regions; [~a,~b,~l,~p(light green)]: generously allowed regions.
- Figure A3** The graph displays the electrostatic interaction energy (in kcal/mol) between the ligand and each single amino acid involved in ligand recognition observed from hypothetical binding modes of ZM-241385 inside the hA_{2A} receptor (**A**), and ligand **116** inside hA_{2A}AR (**B**) and hA₃AR (**C**) binding site.

Table A1. Selected X-ray crystallographic data for **81****Table A2.** Selected bond angles [°] and lengths [Å] for **81**

Ligand	81
Empirical formula	C ₆ H ₆ Cl N ₅
Formula weight	183.61
<i>T</i> [K]	100(2)
Wavelength [Å]	0.71073
Crystal system	Monoclinic
Space group	C2/c
<i>a</i> [Å]	13.885(3)
<i>b</i> [Å]	8.0801(16)
<i>c</i> [Å]	14.805(3)
α [°]	90
β [°]	111.540
γ [°]	90
<i>V</i> [Å ³]	1545.0(5)
<i>Z</i>	8
<i>D_c</i> [Mg m ⁻³]	1.579
μ [mm ⁻¹]	0.439
θ range [°]	2.96 to 27.47
data/restraints / parameters	1745 / 0 / 118
max., min. transmn	0.9290 and 0.7784
final <i>R</i> indices	<i>R</i> 1 = 0.0363
[<i>I</i> > 2 σ (<i>I</i>)]	<i>wR</i> 2 = 0.0987
<i>R</i> indices (all data)	<i>R</i> 1=0.0384, <i>wR</i> 2=0.1004
GOF on <i>F</i> ²	1.122
peak / hole [e.Å ⁻³]	0.495 and -0.236

Ligand	81
N(1)-C(3)	1.335(2)
N(1)-C(6)	1.453(2)
N(2)-C(1)	1.340(2)
N(5)-C(4)	1.339(2)
C(3)-N(1)-N(2)	114.71(13)
C(3)-N(1)-C(6)	127.61(14)
N(2)-N(1)-C(6)	117.67(13)
C(1)-N(2)-N(1)	103.21(12)

$R = \Sigma ||F_o| - |F_c|| / \Sigma |F_o|$, $wR2 = \{\Sigma [w(F_o^2 - F_c^2)^2] / \Sigma [w(F_o^2)^2]\}^{1/2}$. Goodness-of-fit (GOF) = $\{\Sigma [w(F_o^2 - F_c^2)^2] / (n - p)\}^{1/2}$, where *n* is the number of data and *p* is the number of parameters refined.

Table A3. HPLC data of 4-chloro-pyrazolopyrimidine derivatives

ACN(60%): H2O				MeOH(50%): H2O			
Compound	Ret. Time (min)	Area	Area %	Compound	Ret. Time (min)	Area	Area %
81	2.227	5781967	98.210	81	2.550	12711793	99.677
82	3.397	3610977	96.831	82	3.290	24299692	99.542
83	6.047	4514757	100.00	83	6.300	10651419	99.503
84	5.550	3374151	99.351	84	5.890	32279617	99.588
101	2.917	4291782	97.889	101	3.080	23203335	100.00
102	3.337	39412268	99.479	102	3.757	34593321	96.600
103	5.753	39327655	99.859	103	5.660	38059318	99.665
104	3.800	46905660	99.451	104	3.797	4493179	99.585
105	4.233	12402016	100.00	105	4.680	10934814	100.00
106	4.270	19100046	95.569	106	4.780	15050677	95.121
107	7.377	5064005	99.624	107	7.223	10118599	99.497
108	5.293	11313939	95.744	108	5.960	13652921	95.103
109	7.217	28864861	97.897	109	7.983	14111129	97.415
110	8.013	18623701	98.315	110	8.490	11958016	99.658
111	10.907	21506486	95.40	111	11.57	95996198	98.186
112	8.370	27826316	98.422	112	8.590	44458941	97.800
113	6.743	4347049	99.715	113	6.420	31048959	99.517
114	7.377	5064005	99.624	114	7.573	5348241	95.860
115	9.270	4080231	98.781	115	9.057	2260261	96.312
116	6.91	4449642	97.650	116	6.993	4631803	95.010
117	4.513	45034555	99.918	117	4.853	43700086	98.424
118	7.24	13486107	99.400	118	6.910	4449642	97.656
119	11.600	10666104	100.00	119	10.97	19428266	99.130
120	12.387	7360151	98.635	120	11.63	14304110	97.599
121	4.233	6149524	96.276	121	4.960	8840746	99.447
122	5.323	11015801	99.594	122	6.053	5656546	95.100
123	10.020	17883773	98.322	123	10.60	11038020	99.350
124	7.907	4055523	99.527	124	8.430	12304947	97.408

Table A4. C logP values of the pyrazolopyrimidine derivatives

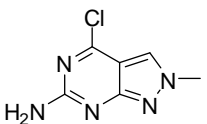
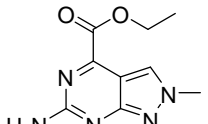
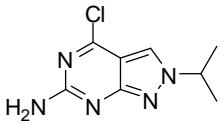
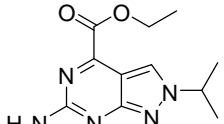
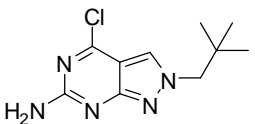
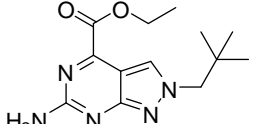
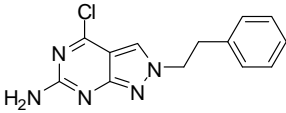
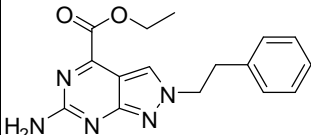
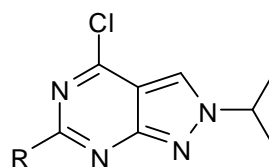
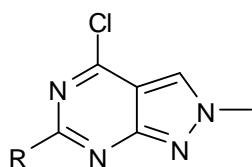
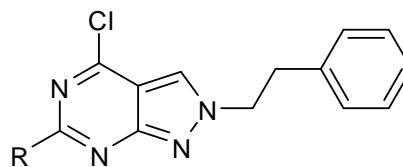
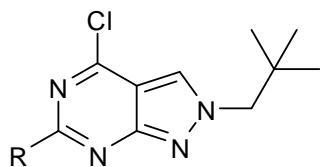
Com pound	Structure	ClogP	Com pound	Structure	C logP
81		0.24	133		-0.32
82		1.08	134		0.52
83		2.10	135		1.53
84		2.34	136		1.76

Table A4 continued.....



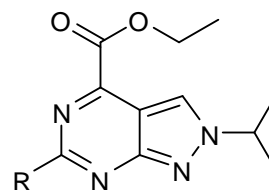
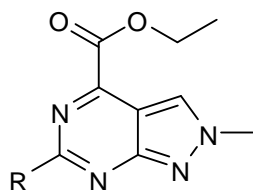
Compound	R	C logP	Compound	R	C logP
101		1.28	105		2.12
102		1.43	106		2.26
103		2.18	107		3.02
104		1.78	108		2.62
117		3.63	118		4.46
121		1.33	122		2.17

Table A4 continued.....



Compound	R	C logP	Compound	R	C logP
109		3.13	113		3.37
110		3.28	114		3.52
111		4.03	115		4.27
112		3.63	116		3.87
119		5.48	120		5.72
123		3.18	124		3.43

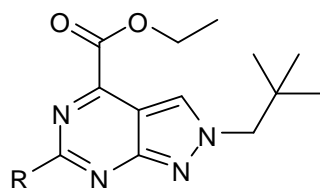
Table A4 continued.....



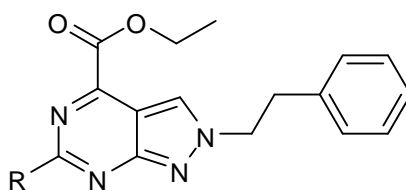
Compound	R	C logP
137		0.71
138		0.85
139		1.60
140		1.21
154		3.06
155		4.79
156		3.49
159		0.76

Compound	R	C logP
141		1.55
142		1.69
143		2.44
144		2.05
157		3.90
160		1.60

Table A4 continued.....



Compound	R	C logP	Compound	R	C logP
145		2.71	147		3.06
146		3.45	161		2.61



Compound	R	C logP	Compound	R	C logP
148		2.81	152		3.67
149		2.95	153		4.11
150		3.70	158		5.15
151		3.31	162		2.86

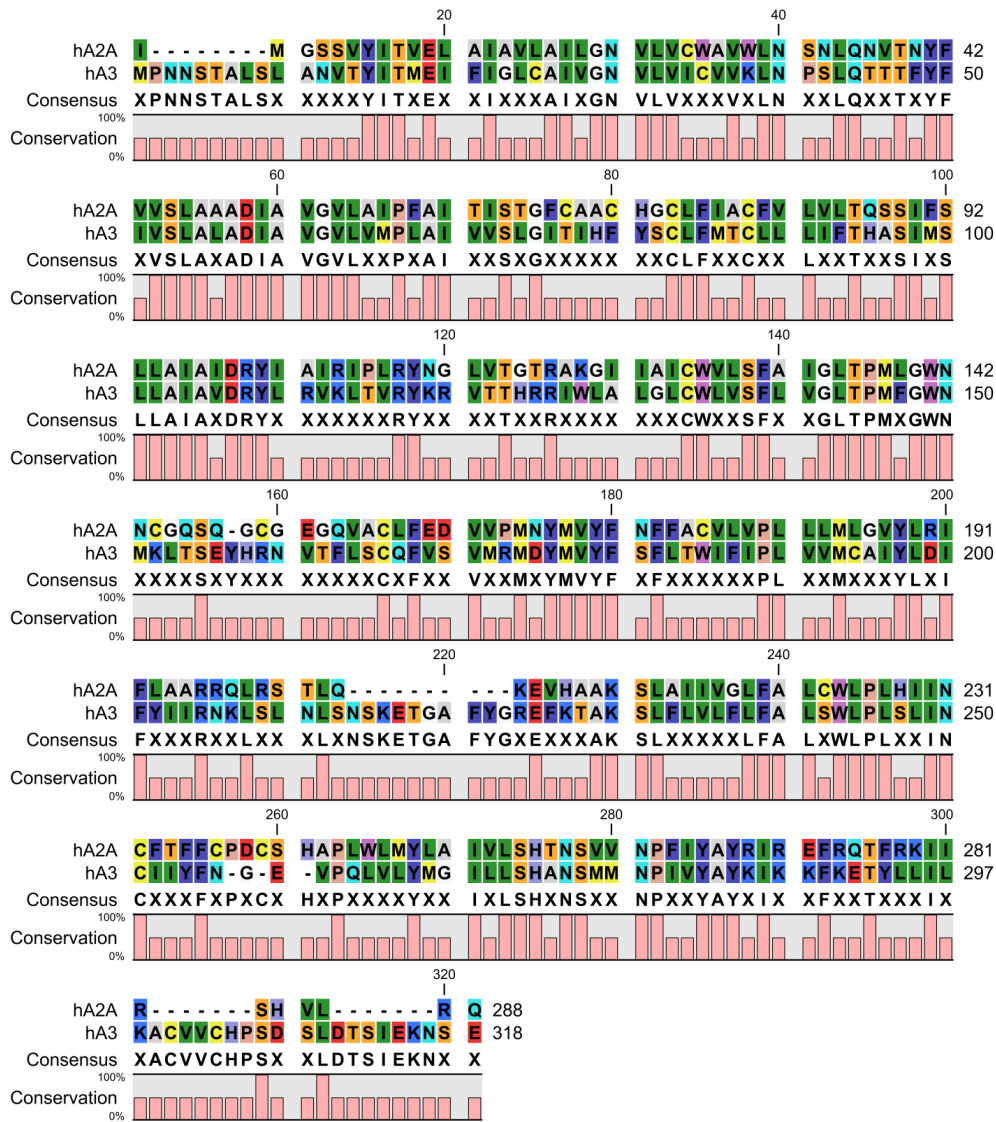


Figure A1. Sequence alignment used to build hA₃ based on hA_{2A} template retrieved by Modeller 9.11

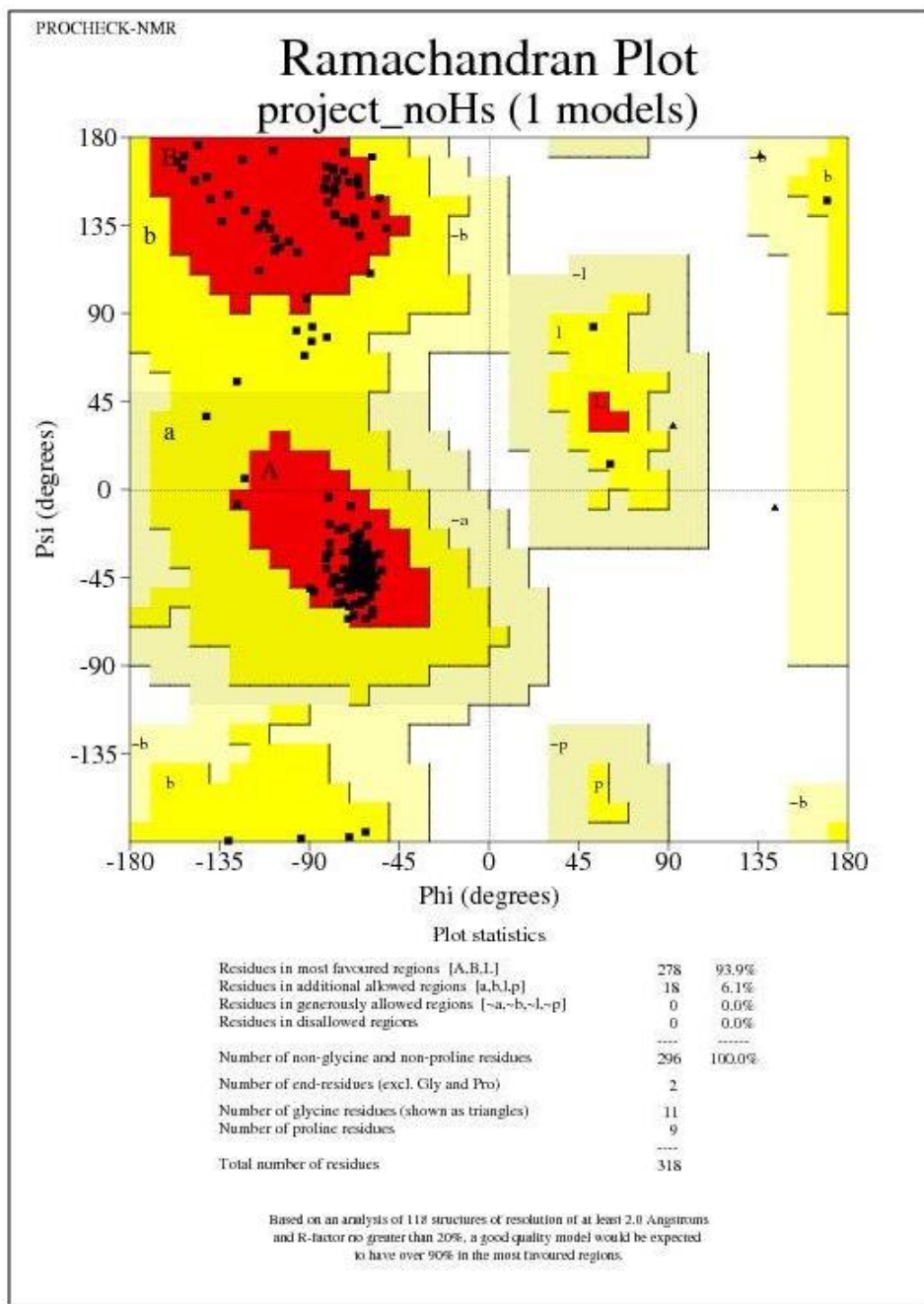


Figure A2. Ramachandran Plot for hA_{2A}AR-based hA₃ homology model ([A,B,L] (red)):most favoured regions; [a,b,l,p (yellow)]: additional allowed regions; [~a,~b,~l,~p(light green)]: generously allowed regions.

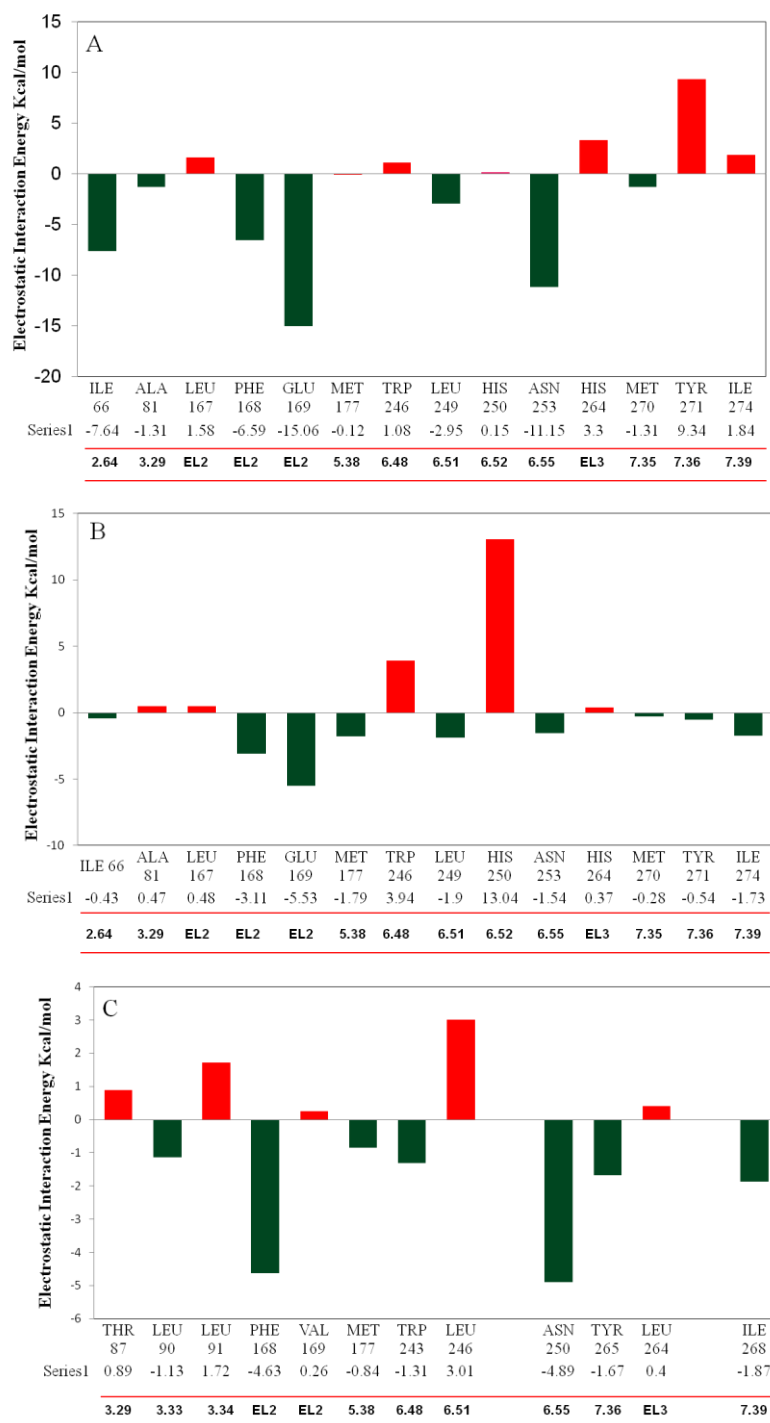


Figure A3. The graph displays the electrostatic interaction energy (in kcal/mol) between the ligand and each single amino acid involved in ligand recognition observed from hypothetical binding modes of ZM-241385 inside the hA_{2A} receptor (A), and ligand 116 inside hA_{2A}AR (B) and hA_{3A}AR (C) binding site.

Table A5. HPLC data of pyrazolopyrimidine-4-carboxylate derivatives

ACN(65%):H2O				MeOH(55%):H2O			
Compound	Ret. Time (min)	Area	Area %	Compound	Ret. Time (min)	Area	Area %
133	2.9	95313883	99.784	133	2.8	17401396	99.70
134	3.2	35262943	99.19	134	2.7	892191	100.00
135	3.5	34708914	100.00	135	3.7	36472694	100.00
136	3.5	12850231	99.470	136	3.1	36702722	100.00
137	3.4	12386174	96.559	137	3.0	31751941	100.0
138	3.5	23447549	95.84	138	3.0	340165	95.617
139	5.8	13386289	99.293	139	5.9	3013438	98.41
140	3.8	11995260	100.00	140	3.6	899335	97.90
141	4.6	10632362	100.00	141	4.0	11091539	100.00
142	4.7	15036842	97.838	142	4.3	15751859	97.78
143	7.3	2963693	98.873	143	6.9	9693421	98.126
144	5.4	18539288	99.13	144	5.0	10282097	98.11
145	6.7	2271874	96.389	145	6.6	18982572	98.91
146	7.9	13812408	97.402	146	8.0	42758757	100.00
147	7.1	43130534	98.406	147	7.1	34446364	100.00
148	3.1	12788841	99.74	148	3.3	32580406	99.76
149	6.1	15921376	97.340	149	6.5	20088939	100.00
150	6.9	12495549	99.684	150	6.7	38023560	100.00
151	7.8	10767741	100.00	151	7.2	21010179	100.00
152	9.1	17621393	100.00	152	10.3	3025011	97.931
153	120	31194331	100.00	153	11.1	9949223	97.776
154	5.4	9787411	97.841	154	5.4	6926709	98.070
155	137	21404761	99.522	155	13.0	5441539	95.552
156	130	30654969	100.00	156	11.6	15453929	100.00
157	8.3	18900479	99.319	157	8.0	21829456	99.716
158	9.3	15823593	97.910	158	9.4	35257764	95.869
159	3.6	3993891	99.372	159	3.8	35623450	100.00
160	4.2	23150840	99.732	160	4.1	29236433	100.00
161	5.5	2383136	97.28	161	5.7	33873733	99.98
162	7.5	15274893	100.00	162	7.7	40996903	100.00